ELSEVIER

Coordination Chemistry Reviews
165 (1997) 315–446

COORDINATION CHEMISTRY REVIEWS

Spectral intensities of transition metal complexes

A.J. Bridgeman, M. Gerloch *

University Chemical Laboratories, Lensfield Road, Cambridge, CB2 1EW, UK

Received 11 November 1996; accepted 21 February 1997

Contents

Abstract 316
1. Introduction 317
2. Electronic and nuclear motions 320
   2.1. The adiabatic Born-Huang and Born-Oppenheimer approaches 321
   2.2. Crude adiabatic basis 322
   2.3. Herzberg-Teller coupling 322
   2.4. The harmonic approximation 323
   2.5. Optical transitions 324
   2.6. The Condon approximation 326
   2.7. The Herzberg-Teller transition moment 328
3. Electric dipole transitions and parity mixing 329
4. Spectral intensities of '*f-f*' transitions 331
   4.1. The static crystal-field model 331
   4.2. Hypersensitive '*f-f*' transitions 335
   4.3. *Pseudo*quadrupole transitions in an inhomogeneous dielectric 336
   4.4. Ligand polarization mechanism 337
   4.5. Alternative views of dynamic coupling 340
   4.6. Early and extensive explorations of the SC + DC model 341
   4.7. Effective operators and covalency 346
   4.8. Ligand polarizability anisotropy 352
   4.9. Overview of '*f-f*' intensities and introduction of '*d-d*' 355
5. The cellular ligand-field model for acentric chromophores 360
   5.1. Cellular ligand-field theory and ligand-field orbitals 361
   5.2. *P*, *t*, and *R* contributions 363
   5.3. Parameterized local transition moments 365
   5.4. Local multipole expansion within a pure *d* basis 370
   5.5. The superposition 372
   5.6. Spectral absorbance 376
   5.7. The chemical and physical significance of the $^{l}\tau_{\lambda}$ parameters 377
   5.8. The signs of the $^{l}\tau_{\lambda}$ parameters 377
   5.9. The *R* contribution 379
   5.10. The magnitudes of CLF intensity and energy parameters 380
   5.11. Qualitative implications of the two-centre expansion 382

* *Corresponding author.*

PII S0010-8545(97)00020-9

5.12. A computational study of the two-centre expansion 385
5.12.1. General trends 385
5.12.2. $P:F$ ratios 387
5.12.3. The importance of the ligand functions 387
5.12.4. A more realistic modelling 388
5.13. Symmetry and degrees of freedom 388
5.14. The functional dependence of static- and dynamic- coupling parameters 391
5.14.1. Static coupling 391
5.14.2. Dynamic coupling 391
5.14.3. Modelling polarizability contributions – an example 393
5.15. Covalency and the CLF approach 395
5.16. Misdirected valency 398
5.17. Coordination voids 400
6. The cellular ligand-field model for centric and near-centric chromophores 400
6.1. Effective operators 401
6.2. Bending vibrational modes 402
6.3. Stretching vibrational modes 407
6.4. Torsional modes 408
6.5. Relationships between the static and vibronic CLF parameters 410
7. A survey of CLF analytical results 413
7.1. The chromophores 413
7.2. Reproduction of experimental data 415
7.2.1. Bis(triphenylphosphine)dichlorocobalt(II) 415
7.2.2. Hexamethyltrendithiocyanatonickel(II) 415
7.2.3. Tetrakis(diphenylmethylarsineoxide)nitrato-cobalt(II) and -nickel(II) nitrates . . 416
7.2.4. (−) (α-isospartien)dichlorocobalt(II) 417
7.2.5. Tetrachloroplatinum(II) and -palladium(II) 419
7.2.6. Tris(ethylenediamine)nickel(II) dinitrate 419
7.2.7. Reproduction of spectral traces 421
7.2.8. Temperature dependence of vibronic intensities 422
7.3. Parameter values 423
7.3.1. Tetrahedral chromophores 424
7.3.2. Trigonal bipyramidal chromophores 428
7.3.3. Square pyramidal chromophores 432
7.3.4. Planar chromophores I 434
7.3.5. Planar chromophores II 437
7.3.6. The reproduction of rotatory strengths 439
7.4. A correlation between bond character and an optical selection rule 441
7.5. Concluding remarks 443
References 444

Abstract

Electronic dipole '*d–d*' transitions in transition metal complexes, and '*f–f*' in lanthanoid species, are formally disallowed. This article describes how they are forced. A broadly chronological review of the literature on '*f–f*' electric dipole transitions focuses upon mechanisms which have been proposed to effect the required parity mixing within functions involved in those transitions. It begins with the "static coupling" (SC) model and, following recognition

of hypersensitive transitions, develops into an exploration of the "dynamic coupling" (DC) model and of their combination (SC+DC) upon which most intensity analyses before the late 1980s have rested. The central importance of effective electric dipole transition operators is emphasized as is the neglect of the effects of covalency in the SC+DC approach. Against this background, the cellular ligand-field (CLF) model of '*d–d*' intensities is presented in detail and the description includes a critique of its relationship with the SC+DC model and of its incorporation, in principle, of all contributions to open-shell intensities, including those deriving from covalency and overlap. The CLF scheme is introduced in two parts, relating first to acentric chromophores in which parity mixing arises within the static environment and then to centric species in which it arises vibronically. An early section of the review briefly summarizes some fundamental concepts relating to normal coordinates and vibronic coupling. The final section provides a survey of the quality and parametrizations of all CLF analyses completed to date. © 1997 Elsevier Science S.A.

1. Introduction

This article addresses the electronic '*d–d*' spectra of coordinated transition metal ions. In particular, it is concerned with the modelling of '*d–d*' intensity distributions. Standard fare for the inorganic chemist includes the violation of the parity selection rule by static means in acentric chromophores and by vibronic means in centric ones; that vibronic intensities are generally an order-of-magnitude weaker and vary markedly with temperature; that spin-forbidden bands are usually much weaker still, and that, by application of group theory, spectral assignments and polarization selection rules are often possible. By and large, however, quantitative reproduction of these spectral intensity distributions has formed little or no part of standard ligand-field analysis. To invert the point: the information content of spectal intensities, as opposed to transition frequencies, has usually been discarded. The aim of the cellular ligand-field model for '*d–d*' spectral intensity distributions that we describe here is to provide a chemically informative scheme with uniform applicability regardless of metal d^n configuration; coordination number, geometry or symmetry; or ligand set. The model is parametric. As such, it is essential that it be well based theoretically, repeatedly successful in reproducing experimental data, and that the parameter values effecting this should vary from system to system in ways which transparently make good bonding and chemical sense.

In this regard, we look to the analysis of other *d* electron properties. For years, this has been dominated by crystal- and ligand-field theories which are characterized by the manipulation of *d* orbital bases under effective hamiltonians that separate two-electron *d–d* interactions from all others:

$$\mathscr{H}_{\mathrm{CF}} = \sum_{i<j} e^2/r_{ij} + \sum_i V_{\mathrm{CF}}(\mathbf{r}_i) + \zeta_0 \sum_i \mathbf{l}_i \cdot \mathbf{s}_i \qquad (1)$$

for crystal-field theory, or

$$\mathscr{H}_{\mathrm{LF}} = \sum_{i<j} U(i,j) + \sum_i V_{\mathrm{LF}}(\mathbf{r}_i) + \zeta \sum_i \mathbf{l}_i \cdot \mathbf{s}_i \qquad (2)$$

for ligand-field theory. The shortcomings of crystal-field theory are very well known and $\mathscr{H}_{CF}$ is mentioned here only to show the mapping of ligand-field theory onto its parent. Interelectron repulsion (ier) is notionally dealt with by the two-electron (d–d) operator U, integrals of which are parametrized with central-field parameters F_2, F_4 (or the Racah equivalents B, C) taking values which differ from their free-ion counterparts under the Coulomb operator e^2/r_{ij}; herein lies the nephelauxetic effect. In $\mathscr{H}_{LF}$, the spin-orbit coupling (soc) parameter ζ similarly takes values that mark it out from ζ_0, the corresponding free-ion value. Both ier and soc operators are "spherical" in that no recognition of molecular point-group symmetry is made. By contrast, molecular geometry *is* built into the crystal- and ligand-field potentials, V_{CF} and V_{LF}. The isomorphism of these two models, exemplified by Eqs. (1) and (2), defines ligand-field theory as freely parametrized crystal-field theory.

Equally characteristic of the ligand-field model is the separation of calculable from non-calculable parts; that is, of angular from radial integrals. Angular considerations establish the d electron splitting in the octahedron as between t_{2g} and e_g orbital subsets. The magnitude of the splitting, Δ_{oct}, relates to radial properties which include the radial forms of various metal and ligand functions and bond length. In high-symmetry molecules, the separation of radial and angular quantities can be immediate and obvious; Δ_{oct} in O_h is architypical. That separation ceases to be simple in complexes with little or no symmetry. It defines, in effect, a scrambling of information relating to molecular angular geometry (the disposition of the ligands around the central metal) with that relating to the nature of the chemical bonds. For the inorganic chemist in particular, this is a matter of considerable importance.

The angular overlap model (AOM) [1–4], properly formulated as cellular ligand-field (CLF) theory [5–9], goes a long way to deconvolute these different pieces of information. At their heart lies a principle of spatial superposition — that the global (molecular) ligand-field potential, V_{LF}, be represented by a sum of local (cellular) potentials, v_{LF}, determined, as closely as possible, solely by locally situated sources of the ligand-field. Those local sources relate to local M–L bonding and antibonding orbitals in the complex so that within the whole CLF structure, parameters relate to discrete M–L bonding. Furthermore, in reflecting the local M–L *pseudo*symmetry, the CLF parameter set subdivides into e_σ, $e_{\pi x}$, $e_{\pi y}$, which provide commentary on bonding modes of different local *pseudo*symmetry. A detailed discussion of the CLF parametrization and of its physicochemical significance has been presented recently [9].

This recognition of the chemical function group — so useful, so long elsewhere in chemistry — provides the power and wide utility of the CLF method. It has been applied [8–10] with unbroken success to the analysis of paramagnetic susceptibilities, electron spin resonance g values and 'd–d' spectral transition energies, quantitatively modelling these properties in molecules, regardless of metal, ligands or geometry, with parameter values that are chemically informative and sensible. We have sought to imbue our CLF model for spectral intensity distributions with these same advantages. One may discern a parallel here between the historical developments of the ligand-field modelling of transition energies with those of 'd–d' intensities. Recognition merely of global geometry and symmetry usefully yields splitting

diagrams and other qualitative insight while the advent of the AOM and CLF approaches provided direct measures of bonding character and the electron distribution in complexes. A similar focus on whole molecules has exploited '*d*–*d*' intensities broadly with respect to selection rules and spectral assignments. Our CLF modelling [11,12] of intensities parametrizes local electric-dipole transition moments with ${}^{L}t_{\lambda}$ variables which mirror the e_{λ} variables of the energy model; $\lambda = \sigma$, πx, πy. The L superscripts, however, relate directly to the nature of the parity mixing within individual metal–ligand bonds and so offer additional bonding information which is complementary to that provided by ligand-field analysis of transition energies. The cellular decomposition, which aims to separate local chemical features, thus provides an enormous gain in information over any global modelling. We have always taken the view that the proper focus for the inorganic chemist in this area is the chemical and bonding information that modelling can yield. Once established, therefore, the model parameters must be describable in mainstream chemical language.

Our presentation of the CLF intensity model is as follows. We begin by drawing attention to the principles underlying our later focus on electronic transitions in systems comprising both electrons and nuclei. A brief, though formal, introduction to the adiabatic separation of electronic and nuclear variables is provided and an outline of vibrational ladders within electronic potentials is made together with some notes on normal coordinates and the coth rule. Section 3 introduces the idea of parity mixing required to circumvent the orbital selection rule, $\Delta\ell = \pm 1$, for electronic transitions. There follows in Section 4 a broadly chronological review of the literature on '*f*–*f*' spectral intensities in the lanthanoid block, for it is here that most of the important contributions to an understanding of forced electric dipole transitions are to be found. The accent throughout is on mechanism. The section includes accounts of the so-called static- and dynamic-coupling models, the construction and symmetry properties of effective transition dipole operators, of "hypersensitive" '*f*–*f*' transitions and the role of ligand polarizabilites. It ends with a comparison between '*f*–*f*' and '*d*–*d*' spectra, which makes connections with the rest of the article. The CLF model, which is central to our review, takes up the remaining three sections. In Section 5, the CLF approach is presented in detail, but in application to acentric chromophores in the first instance. Several discussions and tables not previously published are included here so as to facilitate comparison with the *f* electron work reviewed in Section 4. Of particular importance is Section 5.15 in which the significant advances made by the CLF over the earlier so-called "independent-systems" models are made clear. The CLF model is extended to centric chromophores in Section 6 within a vibronic approach and Section 6.4 describes another previously unpublished aspect of the model. Finally, in Section 7, we survey aspects of the 43 CLF intensity analyses published to date. These include systems acquiring intensity from the static environment alone, from the dynamics of the environment within the vibronic model, and from both. Also included is a brief commentary on the circular dichroism of some chiral chromophores.

In our review of the theoretical work from diverse laboratories, we have followed the original authors' nomenclature almost always. We have done this in the belief

that cross-reference to the original literature — which is not reproduced in full in this article — will be simpler than with the alternative of a unified algebra. Occasional remarks about comparative nomenclature are made where appropriate.

2. Electronic and nuclear motions

Molecular eigensolutions refer, quite generally, to both electrons and nuclei [13,14]. Stationary states are given as solutions to the time-independent Schrödinger equation:

$$\mathcal{H}(q, Q)\Psi(q, Q) = \epsilon\Psi(q, Q). \tag{3}$$

The eigenfunctions, $\Psi(q, Q)$, depend upon electronic and nuclear coordinates (q and Q, respectively) and the hamiltonian may be divided as:

$$\mathcal{H}(q, Q) = \mathcal{H}(q) + H_0(Q) + V(q, Q) \tag{4}$$

in which

$$\mathcal{H}(q) = -\frac{h}{2m}\sum_{\alpha}\nabla_{\alpha}^2 \tag{5}$$

and

$$\mathcal{H}_0(Q) = -\frac{h}{2}\sum_{\eta}\frac{\partial^2}{\partial Q_{\eta}^2} \tag{6}$$

are electronic and nuclear kinetic energy operators in terms of electronic mass, m, and mass-weighted nuclear coordinates, Q_{η}. The potential energy operator:

$$V(q, Q) = V_{nn}(Q) + V_{ee}(Q) + V_{en}(q, Q) \tag{7}$$

includes terms for nucleus–nucleus and electron–electron repulsions and electron–nucleus attraction. Electronic spin-orbit coupling can be included in Eq. (7) if desired.

Analytical solutions for Eq. (3) are not possible because the variables q and Q cannot be separated. Approximate solutions are sought following attempts to separate electronic and nuclear variables according to various levels of approximation. The general strategy is to expand the full molecular wavefunctions, $\Psi_n(q, Q)$, in a basis of *electronic* functions, $\psi_n(q, Q)$:

$$\Psi_i(q, Q) = \sum_{n}\psi_n(q, Q)\chi_{ni}(Q). \tag{8}$$

in which the expansion coefficients, χ, are functions of nuclear coordinates only. If the $\{Q\}$ are taken as internal coordinates, so removing molecular translation and rotations with respect to some laboratory-fixed frame, the $\{\chi\}$ may be identified as the vibrational parts of the wavefunction. Let us also define an *electronic*

hamiltonian,

$$\mathscr{H}_e = \mathscr{H}(q) + V(q, Q) - V_{nn}(Q) \tag{9}$$

and so write the full molecular Schrödinger Eq. (3) in the basis Eq. (8) as:

$$[\mathscr{H}_e(q, Q) + \mathscr{H}_0(Q) + V_{nn}(Q)] \sum_n \psi_n(q, Q)\chi_{ni}(Q) = \epsilon_i \sum_n \psi(q, Q)\chi_{ni}(Q). \tag{10}$$

This expression serves as a starting point for various approximation schemes. We review these in barest outline only.

2.1. *The adiabatic, Born–Huang and Born–Oppenheimer approaches*

Here it is recognized that the nuclei are far more massive than the electrons and conversely that the electrons move much more rapidly than the nuclei. As the nuclei move, it is supposed that the electrons adapt themselves essentially instantaneously to successive nuclear configurations. The electronic Schrödinger equation for each nuclear configuration, Q, is:

$$\mathscr{H}_e(q, Q)\psi_n(q, Q) = E_n(Q)\psi_n(q, Q) \tag{11}$$

and the electronic wavefunctions $\{\psi\}$ depend parametrically on Q. Solutions of Eq. (11) for each Q define the electronic energy functions $\{E\}$.

In the Born–Huang and Born–Oppenheimer approaches, $\{E\}$ and $\{\psi\}$ are deemed to vary slowly with change in nuclear displacements so that coupling between electronic and nuclear motions is ignored and the molecular wavefunctions of Eq. (8) are expressible as single products:

$$\Psi^{\wedge}_{ni}(q, Q) = \psi_n(q, Q)\chi^{\wedge}_{ni}(Q). \tag{12}$$

Functions of this simple product form are termed *adiabatic*; the superscript on the vibrational wavefunctions label the adiabatic approximations involved in simplifying Eq. (8) to Eq. (12) and the separation of variables effected thereby. The adiabatic, Born–Huang (ABH) and Born–Oppenheimer (ABO) approaches are similar, essentially differing in their approximations for the vibrational wavefunctions, χ. In the Born–Oppenheimer scheme, for example, the vibrational functions are given as solutions to:

$$[\mathscr{H}_0(Q) + E_n(Q)]\chi_{ni}(Q) = \epsilon_{ni}\chi_{ni}(Q) \tag{13}$$

and the electronic energy of Eq. (11) serves to define the potential governing the nuclear motion. The BO approximation thus provides the basis for the familiar diagrams we use of nuclear motion taking place in a potential (or on a potential surface) defined by the electronic energy varying as a function of nuclear configuration. When electronic energies are degenerate, or near-degenerate as compared with vibrational frequencies (Kramers' degeneracy excluded), the neglect of coupling leading to Eq. (12) is a poor approximation. The consequent non-separability of the q and Q variables renders the usual "potential energy well" diagrams inadequate

under these circumstances and there result dynamic Jahn–Teller and other non-adiabatic consequences.

2.2. Crude adiabatic basis

The eigenfunctions of Eq. (11) provide just one possible electronic function basis. For many purposes, especially when exploiting molecular symmetry in the establishment of selection rules, the alternative "clamped nuclei" Schrödinger equation,

$$\mathscr{H}_e(q, Q_0)\psi_n(q, Q_0) = E_n\psi_n(q, Q_0) \tag{14}$$

is used to provide an expansion of the full molecular wavefunctions in terms of the electronic functions at the equilibrium nuclear configuration, Q_0:

$$\Psi_i(q, Q) = \sum \psi_n(q, Q_0)\chi_{ni}(Q). \tag{15}$$

Eqs. (11) and (14) are sometimes also referred to as the "dynamic" and "static" equations, respectively. Within the adiabatic approximation and neglect of coupling between electronic and nuclear motions, one obtains:

$$\Psi_{ni}^{\mathrm{CA}}(q, Q) = \psi_n(q, Q_0)\chi_{ni}^{\mathrm{CA}}(Q), \tag{16}$$

analogous to Eq. (12).

The electronic hamiltonians of Eqs. (11) and (14) are simply related:

$$\begin{aligned}\mathscr{H}_e(q, Q) &\equiv \mathscr{H}(q) + V(q, Q) - V_{nn}(Q) \equiv \mathscr{H}(q) + V(q, Q_0) + \Delta V(q, Q) - V_{nn}(Q) \\ &\equiv \mathscr{H}_e(q, Q) + \Delta(q, Q).\end{aligned} \tag{17}$$

In passing, we note that, prior to the adiabatic simplifications, both bases, Eqs. (8) and (15), form complete sets and are therefore equally valid as bases for expansion.

2.3. Herzberg–Teller coupling

It is also the case that ABH, ABO and CA wavefunctions are equally valid expansion bases if we wish to reintroduce the Q dependence from the ABH, ABO or CA limits. The Herzberg–Teller (HT) approach is to expand the electronic wavefunctions in terms of the CA basis:

$$\psi_i(q, Q) = \sum_c a_{ci}(Q)\psi_c(q, Q_0). \tag{18}$$

First-order perturbation theory then gives the approximate adiabatic wavefunctions as:

$$\psi_i(q, Q) = \psi_i(q, Q) + \sum_c a_{ci}(Q)\psi_c(q, Q_0) \tag{19}$$

with expansion coefficients

$$a_{ci}(Q) = \langle c|\Delta V(q, Q)|i\rangle/(E_c(Q_0) - E_i(Q_0)). \tag{20}$$

The perturbation may be expanded as a Taylor series in Q:

$$\Delta V(q, Q)=\sum_r \left(\frac{\partial V(q, Q)}{\partial Q_r}\right)_{Q_0} Q_r+\frac{1}{2}\sum_{r,s}\left(\frac{\partial^2 V(q, Q)}{\partial Q_r \partial Q_s}\right)_{Q_0} Q_r Q_s+\ldots \tag{21}$$

First-order HT coupling includes just the linear term in Eq. (21) while second-order HT coupling includes both linear and quadratic terms. The zeroth limit,

$$\psi_i(q, Q)\approx\psi_i(q, Q_0) \tag{22}$$

is also called the *Condon approximation*. It is important to stress that the HT expansion, to any order, refers only to the *electronic* wavefunction. HT coupling is therefore not properly vibronic coupling, which relates to the coupling of electronic and nuclear motions, for HT functions are adiabatic. We write the molecular wavefunctions to recognize this as:

$$\Psi_{ni}(q, Q)=[\psi_i(q, Q_0)+\sum_c a_{ci}(Q)\psi_c(q, Q_0)]\chi_{ni}^{\mathrm{HT}}(Q). \tag{23}$$

2.4. The harmonic approximation

The inclusion of higher terms in the Taylor expansion Eq. (21) has been argued [15] to be inconsistent with the level of approximation already inherent within the BO scheme. Then to second order in non-degenerate perturbation theory, the E_n of Eq. (11) are given by:

$$E_n(Q)+E_n(Q_0)+\sum_\eta V_\eta^{nn} Q_\eta+\frac{1}{2}\sum_{\eta\mu}\left[V_{\eta\mu}^{nn}+2\sum_{m\neq n}\frac{V_\eta^{nm}V_\mu^{mn}}{E_n(Q_0)-E_m(Q_0)}\right]Q_\eta Q_\mu. \tag{24}$$

The use of such an electronic potential for the nuclear motions constitutes the *harmonic approximation*. Without loss of generality, we may chose coordinates for each electronic state such that $Q=0$ at the potential minimum; that is, $Q_0=0$ and hence, by Eq. (18), $Q_\eta=0$ for all η. Under these circumstances, all linear terms in Eq. (24) vanish. Furthermore, for any one electronic state — and the ground state is the most convenient — the Q may be chosen so that all cross-terms, $Q_\eta Q_\mu$, vanish ($\eta\neq\mu$). Such nuclear coordinates are the so-called *normal coordinates*. A normal coordinate is a single representative of a set of correlated nuclear motions describing a normal mode. The orthogonality of normal vibration modes physically corresponds to the possibility of exciting any one of the complete set of normal modes spanned by a given molecular symmetry without exciting any other; normal modes are uncoupled — independent — orthogonal.

Thus, for a non-degenerate ground state A (no symmetry label implied) in the harmonic approximation, we have the general expression for the potential:

$$E_A(Q)=\frac{1}{2}\sum_\eta k_\eta^A Q_\eta^2, \tag{25}$$

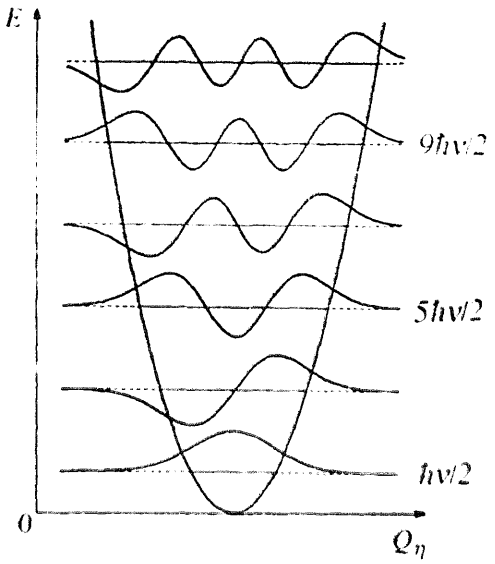

Fig. 1. Vibrational hermite polynomials.

where k_η^A called the *force constants* (for the vibrational normal modes, η, in the electronic ground state potential E_A) are given by

$$k_q^A = V_{\eta\eta}^A. \tag{26}$$

Eq. (25) is a standard equation with well-known solutions. The eigenvalues are:

$$\epsilon_{ni} = \sum_{\eta}^{3N-6} (v_\eta^i + \tfrac{1}{2})h\nu_\eta \tag{27}$$

and the eigenvectors comprise the set of Hermite polynomials. All of this is summarized in the usual "potential-well" diagrams like that shown in Fig. 1. Similar and separate diagrams are drawn for each normal mode, η. Electronic excited state (B) minima need not coincide with that of the ground state. If, following convention and as above, normal coordinates are defined for the ground electronic state, $E_B(Q)$ will not take the simple form of Eq. (25) and the eigenvalues and eigenfunctions of the vibrations in the excited states differ somewhat in value and form from those in the ground state, A. Of course, further departures, in both ground and excited electronic states occur when anharmonicity is taken into account.

2.5. Optical transitions

Electromagnetic radiation comprises simultaneous, orthogonal transverse oscillating electric and magnetic fields. In full detail, the interaction of light with matter is a complex affair. For our purposes, two simplifications can be recognized. First, we assume that the radiation field is weak so that its effects may be taken to first-order by perturbation theory. Effects like two-photon absorption occurring in intense laser fields cannot be treated so simply. In a weak radiation field, we consider [16] a

quantity related to the probability of an optical transition between states α and β. If the light is propagating in the z direction and is linearly polarized parallel to x (meaning the plane of the oscillating *electric* field is xz), the probability of a transition (the intensity), I_x, is proportional to the square of the modulus of:

$$\langle\alpha|ex|\beta\rangle+\langle\alpha|\mu_B\ell_y|\beta\rangle+(2\pi^2 i\omega/c)\langle\alpha|exz|\beta\rangle \tag{28}$$

where μ_B is the Bohr magneton, ℓ_y is the angular momentum operator and ω is the angular frequency of the transition. A sum over all electrons is implied in each integral. The first term in Eq. (28) refers to the induced electric dipole moment arising from the electric component of the electromagnetic field, which is effectively constant over the dimensions of the chromophore when (as is invariably the case for the spectroscopy discussed in this article) those dimensions are very small compared with the light wavelength. The second and third terms in Eq. (28) refer to interaction with the magnetic component of the light and to the quadrupolar interaction with the electric component. Both these terms relate to the curvature of the radiation field over the dimensions of the chromophore and are very small compared with the electric dipole term, roughly in the ratio $1:10^{-6}:10^{-7}$. Our second simplification, therefore, is to neglect all but the electric dipole part.

The electric dipole operator, μ, is the sum of electronic and nuclear vector dipole operators [14,17]:

$$\mu=\mu(q)+\mu(Q). \tag{29}$$

The electric-dipole transition moment, hereafter referred to as the transition moment, $\mathbf{M}^1$, for a transition between the vibronic states ag and bf, where a and b represent electronic functions and g and f, the associated vibrational functions is:

$$\mathbf{M}^1_{ag,\,bf}=\langle ag|\mu(q)+\mu(Q)|bf\rangle. \tag{30}$$

In the adiabatic approximation, this may be separated into two terms:

$$\mathbf{M}^1_{ag,\,bf}=\langle a|b\rangle\langle g|\mu(Q)|f\rangle+\langle g\langle a|\mu(q)|b\rangle f\rangle. \tag{31}$$

Angle brackets, here, indicate integration over electronic coordinates and round ones are used for integration over nuclear coordinates. The first term vanishes unless $a=b$ and so describes a vibrational transition. The second term is usually separated, defining the electronic transition moment as:

$$\mathbf{M}_{ab}(Q)=\langle a(q,Q)|\mu(q)|b(q,Q)\rangle. \tag{32}$$

Using the HT molecular wavefunctions of Eq. (23), together with just the linear coupling of the first-order term in Eq. (21), the second term in Eq. (31) is written

$$\mathbf{M}_{ag,\,bf}=\langle a(q,Q_0)|\mu(q)|b(q,Q_0)\rangle\langle g|f\rangle + \sum_c \frac{\langle a(q,Q_0)|\mu(q)|c(q,Q_0)\rangle\langle c(q,Q_0)|(\partial V(q,Q)/\partial Q_\eta)_{Q_0}|b(q,Q_0)\rangle\langle g|Q_\eta|f\rangle}{E_a(Q_0)-E_c(Q_0)}$$

$$+\sum_{c} \frac{\langle a(q, Q_0)|(\partial V(q, Q_0)/\partial Q_\eta)_{Q_0}|c(q, Q_0)\rangle\langle c(q, Q_0)|\mu(q)|b(q, Q_0)\rangle(g|Q_\eta|f)}{E_b(Q_0)-E_c(Q_0)}. \tag{33}$$

Note that vibrations g and f belong to normal mode, η, which is then known as the inducing mode; the $(g|Q_\eta|f)$ are the inducing integrals. $\mathbf{M}_{ag,bf}$ has been written without the t superscript to indicate that the nuclear moment contribution has been neglected.

2.6. The Condon approximation

In the Condon limit, all but the first term in Eq. (33) are neglected and

$$\mathbf{M}_{ag,\,bf}\langle a(q, Q_0)|\mu(q)|b(q, Q_0)\rangle(g|f) \tag{34}$$

is independent of the nuclear coordinates. The vibronic intensity is then proportional to the vibrational overlap integrals $(g|f)$, also known as the *Franck–Condon (FC) factors*. The FC *principle*, of course, is that electronic transitions take place so rapidly in comparison with the vibrational motion that virtually no changes in nuclear positions or momenta occur in the process; vibronic transitions are then represented as vertical arrows between electronic energy wells in the well-known fashion. The FC factors determine the distribution of intensity between different vibrational excitations within a given electronic transition.

Vibrational wavefunctions vary according to the electronic potential energy as, for example, in Eq. (13). If the electronic states a and b in Eq. (34) have identical potential surfaces (vary identically with respect to nuclear displacements), the vibrational wavefunctions, χ_g and χ_f, are identical (as are their frequencies, v_g and v_f). In these circumstances, the FC factor in Eq. (34) yields a simple orthogonality condition:

$$(g|f) = \delta(v_g, v_f), \tag{35}$$

where the $\{v\}$ are the vibrational quantum numbers of mode η. The vibronic transition Eq. (34) then consists of a single line. In the case of low temperature, when only the $v_a = 0$ vibrational state of the ground electronic state a is populated, the transition corresponds to the 0–0 vibrational excitation ($v_a = 0$; $v_b = 0$), known as the *no-phonon* line.

Two important circumstances arise when the ground and excited electronic levels are associated with non-identical potential surfaces. In the first, we consider the case where they possess identical energy minima (equilibrium nuclear coordinates), but different curvatures (corresponding to different vibrational force constants). Although the orthogonality Eq. (35) no longer holds exactly, it has been shown to be a good approximation for all realistic changes in force constant and, in practice, a single no-phonon line results. The second case arises when the ground and excited potential surfaces are shifted in Q_η (different equilibrium configurations), with or without a change in force constant. These circumstances can only arise for a normal

vibrational mode, η, of A_1 (generally, totally symmetric) symmetry.[1] In essence, this is because only A_1 displacements of the equilibrium geometry are symmetry-preserving. When the equilibrium geometries of ground and excited surfaces differ, Eq. (35) no longer holds, even approximately, and vibronic excitations involving various changes in vibrational quantum number become possible. There results a vibrational progression built upon the no-phonon line, the relative intensities of which vary in a manner depending upon the relative positions of the potential surfaces and upon the relative force constants.

If the ground and excited state frequencies are equal, a particularly simple formula may be derived for the relative intensities of the different vibrational components in the progression:

$$I_n \propto |M_{ab}|^2 e^{-S}(S^n/n!), \tag{36}$$

where I_n is the intensity of the nth vibrational excitation $|b, n\rangle \leftarrow |a,0\rangle$, M_{ab} is the electronic transition moment of Eq. (32) for a given polarization, and S, called the Huang–Rhys parameter, relates to the equilibrium displacement in the coordinate Q_η. Typical patterns of intensity distribution throughout a progression, deriving from Eq. (36) are shown in Fig. 2 Note the word "distribution" here, for the integrated intensity over the whole progression remains constant (and essentially so for $S \leqslant 7$ in the approximation Eq. (36)). When a molecule possesses more than one A_1 vibrational mode and frequency, any member of one of the A_1 progressions may serve as an origin upon which a progression in another A_1 mode may be built.

At higher temperatures, significant populations of other than the $v=0$ vibrational component of the ground electronic state develop. Furthermore, small differences in

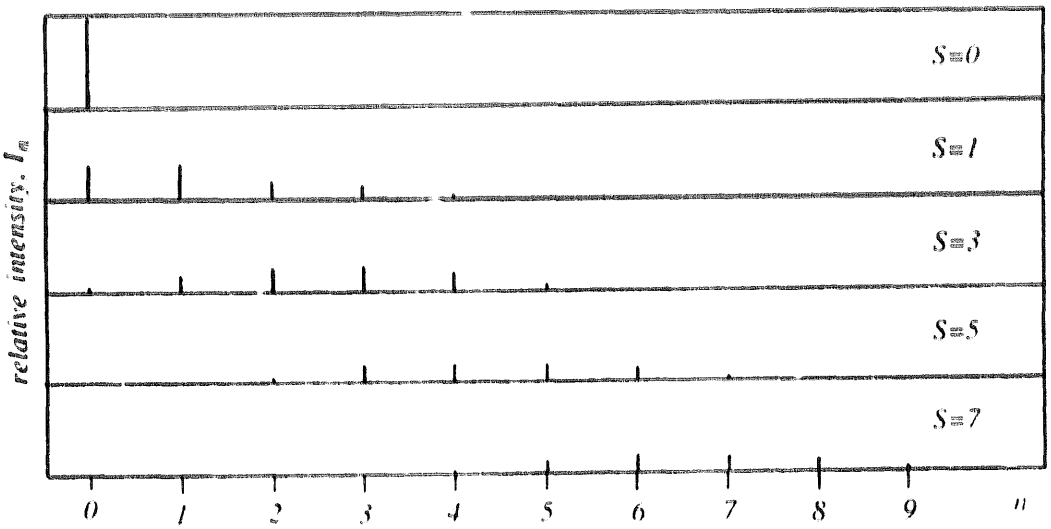

Fig. 2. Intensity distributions as functions of the excited state vibrational quantum number for various values of the Huang–Rhys parameter, S.

[1]Unless there is a change in chromophore geometry and point group symmetry on electronic excitation. We do not pursue this here, but note that the way forward is to consider the highest common sub-group between the two symmetries.

force constant for ground and excited states, a and b, are normal in practice and neither potential surface is truly harmonic. For any or all of these reasons, the spectral absorption usually presents itself as many superimposed progressions with different frequency intervals but unresolved to yield a broad band. Again, we note that while the shape of (intensity distribution in) such bands are determined by FC factors, contributing A_1 vibrations, and Boltzmann distributions within the ground state, the integrated intensity is expected to be governed by the electronic factor $|M_{ab}|^2$.

2.7. The Herzberg–Teller transition moment

A Condon transition moment may vanish by symmetry. A most important class of chromophores for which this is so is the d–d transitions in centric species. The first term in Eq. (33) is then zero and we must consider next the linear terms of HT coupling. The second and third terms in Eq. (33) show that even though $|bf\rangle \leftarrow |ag\rangle$ may be forbidden (by Laporte's rule, for example), $\mathbf{M}_{ag,bf}$ may be non-zero if there exists one or more vibronic states $|cr\rangle$ for which $|cr\rangle \leftarrow |ag\rangle$ or $|cr\rangle \leftarrow |bf\rangle$ is allowed. In effect, the vibrational deformation of the molecule modifies either ground or excited state wavefunctions (or both) by coupling with an allowed transition. For a Laporte forbidden 'd–d' transition, mixing with functions of *ungerade* parity is required.

In the harmonic limit, inducing integrals, $(g|Q_\eta|f)$, are approximately zero unless $v_g = v_f = \pm 1$, where v_g and v_f are the number of quanta in the inducing vibrational mode, η. The electronic transition is thus accompanied by the creation or destruction of *one* quantum of the enabling mode, η, and the vibronic origin corresponds to the no-phonon line plus (or minus) one quantum in the enabling mode. Symmetry allows any number of quanta in any totally symmetric mode to change but none in any other symmetry vibration mode. The resulting spectrum then normally comprises an A_1 progression built on the vibronic origin.

Incorporation of the selection rule for the inducing integrals into Eq. (33) yields the linear HT transition moments:

$$\mathbf{M}_{ag,bf}(Q) = [(v_g^\eta + 1|Q_\eta|v_g^\eta) + (v_g^\eta - 1|Q_\eta|v_g^\eta)] \times \left\{ \sum_c \frac{\langle a(q, Q_0)|\mu(q)|c(q, Q_0)\rangle\langle c(q, Q_0)|(\partial V(q, Q)/\partial Q_\eta)_{Q_0}|b(q, Q_0)\rangle}{E_a(Q_0) - E_c(Q_0)} + \sum_c \frac{\langle a(q, Q_0)|(\partial V(q, Q)/\partial Q_\eta)_{Q_0}|c(q, Q_0)\rangle\langle c(q, Q_0)|\mu(q)|b(q, Q_0)\rangle}{E_b(Q_0) - E_c(Q_0)} \right\}. \quad (37)$$

If both ground and excited vibrational states are harmonic, the inducing integrals in the square bracket of Eq. (37) are given by the simple expressions,

$$(v_g^\eta + 1|Q_\eta|v_g^\eta) = [h(v_g^\eta + 1)/4\pi^2 c\nu_\eta]^{1/2} \quad (38)$$

and

$$(v_g^\eta - 1|Q_\eta|v_g^\eta) = [hv_g^\eta/4\pi^2 c\nu_\eta]^{1/2}, \quad (39)$$

where ν_η is the fundamental frequency (in cm^{-1}) of normal mode η. Other factors being equal, therefore, we note that low frequency modes will be the most effective intensity generators, a result we shall call upon in Section 6.

At low temperatures, only the first term in the square bracket of Eq. (37) is likely to be of importance. The second term gains importance at higher temperatures. That is not the only reason, however, why the magnitude of the sum of vibrational integrals within the square bracket of Eq. (37) changes with temperature. With increasing temperature, increasing population of ground state vibrations with $v_g \neq 0$ occur (the so-called "hot bands"). It can be shown that if HT coupling with a single vibrational mode of frequency v_g is solely responsible for the intensity of an electronic band via Eq. (37), the integrated band intensity changes with temperature according to the *coth rule*,

$$I = I_0 \coth\left(\frac{hcv_g^\eta}{2kT}\right), \tag{40}$$

where I is the intensity at temperature T, and I_0 is the intensity at 0 K. Lohr has shown [19] that Eq. (40) remains valid even if the excited state is anharmonic. When the intensity is determined by several enabling modes, the expression Eq. (40) is replaced by a sum of similar coth rules for each. In favourable circumstances, the empirical temperature dependence of vibronic bands can be analysed to determine the frequency of the enabling mode, when this is unknown, or even to estimate the relative contributions of the inducing modes.

3. Electric dipole transitions and parity mixing

Absorption of light, incident as a plane wave, by chromophores with dimensions typical of metal *d* or *f* electron centres is utterly dominated by the electric dipole process. We shall discuss electric quadrupole and magnetic dipole transitions in special circumstances in due course but for now, and mostly throughout this article, we address electric dipole excitations exclusively. The focus on electric dipole transitions derives from the character of the light — from its small curvature over chromophore dimensions. Selection rules, on the other hand, also relate strongly to the nature of the chromophoric states. For electric-dipole transitions, the Laporte rule requires a change of parity and the orbital selection rule, deriving from the one-photon absorption process with which we are exclusively concerned, then requires a change in ℓ of one unit; $\Delta\ell = \pm 1$. The familiar result is that $s \leftrightarrow p$, $p \leftrightarrow d$, $d \leftrightarrow f$, $f \leftrightarrow g$ etc. are the only electric-dipole, orbital transitions which are allowed. Even more pertinent for transition-metal and lanthanoid spectra is that the electric-dipole transition moments $\langle d|er|d'\rangle$ and $\langle f|er|f'\rangle$ vanish. The experimental fact that '*d–d*' and '*f–f*' transitions *are* observed then requires an explanation. Some say the selection rules are "violated"; others, that the electric-dipole transitions are "forced". There is no question about the accuracy of the selection rules, however, all attention being directed towards a more precise description of the orbitals and states involved in

the optical transition. Implicitly or explicitly, forced electric-dipole transitions arise through parity-mixing processes. The broad principle is illustrated, without loss of generality, with a particular and simple case.

Considering, for example, a nominal *f–f* transition, we recognize the inaccuracy of the description by writing '*f–f*' in quotation marks to signify the impurity of the '*f*' functions. Whatever the origin, it may be that such functions are expressible as:

$$'f' = f + ad + bg \tag{41}$$

in which admixtures of foreign functions with ℓ values not differing from three by one are ignored. An '*f–f*' transition moment is given then by:

$$\langle 'f'|\mathbf{er}|'f''\rangle = \langle f|\mathbf{er}|f'\rangle + a\langle d|\mathbf{er}|f'\rangle + a'\langle f|\mathbf{er}|d'\rangle + b\langle g|\mathbf{er}|f'\rangle + b'\langle f|\mathbf{er}|g'\rangle. \tag{42}$$

The first term vanishes because of the orbital selection rule. The rest survive to the extent that the mixing coefficients *a*, *b* etc. in Eq. (42) differ from zero. The experimental fact that '*f–f*' transitions are very much weaker than fully allowed transitions directly attests the notion that these mixing coefficients are small; we have ignored normalization in Eq. (42) accordingly. Actually, Eq. (42) is a somewhat misleading description of the impurity of the '*f*' function, a point we will return to in due course.

In the late 1950s, Ballhausen and Liehr computed '*d–d*' spectral intensities for some octahedral [20] and tetrahedral [21] complexes within a point-charge model of the metal environment. Violation of the electric-dipole selection rules was deemed to occur through mixing of the odd-parity 4*p* orbitals into the 3*d* under a simple crystal-field potential. In the case of the octahedral complexes, this was taken to arise from *ungerade* molecular vibrations. Despite their use of free-ion *d* orbitals and of unsure estimation of the radial form of the 4*p* orbitals, their calculated intensities differ from those observed by only a factor of about four.

Parity mixing in the tetrahedral $[CoCl_4]^{2-}$ and $[CuCl_4]^{2-}$ ions was presumed to occur via the odd components of the *static* crystal field. Agreement with experiment for these systems was very poor. Inclusion of ligand valence orbitals improved their results considerably and these authors concluded that "covalency" arising from direct overlap of ligand and metal 3*d* orbitals is important so far as the calculation of transition moments is concerned.

It is illuminating at this point to outline the relevance of covalency and overlap for the degree of parity mixing. Let us represent the sets of metal *d* and *p*, and ligand χ orbitals by just single functions. Let us further suppose that direct *d–p* mixing by pure crystal-field perturbations is negligible. The resulting energy matrix under some appropriate covalency hamiltonian $\mathscr{H}_{cov}$ will take the form:

$$\begin{array}{c} \\ d \\ p \\ \chi \end{array} \begin{array}{c} \begin{array}{ccc} d & p & \chi \end{array} \\ \begin{pmatrix} \alpha & 0 & \delta \\ 0 & \beta & \epsilon \\ \delta & \epsilon & \gamma \end{pmatrix} \end{array} \tag{43}$$

where $\alpha=\langle d|\mathscr{H}_{cov}|d\rangle$, $\beta=\langle p|\mathscr{H}_{cov}|p\rangle$, $\gamma=\langle\chi|\mathscr{H}_{cov}|\chi\rangle$, $\delta=\langle d|\mathscr{H}_{cov}|\chi\rangle$ and $\epsilon=\langle p|\mathscr{H}_{cov}|\chi\rangle$. The matrix Eq. (43) does not block off and so all associated eigenfunctions necessarily comprise mixtures of d, p and χ functions

$$\psi=c_1d+c_2p+c_3\chi. \tag{44}$$

In short, overlap between d and χ, and between p and χ ensures d–p mixing in ψ even though, by assumption, direct mixing is negligible.

Electric-dipole transition moments between orbitals ψ and ψ' expanded as in Eq. (42), yield contributions of the type $\langle d|\mathbf{er}|p\rangle$, $\langle p|\mathbf{er}|\chi\rangle$, and $\langle d|\mathbf{er}|\chi\rangle$, for example. The latter two do not vanish as the following simple argument makes clear. The χ functions are conventionally centred on the ligands but may, quite generally, be expressed with respect to the metal centre. We shall describe this in formal terms later, but for now we may write:

$$\chi^L\equiv a_1s^M+a_2p^M+a_3d^M+a_4f^M+\ldots \tag{45}$$

It follows that a contribution to the transition moment $\langle d|\mathbf{er}|\chi\rangle$, for example, comprises terms of the form $\langle d|\mathbf{er}|p\rangle$ and $\langle d|\mathbf{er}|f\rangle$, which generally do not vanish, as well as others, which do. All this may be verbalized by noting that covalent interactions between metal and ligands induce d–p mixing as in Eq. (44) — the p contribution originating on the metal — and also d–p mixing *via* Eq. (45) — the p character originating on the ligands. Within a parametric model, of course, the different origins of the parity-mixing that forces the 'd–d' transition are inseparable. The CLF model that we shall introduce *is* parametric and embodies these simple ideas.

We have reached a position in which the CLF approach may now be formulated in detail, as in the primary literature. We do not do so yet, however, wishing to take advantage of the present review format to place the CLF model in the wider context of developments in the theory of spectral intensities at metal centres. By far the greater part of that research has addressed the 'f–f' transitions in lanthanoid complexes. This subject provides the substance of the next section which ends, however, with a discussion of the important similarities and differences between 'f–f' and 'd–d' transitions.

4. Spectral intensities of 'f–f' transitions

4.1. *The static crystal-field model*

In 1962, Judd [22] and Ofelt [23] published simultaneous but independent models for 'f–f' transitions that are now regarded as seminal contributions to this subject. We shall review Judd's paper in some detail; Ofelt's is somewhat more extensive and we comment on it later. Both approaches envisage forced electric-dipole transitions to arise from parity-mixing induced by an *electrostatic*, crystal-field admixture of d and g orbitals into the f orbitals between which the interesting optical transitions

occur. We consider zeroth-order, initial and final states between which we seek to compute electric-dipole transitions as linear combinations of free-ion functions, $|f^N\alpha JM\rangle$, where $M \equiv M_J$, and α labels any further quantum numbers required to define the state uniquely; for state A, for example:

$$|A\rangle = \sum_{J,\,M} \alpha_{JM} |f^N \alpha JM\rangle. \tag{46}$$

A first-order approximation to the true states is then given by:

$$|B\rangle = \sum_{J,\,M} a_{JM} |f^N \alpha JM\rangle + \sum_k b_k |f^{N-1}(n'\ell')\alpha'' J'' M''\rangle, \tag{47}$$

where

$$b_k = \sum_{J,\,M} a_{JM} \frac{\langle f^{N-1}(n'\ell')\alpha'' J'' M'' | V^o_{CF} | f^N \alpha JM\rangle}{E(\alpha J) - E(\alpha'' J'')}. \tag{48}$$

The expression Eq. (46) thus includes functions from configurations[2] $f^{N-1}d^1$ and $f^{N-1}g^1$, required to yield non-vanishing electric-dipole transition moments, as in Eq. (42). Expansion of the crystal-field potential, V_{CF}, in spherical tensor operators takes the usual form:

$$V_{CF} = \sum_{t,\,p} A_{t,p} D^{(t)}_p, \tag{49}$$

where $D^{(t)}_p$ is the pth component of the operator of rank t. Admixtures of $f^{N-1}d^1$ or $f^{N-1}g^1$ are effected by odd components of the crystal-field potential, of course. By contrast the a_{JM} in Eq. (46) *et seq.* derive from the even components of V_{CF}.

The transition dipole moment operators may also be written in tensorial form as $eD^{(1)}_q$, where q depends upon the direction of the incident radiation. The transition dipole moments between states $|B\rangle$ and $|B'\rangle$ are then:

$$\begin{aligned} e\langle B|D^{(1)}_q|B'\rangle = e \sum_k^1 \sum_{J,\,J',\,M,\,M'} \sum_{t,\,p} a_{JM} a'_{J'M'} A_{t,\,p} \\ \times \left\{ \langle f^N \alpha JM | D^{(1)}_q | f^{N-1}(n'\ell')\alpha'' J'' M'\rangle \frac{\langle f^{N-1}(n'\ell')\alpha'' J'' M'' | D^{(t)}_p | f^N \alpha' J' M'\rangle}{E(\alpha' J') - E(n'\ell'\alpha'' J'')} \right. \\ \left. + \frac{\langle f^N \alpha JM | D^{(t)}_p | f^{N-1}(n'\ell')\alpha'' J'' M''\rangle}{E(\alpha J) - E(n'\ell'\alpha'' J'')} \langle f^{N-1}(n'\ell')\alpha'' J'' M'' | D^{(1)}_q | f^N \alpha' J' M'\rangle \right\}, \end{aligned} \tag{50}$$

where k represents the quantum numbers $n'\,\ell'\,\alpha''\,J''\,M''$ of the excited state configuration $f^{N-1}\,(n'\,\ell')\,\alpha''\,J''\,M''$ being mixed into the zeroth-order state $|A\rangle$.

The structure within the braces of Eq. (50) might be represented pictorially as in Fig. 3 in which we have taken liberties in the shorthand and V^o_{CF} represents the odd $D^{(t)}$ components of the crystal field. The "linkages" between initial and final states (f^N and f'^N) in the upper route relate to the first term in the braces of Eq. (50) and in the lower route to the second term. While the algebra says it all, some prefer to

[2] And of the form $d^0 f^{N+1}$.

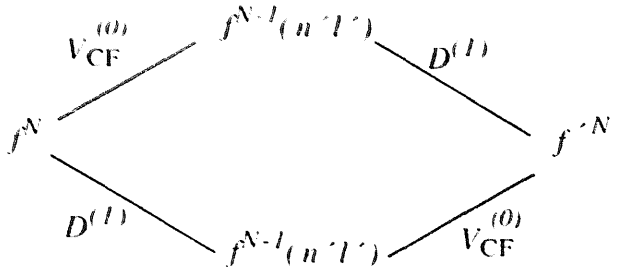

Fig. 3. Linkages between initial, f^N, and final, f'^N, states in the static coupling model.

find verbal description of the various route segments; these can be a help or a hindrance, according to taste. Thus, each linkage in the scheme may quite properly be called a "coupling". The odd components of the crystal field couple the intermediate $f^{N-1}d^1$ and/or $f^{N-1}g^1$ functions to the f or f'. The light electric dipole couples the intermediate states to the $|A\rangle$ and $|A'\rangle$ similarly. Each two-link route can be described as providing the 'f–f' transition by stealing intensity from an allowed interconfigurational $[f^N \leftrightarrow f^{N-1}(n'\ell')]$ transition.

By regrouping the terms within the braces of Eq. (50) we obtain:

$$\{\ldots\} \equiv \langle f^N \alpha J M \left| \frac{D_q^{(1)} | f^{N-1}(n'\ell')\alpha'' J'' M'' \rangle \langle f^{N-1}(n'\ell''\alpha'' J'' M'' | D_p^{(i)}}{E(\alpha' J') - E(n'\ell'\alpha'' J'')} \right.$$
$$\left. + \frac{D_p^{(i)} | f^{N-1}(n'\ell')\alpha'' J'' M'' \rangle \langle f^{N-1}(n'\ell')\alpha'' J'' M'' | D_q^{(1)}}{E(\alpha' J') - E(n'\ell'\alpha'' J'')} \right| f^N \alpha' J' M' \rangle, \qquad (51)$$

which formalizes the equivalence of the double linkage between $\langle A|$ and $|A'\rangle$ with a single linkage describing an *effective* transition moment operator. The effective operator (between the long vertical bars) is of the required *even* parity to couple the same-parity states $\langle A|$ and $|A'\rangle$.

We have laboured our discussion so far, hopefully to facilitate descriptions of other intensity schemes that follow. By contrast, our review of several further, yet very important, aspects of Judd's work will be brief. In large measure, these concern various approximations made to simplify the mathematics and to obtain, as we shall see, a generally useful expression for the 'f–f' transition probabilities for lanthanoid solutions.

The effective operators in Eq. (51) depend upon the energy denominators and hence upon the energies of the components of the ground f^N configuration and of the components of the various excited $f^{N-1}d^1$ and $f^{N-1}g^1$ configurations. Judd considered a series of approximations in order to exploit the closure properties of the expressions $\Sigma|f^{N-1}(n'\ell')\alpha'' J'' M''\rangle\langle f^{N-1}(n'\ell')\alpha'' J'' M''|$. One was the proposition that all states from a given excited configuration may be deemed degenerate — that is, independent of J''. Considerably greater simplification of Eq. (50) was possible, however, if a similar independence of α'' was also assumed. Further "averaging" over n' was also considered — this being equivalent to an anonymous parentage for all $f^{N-1}d^1$ or all $f^{N-1}g^1$ configurations — though not carried forward. It was further assumed that the 'f–f' transition energies of direct concern may be taken as small

compared with the inter-configurational excitations so that $|A\rangle$ and $|A'\rangle$ are deemed to be effectively degenerate within the energy denominators of Eq. (50) also. These various simplifying assumptions led to the derivation of a far more tractable expression than Eq. (50) for the transition moment between $|B\rangle$ and $|B'\rangle$:

$$\langle B|D_q^{(1)}|B'\rangle = \sum_{p,\, t \text{ even}\ \lambda} (2\lambda+1)(-1)^{p+q} A_{tp} \begin{pmatrix} 1 & \lambda & t \\ -q & -p-q & p \end{pmatrix} \Xi(t,\lambda) \times \langle A|U^{(\lambda)}_{p+q}|A'\rangle \tag{52}$$

where U_{p+q} is the $(p+q)$th component of the unit tensor operator $U^{(\lambda)}$ which is itself a sum of unit tensor operators $u^{(\lambda)}(j)$ acting on a single f electron; λ spans 2, 4, 6 to satisfy the vector triangle rule between the $\ell = 3$ f functions of $|A\rangle$ and $|A'\rangle$. The quantity $\Xi(t, \lambda)$ is given by:

$$\Xi(t,\lambda) = 2 \sum_{n'\ell'} (2\ell+1)(2\ell'+1)(-1)^{\ell+\ell'} \begin{Bmatrix} 1 & \lambda & t \\ \ell & \ell' & \ell \end{Bmatrix} \begin{pmatrix} \ell & 1 & \ell' \\ 0 & 0 & 0 \end{pmatrix} \begin{pmatrix} \ell' & t & \ell \\ 0 & 0 & 0 \end{pmatrix} \times \langle n\ell|r|n'\ell'\rangle \langle n\ell|r^t|n'\ell'\rangle / \Delta(n'\ell'), \tag{53}$$

where $\Delta(n'\ell')$ is the mean excitation energy between the configurations f^N and $f^{N-1}(n'\ell')$.

The dependence of Eq. (52) upon q reminds us that this expression is applicable to the computation of the various crystal-field states within the $f^N\alpha J$ manifold and their polarizations. However, Judd was particularly concerned with lanthanoid spectra in solution (the most plentiful data then available) whose crystal-field components are frequently poorly, or not at all, resolved. For these purposes, the dependence of Eq. (52) upon the M and M' quantum numbers can be removed, corresponding to forming a sum over crystal-field component intensities, and this led to his famous equation for the transition probability, P:

$$P = \sum_{\lambda = 2,\, 4,\, 6} \Omega_\lambda v \langle f^N \alpha J \| U^{(k)} \| f^N \alpha' J' \rangle^2. \tag{54}$$

In Judd's model, therefore, all 'f–f' transition probabilities for solution bands are expressible in terms of just three parameters, Ω_λ; $\lambda = 2, 4, 6$, where:

$$\Omega_\lambda = \chi[8\pi^2 m/3h](2\lambda+1) \sum_t (2t+1) B_t \Xi^2(t,\lambda)/(2J+1) \tag{55}$$

and

$$B_t = \sum_p |A_{tp}|^2/(2t+1)^2. \tag{56}$$

χ is the refractive index of the medium.

Initially, Judd [22] put Eq. (54) to the test parametrically. Some 13 transitions each for solutions of $NdCl_3$ and $Nd(ClO_4)_3$ having intensities ranging more than two orders of magnitude, were very well reproduced with (separate) Ω_λ parameter sets; similar successes were achieved for eight transitions in both $ErCl_3$ and

$Er(NO_3)_3$. The efficacy of Eq. (54) in terms of parametrized effective operators was thus well demonstrated, for these systems at least. In a quite separate exercise, Judd attempted to compute the Ω_λ parameter values, *ab initio*. Notwithstanding his need to make bold assumptions about chromophore geometry and matters relating to the radial functions in Eq. (53), he was able to calculate empirically optimized Ω_λ values to within a factor of two for the neodymium systems and of eight for the erbium ones. As Judd [22] remarked, "the agreement is perhaps better than we might reasonably have anticipated".

Another important contribution in Judd's paper [22] is his demonstration that the *form* of Eq. (54) is retained if the interconfigurational mixing derives from vibronic rather than static sources. He pointed out that a good *parametric* fit using Eq. (54) is thus no indicator of the origin of the required parity mixing, a point developed by Newman and Balasubramanian [24] in 1974 whose contribution we consider in some detail in due course.

Judd also drew attention to the peculiar sensitivity of certain '*f–f*' transition intensities to the chemical nature of the lanthanoid environment, identifying Ω_2 as the parameter most dependent upon ligation type. This small detail of his paper gave rise to an important literature in this subject; it forms the subject matter of our next section.

4.2. *Hypersensitive* 'f–f' *transitions*

In 1964, Jørgensen and Judd [25] brought together some empirical observations on the solution spectra of various lanthanoid complexes in which aquo ligands were replaced by acetates, acetylacetonates, phenanthrolines, and of nitrate complexes in both the molten state and as solutions in organic solvents. They noted that while the intensities of most of the narrow '*f–f*' absorptions varied little with respect to ligation (the complexation no doubt changing with regard to both coordination number as well as ligand type), some transition intensities varied by up to two orders of magnitude. These so-called *hypersensitive* transitions shared the selection rule $\Delta J = \pm 2$, and, insofar that Russell–Saunders coupling obtains, $\Delta L = 2$ also. The converse was also true in that all transitions satisfying these conditions were observed to be hypersensitive.

Selection rules for electric quadropole transitions are similar: $\Delta L \leqslant 2$ and, if Russell–Saunders coupling is followed, $\Delta L \leqslant 2$, $\Delta S = 0$. Judd's model [22], reviewed in Section 4.1, is predicated upon the hypothesis that all transitions are forced electric dipole in origin, however, so the first object of the paper by Jørgensen and Judd was to see if the *pseudo*quadrupole selection rules of the hypersensitive intensities in lanthanoid spectra are in conflict with the dipole model. The upshot of a little algebra we need not repeat here is that no formal conflict exists, but that hypersensitivity is uniquely associated with hypersensitive Ω_2 values in Judd's parametrization [22]. Of itself, this did not prove that the empirical hypersensitivity is not truly quadrupolar in nature; only that it can be accommodated *parametrically* within the forced electric dipole model.

As noted earlier, the usual neglect of true quadrupole interaction between

chromophore and radiation field derives from the small dimensions of the absorber relative to the typical wavelengths of an incident plane wave. Jørgensen and Judd put some flesh on this assertion by computing, in an approximate but entirely reasonable model, the magnitude of the Ω_2 parameter to be expected for the 17 300 cm^{-1} absorption in aqueous solutions of Nd(III) ions by a pure quadrupole mechanism; they found it to be some five orders of magnitude smaller than that observed experimentally. They went on to estimate how covalency might affect their estimate and concluded that Ω_2 would be increased by a factor of 20 at most. Altogether, therefore, a pure quadrupolar mechanism was considered to account for a negligible proportion of observed spectral intensities.

Jørgensen and Judd [25] then investigated the possibility that the sensitivity of the Ω_2 parameter might be accountable *quantitatively* within the formalism of the forced electric dipole model of Judd [22]. From the outset, the problem here is to provide a mechanism for the extreme variation in Ω_2 without simultaneously predicting equal, or more likely larger, changes in Ω_4 and Ω_6. We do not repeat their arguments here, however, for even after considering some unrealistic static or vibronic displacements of the lanthanoid ion from its equilibrium site in a complex, Jørgensen and Judd were unable to conceive of more than a tenth of 1% of empirical hypersensitive Ω_2 values arising from the original forced electric dipole model. The value of their efforts lay in demonstrating the absolute need for something new. This, they claimed, lay in a recognition of the inhomogeneous nature of the dielectric environment of the chromophore.

4.3. *Pseudoquadrupole transitions in an inhomogeneous dielectric*

The refractive index of the medium in which the lanthanoid chromophores are located was incorporated merely as a multiplicative constant in Eq. (55) of Judd's original model [22]. The dielectric medium must be recognized, of course, for the radiation field experienced by the chromophore is modified from that of the incident plane wave *in vacuo*. The molecules of the medium are polarized and so establish small, secondary electric dipolar fields throughout the volume. As the incident electric field is oscillatory, so are these secondary fields and an embedded chromophore is subject to all these radiation sources. When the disposition of the polarizable molecules of the medium is cubically symmetric about the chromophore location (or, of higher symmetry yet) the secondary field *gradients* cancel identically. In these circumstances, the only surviving field gradient is that arising from the time variation which defines the wavelength of the incident beam. As discussed above, this gradient is too small to engender pure quadrupole transitions of significant magnitude.

On the other hand, if the distribution of polarizable molecules of the chromophore environment possesses less symmetry with respect to the chromophore, the sum of local (induced) field gradients does not vanish and, because of the close proximity of these molecules to the chromophore, can be profoundly important. Then the chromophore is subject to a net field gradient sufficient to induce quadrupole transitions with significant magnitude. As the origin of this extra field gradient is by induction of the inhomogeneous dielectric environment and is of a magnitude

that depends upon the frequency, we refer to such an intensity-giving mechanism as *pseudo*quadrupolar.

Jørgensen and Judd [25] considered a very simple model in order to gauge the quantitative importance of the inhomogeneous dielectric effect. They envisaged a lanthanoid ion surrounded by a cubic array of environmental molecules — which may be considered as the ligands in a complex — with equal polarizabilities α except for one with polarizability 2α. With reasonable estimates of bond length and mean refractive index, they were able to compute a value for Ω_2 some 5000 times greater than that for a pure quadrupole transition. Although about 30 times smaller than experiment, this estimate clearly demonstrated the possibilities of the proposed mechanism. In this paper, and subsequently, arguments were presented for obtaining much closer agreement with observed intensities.

It was also pointed out that the enhanced intensities, though following electric quadrupole selection rules, are in principle distinguishable from those of pure quadrupole transitions. Thus, while the latter vary as the inverse square of the wavelength, the *pseudo*quadrupole intensities are independent of wavelength (this stems from the dependence of the magnitude of the induced field gradient upon the incident wavelength which serves to cancel the wavelength dependency of pure quadrupole intensities); this is a further reason for the name *pseudo*quadrupolar. Some, albeit equivocal, experimental evidence in support of the *pseudo*quadrupolar nature of hypersensitive transitions of Er(III) by these means was presented.

4.4. *Ligand polarization mechanism*

Some 11 years later, Mason, Peacock and Stewart [26] proposed an apparently quite different model for the hypersensitive lanthanoid intensities. They adopted the so-called "independent systems" representation, in which overlap (and hence covalency) are deemed negligible. They envisaged a two-system model of a lanthanoid complex involving zeroth-order functions of the metal, $|M_k\rangle$, and of a single ligand, $|L_\ell\rangle$, deemed not to overlap. The subsystems are then considered to interact in first order under the intersystem *coulombic* potential, V:

$$V = \sum_{i(M)} \sum_{j(L)} e_i e_j / r_{ij}, \tag{57}$$

where r_{ij} is the distance between the charge e_i of the metal ion and the charge e_j of the ligand. A sum over L is introduced for multiligand chromophores. Corrected functions to first order are written as:

$$|M_a L_0) = |M_a L_0\rangle + \sum_{k,\ell} (E_a - E_k - E_\ell)^{-1} \langle M_k L_\ell | V | M_a L_0 \rangle | M_k L_\ell \rangle \tag{58}$$

in which angle brackets refer to zeroth-order functions and round brackets to "true" functions. The ground state function is $|M_0 L_0)$.

The incident light electric dipole operator is divided into parts acting upon metal electrons only and parts acting on ligand electrons only:

$$D_q^{(1)} = D_q^{(1)}(\mathrm{M}) + D_q^{(1)}(\mathrm{L}) \tag{59}$$

Mason *et al.* [26] presented an expression for the electric dipole moment between states $|M_0L_0\rangle$ and $|M_aL_0\rangle$, corresponding to the transition $|B\rangle \rightarrow |B'\rangle$ in Judd's notation [see Eq. (50) *et seq*]:

$$\begin{aligned}(M_0L_0|Dq^{(1)}|M_aL_0) = &\sum_{k\neq 0}(-E_k)^{-1}\langle M_0L_0|V|M_kL_0\rangle\langle M_k|D_q^{(1)}(\mathrm{M})|M_a\rangle \\ &+\sum_{k\neq a}(E_a-E_k)^{-1}\langle M_kL_0|V|M_aL_0\rangle\langle M_0|D_q^{(1)}(\mathrm{M})|M_k\rangle \\ &+\sum_{\ell\neq 0}(-E_a-E_\ell)^{-1}\langle M_0L_0|V|M_aL_\ell\rangle\langle L_\ell|D_q^{(1)}(\mathrm{L})|L_0\rangle \\ &+\sum_{\ell\neq 0}(E_a-E_\ell)^{-1}\langle M_0L_\ell|V|M_aL_0\rangle\langle L_0|D_q^{(1)}(\mathrm{L})|L_\ell\rangle, \quad (60)\end{aligned}$$

where energies are referred to the ground state, $E_0 = 0$. The first two terms in Eq. (60) are exactly equivalent to the expression Eq. (50) in Judd's electrostatic model [22]. The second two terms are new and provide the focus of the ligand polarization approach of Mason *et al.* They were described [26] as "the coulombic correlation of transient electric dipole moments in the ligands by the transitional charge distribution of the metal ion". Some elaboration of this description might be useful. Within the first two terms of Eq. (60), and by comparison with Judd's Eq. (50), we observe the ligand function L_0 to "go along for the ride" and that the label M in $D_q^{(1)}(M)$ to be superfluous. Each term then comprises a product of linkages between M_0 and M_k by V and $D_q^{(1)}$, as in Fig. 3. The situation within the second two terms of Eq. (60) is rather different. There, simultaneous excitations of the M and L subsystems under the *inter*system coulomb potential, V of Eq. (57) link the initial and final states with the intermediate states $|M_aL_\ell\rangle$ or $|M_0L_\ell\rangle$, and the total linkage is completed via the transient ligand dipoles under $D_q^{(1)}(L)$. In this, so-called *dynamic coupling* (DC) mechanism, therefore, the sources of the electric dipole intensity of the metal '*f*–*f*' transitions are transition moments based upon the ligands.

Within the ML product basis, it is natural to factor the intersystem coulombic potential, $V_{ML} \equiv V$, into parts referring, as far as possible, to the metal and ligand subsystems separately. This is effected using a bipolar expansion in products of multipole moments centred on the two non-overlapping charge distributions: standard tensor algebra is available [27,28]. The expansion is restricted to the lowest-order non-vanishing multipole in each system. For the ligand, this is a dipole (the ligand monopoles having been dealt with within the electrostatic model discussed earlier). Multipoles of order, $\lambda = 2, 4, 6$ are considered for the metal system, commensurate with transitions within a pure f^n configuration. With these restrictions, the bipolar expansion of V_{ML} is given by:

$$V_{ML}^{(0)} = -\sum_{\lambda}[(2\lambda+3)(2\lambda+1)(\lambda+1)]^{1/2}[D^{(1)}D^{(\lambda)}G^{(\lambda+1)}]^{(0)}, \quad (61)$$

where

$$D_L^{(1)} = -e\sum_j r_{jL}C^{(1)}(\theta,\phi)_{jL}, \quad (62)$$

$$D_M^{(\lambda)} = -e\sum_i r_{iM}C^{(\lambda)}(\theta,\phi)_{iM}, \quad (63)$$

$$G_{ML}^{(\lambda+1)} = (R_{ML})^{-(\lambda+2)} C^{(\lambda+1)}(\Theta, \Phi)_{ML}. \tag{64}$$

The $C^{(k)}$ are sets of spherical, irreducible tensors $C_q^{(k)}$ defined in standard form to the spherical harmonics:

$$C_q^{(k)} = (4\pi/(2k+1)) Y_q^{(k)}; q = k, k-1, \ldots, -k. \tag{65}$$

The scalar nature of V_{ML} in Eq. (61), as part of the hamiltonian for the ML system, is established by taking the scalar coupling of the three tensors Eqs. (62)–(64), as indicated by the zero-rank superscripts in Eq. (61). Overall, the desired separation is evident, the ligand dipole tensor given by Eq. (62) and the metal quadrupole, hexadecapole and 2^6 tensors by Eq. (63). The so-called geometric tensor $G_{ML}^{(\lambda+1)}$ of Eq. (64) cannot be factored between the subsystems, of course, depending as it does upon the relative disposition of metal and ligands, reference frames for which are shown in Fig. 4. The advantage of the bipolar expansion Eq. (61) is that of allowing all ligand-dependent quantities to be collected together into a so-called environmental tensor $F^{(t)}$ leaving only the metal multipole operators $D^{(\lambda)}$; $\lambda = 2, 4, 6$, to connect pure f^n states. In this way, an effective, even-parity operator set for the DC mechanism, akin to the structure in Eq. (51), may be constructed. One further, powerful feature emerges. The problematic sum over excited ligand states within the DC terms of Eq. (60) is incorporated into an electric dipole polarizability tensor, $\alpha^{(k)}$, which is, in principle at least, an experimentally accessible quantity:

$$\alpha^{(k)} = -\sum_{\ell} (-1)^k [\langle L_0 | D^{(1)} | L_\ell \rangle \langle L_\ell | D^{(1)} | L_0 \rangle]^k (E_a - E_\ell)^{-1}$$
$$- [\langle L_0 | D^{(1)} | L_\ell \rangle \langle L_\ell | D^{(1)} | L_0 \rangle]^k (E_a + E_\ell)^{-1}. \tag{66}$$

The effective electric dipole transition moment operator for the DC model, acting within a pure f^n basis is given by:

$$\mu_{\text{eff}}^{(1)DC} = \sum_{L} \sum_{t,\lambda} c(\lambda) [F^{(t)} D^{(\lambda)}]^{(1)}, \tag{67}$$

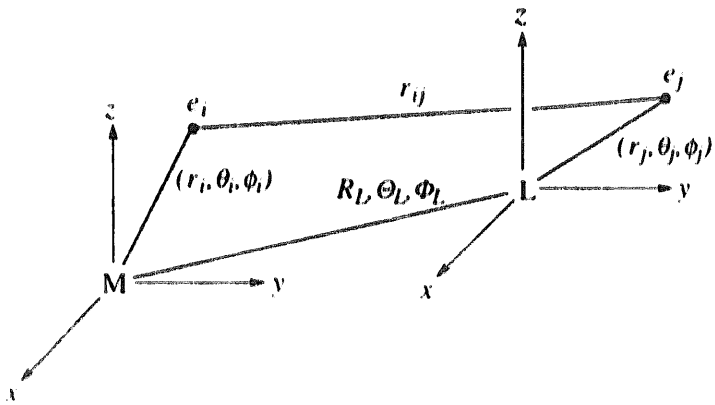

Fig. 4. Coordinates for metal and ligand electrons.

where

$$c(\lambda)=[(2\lambda+3)(2\lambda+1)(\lambda+1)]^{1/2}$$

and

$$F^{(t)}=(-1)^k[(2k+1)(2t+1)/3]^{1/2}\begin{Bmatrix}\lambda+1 & k & t\\ 1 & \lambda & 1\end{Bmatrix}[\alpha^{(k)}G^{(\lambda+1)}]^{(t)}. \tag{68}$$

A sum over L for a multiligand complex has been included in Eq. (67).

The foregoing sketch of the DC theory of Mason *et al.* [26], resting heavily upon an excellent review [29] by Stewart, has been presented at the present level of detail to highlight the role of ligand polarizabilities and to provide a link to important extensions we discuss later. We break off from our introduction of new ideas at this point, however, to assess the relative merits of the ligand polarizability and inhomogeneous dielectric approaches.

4.5. Alternative views of dynamic coupling

Mason et al. [26] applied their original ligand polarization model to hypersensitive transitions in some neodymium, erbium and holmium complexes and were able to report quite good reproduction of experimental intensities. They pointed to the "failure" of the Jørgensen and Judd model in suggesting an Ω_2 parameter of only about 1/30 of the corresponding empirical value — notwithstanding the acknowledged crudity of the early, exploratory calculations — and asserted that the inhomogeneous dielectric approach did "not take into account the correlation between ligand polarization moments and the transition moment of the metal ion implied by [the DC terms of Eq. (60)]". For a while, the inhomogeneous dielectric and ligand polarization mechanisms for hypersensitive transitions stood in competition or, at any rate, were complementary. Mason *et al.* clearly considered the effects of the inhomogeneous dielectric to be additional, but small, with respect to those of their ligand polarizability mechanism. In 1979, however, Judd [30] demonstrated in both general terms and in detail that the two mechanisms are one and the same.

His general observation was to note that two perturbations are involved in each approach. One of them modifies the wavefunctions which are then used to calculate matrix elements of the other; it makes no difference which perturbation one begins with. To be specific: in the inhomogeneous dielectric picture, light is considered to perturb (polarize) the ligands which are then taken to interact with the metal f electrons through the electrostatic potential; in the ligand polarization scheme, the metal f electrons are deemed to perturb the ligands *via* the coulombic potential and the polarized ligands then interact with the light.

Judd went on to derive the exact same expression for the effect from each standpoint: we need not repeat the details here. Most importantly, having demonstrated the identity of the two approaches, Judd emphasized that one should not invoke both in any system for that would simply be a case of double counting. He also demonstrated that the reportedly greater efficacy of the model of Mason *et al.*

in reproducing experimental intensities was really due to the approximate and undetailed nature of the calculations originally offered by Jørgensen and Judd [25]. Henceforth, with Mason *et al.* [26] and Richardson *et al.* (*vide infra*), we shall refer to this "two-in-one" model as the *dynamic coupling* (DC) mechanism. Judd's [22] (and Ofelt's [23]) original, electrostatic model will be called the *static coupling* (SC) mechanism. Thus, in the SC model, the ligand charge distribution is deemed unresponsive (not coupled with) the radiation field while the DC model relates to charge distributions on the ligand which *are* (dynamically) perturbed by the light. Both models were introduced as crystal-field models; neither incorporates overlap or covalency. In both cases, the metal environment provides the linkage between initial and final f functions; in the SC process, it is established by fixed, hard point charges (in a classical electrostatic manner), while in the DC mechanism, it is the polarizability of the ligands that is considered.

While the inhomogeneous dielectric and ligand polarizability views of the DC mechanism relate to the same physics, the latter seems more amenable to numerical evaluation. Stewart [29] makes the point that the *explicit* treatment of correlation was missing from the earlier model of Jørgensen and Judd [25]. One way to illustrate this begins with the expression Eq. (61) for the intersystem coulombic potential V_{ML}. The identical expression is used to describe the electro*static* potential between permanent moments. Within the ligand polarization view of the DC mechanism, it has an electro*dynamic* interpretation as it relates to the correlation of transition moments in the metal and ligand subsystems. That correlation process may be represented pictorially and so help qualitative and intuitive assessment of resultant electric dipole intensities. Two examples are presented in Fig. 5.

The correlation results from a first-order perturbation and so leads to a lowering of energy of the ML_N system. The representations in Figs. 5(a and b) indicate instantaneous phases of transition moments in their lowest energy arrangements. One immediate utility of such diagrams is evident from Fig. 5(b), showing the negative interference between the resultant dipoles of the equatorial $[ML_3]$ ligand set and that of the $[ML_6]$ trigonal prismatic set. *The efficacy of the DC mechanism thus depends closely upon the geometry and symmetry of the chromophore.* While such dependence is more generally and formally dealt with group theoretically, diagrams like these illustrate the concept in a direct and transparent manner. Stewart [29] properly reminds us of the philosophical shortcomings of such diagrams, however, but their utility as conceptual aids survives.

4.6. *Early and extensive explorations of the SC + DC model*

The ligand polarization and inhomogeneous dielectric models describe the same intensity-giving mechanism and must not be taken together, but the SC and DC sources of forced-electric dipole intensity relate to quite separate contributions and should be summed.

Both mechanisms describe "non-overlap", coulombic correlations between metal- and ligand-centred multipoles. The SC contribution to the effective, transition dipole operator relates to the leading monopoles, or point-charges of the ligands; the DC

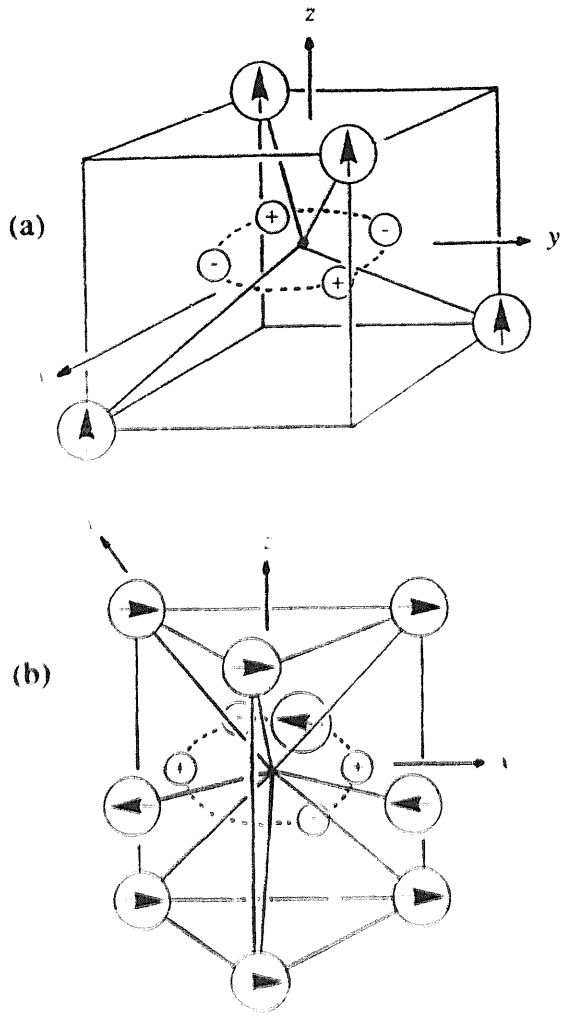

Fig. 5. (a) The coulombic correlation between the z components of the ligand dipole transition moments and the xy component of a d–d quadrupole transition moment in a tetrahedral system; (b) the same for ligands in a nine-coordinate trigonal lanthanoid complex correlating with the x^2-y^2 components of the electric quadrupole f–f transition moment.

contribution concerns the second (and, for reasons of tractability, final) terms in the ligand multipole expansion — the ligand dipoles. Let us emphasize also that both contributions are made to the transition dipole moment operator, which is a vector, rather than to the consequent intensity, which is a scalar. A short communication by Richardson [31] at this time referred to "interference effects" between "SC and DC mechanisms". In effect, his point was that SC and DC contributions contribute *vectorially*. The upshot is that the net computed transition dipole moment can suffer partial cancellation effects. Consider, for example, that the phases (orientation) of the calculated SC and DC component moments are either exactly aligned or opposed (in-phase or out-of-phase): their contributions to the total intensity will then add or subtract arithmetically. More generally, SC and DC moments can be oriented at any relative angle and so result in intensities that are partially attenuated by these "interference effects". Particular examples presented by Richardson

indicated some significance of these effects and so emphasized the importance at the time of not seeking to interpret '*f–f*' intensities either by SC or DC contributions alone, or by any naive supposition that their intensity contributions would be arithmetically additive.

Just before this note, Richardson *et al.* [32] published the first full-scale computational exploration of '*f–f*' intensities resting upon the mechanistic developments that we have described so far. The present review focuses particularly on the CLF model for '*d–d*' intensities although, as indicated earlier, that is best done against a background of the important advances which have been made for '*f–f*' intensities. Accordingly, we make no attempt here to exhaust the extensive literature on lanthanoid spectra. Our review of the detailed study by Richardson *et al.* [32] is, therefore, by way of a sketch and summary only.

Their paper addressed three main issues: the relative importance of SC and DC contributions to various forced, electric-dipole '*f–f*' transitions; the varying magnitude of magnetic-dipole contributions; and the role of chromophore geometry. All calculations of intensity were predicated upon point-charge, electrostatic modelling of transition energies. By and large, this was non-parametric[3] in that crystal-field splittings were computed from metal and ligand charges, ligand coordinates, and best available 4*f* radial wavefunctions for the various lanthanoid ions. Some problems with this procedure were identified by the authors and have been returned to in later years [33]. However, as all subsequently calculated intensities in this study were summed over each appropriate crystal-field multiplet, with random (solution) orientation of the chromophore — that is, "level-to-level" intensities — it was argued that a precise accounting of the crystal-field levels was less important than of the parent *J* levels. Computation of the SC and DC contributions to the forced electric dipole intensities were similarly non-parametric, relating to the same fixed point-charges used for the calculation of energies and to fixed estimates of ligand polarizabilities. The latter were deemed isotropic, a point we return to in due course. Magnetic dipole transitions are formally allowed within the pure f^n basis so that contributions from SC or DC sources were ignored at this time.

The calculations related to various lanthanoid ions; Ln = Pr, Eu, Tb, Ho; situated in several acentric environments (vibronic contributions were not considered). Several types of nine- and seven-coordinate sites were studied. Type I was the LnL_9 tricapped, trigonal prismatic structure, subdivided into two variations. As shown in Fig. 6; IR refers to the regular geometry (D_{3h} symmetry), and ID to the distorted geometry in which opposite triangular faces are rotated away from the exactly eclipsed geometry of the IR system to leave D_3 symmetry. Type II describes an idealization of the known geometry of Ln(chelate)$_3$ species, in particular of [Ln(oxydiacetate)$_3$]$^{3-}$ ions in which the tridentate chelates bind at both terminal triangular faces of a nominal trigonal prism and at an equatorial capping site. The point-group symmetry of metal plus donor atoms ranges from D_{3h}, when opposite "axial" sites are eclipsed, to D_3, when they are not. Type III geometry, for seven-coordination with C_{3v} symmetry, refers to the LnL_9 structure in which three "axial"

[3]We use "parametric" to mean empirically variable.

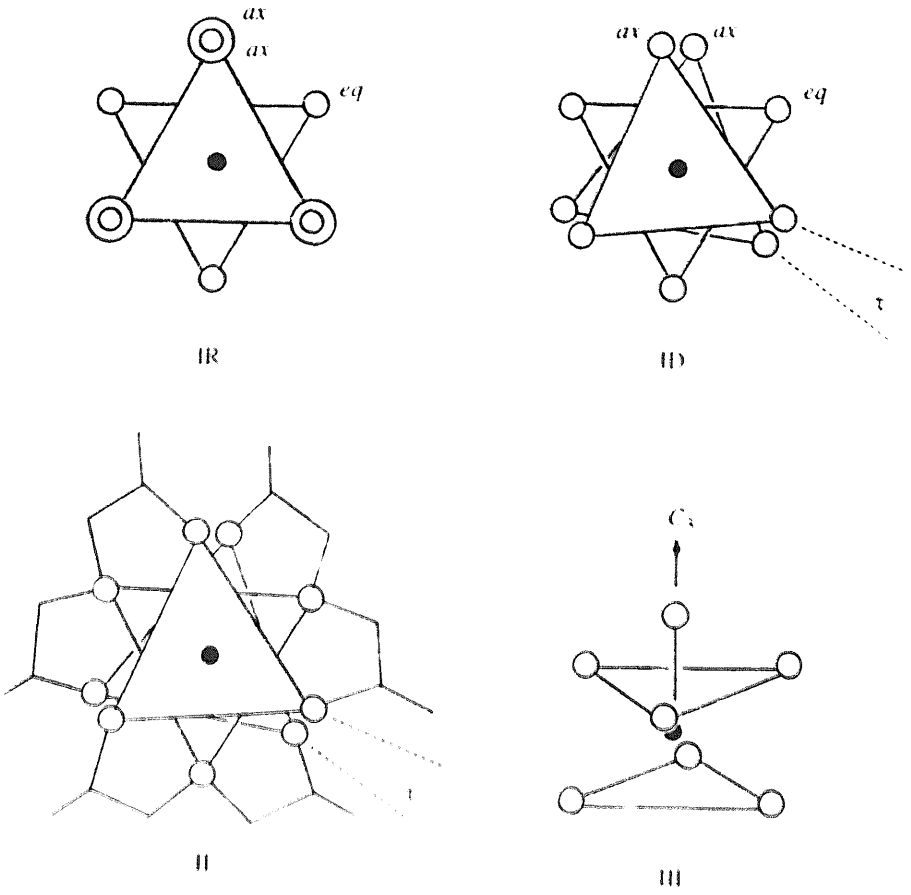

Fig. 6. Geometries in regular and distorted nine-coordinate, and in seven-coordinate lanthanoid complexes.

ligands are replaced by one, lying on the C_3 axis. Variations in the metal environment were modelled by different rotation angles (τ in the ID and II structures) and by different charge distributions for the terdentate oxydiacetate chelates. Full details are given in the original paper [32].

The results of the calculations of Richardson *et al.* [32] were presented in more than 10 lengthy tables. Their main conclusions are summarized by the selections presented in Tables 1–3. We note the following points. (1) Calculated magnetic dipole strengths, though frequently relatively small, are occasionally large and even larger than those for the forced electric dipole contribution; Richardson *et al.* note that these results accord with experiment in all cases where data is available. (2) The relative contributions of dynamic and static coupling to the electric dipole strengths vary considerably; the first two entries in Table 3 directly show the order of magnitude of DC contributions in the regular type I geometry by comparing SC with SC+DC computations, for example. (3) The role of geometry is evident throughout the tables; in particular, the hypersensitivity of the $^5I_8 \rightarrow {}^5G_6$ transition in the seven-coordinate holmium chromophore is very large, though this derives in part from changes to the SC contribution brought about by the changed geometry (IR→III types).

Table 1
Selected dipole strengths for $[Pr(ODA)_3]^{3-}$ and $[Tb(ODA)_3]^{3-}$ chromophores: ODA = oxydiacetate. Rotation angle, $\tau = 16°$

Complex	Transition	MD[a]	ED[a]	DC/SC
$[Pr(ODA)_3]^{3-}$ type II[b]	$^3H_4 \rightarrow {}^3H_5$	948	8030	0.012
	$\rightarrow {}^3H_6$	2.3	1950	0.002
	$\rightarrow {}^3F_2$	11.9	5180	0.101
	$\rightarrow {}^3F_3$	9.3	9650	0.006
	$\rightarrow {}^3F_4$	14.8	6460	0.003
$[Tb(ODA)_3]^{3-}$ type II[b]	$^7F_6 \rightarrow {}^7F_5$	1700	1230	0.290
	$\rightarrow {}^7F_4$	7	740	0.052
	$\rightarrow {}^7F_3$	2.4	601	0.002

[a] Dipole strengths/$10^{-6}D^2$.
[b] See Eq. (32) for charge and polarizability distributions amongst the donor atoms.

Table 2
Selected dipole strengths for EuL_9 chromophores

Complex	$^7F_J \rightarrow {}^7D_J$	MD[a]	ED[a]	DC/SC
ID[b] $\tau = 16°$	$0 \rightarrow 1$	181	0.14	$< 10^{-2}$
	$0 \rightarrow 2$	0.01	82.4	0.01
ID[b] $\tau = 8°$	$0 \rightarrow 1$	180	0.08	$< 10^{-2}$
	$0 \rightarrow 2$	$< 10^{-2}$	94.2	0.05
IR[c]	$0 \rightarrow 1$	181	$< 10^{-2}$	$< 10^{-2}$
	$0 \rightarrow 2$	$< 10^{-2}$	1.13	35.8

[a] Dipole strengths/$10^{-8}D^2$.
[b] Unequal equatorial and "axial" ligations; see [32].
[c] Equal ligations.

The last issue re-emphasizes an important point about the calculation of '*f–f*' (and of '*d–d*') intensities. We have focussed our discussions most particularly upon the question of mechanism. However, the role of gross chromophore geometry and symmetry is equally important. The *pseudo*quadrupolar selection rules discussed earlier derive in part from the spherical symmetry of the free ion and determine which transitions *may* be hypersensitive. Whether they are or not, and to what extent, is then further determined by the chromophore point-group symmetry — the symmetry of the environment. The partial cancellation of the DC contribution in the tricapped, trigonal prismatic structure was illustrated directly in Fig. 5(b) for example. That both static and dynamic contributions may be sensitively dependent upon geometry and symmetry is similarly exemplified by the requirement that both must vanish in centrosymmetric environments (we ignore vibronic contributions here). Overall, therefore, the wide range of some '*f–f*' intensities (the hypersensitive ones in particular) is due as much to variations in chromophore coordination number and geometry as to the efficacy of the dynamic coupling mechanism and the magnitudes of the ligand polarizabilities. Naturally, both considerations are properly

Table 3
Selected dipole strengths for HoL_9 and HoL_7 chromophores [32]

Complex	Transition	MD[a]	ED[a]	DC/SC
IR	$^5I_8 \rightarrow {}^5I_7$	2160	220	0.005
	$\rightarrow {}^5K_8$	101	24	0.078
	$\rightarrow {}^5G_6$	0.7	94	1.74
	$\rightarrow {}^5G_5$	0.1	27	0.004
	$\rightarrow {}^3K_7$	2.1	6	0.011
IR[b]	$^5I_8 \rightarrow {}^5I_7$	2160	221	0
	$\rightarrow {}^3K_8$	101	22	0
	$\rightarrow {}^5G_6$	0.7	43	0
	$\rightarrow {}^5G_5$	0.1	26	0
	$\rightarrow {}^3K_7$	2.1	6	0
III	$^5I_8 \rightarrow {}^5I_7$	2142	220	0.572
	$\rightarrow {}^3K_8$	102	87	2.21
	$\rightarrow {}^5G_6$	0.6	5315	4.24
	$\rightarrow {}^5G_5$	0.1	158	0.19
	$\rightarrow {}^3K_7$	2.1	11	1.24

[a] Dipole strength/$10^{-6}D^2$.
[b] As for entries above, but with ligand polarizabilities set at zero.

included within the formal algebra of the model. So these variations reflect the changing character of the relevant wavefunctions rather than of some mysterious trends in the underlying physics.

Richardson *et al.* [32] noted that: "Full scale quantitative calculations of 4*f*–4*f* intensities in low-symmetry lanthanide complexes remain a difficult undertaking ..." and go on to claim, with justification, that their results "suggest that the intensity model (SC + DC) provides a reasonably good basis for carrying out such calculations and within which new parametrization schemes can be developed." Part of that development arose out of an important contribution to the subject by Newman and Balasubramanian [24] that we now review.

4.7. *Effective operators and covalency*

An important contribution [24] with implications for '*d*–*d*' as well as '*f*–*f*' transition intensities is that by Newman and Balasubramanian in 1974. It begins by addressing certain features of Ofelt's [23] parametrization scheme. Ofelt's model, and Axe's [34] subsequent modification of it, was developed from an identical view of electrostatic configurational mixing as that taken by Judd [22]. It was somewhat more specific, however, and established a parametrization scheme that related to the symmetry of the electrostatic field in which the lanthanoid atom is situated. At a purely *parametric* level, Judd's three Ω_λ ($\lambda = 2, 4, 6$) coefficients subsumed the parentage of admixed configurations and the overall chromophore symmetry. Ofelt's scheme kept such matters parametrically separate with quantities labelled $A_q^k(\ell)$. The (k, q) labels refer to odd components of the crystal-field potential giving rise to the required parity mixing, while ℓ ($= 2, 4$) labels the *d* or *g* character of the admixed

configurations. The number of $A_k^q(\ell)$ required in any given system depends upon the chromophore symmetry but is always greater than three. Estimates of the relative signs and magnitudes of the $A_k^q(\ell)$ for different ℓ can be made within a simple electrostatic model. Work by Krupke and Gruber [35] and Becker [36], however, had not supported such estimates although good *parametric* reproduction of observed intensity distributions within the Ofelt and Axe schemes had been achieved. As emphasized by Newman and Balasubramanian, the electrostatic models of Ofelt and Axe were successful with respect to the number of parameters required in those particular species but not with respect to some of their relative magnitudes.

Newman and Balasubramanian pointed out that Judd's parametrization really only depends upon the one-particle nature of the crystal field. They further reminded us of Judd's demonstration [22] that, *parametrically* Eq. (54) serves equally well for any dynamic (vibronic) crystal-field contributions to the parity-mixing process. They posed the question, therefore, as to whether the Ofelt and Axe parameters provide the most general description of transition amplitudes between crystal-field-split states. In particular, Newman and Balasubramanian had in mind the possible role of covalency as an intensity generator. That suggestion had previously been made by Reisfeld *et al.* [37] and by Jaeger and Englman [38]; it sits well, in general terms, with the established relevance of covalency and overlap for crystal-field modelling of transition energies. In passing, we note the different language used in this area and in mainstream inorganic chemistry. In the latter, we use Eq. (1) to summarize crystal-field theory as a purely electrostatic approach and Eq. (2) for ligand-field theory deemed to include all contributions including covalency (see [5,7,18]). Within the lanthanoid literature currently being reviewed, the name "crystal-field" is taken to be general enough to encompass all field sources and must be interpreted within each given context.

So Newman and Balasubramanian sought to generalize Judd's approach. Before looking at their contribution, recall the structure of Eq. (51) in which the terms between the long vertical bars describe, *inter alia*, an even-parity *effective* operator coupling the like-parity bra and ket states under the light. The question for Newman and Balasubramanian was, in effect, to describe such an effective operator in the most general (that is, least specific) way. They observe that mixed parity states resulting from covalency, overlap *and* configuration interaction into the $4f^N$ open shell states $|4f^N\alpha JJ_z\rangle$ can be written quite generally as:

$$|\alpha JJ_z\rangle = (1+Q)|4f^N\alpha JJ_z\rangle, \tag{69}$$

where Q is a non-local operator. It is assumed only that Q can be taken as a one-electron operator. It may be divided into even (g) and odd (u) components:

$$Q = Q_g + Q_u. \tag{70}$$

Ligand-field splittings relate to the even part of Q via matrix elements of the kind, $\langle 4f^N\alpha' J' J'_z|Q_g|4f^N\alpha JJ_z\rangle$.

Static contributions (SC) — which include any vibronic contributions also — to

forced electric dipole transitions may be written as:

$$(\alpha' J' J'_z | P_\rho | \alpha J J_z) = \langle 4f^N \alpha' J' J'_z | Q_u P_\rho + P_\rho Q_u | 4f^N \alpha J J_z \rangle, \tag{71}$$

where $Q_u P_\rho + P_\rho Q_u$ is a non-local, one-electron vector operator, V_ρ, corresponding to the vectorial nature of the electric dipole operator $P_\rho (\rho = 1, 0, -1)$.

Newman and Balasubramanian then expand V_ρ as superpositions of components of localized vector fields having the same matrix elements as the non-local operator in the open-shell states $|4f^N \alpha J J_z\rangle$:

$$Q_u P_\rho + P_\rho Q_u \equiv V_\rho = \sum_{KQ} V_Q^K(\rho) U_Q^{(K)}, \tag{72}$$

where $U_Q^{(K)}$ is a sum of single-electron, unit tensor operators. This simple argument established the parameters $V_Q^K(\rho)$ to have far more general validity than those of Judd or Ofelt in that contributions from overlap and covalency had not been ignored. Newman and Balasubramanian claim that the closure approximations required in the models of Judd and Ofelt are related to the present restriction to one-electron operators. By way of emphasis: the Judd and Ofelt models are specifically electrostatic, configuration-mixing in kind; we shall discuss some equally specific, covalency type contributions in due course, but the arguments given above show that, parametrically, all kinds of one-electron parity-mixing may be properly subsumed within an effective vector operator like Eq. (72).

The incompleteness of the electrostatic, point-charge scheme is dramatically illustrated by symmetry analysis of the vector field, V_ρ. Newman and Balasubramanian offered two views. The V_ρ of Eq. (72) comprise three distinct expansions, one for each value of ρ — the electric dipole polarization. The number of parameters, $V_Q^K(\rho)$, for each ρ may be determined for a given chromophore site symmetry by finding the number of occurrences of the irreducible representations of that site symmetry corresponding to each component of the vector basis in each of the full rotation group representations $D^{(2)}$, $D^{(4)}$ and $D^{(6)}$. Results for three site symmetries of interest are given in Table 4(a). The numbers of requisite V_Q^K parameters are greater than those spawned by Ofelt's electrostatic model and successfully employed by Krupke and Gruber [35] or by Becker [36]. The reason for this mismatch is somewhat opaque in the presentation so far. It was resolved by Newman and Balasubramanian from an alternative but entirely equivalent formulation of the effective vector operator V.

In this, the vector field, V, is not expressed by three simply resolved components as in $V(\rho)$ of Eq. (72) but rather *in toto* as an expansion in *vector* spherical harmonics:

$$V = \sum_{JKM} A_{JKM} Y_{JKM}, \tag{73}$$

where the vector spherical harmonics couple the tensors of the potential with the base vectors and are defined by Edmonds [39]:

$$Y_{JKM} = \sum_{Q\rho} Y_{KQ}(\theta, \phi) e_\rho (KQ, 1\rho | JM), \tag{74}$$

Table 4
Vector field parameterizations, after Newman and Balasubramanian [24]

Site symmetry	K	(a) Parameters $V_Q^K(\rho)$			(b) Parameters A_{JKM}		
		Number for $\rho=\sigma$	Number for $\rho=\pi$	Totals	Number for $J=K$	Number for $J=K\pm1$	Totals
D_{2d}	2	1	1	2	1	1	2
	4	1	2	3	1	2	3
	6	2	3	5	2	3	5
	All	4	6	10	4	6	10
D_{3h}	2	0	1	1	0	1	1
	4	1	2	3	1	2	3
	6	1	2	3	1	2	3
	All	2	5	7	2	5	7
$C_{\infty v}$	2	1	1	2	0	2	2
	4	1	1	2	0	2	2
	6	1	1	2	0	2	2
	All	3	3	6	0	6	6

where the parameters, A_{JKM}, are given by

$$A_{JKM}=(-1)^{\rho}\sum_{Q\rho}(KQ,\,1\rho|JM)V_Q^K(-\rho). \tag{75}$$

An immediate advantage of this formulation is that rotation of coordinates only affects the suffix M, so simplifying the development of a superposition model, as we shall outline shortly. In Table 4(b) are listed the numbers of non-zero parameters, A_{JKM}, for the same site symmetries considered in Table 4(a), which emerge from the new formulation. These are obtained by finding the number of totally symmetric irreducible representations with even parity in $D^{(J)}$ for $J=K\pm1$ and with odd parity in $D^{(J)}$ for $J=K$. As required by the equivalence of the two expansions Eqs. (72) and (73), the total number of parameters required is the same [for each site assignment in Table 4(a and b)]. However, those with $J=K\pm1$ are the only ones to emerge from the electrostatic models of Judd, Ofelt or Axe. Newman and Balasubramanian had thus identified the "extra" parameters of the general effective operator Eqs. (72) and (73) to be those characterized by $J=K$. The question therefore arises as to what physical processes these extra parameters can model.

Newman and Balasubramanian first showed what the $J=K$ parameters cannot model. They considered the case that V might derive from the superposition of vector fields contributed by individual ligands represented as local point-charges or point-dipoles (we do not include any idea of polarizability of the ligands in this). Inspection of Table 4(b) shows that no $J=K$ parameters arise for the site symmetry $C_{\infty v}$ (appropriate for the axial field of an individual electrostatic M–L interaction). Superposition of several, discrete local fields involves the rotation of each into a

common frame, followed by summation:

$$A^G_{JKM} = \sum_i \bar{A}^L_{JK}(R_i) D^{(J)*}_{M0}(\theta_i, \phi_i)^L, \tag{76}$$

where L and G superscripts refer to local and global environments and the $\bar{A}^L_{JK}(R_i)$ are local, "intrinsic" parameters for ligand i. As $J=K$ parameters are absent in the local C_∞ environment, the sum Eq. (76) inevitably excludes them from *any* global site symmetry also. Newman and Balasubramanian therefore conclude that the successful *parameteric* reproduction of experimental intensities for the ethyl sulphate complex of Tm^{3+} by Krupke and Gruber [35] using only five $J=K\pm1$ variables is to be attributed to the validity of the superposition principle rather than to the relevance of the original electrostatic modelling of Judd or Ofelt. This conclusion rests, it must be emphasized, upon the assumption that all contributions to the local vector fields — from covalency as well as from configuration mixing *via* an electrostatic process — are axially symmetric. Conversely and by way of emphasis, the need for the $J=K$ parameters that the most general forms of effective operator Eqs. (72) and (73) require will arise if either the superposition assumption is invalid (equivalent to interaction between local ligations) or the local vector fields are not axially symmetric with respect to the local M–L bonds. All this was to be taken on board by Richardson *et al.* in their later work, as we shall see.

Newman and Balasubramanian, however, made one more important contribution in their 1975 paper [24]. Given the superposition assumption, which is widely accepted, and that the local fields in the object systems are axial — which may well be a reasonably good assumption — their argument above demonstrated that the relevance of the electrostatic model was not secure. That it is surely inadequate, however, only emerged from a more detailed perusal of the detailed predictions of the electrostatic scheme. We summarize it in barest outline only. It was shown that when the operator $Q_u P_\rho + P_\rho Q_u$ of Eq. (72) is assumed further to involve a non-local operator Q_u which can be approximated by a superposition of local spherical harmonics, as appropriate for an electrostatic model, the ratios between certain pairs of A_{JKM} parameters are fully determined by the quantum numbers:

$$r_J = A_{J,\,J+1,\,M}/A_{J,\,J-1,\,M} = -(J+1/J)^{1/2}. \tag{77}$$

The phenomenological parameters from the analyses by Becker and by Krupke and Gruber, however, were found to describe positive such ratios, r_J, in all cases. These workers had already recognized this problem and Becker [35] had suggested a possible solution to it. He had noted that Q_u can be factored into a projection operator $\hat{S}$ acting on an odd parity electrostatic field function V_u. This is based upon the approximation that the projection is taken over a sufficiently extensive set of states to be replaced by unity. However, Becker pointed out [36] that the occupied states involve a projection operator of opposite sign to that from the excited states, so that $\hat{S}$ should be replaced by $\hat{S}$(excited) $-$ $\hat{S}$(occupied). He therefore proposed that the solution to the sign problem above lay in significant contributions from (occupied) $3d$ and $4d$ configuration interaction as well as from (unoccupied) $5d$. Newman and Balasubramanian tested this proposition but

found such contributions to be negligible. So the failure of the pure electrostatic model remains. On the other hand, they pointed out that contributions from occupied *ligand* states could well be important enough to account for the sign reversal sought above; their suggestion was supported by other observations. Altogether, Newman and Balasubramanian concluded that while a pure electrostatic modelling of forced electric dipole transitions is unsupportable, indirect evidence for the relative importance of covalency and overlap contributions to parity mixing is to hand.

Ten years later, in 1984, Poon and Newman [40] returned to this theme. Their aim was to make more detailed estimates of the magnitudes of ($K=J\pm1$) intensity parameters within an explicit covalency model; in particular, to compare parameter ratios calculated on an overlap basis with those derived from the electrostatic model. In the years between the Newman/Balasubramanian and Poon/Newman papers, the importance of ligand polarizabilities and the dynamic coupling mechanism had come to the fore. The failure of the static mechanism to account for various empirical intensity parameter ratios had been addressed by Richardson and his colleagues [41], claiming that the DC mechanism could successfully put the matter right. Their work, however, sharpened the focus of that by Poon and Newman who noted that if intensity parameter ratios calculated by the SC and covalency models were found to differ significantly, the claim of Reid *et al.* [41] for the importance of the DC contribution could be unsupportable.

The basis of Poon and Newman's overlap model is very simple. The required parity mixing for forced electric dipole transitions is deemed to arise from the formation of molecular orbitals between lanthanoid $4f$ functions (ϕ) and ligand wavefunctions (χ). For a single-ligand case, they write:

$$\phi'_m = N_m^{-1/2}(\phi_m - \sum_\tau \lambda_{m\tau}\chi_\tau), \tag{78}$$

where the sum extends over various outer-shell ligand functions ($\tau = s, p\sigma, p\pi$). The normalization factor is defined by:

$$N_m = 1 - 2\sum_\tau \lambda_{m\tau}S_{m\tau} + \sum_\tau \lambda_{m\tau}^2, \tag{79}$$

where $S_{m\tau} = \langle\phi_m|\chi_\tau\rangle$. Unlike ϕ_m, ϕ'_m does not have definite parity so that non-vanishing electric dipole transition matrix elements of the type $\langle\phi'_{m1}|\mathbf{er}|\phi'_{m2}\rangle$ exist:

$$\langle\phi'_{m1}|\mathbf{er}|\phi'_{m2}\rangle = (N_{m1}N_{m2})^{-1/2}(-\sum_\tau (\lambda_{m2\tau}\langle\phi_{m1}|\mathbf{er}|\chi_\tau\rangle + \lambda^*_{m1\tau}\langle\chi_\tau|\mathbf{er}|\phi_{m2}\rangle + \sum_{\tau,\tau'} \lambda^*_{m1\tau}\lambda_{m2\tau'}\langle\chi_\tau|\mathbf{er}|\chi_{\tau'}\rangle). \tag{80}$$

Calculations of the magnitudes of such matrix elements rest upon estimates of the various overlap integrals and mixing coefficients appearing in these expressions. It is clear that these estimates and the adoption of so simple a model of covalency will limit the accuracy with which the intensity parameters which depend on them may be computed. The notions inherent in a point-charge description of the SC computations are probably no less limiting. Nevertheless, it is of interest to compare the results.

Table 5 lists local or "intrinsic" parameter values [the $\bar{A}^L_{JK}$ of Eq. (76)] calculated by Poon and Newman within their covalency and electrostatic models and compared with empirical values reported by Reid *et al.* The experimental values are all of the same sign, except for the very uncertain value of $\bar{A}_{76}$, as was the case for the data of Krupke and Gruber and of Becker, discussed earlier. *Neither* the covalency nor the electrostatic (SC) models reproduce this feature although, as Poon and Newman point out, "it is conceivable that a pattern of cancellation could exist between these and other contributions such as screening that would produce such a result". They go on, however, to acknowledge the more likely explanation, already advanced by Reid and Richardson [42,43], and by Reid *et al.* [41], that ligand polarization contributions within the DC mechanism which only affect the $J=K-1$ parameters are sufficiently large to change their sign. This support for the relevence of the DC contribution does not rule out any contribution from covalency, however. The crudity of the models indicated above must be borne in mind.

4.8. Ligand polarizability anisotropy

We return, meanwhile, to the ligand polarization model. In 1980, Kuroda *et al.* [44] extended this approach in an important way. As originally developed, and presented so far, it was supposed that the ligands could be represented by isotropic polarizabilities. While such a simplification might be supportable for monatomic halogen ligators, for example, it is called into question for more complex species whose electron distributions are known to be anisotropic. While the development of the ligand polarization mechanism by Kuroda *et al.* appears to be the first to address this issue *explicitly*, it had been signalled in the earlier work of Newman and Balasubramanian, as we shall see. Apart from the particulars of the work of Kuroda *et al.* in application to $[Eu(digly)_3]^{3+}$ and $[Eu(H_2O)_9]^{3+}$ chromophores, we note a central, incisive point in their contribution. That was their demonstration that a non-vanishing, resultant electric dipole moment — as experimentally observed — was satisfactorily reproduced with anisotropic ligands while a corresponding calculation based on isotropic polarizabilities yielded an identically zero result. They went on to describe extensions of the selection rules established by the

Table 5
Calculated Pr^{3+}–Cl^- single-ligand, "intrinsic" parameters $\bar{A}_{JK}$ (in 10^{-11} cm) calculated by Poon and Newman [40] for covalency and electrostatic configuration interaction mechanisms. The empirical data are for Pr^{3+}:$LaAlO_3$ after Reid *et al.* [41]

	Covalency and overlap	Electrostatic configuration interaction	Empirical for Pr^{3+}:$LaAlO_3$
$\bar{A}_{12}$	1.26	−55.6	
$\bar{A}_{32}$	−1.54	3.05	−3.6 ± 0.8
$\bar{A}_{34}$	2.53	−6.39	−19.6 ± 4.1
$\bar{A}_{54}$	−2.83	0.46	−17.0 ± 0.7
$\bar{A}_{56}$	4.54	−1.32	−30.0 ± 1.6
$\bar{A}_{76}$	−4.90	0.00	62 ± 50

more restrictive earlier model. Overall, their demonstration of the importance of anisotropic ligand polarizabilities in general was therefore well founded on a clear-cut symmetry-based example.

In 1983, Stewart [45], and Reid and Richardson [43,46], independently published generalized treatments of the DC mechanism with respect to anisotropic ligand polarization contributions in this way. Many applications to real lanthanoid chromophores, especially by Richardson and his group, have since exploited these detailed expositions of the theory. As indicated already, our goal in the present article is to describe the CLF model for '*d–d*' intensities against the background of mechanistic understanding that has emerged from the '*f–f*' literature. A detailed description of the complete ligand polarization model is not appropriate here, therefore. However, a summary of it and its relationship to the work of Newman and Balasubramanian — along the lines of the recent review by Stewart [29] — is informative.

Recall Eq. (66), expressing the ligand polarizability tensor in terms of sums of dipole moments amongst the ligand states. In other contexts, it is usual to express the tensor $\alpha^{(k)}$ as a second-rank Cartesian tensor. In spherical symmetry, however, it may be reduced into three irreducible components: the isotropic, mean polarizability when $k=0$; an antisymmetric anisotropy for $k=1$; and a symmetric anisotropy with $k=2$. For the present purpose, the odd, antisymmetric component is irrelevant, but we need to consider the even $k=0$ and $k=2$ tensors. For convenience' sake we note again earlier expressions for the effective DC dipole moment operator [Eqs. (67) and (68)]:

$$\mu_{\mathrm{eff}}^{(1)\mathrm{DC}} = \sum_{L} \sum_{t,\lambda} c(\lambda)[F^{(t)} D^{(\lambda)}]^{(1)},$$

where

$$c(\lambda) = [(2\lambda+3)(2\lambda+1)(\lambda+1)]^{1/2}$$

and

$$F^{(t)} = (-1)^k [(2k+1)(2t+1)/3]^{1/2} \begin{Bmatrix} \lambda+1 & k & t \\ 1 & \lambda & 1 \end{Bmatrix} [\alpha^{(k)} G^{(\lambda+1)}]^{(t)}.$$

For the isotropic polarizability:

$$F^{(t)}(k=0) = (1/3)\alpha^{(0)} G^{(\lambda+1)} = -(1/\sqrt{3})\bar{\alpha} G^{(\lambda+1)}, \tag{81}$$

where $\bar{\alpha} = (\alpha_{xx} + \alpha_{yy} + \alpha_{zz})/3$ is the mean ligand polarizability.

Now, writing

$$\langle A|\mu_{\mathrm{eff}}^{(1)}|B\rangle = \sum_{L} \sum_{t,\lambda} c(\lambda)[F^{(t)} \langle A|D^{(\lambda)}|B\rangle]^{(1)} \tag{82}$$

for a forced electric dipole matrix element between pure f states $\langle A|$ and $|B\rangle$ is quite general in that it serves equally for electrostatic (SC) contributions as well as for dynamic (DC). The nature of the environmental tensor $F^{(t)}$ depends upon which mechanism is being considered, however, and the allowed values of t vary accord-

Table 6
Contributions to SC and DC models[a]

	SC	Isotropic DC	General DC
$F^{(t)}$	$\sim \Xi(t, \lambda) A_p^t$	$\sim \bar{\alpha} G^{(\lambda+1)}$	$\sim [\alpha^{(k)} G^{(\lambda+1)}]^{(t)}$
t	$\lambda \pm 1$	$\lambda \pm 1$	$\lambda, \lambda \pm 1$

[a]First row describes the significant parts of the environmental tensor $F^{(k)}$. Second row lists the restrictions upon t.

ingly. Firstly, the triangle rule places restrictions upon the coupling of the effective dipole operator, Eq. (67) such that $t = \lambda - 1, \lambda, \lambda + 1$. Further restrictions are established by the parities of the coupled tensors in Eq. (67). Thus, the dipole operator μ has odd parity and so determines a similar odd parity for the coupling $[F^{(t)} D^{(\lambda)}]^{(1)}$. The multipole operator $D^{(\lambda)}$ ($\lambda = 2, 4, 6$) is of even parity and therefore $F^{(t)}$ must have odd parity. The odd parity of $G^{(\lambda+1)}$ in Eq. (68) then requires $\alpha^{(k)}$ to have even parity so leading to our neglect of the antisymmetric component ($k = 1$) of α above.

For the electrostatic SC contribution, $F^{(t)}$ is proportional to $\Xi(t, \lambda) A_p^t$ where the A_p^t are odd parity crystal-field parameters. In this case, then, t must be odd and its range limited overall to $t = \lambda \pm 1$ as discussed earlier. For the isotropic DC contribution, Eq. (81) establishes $t = \lambda + 1$ only: again t is odd. On the other hand, for the $k = 2$, anisotropic DC contribution, application of the triangle rule and parity in Eq. (68) establishes the full range for t: $t = \lambda, \lambda \pm 1$. These various relationships between t and λ are summarized in Table 6.

An interesting pictorial summary of these connections between the multipolarity λ of a transition and the allowed values of the rank t of the environmental tensor $F^{(t)}$ is shown in Fig. 7. This highlights, for example, that a rank 3 parameter ($t = 3$) has contributions from both $\lambda = 2$ and $\lambda = 4$ transitions in the SC model but only from a $\lambda = 2$ transition in the (original) isotropic DC model. We have seen that the "quadrupolar" transitions (as opposed to hexadecapole or 2^6-pole) are uniquely hypersensitive. The figure makes plain how this unique selection of $\lambda = 2$ is possible in the SC scheme only for polar ($t = 1$) crystal-field parameters, as the $t = 3$ parameters contribute to both $\lambda = 2$ and $\lambda = 4$ transitions. Experimentally, however, hypersensitivity is not restricted to chromophore sites possessing polar crystal-field components.

The full range of contributions for the general, anisotropic DC mechanism is apparent from Fig. 7. In particular, the $t = \lambda$ terms are uniquely associated with the concept of anisotropic ligand polarizabilities, although these terms vanish identically

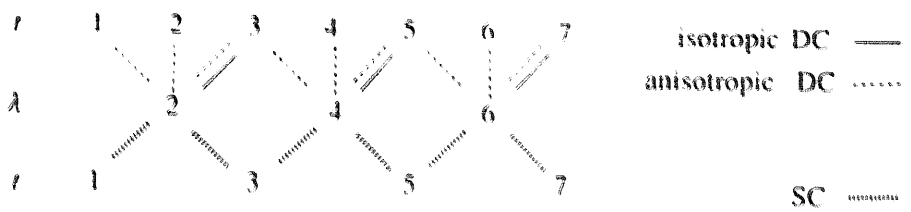

Fig. 7. Possible values of t for SC and DC models.

also for cylindrical ligation; that is, for anisotropic but axially symmetric ligand polarizabilities whose principal axis is directed along the local M–L vector. All this, of course, directly correlates with the contribution (the $J=K$ terms) of Newman and Balasubramanian [24] discussed earlier. Their development was purely group-theoretical, however, so that the present neglect of overlap and covalency is not essential. A corollary here is that selection rules cannot differentiate between an independent-systems approach and any overlap-based modelling of forced, electric-dipole intensities.

4.9. *Overview of* 'f–f' *intensities and introduction to* 'd–d'

An accounting for the spectral intensities of lanthanoid '*f–f*' intensities has been an ambitious program; a great deal has been achieved since 1962. One may discern a number of contrasting strands: symmetry and angular quantities versus radial properties; electrostatic versus covalency interactions between metal and environment; "term" spectra versus detailed ligand-field components; magnetic dipole versus electric multipole contributions. Most of the development has been concerned with forced electric dipole transition moments in which the parity and orbital selection rules that deny pure *f–f* intensities in free lanthanoid ions are partially circumvented by a variety of parity-mixing processes. We have taken a somewhat historical journey through these matters. With the benefit of hindsight, we might cut the cake differently.

While in no way minimizing the magnificent contributions of Judd and Ofelt or of the Mason and Richardson groups, one may look at those of Newman and Balasubramanian as providing an insightful focus from which to build an overview of this technically complex field. That all one-electron contributions to forced electric dipole transitions are formally collected within an effective operator like Eq. (72) provides a unity to the diverse enterprises outlined in the foregoing pages. The generality of the concept separates problematic radial features from purely angular quantities which may be dealt with fully and explicitly. The latter provide for an applicable, mathematical modelling of intensities and define all appropriate selection rules. The former leave the question of mechanism vague; this may be seen as both a strength and a weakness. The weakness is obvious, of course, given the natural desire to establish non-parametric, *quasi ab initio*, accounting of these open-shell spectra. In this regard, the importance of the various stages of the independent-systems approach are evident. One is to remember that the hypersensitive '*f–f*' transition intensities are observed experimentally to vary over three orders of magnitude. It is clearly persuasive that their explicit modelling in terms of non-parametric ligand charges and polarizabilities has been able to reproduce all qualitative aspects of experimental intensity distributions and to account for absolute intensities usually to within a factor of two or so. That more perfect agreements between observed and calculated oscillator strengths have not generally been achieved is surely an indication that theoretical restriction to the more tractable coulombic mechanisms is not wholly warranted and that the consequences of covalency remain to be assessed. Conversely, that the agreement is as good as it is suggests something real

in those mechanistic constructions. Nevertheless, to repeat an earlier point, the relevance of the angular theory and its associated selection rules does not, of itself, argue for or against overlap and covalency contributions.

The non-parametric modelling within the SC + DC scheme, especially in the hands of the Richardson group, has naturally included a simultaneous modelling of '*f–f*' transition *energies*. Earlier efforts in this direction were not without problems, but some more recent work [33] in which various two-electron, ligand-field contributions are recognized, appear to be very successful. One is bound to recall however, and certainly with regard to corresponding '*d–d*' transitions, that non-parametric computations of ligand-field spectral energies have always met with limited success. There are even serious interpretative problems with parametric ligand-field schemes like the angular overlap model (AOM). We have discussed this at length in a recent review [9] and so do not repeat these matters here except with respect to one centrally important issue. In modelling *d* electron properties by ligand-field theory — and, in particular, that variation which employs a spatial superposition over discrete ligations known as cellular ligand-field (CLF) theory — one is to recognize that we are seeking to account for experimental observations on a molecule *as it is* rather than on a promolecule — meaning the notional structure of the same geometry before chemical bonding has taken place. The promolecular situation is not far removed from the zeroth order state in an independent systems approach. An important assumption within the AOM is that of ligation additivity — of the independence of local perturbations. Following the give-and-take of electron redistribution on chemical bonding, however, local bonding properties inevitably reflect the remaining environment: the *trans* effect is just one example of this. The consequence is that any molecular orbital description of a given M–L bond in terms of prior atomic or ionic orbitals (of the promolecule) must necessarily also include such orbitals from atoms of ligands other than that for which such a description is being formed. In this sense, therefore, chemical bonding ensures that, to some extent at least, separate ligations are not wholly independent. On the other hand, *parametrization* of the molecule as is — as formed — *can* adequately factor the resultant ligand field as a sum of discrete perturbations. The problem then devolves into one of interpretation for, without the benefit of some accurate (and essentially presently unattainable) *ab initio* computation of the rearranged electron distribution, one no longer has available the knowledge to construct some non-parametric approach. Interpretations of CLF parameter optimizations must then be made on a qualitative basis. With insight and intuition they can be rewarding nonetheless.

All of this seems pertinent for the interpretation of open-shell spectral *intensities* also. The coupling of different ligations through chemical bonding will occur via the appropriate valence shells. It has been argued that the participation of *d* orbitals in such shells is small (in complexes to which ligand-field models are applied — Werner-type species) and no doubt even smaller for *f* orbitals in lanthanoid species. However, the small *d* or *f* orbital overlaps with the ligands in no way diminishes the ligand–ligand coupling within the bonding. The relevance of this in our present context is that estimates of the magnitudes and anisotropies of ligand polarizabilities — and, of course, of the radial part of the metal *f* orbitals — cannot be made with great

confidence. It is only too possible that the considerable success to be had within the SC+DC independent-systems modelling with fixed (non-parametric) estimation of these quantities is owed to happy, partial compensation for the neglect of covalency by poor descriptions of the polarizabilities of bonded ligands. To emphasize these points: the ligands in a complex are bound to involve different electron distributions to the corresponding free ligands, and the effects of covalency are by no means limited to consideration of overlap with the metal *f* orbitals. Hints along these lines are to be found in the '*f–f*' intensity literature from time to time. Both Judd [30] and Newman [40] have suggested that earlier modelling successes might have been somewhat fortuitous given the neglect of both "shielding" and "anti-shielding" contributions from electron densities elsewhere in a chromophore.

We have mentioned the weakness of Newman's approach [24] leaving the question of mechanism somewhat vague. Its strength, on the other hand, is its ability to sequester all mechanisms even though subsequent interpretation must be qualitative. We espouse the openness of the effective operator approach. The CLF intensity models of the next sections exemplify it. Before turning to that model, which has been developed for the '*d–d*' transition intensities of the main transition block, let us review some of the differences between the *d* and *f* electron systems.

The looks of '*f–f*' and '*d–d*' spectra are quite obviously different. Compare, for example, that for a saturated aqueous solution of neodymium ions with that for tetrachlorocobalt(II) ions, shown in Fig. 8. The '*d–d*' spectrum is characterized by

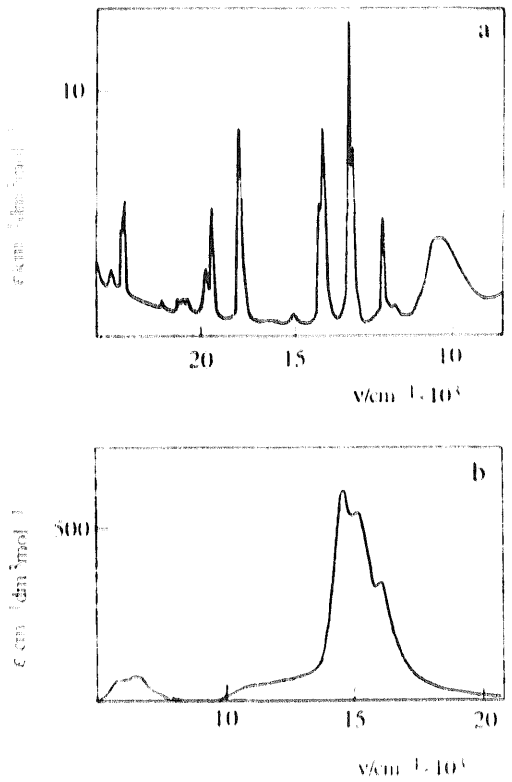

Fig. 8. (a) Electronic '*f–f*' spectrum of a saturated aqueous solution of Nd^{3+} ions; (b) electronic '*d–d*' spectrum of a solution of $[CoCl_4]^{2-}$.

much larger extinction coefficients and very broad bands split in the ligand field by several thousand wavenumbers. The '*f–f*' trace typically displays many more bands, which are narrow and with much smaller extinction coefficients. It is usual in inorganic chemistry teaching texts to account for all these differences in terms of the 4*f* electrons being much more core-like than the 3*d*. While this explanation is undoubtedly correct, it is superficial and is worth elaboration.

Firstly, consider the question of splittings. The mean radii of 4*f* electrons in Ln^{3+} ions is not too different from that of 3*d* electrons in M^{2+} ions of the first main transition period. On the other hand, bond lengths in lanthanoid complexes are probably some 25% longer than their counterparts in first-row, 3*d*, complexes; the 4*f* orbitals are indeed more "buried" beneath the valence shell than are the 3*d* orbitals. An explanation of the small *f* electron, ligand-field splittings — measured in tens or hundreds of wavenumbers rather than the thousands for *d* systems — readily comes to hand in terms of a point-charge, crystal-field model. It also follows in cellular ligand-field theory where the sources of the splittings are recognized as the bonding electron density. In short, the longer lanthanoid bond lengths establish smaller energy splittings.

Secondly, a view of band widths as reflecting the variations of ligand-field splittings with vibrations in the chromophore (in particular, with symmetric, bond-stretching, "breathing" modes) immediately rationalizes the narrower bands in the lanthanoid series as even a similar percentage variation of the ligand-field splitting necessarily results in much smaller absolute variations in band width. Again, the longer lanthanoid bond lengths and more core-like character of the 4*f* orbitals are, by and large, responsible for the narrow bands in these chromophores.

The third issue, and of particular interest for the present article, concerns the intensities of these spectra. Before discussing theoretical aspects, consider the facts. If we compare just one '*f–f*' band from Fig. 8(a) with one '*d–d*' from Fig. 8(b), we observe a change from $\epsilon \approx 10$, say, to $\epsilon \approx 500$ together with an increase in band width (say, width at half-height) from approximately 20 to approximately 1000 cm^{-1}. In short, the '*d–d*' band is some 2500 times more intense. Taking different bands might vary this figure by about an order of magnitude. On the other hand, assuming that all these bands are predominantly of the forced electric dipole type, a better comparison between '*f–f*' and '*d–d*' spectral intensities is probably made with respect to dipole strengths summed over all ligand-field bands. The argument here is that all types of coulombic, spin-orbit and ligand-field perturbations serve to distribute the necessary parity-mixing throughout the relevant manifolds. Dipole strengths exclude the frequency dependence of oscillator strength, of course, but we might estimate that the total dipole strength in a typical lanthanoid spectrum of the type shown in Fig. 8(a) is only approximately 200 times smaller than that of the '*d–d*' spectrum shown in Fig. 8(b). In other words, the '*f–f*' intensity is spread over many more transitions than is the '*d–d*'. We acknowledge that these estimates are rough but they serve to demonstrate that the difference in '*d–d*' and '*f–f*' intensities are not as great as they first appear.

Finally, we turn to the theoretical prediction of these relative intensities. In 1975, Gale *et al.* [47] published a note on the '*d–d*' intensities in a number of tetrahedral

tetrahalocobalt(II) and -nickel(II) species. They ignored the SC contribution, pointing to the early calculations of Ballhausen and Liehr [21] whose electrostatic modelling led to calculated oscillator strengths some two or three orders of magnitude smaller than experiment. Instead, they computed intensities just within the DC model of Mason, Peacock and Stewart [26]. Taking metal charges at the ionic limit of M^{2+}, Gale *et al.* [47] calculated intensities within a factor of about two of the experimental values and also showed that they had a further factor of 4.3 in hand should the metal atoms be given zero charge as a result of covalent bonding. As they put it, allowance for the nephelauxetic effect could bring calculated and experimental intensities into close correspondence. This agreement refers to overall intensity, by the way, for their reproduction of the intensity distribution was rather less good. Again, this is reminiscent of the quality of fit that had been generally achieved for lanthanoid spectra. Nevertheless, the point here is that the DC approach used in a near-non-parametric manner, was essentially equally as successful in (this example, at least) the *d* block as in the *f*. Given our general proposition that "mean" '*d*–*d*' intensities are some 200 times stronger than "mean" '*f*–*f*', it is of interest to pinpoint theoretically the main sources of this difference within the DC, independent-systems modelling that has been used in both types of system.

For this, we refer to the bipolar expansion of the coulombic perturbation, $V^{(0)}_{ML}$, given in Eqs. (61)–(64). Let us consider the determinants of its magnitude as between a single M–L bond in a lanthanoid complex and one of the first *d* period, and with common ligand, L. Differences therefore relate to the metal multipole Eq. (63) and the geometric tensor Eq. (64). As shown earlier by Mason *et al.* [26], it is the quadrupole term ($\lambda = 2$) which contributes most to the DC process. Within final expressions for the intensity we must compare squares of r_{iM} and R^{-4}_{ML}. Values of $\langle 4f|r^2|4f\rangle$ for lanthanoid ions are not very different from those of $\langle 3d|r^2|3d\rangle$ for the first row *d*-block ions; they are within a factor of two of one another, depending upon the particular ions considered. Metal–ligand bond lengths might be 25% greater in the *f* series (for Ln–Cl, say, 2.9 Å might be typical; for Co^{II}–Cl, 2.5 Å). So $R^8_{ML}(Co)/R^8_{ML}(Ln)$ is of the order 5–10, say. Overall, therefore, an increase in intensity from the DC mechanism due to the intrinsic properties of the metal and bond-length on replacing a lanthanoid complex by a first-row, main transition block complex is unlikely to be by more than a factor of 20, and quite probably by considerably less. Yet Gale et al. [47] were readily able to model the '*d*–*d*' intensities in $[CoCl_4]^{2-}$ and similar ions. What, therefore, is responsible for the significantly greater intensities in '*d*–*d*' spectra? As mentioned several times throughout this article, our focus on mechanism should not blind us to the role of geometry. The point here is that most, though not all, commonly studied lanthanoid complexes approximate the tricapped, trigonal prismatic geometry of the nonahydrate. For these, the summation of contributions from separate ligations results in a significant degree of cancellation within the effective transition dipole moment operator and hence intensities. Intensities calculated for the four-coordinate *d* electron chromophore of our present choice decrease rapidly and non-linearly as that geometry is changed from tetrahedral to square planar, for example. All in all, therefore, our general perception that '*d*–*d*' intensities are much greater than '*f*–*f*' is owed in large

measure to our making comparisons between systems with very different coordination geometries, and, of course, to the more even intensity distributions over many more transitions in the *f* electron systems. Overall, therefore, we might expect rather similar models and mechanisms to be relevant in the two types of chromophore.

We anticipate one exception to this generalization; this concerns magnetic dipole transitions. Subject to the detailed nature of the transition considered, these are potentially fully allowed within open *d* or *f* shells. Their intensities can be well estimated without recourse to configurational mixing. On average, it is to be expected that magnetic dipole intensities will be somewhat smaller in the *d* block than in the *f* (essentially due to the decrease of the azimuthal quantum number from $\ell = 3$ to $\ell = 2$). Given the rather greater intensities due to the forced electric dipole mechanisms, one expects, therefore, that the neglect of magnetic dipole intensities for non-circularly dichroic spectroscopy should be acceptable. Accordingly, we do not consider them further in this article.

We turn at last to the CLF model that we have developed over the past decade or so and which has been successfully applied to more than 40 '*d*–*d*' spectra. The model considers forced, electric dipole transitions only and incorporates the concepts of a parametric, effective transition moment operator, and of a ligation superposition tailored closely to general concepts of bonding established elsewhere throughout chemistry.

5. The cellular ligand-field model for acentric chromophores

The remainder of the present article addresses our CLF model as applied so far to '*d*–*d*' spectra; it is divided into two main parts. The first concerns acentric chromophores in which forced electric dipole transitions acquire intensity through parity mixing that is permanently established by the coordination environment. We refer to this as the CLF *static* model [11]; not to be confused with the static coupling mechanism of the previous pages. Later, in Section 6, we shall consider a CLF *vibronic* model [12] directed towards centric chromophores in which the necessary parity mixing is established by appropriate *ungerade* vibrational modes. The possibility of intensity arising from both static and dynamic sources in near-centric environments will also be considered in the Section 6. The "vibronic" model shares a common structure and parametrization scheme with the "static" model.

The CLF approach possesses three main characteristics. Firstly, it exploits the concept of an effective, even-parity, transition moment operator acting within a pure *d* basis, as first described by Judd [22] and later generalized by Newman and Balasubramanian [24]. Secondly, it employs the principle of spatial superposition as also formalized by the latter workers and carried forward by the Mason and Richardson groups in both the lanthanoid and main transition series. Thirdly, and crucially characteristic of the CLF approach, is a parametrization of each local ligation's contribution to forced electric dipole moments in a manner that reflects chemical functionality. Thus, a recognition of the σ and π character of local metal–ligand bonding is built into the model from the outset.

In view of our remarks about the, essentially incalculable, role of covalency — about which more in due course — the CLF model is parametric and so addresses intensity distributions rather than absolute oscillator strengths by any *ab initio* route. The aim, then, is to construct a description of relative '*d–d*' intensities from the computation of electric dipole transition moments within a pure d ($\ell = 2$) basis using even-parity, effective operators. These are constructed for the complete, "global" chromophore as multipole expansions. The global multipole coefficients are built by superposition of analogous "local" multipole expansions which refer to transition moment contributions from each ligation. In turn, the local multipole coefficients are expressed in terms of local transition dipole moments that define the intrinsic model parameters. Our presentation conveniently begins with the definition of the CLF intensity parameters, proceeding stepwise to a global description of the approach that effectively corresponds to the starting point of the work of Judd [22] or of Newman and Balasubramanian [24] for the f electron systems. First, however, we remind the reader of the character of cellular ligand-field theory in its broader context.

5.1. *Cellular ligand-field theory and ligand-field orbitals*

The CLF model derived from attempts by Gerloch and Woolley [5–8] to comprehend the successes of earlier ligand-field studies of transition energies and magnetic properties in transition metal complexes. The central idea was to trace a linkage between the well-established structures of quantum chemistry at large and those, rather *ad hoc*, procedures of ligand field theory. In so doing, the sources of the effective ligand-field potential were identified and a qualitative understanding of the chemical significance of ligand-field parameters was established. These latter features for d electron energies have been reviewed in considerable detail recently [9]. It is therefore inappropriate to repeat that material in this article. Our remarks in the present section draw freely from that review and the earlier work of Gerloch and Woolley [5–8].

As ligand-field parameters are one-electron integrals, we focus on a one-electron hamiltonian H comprising, as usual, a sum of kinetic and potential energy terms, i.e. T and U, respectively. Let U be taken as that formally established by density functional theory for the molecular ground state. Then orbital eigenvectors ξ of $H = T + U$ satisfy the condition that molecular groundstate electron densities are given by the simple sum $\Sigma_i \xi_i \xi_i$ over populated orbitals without additional terms for exchange and correlation. In this regard, the $\{\xi\}$ may be regarded as "best" orbitals for the molecular groundstate [48,49]. In practice, of course, they are as difficult to calculate as by other *ab initio* schemes. The parametric nature of ligand-field theory recognizes this unfortunate but overarching difficulty. The molecular hamiltonian, H, includes *all* relevant determinants of the ground state density, of course. Now ligand-field procedures conventionally separate *d–d* from *d*–other interactions, in the manner of Eq. (1). To mimic that construction, we replace $U(\rho)$, which is a functional of the total electron density in the groundstate, by $V(\rho - \rho_d)$, a functional of all groundstate density except that of the d electrons. The d orbitals are defined

(cyclically) in a moment. We then define *ligand-field orbitals*, ψ^{LFO}, as solutions to the equation:

$$(\mathscr{H} - E_n)\psi_n = 0 \tag{83}$$

with

$$\mathscr{H} = T + V \tag{84}$$

The $\{\psi\}$ may be written as linear combinations of fragment orbitals, but, unlike the familiar LCAO molecular orbital formalism, we choose fragment orbitals that refer to $\mathscr{H}$ divided into its mean spherical — and aspherical — components:

$$\mathscr{H} = \mathscr{H}^{(0)} + \mathscr{H}^{(1)}, \tag{85}$$

corresponding to the functional V being divided into its spherical, $\langle V \rangle$, and aspherical, V', parts:

$$V = \langle V \rangle + V'. \tag{86}$$

Solutions for

$$H^{(0)}\phi = (T + \langle V \rangle)\phi = \epsilon\phi \tag{87}$$

are of the usual central-field type with angular parts which may be labelled by the letters, *s*, *p*, *d*, *f*... It is the electron density associated with these *d* orbitals which was notionally subtracted in $V(\rho - \rho_d)$. Furthermore, it is these same *d* orbitals that form the "pure" *d* orbital basis employed within all ligand-field calculations. Their radial form is generally unknown to us because the foregoing procedure is merely formal. However, that form is dictated by the mean of the total molecular hamiltonian constructed for the groundstate. It differs from complex to complex. Its variability includes all consequences of covalency throughout the complex including those arising from the nephelauxetic effect: the latter also affects the two-electron *d–d* interactions of course. Overall, then, the solutions for Eq. (84) are written as

$$\psi^{LFO} = c_d\phi_d + c_r\phi_r, \tag{88}$$

in which ϕ_d are appropriate "mean" *d* orbitals ["mean" because they span the "mean" or spherical hamiltonian, $H^{(0)}$, in Eq. (87)], and ϕ_r comprise all other functions required to span the rest of $\mathscr{H}^{(0)}$ as well as of $\mathscr{H}^{(1)}$. These "rest" functions (meaning "remaining") include all metal-originating functions (other than the basis *d* orbitals) plus all ligand-originating functions. Once again, the *complete* molecular hamiltonian for the molecular groundstate has been included in their formal definition.

The significance of the adjective "mean" must be extended, however. In order to regenerate the empirical efficacy of the ligand-field method in which the same ligand-field hamiltonian Eq. (1) is employed throughout the ligand-field domain (the open *d* shell), we must assume that the "best" orbitals defined by density functional theory for the groundstate will suffice also for all ligand-field states or, perhaps, that

these best orbitals are to be taken as some average over best orbitals for each ligand-field state. The mean is defined by the system, not by us.

Subsequent parametric calculation of *d* orbital energies and other properties in terms of the pure, "mean", *d* orbital basis, together with interpretation in terms of the ligand-field orbitals, ψ^{LFO}, of Eq. (90) thus includes *all* the "spherical" (central–field) *d–d* interactions, conventionally parametrized within the Condon–Shortley, F_k, or Racah schemes. It is to be emphasized that the parametric nature of all ligand-field calculations is forced by our quantitative ignorance of the detailed consequences of the primary bonding within a complex. Both the exact radial form of the basis *d* orbitals [ϕ_d in Eq. (90)] — which will assuredly differ from that in the corresponding free metal ion — and the detailed form of the "rest" orbitals, ϕ_r, are unknown and their characteristics must be subsumed within the system parameters. Parametric ligand-field models, including those for spectral intensities, therefore excuse us from the enormously difficult task of computing the primary bonding in object molecules. The best we can hope for, apart from good reproduction of observed ligand-field properties, is a semi-quantitative understanding of emerging parameter values in terms of broad-based chemical concepts. For '*d–d*' intensities, we discuss this in due course.

5.2. P, F *and* R *contributions*

The *cellular* ligand-field model refers to a spatial superposition of the ligand-field over disjoint regions of space we call *cells*. Usually, and for our present purposes always, each cell encloses one ligation.

Let us partition the global ligand-field orbitals, ψ^{LFO} described in the preceding section, into local, cellular orbitals $\{\psi_\lambda\}$ which may be taken as real without loss of generality. For cell *c*, we write [11]:

$$\psi_\lambda^c = N_\lambda(d_\lambda^c + b_\lambda^c \phi_\lambda^c), \tag{89}$$

where *d* [$\equiv \phi_d$ in Eq. (88)] is the (metal-centred) mean *d* orbital and ϕ describes the "rest" orbitals (metal non-*d* plus all ligand functions, including those from all other ligands if, after bond formation, they contribute to the region of cell, *c*). Following recognition of the efficacy of ligand-field theory and its implications for the near uncoupling of *d* orbitals from the rest, as described in full elsewhere [5–9], we shall approximate the normalization constant N_λ as unity. In order to forge a close link with conventional views of chemical bonding, functions are labelled by λ according to classifications in terms of real, Cartesian *d* parentage, or with respect to local $C_{\infty v}$ or C_{2v} ligation *pseudo*symmetry:

$$\lambda = \{z^2, xz, yz, xy, x^2-y^2\};\ \text{or}\ \{\sigma\ \pi\ \delta\},\ C_{\infty v};\ \text{or}\ \{\sigma, \pi x, \pi y, \delta xy, \delta x^2-y^2\},\ C_{2v}. \tag{90}$$

The mixing coefficients b_λ are set to zero in the case of local δ interaction as is common practice in CLF energy analysis.

The $\{\phi_\lambda\}$ of Eq. (89) include ligand-centred components. We form equivalent

cellular orbitals all of whose constituents are referred to the metal atom: this is notionally achieved *via* a two-centre, multipole expansion:

$$\psi^c_{z^2} = d^c_{z^2} + \sum_{\ell} a^c_{\ell\sigma}{}^{\ell}\chi^c_{\sigma}$$

$$\psi^c_{xz} = d^c_{xz} + \sum_{\ell} a^{\ell}{}_{\pi x}{}^{\ell}\chi^c_{\pi x}$$

$$\psi^c_{yz} = d^c_{yz} + \sum_{\ell} a^c_{\ell xy}{}^{\ell}\chi^c_{\pi y}$$

$$\psi^c_{xy} = d^c_{xy}$$

$$\psi^c_{x^2-y^2} = d^c_{x^2-y^2}. \tag{91}$$

The index ℓ labels the azimuthal quantum number of the angular parts of those non-*d* functions originating either on the metal or, *via* the two-centre multipole expansion, on the ligand. The mixing coefficients $\{a\}$ subsume the $\{b\}$ of Eq. (89).

Matrix elements of the electric dipole operator $e\mathbf{r}$, in this basis of cellular orbitals, each comprise three parts:

$$e\langle\psi^c_{\lambda}(r)|r^c|\psi'^c_{\lambda'}(r)\rangle = k^c|\langle\hat{d}^c_{\lambda}|\hat{r}^c|\hat{d}'^c_{\lambda'}\rangle \qquad \text{I}$$

$$\left.\begin{aligned} &+\sum_{\ell'} \bar{a}^c_{\ell'\lambda'}\langle\hat{d}^c_{\lambda}|\hat{r}^c|^{\ell'}\hat{\chi}'^c_{\lambda'}\rangle \\ &+\sum_{\ell} \bar{a}^c_{\ell\lambda}\langle^{\ell}\hat{\chi}^c_{\lambda}|\hat{r}^c|\hat{d}^c_{\lambda'}\rangle \end{aligned}\right\} \qquad \text{II}$$

$$+\sum_{\ell}\sum_{\ell'} {}^{\ell\ell'}k^c_{\lambda\lambda'}\langle^{\ell}\hat{\chi}^c_{\lambda}|\hat{r}^c|^{\ell'}\hat{\chi}'^c_{\lambda'}\rangle. \qquad \text{III} \tag{92}$$

in which radial and angular quantities are separated using the notation, $\mathbf{r} \equiv r\hat{r}$, and all radial parts are sequestered into the coefficients

$$k^c \equiv e\langle d^c(r)|r^c|d'^c(r)\rangle,$$

$$\bar{a}^c_{\ell\lambda} \equiv e a^c_{\ell\lambda}\langle d(r)|r^c|^{\ell}\chi'^c_{\lambda}(r)\rangle,$$

and

$${}^{\ell\ell'}k^c_{\lambda\lambda'} \equiv e a^c_{\ell\lambda} a^c_{\ell'\lambda'}\langle^{\ell}\chi^c_{\lambda}(r)|r^c|^{\ell'}\chi'^c_{\lambda'}(r)\rangle, \tag{93}$$

and where all functions and operators are referred to the metal atom as origin; all *d* functions have a common radial form.

The matrix elements Eq. (92) are local electric dipole transition moments and provide the basis of the parametrization scheme in our CLF model. The electric-dipole selection rule, $\Delta\ell = \pm 1$, removes term I in Eq. (92) as a source of intensity. It similarly establishes that terms II make contributions only for ℓ, $\ell' = 1$ or 3: henceforth, we refer to these as *P* and *F* contributions, respectively. In term III, a double, infinite sum remains, even though $|\ell - \ell'|$ must be unity, and we label

intensity deriving purely from the "rest" functions $\{\chi_\lambda\}$ collectively as the R contribution.

5.3. *Parametrized local transition moments*

The CLF model [11] is developed for local ligation *pseudo*symmetry C_{2v}. This is sufficiently general at this stage in that it relates (a) directly to interactions between metal and ligands like pyridine where π bonding properties parallel and perpendicular to the ring plane may differ; and (b) indirectly, to bonding with so-called "linear" ligators like the halogens where the relationship $\pi x = \pi y$ raises the local symmetry to $C_{\infty v}$. Extension of the model to local C_s symmetry or less is discussed later under "misdirected valency". In C_{2v} symmetry, components of the radius vector $\mathbf{r}$, and of the d_λ and χ_λ parts of the cellular orbitals transform as shown in Table 7; δ-type non-d functions are omitted as before. Explicit angular forms of all relevant operators and functions required are given in Eq. (94):

$$
\begin{aligned}
\hat{r}_z &= C_0^{(1)} \\
\left.\begin{aligned}\hat{r}_x &= (C_{-1}^{(1)} - C_1^{(1)})/\sqrt{2} \\ \hat{r}_y &= i(C_{-1}^{(1)} + C_1^{(1)})/\sqrt{2}\end{aligned}\right\} & C_q^{(k)} = [4\pi/(2k+1)]^{1/2}\, Y_q^{(k)} \\
\hat{d}_{z^2} &= Y_0^{(2)} \\
\hat{d}_{xz} &= (Y_{-1}^{(2)} - Y_1^{(2)})/\sqrt{2} \\
\hat{d}_{yz} &= i(Y_{-1}^{(2)} + Y_1^{(2)})/\sqrt{2} \\
\hat{d}_{xy} &= i(Y_{-2}^{(2)} - Y_2^{(2)})/\sqrt{2} \\
\hat{d}_{x^2-y^2} &= (Y_{-2}^{(2)} + Y_2^{(2)})/\sqrt{2} \\
{}^{\ell}\hat{\chi}_\sigma &= Y_0^{(\ell)} \\
\left.\begin{aligned}{}^{\ell}\hat{\chi}_{\pi x} &= (Y_{-1}^{(\ell)} - Y_1^{(\ell)})/\sqrt{2} \\ {}^{\ell}\hat{\chi}_{\pi y} &= i(Y_{-1}^{(\ell)} + Y_1^{(\ell)})/\sqrt{2}\end{aligned}\right\} & \ell \text{ odd.}
\end{aligned}
\tag{94}
$$

These functions, together with the neglect of δ mixing in the cellular orbitals and by noting the selection rules implicit in Table 7, yield a reduction to just nine, unique non-zero matrix elements under $\mathbf{r}$ from the possible total 45, as shown in Table 8.

Table 7
Transformation properties of components of the radius vector r and of metal d and local ligand orbitals

C_{2v} irrep.	r_α	d_λ	χ_λ
a_1	z	z^2, x^2-y^2	σ
a_2		xy	
b_1	x	xz	πx
b_2	y	yz	πy

Table 8
Occurrence of non-zero transition moments in local C_{2v} symmetry

	z^2	xz	yz	xy	x^2-y^2
z^2	r_z	r_x	r_y	0	0
xz	r_x	r_z	0	r_y	r_x
yz	r_y	0	r_z	r_x	r_y
xy	0	r_y	r_x	0	0
x^2-y^2	0	r_x	r_y	0	0

Thus, $\langle xy|\hat{r}|xy\rangle$ and $\langle x^2-y^2|\hat{r}|x^2-y^2\rangle$ vanish following the neglect of δ mixing; $\langle xy|\hat{r}|z^2\rangle$ and $\langle x^2-y^2|\hat{r}|z^2\rangle$ because r does not connect functions with m_ℓ values differing by more than unity; and the symmetry properties summarized in Table 7 ensure that $\langle yz|\hat{r}|xz\rangle$ also vanishes and, further, that all remaining non-zero elements are mutually exclusive with respect to the components of $\mathbf{r}$.

To evaluate the local matrix elements on the LHS of Eq. (92), we first consider contributions of type II. Using the standard formula [8] for the evaluation of angular integrals:

$$\langle k'q'|C_Q^{(K)}|kq\rangle = (-1)^{q'}[(2k'+1)(2k+1)]^{1/2}\begin{pmatrix} k' & K & k \\ -q' & Q & q \end{pmatrix}\begin{pmatrix} k' & K & k \\ 0 & 0 & 0 \end{pmatrix} \tag{95}$$

we find, for example, that

$$\langle d_{z^2}|er_z|\chi_\sigma\rangle = \left(\frac{4}{15}\right)^{1/2} a^c_{1\sigma} + \left(\frac{9}{35}\right)^{1/2} a^c_{3\sigma} \tag{96}$$

or that

$$\langle d_{xz}|er_z|\chi_{\pi x}\rangle = \left(\frac{1}{5}\right)^{1/2} a^c_{1\pi x} + \left(\frac{8}{35}\right)^{1/2} a^c_{3\pi x}. \tag{97}$$

Eleven such integrals arise and are listed in Table 9.

Combination of these integrals within Eq. (92) then yields the matrix elements we require. For example,

$$\langle z^2|er_z|z^2\rangle = 2\left(\frac{4}{15}\right)^{1/2} a^c_{1\sigma} + 2\left(\frac{9}{35}\right) a^c_{3\sigma} + \sum_{\ell,\ell'} k^c_{\sigma\sigma}\langle \ell^c\chi^c_\sigma|r_z|\ell'^c\chi^c_\sigma\rangle, \tag{98}$$

the first two terms describing the P and F contributions to II in Eq. (92) and the third, the R contributions of III. We now define the basic parameters of the CLF model as:

$${}^L\tilde{t}_\lambda = e\langle d^c_\lambda(r)|r^c|a^c_{\ell\lambda}(r)^\ell\chi^c_\lambda(r)\rangle\langle \hat{d}^c_\lambda|\hat{r}^c_z|^\ell\chi^c_\lambda\rangle; \quad L = P, F \tag{99}$$

and

$${}^R\tilde{t}_\lambda = e\sum_{\ell,\ell'} a^c_{\ell\lambda}a^c_{\ell'\lambda'}\langle \ell^c\chi^c_\lambda(r)|r^c|\ell'^c\chi^c_{\lambda'}(r)\rangle\langle \ell^c\chi^c_\lambda|\hat{r}^c_z|\ell'^c\chi^c_{\lambda'}\rangle. \tag{100}$$

Table 9
Non-zero local transition moments in C_{2v} symmetry

$$\langle d_{z^2}|r_z|\chi_\sigma\rangle = \left(\frac{4}{15}\right)^{1/2} \tilde{a}_{1\sigma} + \left(\frac{9}{35}\right)^{1/2} \tilde{a}_{3\sigma}$$

$$\langle d_{xz}|r_z|\chi_{\pi x}\rangle = \left(\frac{1}{5}\right)^{1/2} \tilde{a}_{1\pi x} + \left(\frac{8}{35}\right)^{1/2} \tilde{a}_{3\pi x}$$

$$\langle d_{yz}|r_z|\chi_{\pi y}\rangle = \left(\frac{1}{5}\right)^{1/2} \tilde{a}_{1\pi y} + \left(\frac{8}{35}\right)^{1/2} \tilde{a}_{3\pi y}$$

$$\langle d_{z^2}|r_z|\chi_{\pi x}\rangle = -\left(\frac{1}{15}\right)^{1/2} \tilde{a}_{1\pi x} + \left(\frac{6}{35}\right)^{1/2} \tilde{a}_{3\pi x}$$

$$\langle d_{x^2-y^2}|r_x|\chi_{\pi x}\rangle = \left(\frac{1}{5}\right)^{1/2} \tilde{a}_{1\pi x} - \left(\frac{1}{70}\right)^{1/2} \tilde{a}_{3\pi x}$$

$$\langle d_{xy}|r_x|\chi_{\pi y}\rangle = \left(\frac{1}{5}\right)^{1/2} \tilde{a}_{1\pi y} - \left(\frac{1}{70}\right)^{1/2} \tilde{a}_{3\pi y}$$

$$\langle d_{xz}|r_x|\chi_\sigma\rangle = \left(\frac{1}{5}\right)^{1/2} \tilde{a}_{1\sigma} - \left(\frac{3}{35}\right)^{1/2} \tilde{a}_{3\sigma}$$

$$\langle d_{z^2}|r_y|\chi_{\pi y}\rangle = -\left(\frac{1}{15}\right)^{1/2} \tilde{a}_{1\pi y} + \left(\frac{6}{35}\right)^{1/2} \tilde{a}_{3\pi y}$$

$$\langle d_{x^2-y^2}|r_y|\chi_{\pi y}\rangle = -\left(\frac{1}{5}\right)^{1/2} \tilde{a}_{1\pi y} + \left(\frac{1}{70}\right)^{1/2} \tilde{a}_{3\pi y}$$

$$\langle d_{xy}|r_y|\chi_{\pi x}\rangle = \left(\frac{1}{5}\right)^{1/2} \tilde{a}_{1\pi y} - \left(\frac{1}{70}\right)^{1/2} \tilde{a}_{3\pi x}$$

$$\langle d_{yz}|r_y|\chi_\sigma\rangle = \left(\frac{1}{5}\right)^{1/2} \tilde{a}_{1\sigma} - \left(\frac{3}{35}\right)^{1/2} \tilde{a}_{3\sigma}$$

Following this, referring to Eq. (93), we express Eq. (98) as:

$$\langle z^2|er_z|z^2\rangle = 2^P\tilde{t}_\sigma + 2^F\tilde{t}_\sigma + {}^R\tilde{t}_\sigma. \tag{101}$$

Similarly,

$$\langle xz|er_z|xz\rangle = 2\left(\frac{1}{5}\right)^{1/2} \tilde{a}^c_{1\pi x} + 2\left(\frac{8}{35}\right)^{1/2} \tilde{a}^c_{3\pi x} + \sum_{\ell,\ell'} {}^{\ell\ell'}k^c_{\pi x,\,\pi x}\langle {}^\ell\chi^c_{\pi x}|r_z|{}^{\ell'}\chi'^c_{\pi x}\rangle$$

$$= 2^P\tilde{t}^c_{\pi x} + 2^F\tilde{t}^c_{\pi x} + {}^R\tilde{t}^c_{\pi x}, \tag{102}$$

and

$$\langle yz|er_z|yz\rangle = 2^P\tilde{t}_{\pi y} + 2^F\tilde{t}_{\pi y} + {}^R\tilde{t}_{\pi y}. \tag{103}$$

A further simplification is introduced in the expansion of the remaining six off-diagonal elements in Table 8. Consider, for instance, the element $\langle xz|er_x|z^2\rangle$:

$$\langle xz|er_x|z^2\rangle = \left(\frac{1}{5}\right)^{1/2} \tilde{a}^c_{1\sigma} - \left(\frac{1}{5}\right)^{1/2} \tilde{a}^c_{1\pi y} - \left(\frac{3}{35}\right)^{1/2} \tilde{a}^c_{3\sigma} + \left(\frac{6}{35}\right)^{1/2} \tilde{a}^c_{3\pi y}$$

$$+ \sum_{\ell,\ell'} {}^{\ell\ell'}k^c_{\pi x,\,\sigma}\langle {}^\ell\chi^c_{\pi x}|r_x|{}^{\ell'}\chi'^c_\sigma\rangle \tag{104}$$

The first four terms arise from parity mixing contributions of the form $\langle d_{xz}|er_x|\chi_\sigma\rangle$ and $\langle\chi_{\pi x}|er_x|d_{z^2}\rangle$, factors already contained within the definitions of ${}^{P}t_\lambda$ and ${}^{F}t_\lambda$. The last term in Eq. (104), however, is new and will be different for each of the six off-diagonal matrix elements in Table 8. In order to minimize the degree of parametrization in the CLF model, we neglect all contributions of this kind; that is, all terms of type III in Eq. (92) for which $\lambda \neq \lambda'$. Support for this stratagem also derives from the following observations.

We express the cellular orbitals in terms of metal-centred and ligand-centred parts:

$$\psi_\lambda = M_\lambda + c_\lambda L_\lambda \tag{105}$$

once more setting the normalization coefficient to unity. Non-zero components of the L type transition moment in the local bond direction may be expanded as:

$$\langle L_\lambda|r_z(M)|L_\lambda\rangle = \langle L_\lambda|R|L_\lambda\rangle + c_\lambda^2\langle L_\lambda|rz(L)|L_\lambda\rangle, \tag{106}$$

where R is the local M–L bond length and r_z(M) and r_z(L) are the z components of the transition electric dipole moment operator (in units of e) referred to metal and ligand centres, respectively. As the c_λ are presumed to be small in ligand-field orbitals (in line with our approximating the normalization coefficient to unity), it is apparent that the $\langle L_\lambda|r_z(\mathrm{M})|L_\lambda\rangle$ are dominated by $\langle L_\lambda|R|L_\lambda\rangle$. For the corresponding moments in directions perpendicular to the bond, we have:

$$\langle L_\lambda|r_\perp(\mathrm{M})|L_{\lambda'}\rangle = c_\lambda c_{\lambda'}\langle L_\lambda|r_\perp(\mathrm{L})|L_{\lambda'}\rangle \tag{107}$$

because $\langle L_\lambda|R|L_{\lambda'}\rangle = R\delta_{\lambda\lambda'} = 0$ when $\lambda \neq \lambda'$ as required for $r_x \neq r_z$. Hence, the neglect of contributions of the type Eq. (107) is justified if $c_\lambda c_{\lambda'}\langle L_\lambda|r_\perp(\mathrm{L})|L_{\lambda'}\rangle \ll R$. Accordingly, type III contributions to Eq. (92) are neglected for light components in local x and y directions.

Following this simplification, Eq. (104) reduces to:

$$\langle xz|er_x|z^2\rangle = \left(\frac{1}{3}\right)^{1/2}\left(\frac{3}{2}{}^{P}\tilde{t}_\sigma - {}^{P}\tilde{t}_{\pi y}\right) + \left(\frac{1}{3}\right)^{1/2}\left(\frac{3}{2}{}^{F}\tilde{t}_{\pi y} - {}^{F}\tilde{t}_\sigma\right). \tag{108}$$

The completed list of non-zero local transition matrix elements in Table 8, evaluated in this way, is given in Table 10. That no intrinsic parameters need be defined with respect to r_x or r_y arises from the explicit evaluation of appropriate angular integrals using Eq. (97).

In passing, we note that all analogous P and F contributions to matrix elements under r_x and r_y are opposed; for example, the signs with ${}^{P}\tilde{t}_\sigma$ and ${}^{F}\tilde{t}_\sigma$ are opposite in $\langle xz|er_x|z^2\rangle$. This may be unexpected; that the algebra of the angular integrals *via* Eq. (95), which yielded these signs, is correct, however, is confirmed by the following pictorial argument. Consider the contribution $\langle d_{xz}|er_x|\chi_\sigma\rangle$ to the matrix element $\langle xz|er_x|z^2\rangle$; in particular, the operation of r_x upon χ_σ. The only parts of χ_σ which are relevant for the present purposes are p_σ and f_σ referred to the metal centre. The action of r_x upon p_σ is shown in Fig. 9(a) and upon f_σ in Fig. 9(b). The phasing of $r_x p_\sigma$ exactly matches that of d_{xz}, so yielding a positive value for $\langle d_{xz}|r_x|{}^{p}\chi_\sigma\rangle$. However, the amplifying nature of the r_x operator — multiplying more distant (greater x) parts of a χ function more than less distant parts — means that the "secondary"

Table 10
Non-zero, forced electric dipole transition moments for a ligation with local C_{2v} pseudosymmetry expressed in terms of the intrinsic parameter set ${}^{L}t_{\lambda}$; $L=P, F, R$; $\lambda=\sigma, \pi x, \pi y$

$$\langle z^2|er_z|z^2\rangle = 2{}^{P}\tilde{t}_{\sigma} + 2{}^{F}\tilde{t}_{\sigma} + {}^{R}\tilde{t}_{\sigma}$$
$$\langle xz|er_z|xz\rangle = 2{}^{P}\tilde{t}_{\pi x} + 2{}^{F}\tilde{t}_{\pi x} + {}^{R}\tilde{t}_{\pi x}$$
$$\langle yz|er_z|yz\rangle = 2{}^{P}\tilde{t}_{\pi y} + 2{}^{F}\tilde{t}_{\pi y} + {}^{R}\tilde{t}_{\pi y}$$
$$\langle xz|er_x|z^2\rangle = \left(\frac{1}{3}\right)^{1/2}\left(\frac{3}{2}{}^{P}\tilde{t}_{\sigma} - {}^{P}\tilde{t}_{\pi x}\right) + \left(\frac{1}{3}\right)^{1/2}\left(\frac{3}{2}{}^{F}\tilde{t}_{\pi x} - {}^{F}\tilde{t}_{\sigma}\right)$$
$$\langle yz|er_y|z^2\rangle = \left(\frac{1}{3}\right)^{1/2}\left(\frac{3}{2}{}^{P}\tilde{t}_{\sigma} - {}^{P}\tilde{t}_{\pi y}\right) + \left(\frac{1}{3}\right)^{1/2}\left(\frac{3}{2}{}^{F}\tilde{t}_{\pi y} - {}^{F}\tilde{t}_{\sigma}\right)$$
$$\langle x^2-y^2|er_x|xz\rangle = {}^{P}\tilde{t}_{\pi x} - \frac{1}{4}{}^{F}\tilde{t}_{\pi x}$$
$$\langle x^2-y^2|er_y|yz\rangle = -{}^{P}\tilde{t}_{\pi y} + \frac{1}{4}{}^{F}\tilde{t}_{\pi y}$$
$$\langle xy|er_y|xz\rangle = {}^{P}\tilde{t}_{\pi x} - \frac{1}{4}{}^{F}\tilde{t}_{\pi x}$$
$$\langle xy|er_x|yz\rangle = {}^{P}\tilde{t}_{\pi y} - \frac{1}{4}{}^{F}\tilde{t}_{\pi y}$$

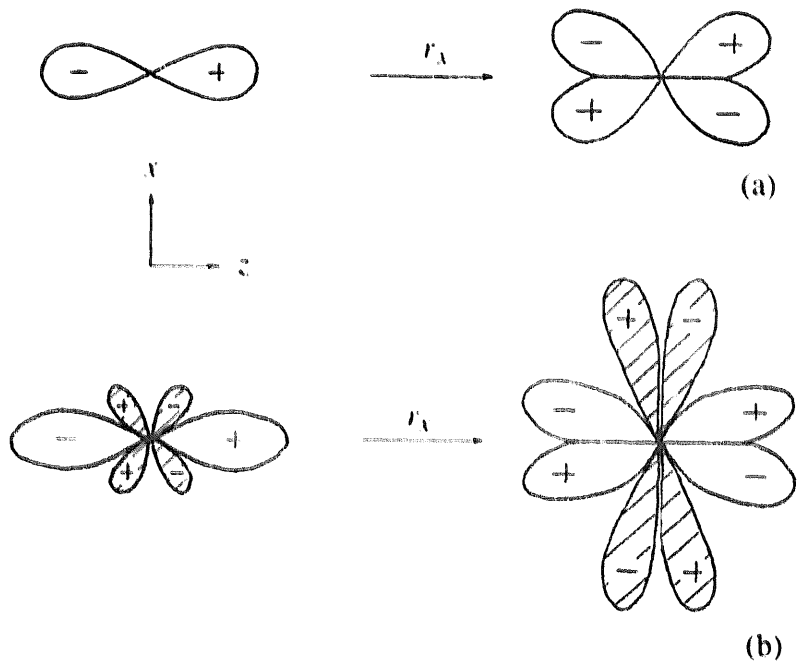

Fig. 9. (a) The results of operating with r_x upon p_z orbital and (b) upon an f_{z^3} orbital.

lobes of the f_{σ} function (shown hatched) are amplified more than the "primary" lobes directed about the z axis. Subsequent overlap of $r_x f_{\sigma}$ with d_{xz} is now dominated by the amplified, "secondary" lobes of $r_x f_{\sigma}$ whose phasing is opposite to that of d_{xz} and a negative value for $\langle d_{xz}|r_x|^{f}\chi_{\sigma}\rangle$ results.

The matrix elements in Table 9 are all expressed within the local cellular orbital basis. We now consider their equivalents within a pure d basis.

5.4. Local multipole expansion within a pure *d* basis

We seek to replace the odd-parity, electric dipole operators er^c_α acting within the mixed-parity, cellular orbitals ψ^{LFO} by effective, even-parity operators, eT^c_α, acting within the equivalent, locally-referred, pure *d* orbital basis:

$$\langle \psi^c_i | er^c_\alpha | \psi^c_j \rangle \equiv \langle d^c_i | eT^c_\alpha | d^c_j \rangle; \quad \alpha = x, y, x. \tag{109}$$

As the $\{\psi\}$ were defined in Cartesian form, as in Eq. (90), so also are the pure *d* functions in Eq. (109). Following this, by reference to Table 9, we have, for example:

$$\langle d_{z^2} | eT_z | d_{z^2} \rangle = 2^P \tilde{t}_\sigma + 2^F \tilde{t}_\sigma + {}^R\tilde{t}_\sigma. \tag{110}$$

This, and analogous expressions are listed in Table 11 but in a manner which separates the *P*, *F* and *R* types.

We now form three multipole expansions of the $\{T^c_\alpha\}$:

$$T^c_\alpha = \sum_{k,q} \omega^c_{kq\alpha}(r) C^{(k)}_q; \quad \alpha = x, y, z \tag{111}$$

in which the $\{C^{(k)}\}$ are spherical tensor operators of rank *k*. Writing the pure, Cartesian *d* functions on the right-hand side of Eq. (109) and of Table 11 as $\{R(d)\cdot\hat{d}\}$, we consider the matrix elements:

$$\begin{aligned}\langle d^c_i | eT^c_\alpha | d^c_j \rangle &= \langle R(d)\hat{d}_i | \sum_{kq} e\omega^c_{kq\alpha}(r) C^{(k)}_q | R(d)\hat{d}_j \rangle \\ &= \sum_{kq} \langle R(d) | e\omega^c_{kq\alpha}(r) | R(d) \rangle \langle \hat{d}_i | C^{(k)}_q | \hat{d}_j \rangle \\ &= \sum_{kq} c^c_{kq\alpha}(r) \langle \hat{d}_i | C^{(k)}_q | \hat{d}_j \rangle.\end{aligned} \tag{112}$$

The common radial parts of the five *d* functions, $R(d)$, ensure that Eq. (112) is unchanged if the Cartesian *d* functions are replaced throughout by their complex equivalents $|\ell = 2, m_\ell\rangle \equiv d_m$. In this latter form, they are easily evaluated using Eq. (95).

The vector triangle rule implicit in both 3-*j* symbols of Eq. (95) establishes the range of the tensor ranks in Eq. (111). This, together with parity, determines *k* as 2 and 4 only, within a pure *d* basis. The further requirement that $-q' + Q + q = 0$ in the first 3-*j* symbol of Eq. (94) restricts the number of terms in the multipole expansion which can connect any two given basis functions. For example, only $C^{(2)}_1$ and $C^{(4)}_1$ are effective in the *d* matrix elements, $\langle d_2 | eT^c_\alpha | d_1 \rangle$ and $\langle d_1 | eT^c_\alpha | d_0 \rangle$. Using Eq. (97), we find:

$$\langle d_2 | eT^c_\alpha | d_1 \rangle = \frac{1}{7}(6)^{1/2} c^c_{21\alpha}(r) - \frac{1}{21}(5)^{1/2} c^c_{41\alpha}(r) \tag{113}$$

and

$$\langle d_1 | eT^c_\alpha | d_0 \rangle = \frac{1}{7} c^c_{21\alpha}(r) + \frac{1}{21}(30)^{1/2} c^c_{41\alpha}(r). \tag{114}$$

Table 11
Matrices of the effective transition moment operators within the pure Cartesian d basis. Only the lower triangles of the symmetric matrices are listed. Matrix elements with respect to the three spatial components ($\alpha = x, y, z$) of the operators are mutually exclusive

${}^{P}T^{c}_{\alpha}$	d_{z^2}	d_{xz}	d_{yz}	d_{xy}	$d_{x^2-y^2}$
d_{z^2}	$2^{P}\tilde{t}_{\sigma}$				
d_{xz}	$\left(\frac{1}{3}\right)^{1/2}\left(\frac{3}{2}{}^{P}\tilde{t}_{\sigma} - {}^{P}\tilde{t}_{\pi x}\right)$	$2^{P}\tilde{t}_{\pi x}$			
d_{yz}	$\left(\frac{1}{3}\right)^{1/2}\left(\frac{3}{2}{}^{P}\tilde{t}_{\sigma} - {}^{P}\tilde{t}_{\pi y}\right)$	0	$2^{P}\tilde{t}_{\pi y}$		
d_{xy}	0	${}^{P}\tilde{t}_{\pi x}$	${}^{P}\tilde{t}_{\pi y}$	0	
$d_{x^2-y^2}$	0	${}^{P}\tilde{t}_{\pi x}$	$-{}^{P}\tilde{t}_{\pi y}$	0	0

${}^{F}T^{c}_{\alpha}$	d_{z^2}	d_{xz}	d_{yz}	d_{xy}	$d_{x^2-y^2}$
d_{z^2}	$2^{F}\tilde{t}_{\sigma}$				
d_{xz}	$\left(\frac{1}{3}\right)^{1/2}\left(\frac{3}{2}{}^{F}\tilde{t}_{\pi x} - {}^{F}\tilde{t}_{\sigma}\right)$	$2^{F}\tilde{t}_{\pi x}$			
d_{yz}	$\left(\frac{1}{3}\right)^{1/2}\left(\frac{3}{2}{}^{F}\tilde{t}_{\pi y} - {}^{F}\tilde{t}_{\sigma}\right)$	0	$2^{F}\tilde{t}_{\pi y}$		
d_{xy}	0	$-\frac{1}{4}{}^{F}\tilde{t}_{\pi x}$	$-\frac{1}{4}{}^{F}\tilde{t}_{\pi y}$	0	
$d_{x^2-y^2}$	0	$-\frac{1}{4}{}^{F}\tilde{t}_{\pi x}$	$\frac{1}{4}{}^{F}\tilde{t}_{\pi y}$	0	0

${}^{R}T^{c}_{\alpha}$	d_{z^2}	d_{xz}	d_{yz}	d_{xy}	$d_{x^2-y^2}$
d_{z^2}	$2^{R}\tilde{t}_{\sigma}$				
d_{xz}	0	$2^{R}\tilde{t}_{\pi x}$			
d_{yz}	0	0	$2^{R}\tilde{t}_{\pi y}$		
d_{xy}	0	0	0	0	
$d_{x^2-y^2}$	0	0	0	0	0

Solving Eqs. (113) and (114) as a pair of simultaneous equations in $c_{21\alpha}(r)$ and $c_{41\alpha}(r)$ yields:

$$c_{21\alpha}(r) = 6^{1/2}\langle d_2|eT^{c}_{\alpha}|d_1\rangle + \langle d_1|eT^{c}_{\alpha}|d_0\rangle \tag{115}$$

and

$$c_{41\alpha}(r) = 3\left(\frac{1}{5}\right)^{1/2}\left[-\langle d_2|eT^{c}_{\alpha}|d_1\rangle + 6^{1/2}\langle d_1|eT^{c}_{\alpha}|d_0\rangle\right]. \tag{116}$$

Equivalent expressions for c coefficients with q negative can be found explicitly — here, by considering the matrix elements $\langle d_1|\cdot|d_2\rangle$ and $\langle d_0|\cdot|d_1\rangle$ — or from the

condition:

$$c_{kq\alpha} = (-1)^q c^*_{k,-q\alpha}; \quad \alpha = x, y, z. \tag{117}$$

More useful for our present purposes is to express the $c_{kq\alpha}(r)$ of Eqs. (115) and (116) and the like, in terms of the real Cartesian d basis. After some tedious algebra, one finds, for example:

$$\mathrm{Re}[c^c_{21\alpha}(r)] = -\left(\frac{1}{2}\right)^{1/2} [3^{1/2}\langle d_{yz}| \cdot |d_{xz}\rangle + 3^{1/2}\langle d_{xz}| \cdot |d_{x^2-z^2}\rangle + \langle d_{xz}| \cdot |d_{z^2}\rangle] \tag{118}$$

and

$$\mathrm{Im}[c^c_{21\alpha}(r)] = \left(\frac{1}{2}\right)^{1/2} [-3^{1/2}\langle d_{yz}| \cdot |d_{x^2-y^2}\rangle + 3^{1/2}\langle d_{xz}| \cdot |d_{xy}\rangle + \langle d_{yz}| \cdot |d_{z^2}\rangle], \tag{119}$$

where Re and Im are the real and imaginary parts of the complex quantity $c_{21\alpha}(r)$. A more complete list of $c_{kq\alpha}(r)$ coefficients derived in this way for an $\ell = 2$ basis is given in Table 12. In passing, note: (1) the expressions in Table 12 differ by a factor of $(4\pi/(2k+1))^{1/2}$ from those given earlier [50] due to the present multipole expansion in spherical $C^{(k)}_q$ tensors rather than in spherical harmonics, $Y^{(k)}_q$; and (2) the same expressions serve for all one-electron operators so that, with appropriate dimensions, the dot can refer to the present effective transition dipole operator or to the effective ligand-field potential for which this table was originally constructed.

The matrix elements on the right-hand side of the expressions in Table 12 have been given, in the present context, by the entries in Table 11 and so we have established the relationships between the local multipole coefficients of Eq. (112) for each local, radiation polarization, α', and the intrinsic local transition parameters, ${}^{L}t_{\lambda}$, of Eqs. (98) and (99). They are listed in Table 13.

The multipole expansions listed in Table 13 refer to Cartesian components of the electric dipole operator $\alpha = x, y, z$. Equivalent expressions in the spherical basis may be formed using the relationships:

$$T_z = T_0; \quad T_{\pm 1} = \mp (T_x \pm iT_y)/\sqrt{2} \tag{120}$$

and these are listed in Table 14 for $T \pm 1$.

5.5. *The superposition*

Our aim is to find expressions which describe forced electric dipole moments in the whole, multiligand chromophore for incident radiation which is polarized in an arbitrary direction. Eq. (112), together with Table 13 provides one-electron matrix elements arising from radiation polarized in the specific x, y or z directions defined

Table 12
General relationships between spherical tensor coefficients and any one-electron operator within the real d basis

(a) Real parts of $c_{kq}(r)$

$$c_{00} = \frac{1}{5}[\langle d_{z^2}|\cdot|d_{z^2}\rangle + \langle d_{xz}|\cdot|d_{xz}\rangle + \langle d_{yz}|\cdot|d_{yz}\rangle + \langle d_{xy}|\cdot|d_{xy}\rangle + \langle d_{x^2-y^2}|\cdot|d_{x^2-y^2}\rangle]$$

$$c_{20} = \left(\frac{1}{4}\right)^{1/2}[2\langle d_{z^2}|\cdot|d_{z^2}\rangle + \langle d_{xz}|\cdot|d_{xz}\rangle + \langle d_{yz}|\cdot|d_{yz}\rangle - 2\langle d_{xy}|\cdot|d_{xy}\rangle - 2\langle d_{x^2-y^2}|\cdot|d_{x^2-y^2}\rangle]$$

$$c_{22} = \left(\frac{3}{4}\right)^{1/2}[\langle d_{xz}|\cdot|d_{xz}\rangle - \langle d_{yz}|\cdot|d_{yz}\rangle - 4(3)^{1/2}\langle d_{x^2-y^2}|\cdot|d_{z^2}\rangle]$$

$$c_{40} = \frac{6}{5}\left[\frac{3}{2}\langle d_{z^2}|\cdot|d_{z^2}\rangle - \langle d_{xz}|\cdot|d_{xz}\rangle - \langle d_{yz}|\cdot|d_{yz}\rangle - \frac{1}{4}\langle d_{xy}|\cdot|d_{xy}\rangle - \frac{1}{4}\langle d_{x^2-y^2}|\cdot|d_{x^2-y^2}\rangle\right]$$

$$c_{42} = 3\left(\frac{1}{10}\right)^{1/2}[(3)^{1/2}\langle d_{xz}|\cdot|d_{xz}\rangle - \langle d_{yz}|\cdot|d_{yz}\rangle + \langle d_{x^2-y^2}|\cdot|d_{z^2}\rangle]$$

$$c_{21} = -\left(\frac{1}{2}\right)^{1/2}[3^{1/2}\langle d_{yz}|\cdot|d_{xy}\rangle + 3^{1/2}\langle d_{xz}|\cdot|d_{x^2-z^2}\rangle + \langle d_{xz}|\cdot|d_{z^2}\rangle]$$

$$c_{41} = 3\left(\frac{1}{5}\right)^{1/2}\left[\frac{1}{2}\langle d_{yz}|\cdot|d_{xy}\rangle + \frac{1}{2}\langle d_{xz}|\cdot|d_{x^2-y^2}\rangle - (3)^{1/2}\langle d_{xz}|\cdot|d_{z^2}\rangle\right]$$

$$c_{43} = 3\left(\frac{7}{20}\right)^{1/2}[\langle d_{yz}|\cdot|d_{xy}\rangle - \langle d_{xz}|\cdot|d_{x^2-y^2}\rangle]$$

$$c_{44} = 3\left(\frac{7}{40}\right)^{1/2}[\langle d_{x^2-y^2}|\cdot|d_{x^2-y^2}\rangle - \langle d_{xz}|\cdot|d_{xy}\rangle]$$

(b) Imaginary parts of $c_{kq}(r)$

$$c_{21} = \left(\frac{1}{2}\right)^{1/2}[\langle d_{yz}|\cdot|d_{z^2}\rangle + (3)^{1/2}\langle d_{xz}|\cdot|d_{xy}\rangle - (3)^{1/2}\langle d_{yz}|\cdot|d_{x^2-y^2}\rangle]$$

$$c_{22} = \left(\frac{1}{2}\right)^{1/2}[\langle d_{xy}|\cdot|d_{z^2}\rangle - (3)^{1/2}\langle d_{xz}|\cdot|d_{yz}\rangle]$$

$$c_{41} = 3\left(\frac{1}{5}\right)^{1/2}\left[(3)\frac{1}{2}\langle d_{yz}|\cdot|d_{z^2}\rangle + \frac{1}{2}\langle d_{yz}|\cdot|d_{x^2-y^2}\rangle - \frac{1}{2}\langle d_{xz}|\cdot|d_{xy}\rangle\right]$$

$$c_{42} = -3\left(\frac{1}{10}\right)^{1/2}[(3)^{1/2}\langle d_{xy}|\cdot|d_{z^2}\rangle + 4\langle d_{xz}|\cdot|d_{yz}\rangle]$$

$$c_{43} = 3\left(\frac{7}{20}\right)^{1/2}[\langle d_{xz}|\cdot|d_{xy}\rangle + \langle d_{yz}|\cdot|d_{x^2-y^2}\rangle]$$

$$c_{44} = -3\left(\frac{7}{10}\right)^{1/2}[\langle d_{x^2-y^2}|\cdot|d_{xy}\rangle$$

for a single ligation. The local, effective operators in Eq. (112) are:

$$eT^c_\alpha = \sum_{k,\,q'} c^c_{kq'\alpha'}(r)C^{(k)}_{q'}, \tag{121}$$

where primes emphasize the local reference frame.

The relationships between local and global frames may be expressed either in terms of a set of Euler angles, $(\alpha'^c, \beta'^c, \gamma'^c) \equiv \hat{R}^c$, for short, or in terms of a matrix

Table 13
Relationships between local multipole coefficients and local transition parameters

(a) For ${}^{P}T_z$, ${}^{F}T_z$, ${}^{2R}T_z$

$$c_{00} = \left(\frac{2}{5}\right)\left(\tilde{t}_\sigma + \tilde{t}_{\pi x} + \tilde{t}_{\pi y}\right)$$

$$c_{20} = \left(2\tilde{t}_\sigma + \tilde{t}_{\pi x} + \tilde{t}_{\pi y}\right)$$

$$c_{22} = (3)^{1/2}\left(\tilde{t}_{\pi x} - \tilde{t}_{\pi y}\right)$$

$$c_{40} = \left(\frac{6}{5}\right)\left(3\tilde{t}_\sigma - 2\tilde{t}_{\pi x} - 2\tilde{t}_{\pi y}\right)$$

$$c_{42} = 3\left(\frac{2}{5}\right)^{1/2}\left(\tilde{t}_{\pi x} - \tilde{t}_{\pi y}\right)$$

(b) For ${}^{P}T_x$

$$c_{21} = -\left(\frac{1}{40}\right)^{1/2}\left(4^{P}\tilde{t}_{\pi x} + 6^{P}\tilde{t}_{\pi y} + 3^{P}\tilde{t}_\sigma\right)$$

$$c_{41} = -3\left(\frac{1}{20}\right)^{1/2}\left(3^{P}\tilde{t}_\sigma - 3^{P}\tilde{t}_{\pi x} - 3^{P}\tilde{t}_{\pi y}\right)$$

$$c_{43} = 3\left(\frac{7}{20}\right)^{1/2}\left(3^{P}\tilde{t}_{\pi y} - {}^{P}\tilde{t}_{\pi x}\right)$$

(c) For ${}^{F}T_x$

$$c_{21} = -\frac{1}{4}\left(\frac{1}{6}\right)^{1/2}\left(3^{F}\tilde{t}_{\pi x} - 3^{F}\tilde{t}_{\pi y} - 4^{F}\tilde{t}_\sigma\right)$$

$$c_{41} = \frac{3}{8}\left(\frac{1}{5}\right)^{1/2}\left(8^{F}\tilde{t}_\sigma - 13^{F}\tilde{t}_{\pi x} - {}^{F}\tilde{t}_{\pi y}\right)$$

$$c_{43} = -\frac{3}{8}\left(\frac{7}{5}\right)^{1/2}\left({}^{F}\tilde{t}_{\pi y} - {}^{F}\tilde{t}_{\pi x}\right)$$

(d) For ${}^{P}T_x$

$$c_{21} = i\left(\frac{1}{40}\right)^{1/2}\left(4^{P}\tilde{t}_{\pi y} + 6^{P}\tilde{t}_{\pi x} + 3^{P}\tilde{t}_\sigma\right)$$

$$c_{41} = 3i\left(\frac{1}{20}\right)^{1/2}\left(3^{P}\tilde{t}_\sigma - 3^{P}\tilde{t}_{\pi y} - {}^{P}\tilde{t}_{\pi x}\right)$$

$$c_{43} = -3i\left(\frac{7}{20}\right)^{1/2}\left({}^{P}\tilde{t}_{\pi y} - {}^{P}\tilde{t}_{\pi x}\right)$$

(e) For ${}^{F}T_y$

$$c_{21} = \frac{i}{4}\left(\frac{1}{6}\right)^{1/2}\left(3^{F}\tilde{t}_{\pi y} - 3^{F}\tilde{t}_{\pi x} - 4^{F}\tilde{t}_\sigma\right)$$

$$c_{41} = -3\frac{i}{8}\left(\frac{1}{5}\right)^{1/2}\left(8^{F}\tilde{t}_\sigma - 13^{F}\tilde{t}_{\pi y} - {}^{F}\tilde{t}_{\pi x}\right)$$

$$c_{43} = 3\frac{i}{8}\left(\frac{7}{5}\right)^{1/2}\left({}^{F}\tilde{t}_{\pi y} - {}^{F}\tilde{t}_{\pi x}\right)$$

Table 14
Relationships between local multipole coefficients for $T_{\pm 1}$ and local transition parameters

(a) For T_{+1}

$$c_{21}=\frac{1}{2}\left(\frac{1}{3}\right)^{1/2}[3^P\tilde{t}_\sigma+5^P\tilde{t}_{\pi x}+5^P\tilde{t}_{\pi y}-2^F\tilde{t}_\sigma]$$

$$c_{41}=\frac{3}{4}\left(\frac{1}{10}\right)^{1/2}[12^P\tilde{t}_\sigma-8^P\tilde{t}_{\pi x}-8^P\tilde{t}_{\pi y}-8^F\tilde{t}_\sigma+7^F\tilde{t}_{\pi x}+7^F\tilde{t}_{\pi y}]$$

$$c_{43}=\frac{3}{4}\left(\frac{7}{10}\right)^{1/2}[4^P\tilde{t}_{\pi x}-4^P\tilde{t}_{\pi y}-{}^F\tilde{t}_{\pi x}+{}^F\tilde{t}_{\pi y}]$$

(b)For T_{-1}

$$c_{21}=\frac{1}{4}\left(\frac{1}{3}\right)^{1/2}[2^P\tilde{t}_{\pi x}-2^P\tilde{t}_{\pi y}-3^F\tilde{t}_{\pi x}+3^F\tilde{t}_{\pi y}]$$

$$c_{41}=\frac{3}{2}\left(\frac{1}{10}\right)^{1/2}[2^P\tilde{t}_{\pi x}-2^P\tilde{t}_{\pi y}-3^F\tilde{t}_{\pi x}+3^F\tilde{t}_{\pi y}]$$

$$c_{43}=0$$

(c) For $T_{\pm 1}$

$$c_{k,-q}(\pm 1)=c_{k,q}(\mp 1)$$

of direction cosines, $\mathscr{L}^c$. The local effective operators of Eq. (121) are then expressed relative to the global reference frame of the complete chromophore, either by:

$$eT^c_\alpha=\sum_{\alpha',\alpha}\sum_k\sum_{q,q'}\mathscr{L}^c_{\alpha'\alpha}c^c_{kq'\alpha'}(r)\mathscr{D}^{(k)}_{q'q}(\hat{R}^c)C^{(k)}_q \tag{122}$$

for local Cartesian multipole expansions, as in Table 13, or by

$$eT^c_n=\sum_{n'n}\sum_k\sum_{qq'}\mathscr{D}^{(1)}_{n'n}(\hat{R}^c)c^c_{kq'n'}(r)\mathscr{D}^{(k)}_{q'q}(\hat{R}^c)C^{(k)}_q \tag{123}$$

for the spherical expansions of Table 14. The Wigner rotations $\mathscr{D}^{(k)}$ transform the tensors of Eq. (121) into the global frame and either $\mathscr{D}^{(1)}$ or $\mathscr{L}$ take account of the arbitrary (but fixed) polarization of the incident light. Finally, summing of contributions from all ligations yields the global, effective dipole operators:

$$eT_\alpha=\sum_c\sum_{\alpha\alpha'}\sum_k\sum_{qq'}\mathscr{L}^c_{\alpha'\alpha}c^c_{kq'\alpha'}(r)\mathscr{D}^{(k)}_{q'q}(\hat{R}^c)C^{(k)}_q \tag{124}$$

or

$$eT_n=\sum_c\sum_{nn'}\sum_k\sum_{qq'}\mathscr{D}^{(1)}_{n'n}(\hat{R}^c)c^c_{kq'n'}(r)\mathscr{D}^{(k)}_{q'q}(\hat{R}^c)C^{(k)}_q. \tag{125}$$

Global transition moment matrix elements within a many-electron, pure d basis of states expressed as $\{L\ S\ J\ M_J\}$ are then evaluated using standard tensor operator techniques [8]. However, we need to compute such integrals within the basis of ligand-field states $\{\Psi\}$ deriving from prior ligand-field analysis of transition energies;

the cellular ligand-field orbitals of Eq. (89), to which the intrinsic CLF transition parameter definition Eqs. (100) and (101) relate, are established by that same ligand field. The ligand-field states $\{\Psi\}$ are, of course, expressed as linear combinations of the $\{L\ S\ J\ M_J\}$:

$$\Psi_I = \sum_i a_{iI}(r)\Phi_i; \quad \Phi_i \equiv |L\ S\ J\ M_J\rangle_i \tag{126}$$

where the expansion coefficients $\{a\}$ are established by diagonalization under Eq. (2). Altogether, therefore, the global matrix elements of the effective transition dipole operators within the many-electron, ligand-field basis are given by:

$$\langle \Psi_I | eT_\alpha | \Psi_J \rangle = \sum_c \sum_{\alpha'\alpha} \sum_k \sum_{qq'} \sum_{ij} a^*_{iI}(r) a_{jJ}(r) \mathscr{L}^c_{\alpha'\alpha} c^c_{kq'\alpha'}(r) \mathscr{D}^{(k)}_{q'q}(\hat{R}^c) \langle \Phi_i | C^{(k)}_q | \Phi_j \rangle \tag{127}$$

or

$$\langle \Psi_I | eT_n | \Psi_J \rangle = \sum_c \sum_{n'n} \sum_k \sum_{qq'} \sum_{ij} a^*_{iI}(r) a_{jJ}(r) \mathscr{D}^{(1)}_{n'n}(\hat{R}^c) c^c_{kq'\alpha'}(r) \mathscr{D}^{(k)}_{q'q}(\hat{R}^c) \langle \Phi_i | C^{(k)}_q | \Phi_j \rangle. \tag{128}$$

As Cartesian transition moments are the more convenient at this stage, Eq. (127) is our favoured expression.

5.6. *Spectral absorbance*

We are generally interested in spectral transitions between degenerate or near-degenerate manifolds; this is particularly true for the broad features of '*d–d*' bands. Consider, therefore, transitions between the N_A members of an effectively degenerate manifold A and the N_B members of a similar manifold B. We do not know, *a priori*, along which directions principal optical absorptions occur in a general, low-symmetry chromophore. So we construct a second-rank (Cartesian) tensorial representation of spectral absorbance from which principal absorbances and their orientations may be determined by diagonalization. For the transition manifold A→manifold B, a general element of the absorbance tensor A^{AB} is given by

$$A^{AB}_{\alpha\beta} = K \sum_{I \in A} \sum_{J \in B} \langle \Psi_I | eT_\alpha | \Psi_J \rangle \langle \Psi_J | eT_\beta | \Psi_I \rangle, \tag{129}$$

where $K = L\pi\nu/3\epsilon_0 hc$ and L is Avagadro's number. This quantity has been shown [11] to be invariant to a unitary transformation that scrambles the eigenvectors within manifold A and within manifold B, separately; hence, principal absorbances and their orientations so computed are independent of the choice of global reference frame.

Mean absorbances, to be compared with intensities derived from experiments on solutions are given by the traces of A^{AB} as usual. For polarization studies on single crystals, comparisons between calculation and experiment are made only after appro-

priate tensorial summation over crystallographically equivalent chromophoric units and transformation into the (experimental) crystal frame by conventional methods [8].

5.7. The chemical and physical significance of the ${}^{L}t_{\lambda}$ parameters

We have been occupied in the immediately preceding sections with a summary of the structure of the CLF intensity model as constructed for acentric chromophores. In due course, we will describe its extension for centric species and vibronically derived intensity. Before that, however, let us take stock and consider the parameters which are at the core of the approach. There are two broad classes of consideration we must make: the connections between the parameter values and chemical structure to be expected within the CLF structure itself, and the relationships between both parameters and model structure of the CLF scheme and of the SC + DC constructs which we have reviewed earlier. We proceed in this order.

We begin with the signs of the CLF intensity parameters and their relationships with the signs of CLF energy parameters; a straightforward correlation emerges. This is followed by some general observations on the magnitudes of the ${}^{L}t_{\sigma}$ and ${}^{L}t_{\pi}$ parameters in relation to their e_{σ} and e_{π} counterparts, and on the relative unimportance of the ${}^{R}t_{\lambda}$ contribution from Eq. (95). Of particular significance is the ratio of the P and F type contributions, which are discussed qualitatively at first and then with respect to some quantitative modelling computations of the two-centre expansion which takes us from Eqs. (89) to (91). Only after all this do we place the CLF model within the broader context of intensity theory described earlier.

5.8. The signs of the ${}^{L}t_{\lambda}$ parameters

The CLF model is centred around the cellular orbitals Eq. (89). As explicit forms for these are unavailable without (currently intractable) prior computation of the electronic distribution throughout the object chromophore, their form is notional and properties depending upon them are parametrized. In relation to the schemes in Fig. 10, which is only intended as a rough summary of the material reviewed in Section 5.1, we write a dominant contribution to a σ bond orbital, ϕ^{b}_{σ}, as:

$$\phi^{b}_{\sigma} \sim Ms + Mp_{\sigma} - L_{\sigma}, \tag{130}$$

in which the magnitudes but not the signs of the mixing coefficients are subsumed into the constituent metal s or p, and ligand σ functions. The negative sign in Eq. (130) arises from our taking coparallel axis frames on metal and ligand with z being directed along the M–L vector. The corresponding π bond orbital, ϕ^{b}_{π}, is:

$$\phi^{b}_{\pi} \sim Mp_{\pi} + L_{\pi}. \tag{131}$$

The same expression suffices even for the higher-lying (mostly) ligand function on the right-hand side of Fig. 10(c) for while that may be antibonding within the ligand, it is still bonding with respect to the metal.

The corresponding ligand-field orbitals, $\{\psi^{\mathrm{LFO}}\}$, arising after interaction with the

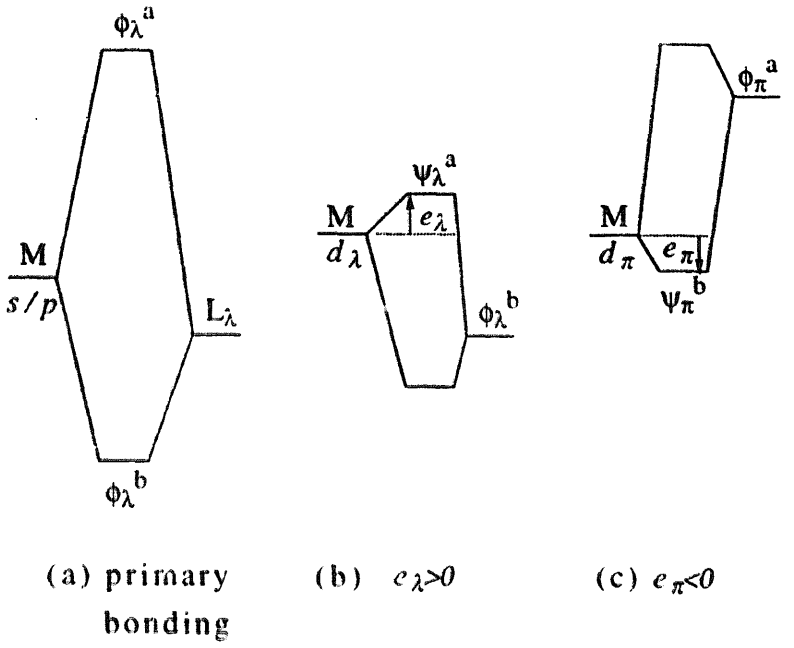

Fig. 10. (a) Bond orbitals, ϕ_λ^b, result from the primary bonding interaction of metal s and p orbitals with a ligand. The bond orbitals interact with the metal d orbitals to yield ligand-field orbitals, ψ_λ, defining positive e_λ values in (b) or negative e_π values in (c).

mean d orbitals are:

$$\begin{aligned}
&\text{for } e_\sigma > 0: \quad \psi_\sigma^a \sim Md_{z^2} - Ms - Mp_z + L_\sigma \\
&\text{for } e_\pi > 0: \quad \psi_\pi^a \sim Md_\pi - Mp_\pi - L_\pi \\
&\text{for } e_\pi < 0: \quad \psi_\pi^b \sim Md_\pi + Mp_\pi + L_\pi.
\end{aligned} \tag{132}$$

In these expressions, the metal d, s and p functions are referred to the metal centre, but the ligand L_σ and L_π functions are referred to the ligand. Let us now refer these ligand functions to the metal as origin *via*, for now, an unspecified, two-centre multipole expansion, retaining only metal-centred orbitals of p and f character. The latter restriction is made because of the use of the $\{\psi\}$ within integrals under the electric-dipole operator, of course. For the same reason, the contribution from the Ms function is also dropped. The remaining parts of the $\{\psi^{\mathrm{LFO}}\}$, all referred to the metal centre and so equivalent to Eq. (91), take the forms:

$$\begin{aligned}
&\text{for } e_\sigma > 0: \quad \psi^a \sim Md_\lambda - Mp_\lambda - {}^pL_\lambda - {}^fL_\lambda \\
&\text{for } e_\pi < 0: \quad \psi^b \sim Md_\pi - Mp_\pi + {}^pL_\pi + {}^fL_\pi,
\end{aligned} \tag{133}$$

where $\{{}^\ell L_\lambda\}$ are the metal-centred parts of $\{L_\lambda\}$ with p or f character. The signs associated with the $\{L_\lambda\}$ arise from the signs in Eq. (132) together with a reversal for the two-centre expansion of the σ function.

Reference to the parameter definitions in Eqs. (99) and (100) then establishes the signs of ${}^p\tilde{t}_\lambda$ and ${}^f\tilde{t}_\lambda$ as consistently opposite to those of the corresponding energy

parameters, e_λ; that of ${}^{R}\tilde{t}_\lambda$ will always be positive. For convenience and correspondence with the literature on the CLF intensity model, we now redefine the intrinsic parameters as:

$$ {}^{P}t_\lambda = -{}^{P}\tilde{t}_\lambda; \quad {}^{F}t_\lambda = -{}^{F}\tilde{t}_\lambda; \quad {}^{R}t_\lambda = {}^{R}\tilde{t}_\lambda \tag{134} $$

and observe that the signs of both e_λ and ${}^{L}t_\lambda$ ($L=P$, F) relate to ligand donor/acceptor function in the same way. The origins of this irritating sign change are not mysterious. In Eq. (89) *et seq.*, positive signs were used throughout, without prejudice. The signs in Eqs. (132) and (133) recognize the major *bonding* role of the bond orbitals together with their subsequent *bonding* or *antibonding* status with respect to the mean *d* orbitals, according to circumstances. The ensuing definitions in Eq. (134) then form a natural choice.

5.9. *The* R *contribution*

In terms of the cellular orbitals, Eq. (89), the ${}^{L}t_\lambda$ parameters take the form $b_\lambda^c\langle d_\lambda^c|er_z^c|\phi_\lambda^c\rangle$ for $L=P$, F and $b_\lambda^{c2}\langle\phi_\lambda^c|er_z^c|\phi_\lambda^c\rangle$ for $L=R$. With the $\{\phi_\lambda^c\}$ referred to the ligand's origin, $\langle\phi_\lambda^c|r_z^c|\phi_\lambda^c\rangle$ is of the order of the M–L bond length, say, 2–3 Å. We present computations shortly which suggest that $\langle d_\lambda^c|r_z^c|\phi_\lambda^c\rangle$ integrals are of the order of 0.2 Å or less. The cellular mixing coefficients, b_λ^c, are likely to be 0.1 or less. Hence, ${}^{R}t_\lambda$ parameters are expected to be no more than about 10% of the corresponding ${}^{P,F}t_\lambda$ values. Often, therefore, the *R* contribution might well be negligible. If, however, the global chromophore symmetry corresponds to that of a regular or a skewed bipyramid or antibipyramid, the overall *R* contribution will tend to vanish completely, as the following argument shows.

As discussed after Eq. (104), *R*-type contributions for components of incident radiation oriented perpendicular to any local bond are negligible compared with those lying parallel to the bond. Uniquely for the *R* contribution, therefore, we only include local transition moments that are parallel to the bond vectors. Let θ_A etc. be the angle subtended by bond vector *A* etc. and some fixed global vector. The resultant transition moment ${}^{R}Q$ arising from local *R* contributions is then:

$$ {}^{R}Q = q_A\cos\theta_A + q_B\cos\theta_B + \ldots, \tag{135} $$

where the $\{q\}$ are the local *R*-type transition moments. The sum ${}^{R}Q$ will vanish when the geometrical arrangement of ligations in a complex is characterized by one of two symmetries, namely: (1) when the whole complex possesses C_{nh} symmetry ($n\geqslant 2$); or (2) when exactly half of the ligations possessing C_n ($n\geqslant 2$) symmetry may be related to the other half, after an arbitrary rotation about the principal axis, by reflection in a mirror plane normal to that axis. These geometrical descriptions identify two types of coordination polyhedron; regular bipyramids and regular antibipyramids, whether skewed or not. Included amongst these are trigonal and pentagonal bipyramids, the tetrahedron, and planar, equilateral triangles. Many real molecular geometries conform exactly or approximately to these types. Altogether,

following the reasoning in both preceding paragraphs, CLF intensity analyses to date have almost always omitted further reference to the ${}^{R}t_{\lambda}$ parameters.

5.10. The magnitudes of CLF intensity and energy parameters

The CLF model considers '*d–d*' spectral intensity as a ligand-field property with some connections with '*d–d*' transition energies or various paramagnetic attributes of the ligand-field regime. It is to be expected, therefore, that experimentally determined e_{λ} and ${}^{L}t_{\lambda}$ parameters will reflect aspects of the same electronic distribution within a given complex, albeit in different ways.

The dominant parts of CLF energy parameters are given [7–9] by:

$$e_{\lambda} \sim |\langle d_{\lambda}|V'|\chi_{\lambda}\rangle|^2/(\epsilon_d - \bar{\epsilon}_{\chi}), \tag{136}$$

where V' was defined in Eq. (86) and the $\{\chi\}$ are bond orbitals, as compared with the P or F type intensity parameters taking the form

$${}^{L}t_{\lambda} \sim \langle d_{\lambda}|er_z|\chi_{\lambda}\rangle;\ \lambda = P, F. \tag{137}$$

One determinant of there being a significant contribution to e_{λ} is the existence of one or more, spatially and energetically proximate bond orbitals χ_{λ} to the mean d orbitals. Many of the subtleties in this proposition have been reviewed at length recently [9] and will not be repeated here. One obvious example, however, with particular relevence to our present subject is the case of a near-vanishing e_{π} value for amine ligators which lack any low-lying π function. The same circumstances would lead us to expect the lack of any significant π contribution within the local ligand-field orbital, ψ^{LFO}. In short, we anticipate that vanishing ${}^{P}t_{\pi}$ and ${}^{F}t_{\pi}$ intensity parameters should accompany vanishing e_{π} energy parameters. As any CLF intensity analysis is predicated upon a prior ligand-field analysis of energies, it might seem reasonable to neglect ${}^{L}t_{\pi}$ parametrization in *all* systems characterized by near zero e_{π} values. Such a simplifying assumption might be reasonable in the case of amine ligations, for example, for there are good theoretical (bonding) reasons suggested from outside the model in support. In general, however, a parallelism between the magnitudes of intensity and energy parameters may not be secure. This doubt rests on the different natures of the two operators in Eqs. (136) and (137). The operator V' arises from those local parts of the molecular ligand-field potential that do not form part of the mean, spherically symmetric, term $\langle V\rangle$ in Eq. (86); it is expected to be maximized in roughly those regions of space where χ_{λ} is maximal. The integral in Eq. (136) might thus be considered, very approximately, as a scaled overlap integral, $\langle d_{\lambda}|\chi_{\lambda}\rangle$. By contrast, the electric dipole operator, er_z, in Eq. (137), increases linearly with distance from the metal centre and so $\langle d_{\lambda}|er_z|\chi_{\lambda}\rangle$ might be viewed as a similar overlap integral weighted progressively towards the ligand centre. In this sense, we see the intensity parameters as more "outer" properties than their energy counterparts. In practice, therefore, it is to be expected that t_{π}:t_{σ} ratios will often be greater than the corresponding e_{π}:e_{σ} ratios. Examples presented in Section 7 of this article provide empirical support for this proposal.

Generally, both e_λ and ${}^{L}t_\lambda$ ($L=P$, F) parameter values should decrease with increasing bond length and, other things being equal, such is observed to be the case. Both types of parameter should reflect the same symmetry functionality (σ, π) in the chemical bond. However, the properties being parametrized by the $\{e\}$ and the $\{t\}$ are different and it is to be expected that these parameter sets will reflect the underlying bonding in different ways. We can thus hope that an analysis of intensity distribution will provide a more informative probe of the ligation chemistry than one of transition energies alone. The key for exploiting the broader technique lies in the nature of the "double layer" of intensity parameters relative to energy variables. By this is meant that, even neglecting the R type intensity contribution as noted earlier, there remains a "working set" of intensity variables which exactly doubles that of the corresponding energy analysis, as shown in Table 15.

Our next topic, therefore, is the relative roles of the P and F contributions to intensity. Much is to be learned from a study of the two-centre expansion of ligand functions onto the metal. Before doing this, however, recall the general form of the ligand-field orbitals $\{\psi^{\mathrm{LFO}}\}$ of Eq. (89) and our remarks in Section 3. The $\{\psi^{\mathrm{LFO}}\}$ comprise mean d orbitals together with small admixtures of the bond orbitals — the $\{\phi\}$ of Eqs. (130) and (131). The mixing coefficients $\{b\}$ in Eq. (89) *are* expected to be small in view of the weak coupling between the d functions and all others; the weakness of that coupling is evidenced by the efficacy of the whole of ligand-field theory, as discussed in [7–9]. Variations in the magnitudes of the b coefficients from ligation to ligation will affect P and F intensity contributions proportionately equally. As these coefficients cannot, at present, be computed with suitable accuracy, connections between the overall magnitudes of ${}^{P,F}t_\lambda$ parameters and chemistry must remain empirical and be established by experience. Next, we recall how the admixed bond orbitals — the "rest" functions of Eq. (88) — comprise both metal-originating and ligand-originating functions. As discussed in Section 3, the metal-originating functions can arise by electrostatic (crystal-field) means or by "covalency". For complexes of the main transition series it is unlikely that serious consideration to f orbital admixtures by these means need be given. The extent of such p orbital mixing will, no doubt, depend upon the global, molecular symmetry and is a point we will illustrate in Section 7.3.5. In general, however, we anticipate that the greater part of any bond orbital will derive from the ligand because (a) metal–ligand bonding is much weaker than most intraligand bonding (weaker dative covalency in the language of yesteryear) and (b), another aspect of (a), just one (s) metal orbital (plus some small contributions from the p set) is shared by many ligands while the latter

Table 15
Parameters in the CLF models (excluding ${}^{R}t_\lambda$)

Energy parameters	Intensity parameters
e_σ	${}^{P}t_\sigma$, ${}^{F}t_\sigma$
$e_{\pi x}$	${}^{P}t_{\pi x}$, ${}^{F}t_{\pi x}$
$e_{\pi y}$	${}^{P}t_{\pi y}$, ${}^{F}t_{\pi y}$

devote one orbital (or possibly more) wholly to the metal. The dominance of ligand functions within the bond orbitals $\{\phi\}$ thus suggests that the major influences over the ${}^{P,F}t_\lambda$ intensity parameters might be gauged from a focus upon the ligand-centred components in Eq. (133). So we look now at the multipolar expansion of ligand functions onto the metal centre. Once more, we draw attention to one further caveat which warns us that a complete understanding of the relative roles of *P*- and *F*-type contributions to intensity is not to be expected from the approach we are about to describe. The point here is to recall that all ligand-field phenomena are properties of real — formed — molecules rather than of promolecules. As a result of the usual give-and-take in bond formation, the character of any one bond will depend in part upon all bonds, not just upon the local atomic constituents — the *trans* effect illustrates the point. Consequently, we are to expect that the "best orbitals" within a given cellular region will include contributions from orbitals originating from all ligands in the system. All these may, of course, be referred to the object ligand centre as origin, in which case all that follows notionally includes these contributions. Our warning, therefore, is that while trends may be deduced from the following analysis, empiricism remains the ultimate arbiter for what are, after all, *parameters*.

5.11. *Qualitative implications of the two-centre expansion*

Multipole expansion of a ligand-centred function onto the metal can be made in two ways. In one, the expansion functions are defined with respect to fixed radial parts and so might comprise the set $\{1s, 2s, 3s,\ldots; 2p, 3p, 4p,\ldots; 3d, 4d,\ldots; 4f, 5f,\ldots\}$. In the other, we take just one angular function of each kind (ℓ value) — $\{s, p, d, f,\ldots\}$ — with radial parts defined by the expansion process. In a later section, explicit expressions for this will be described. The second procedure is more convenient for our present purposes as we wish to focus on those expansion functions of just *p* or *f* character, and, as the exact form of any ligand function is unknown to us in practice, the consequent transition moments are parametrized anyway.

For concreteness' sake, let us consider the expansion of a ligand σ function:

$$L_\sigma = a_s s + a_p p_\sigma + a_d d_\sigma + a_f f_\sigma + \ldots, \tag{138}$$

where the functions on the right are referred to the metal. The ultimate success of this expansion may be visualized as in Fig. 11. Two aspects of this construction are of immediate interest. First, we note how the loss of amplitude near the metal arises from cancellations of odd- and even-parity metal functions in the sum. Secondly, we observe the increasing directedness of the ligand-pointing lobes with increasing azimuthal quantum number; equivalently, we note the decreasing angle subtended at the metal by the nodal cones of the σ lobes. In essence, this is forced by the ever increasing number of lobes to be accommodated within the metal sphere with increasing ℓ value. This second feature provides a guide for qualitative predictions about the relative magnitudes of *P* and *F* type contributions to forced electric-dipole transition moments.

The point here is that the expansion coefficients, a_s, a_p, a_d, a_f etc. in Eq. (138)

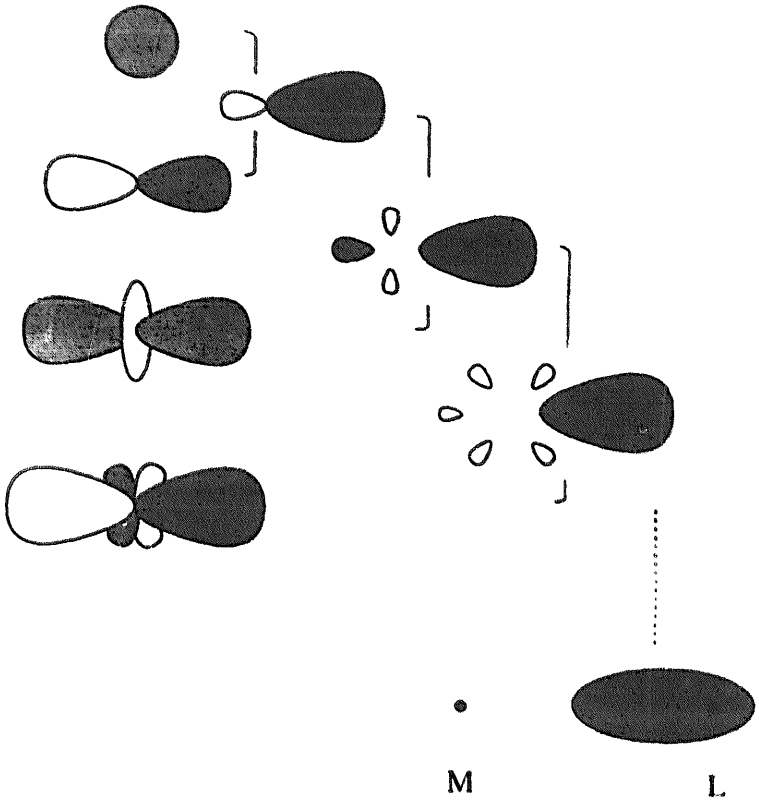

Fig. 11. Illustrating how a superposition of metal-centred functions can reconstruct a ligand-centred function.

are determined by both bond length and the character of the L_σ orbital. Both bond length and lateral spread of the ligand function are relevant. Consider the contribution $a_\mu p_\sigma$ in Eq. (138). We might suppose the reproduction of a chlorine 3*s* function, say, at short and long distances to be achieved in part by small and large radial coefficients a_p, respectively, as in Fig. 12. However, at the same time that we satisfy the reproduction of the more distant ligand function, we form a ligand orbital of greater lateral diffuseness. While the same is true of all the expansion functions in Eq. (138), it is less so for the more highly directed f_σ function, for example. Qualitatively, therefore, we expect that, other factors being constant, longer bond lengths involve relatively greater contributions from higher-order multipoles in the two-centre expansion. Note how this conclusion about bond length is intimately bound up with the nodal cone angles of the expansion functions themselves.

Similar reasoning may be applied when comparing less and more directed ligand functions. A chlorine (3)sp_z hybrid donor function approaches the metal more closely on average than a (3)*s* at the same bond length, for example. Other factors

Fig. 12. Smaller mixing coefficient a_p for shorter M–L bonds on the left and a larger one for longer M–L bonds on the right. Both radial and lateral dimensions are affected.

being constant once more, a two-centre expansion of a more metal-directed, or polarized, ligand function will result in a relatively greater contribution from a metal-centred p_σ function and a relatively smaller one from an f_σ function than for a less donating ligand.

The same conclusions can be reached from a different, but equivalent, viewpoint. In Fig. 13(a and b) we sketch the nodal cones of the metal p_σ and f_σ expansion functions. From Fig. 12(c), we observe how that (hatched) part of a ligand σ function which falls outside the f_σ nodal cone cannot be represented by a metal f_σ expansion function but can by a metal p_σ. It is also clear that this result will pertain especially to ligand orbitals which are more diffuse laterally.

To the extent that the relative magnitudes of the ${}^{P}t_\sigma$ and ${}^{F}t_\sigma$ parameters directly follow the two-centre expansion which transforms Eq. (89) into Eq. (91), we may list three qualitative trends based on the foregoing arguments:
Increasing contributions from p expansion functions and decreasing ones from f functions, so leading to increasing ${}^{P}t_\sigma:{}^{F}t_\sigma$ ratios, will be associated with:
(1) shorter bond lengths;
(2) ligand functions which are more directed, or polarized, towards the metal; and
(3) ligand functions which are laterally more diffuse.

As ever, other factors being constant.
The last two trends might operate in opposition on occasion. Consider a series of ligations involving increasing ligand→metal donation — perhaps following appropriate substitutions on the donor atom. Firstly, we anticipate the greater donicity to be manifested by greater polarization of the ligand function toward the metal and so, by (2), expect an increase in the ${}^{P}t_\sigma:{}^{F}t_\sigma$ ratio. As the donicity increases further, however, electron density drifts further from the spherical, atomic field of the donor atom into the bond region whose field is increasingly established by the metal and ligand together. The bond electron density will tend to concentrate more about the metal–ligand vector and so characterize a "tight" bond. This narrower

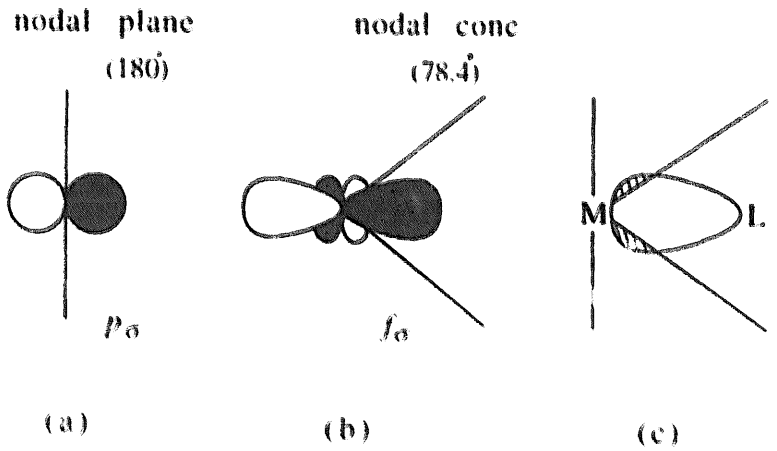

Fig. 13. (a) The nodal plane of a p_σ orbital. (b) The nodal cone of an f_σ function. (c) Those parts of a ligand function lying outside the nodal cone of f_σ are better reproduced by a metal-centred p_σ expansion function.

bond orbital will then be modelled in the two-centre expansion by increasing f character more than increasing p and, by (1.3), we expect to observe a decrease in the ${}^{P}t_{\sigma}:{}^{F}t_{\sigma}$ ratio. We shortly present some computational studies in support of this qualitative argument.

Qualitatively, we expect similar trends to those listed above for σ interactions to be relevent for π bonding. One may discern factors, however, which suggest that the relative contribution of F terms should be more pronounced for π bonding than for σ. Thus, ligand π functions will generally overlap with metal p_{π} functions less than ligand σ functions do with the metal s or p_{σ} functions. Migration of ligand π electron density towards the metal may frequently be less than σ, therefore, and its greater mean distance from the metal will, by (1.1) above, favour larger ${}^{F}t_{\pi}:{}^{P}t_{\pi}$ ratios. Secondly, reproduction of more distant ligand orbitals within the two-centre expansion is, as discussed above, partly effected through larger radial functions — the $\{a\}$ of Eq. (138). The consequent, but unwanted, lateral expansion is of greater significance for π functions than for σ, however, and will be offset by relatively larger contributions from f_{π} rather than p_{π}. Opposed to these two factors favouring relatively greater F contributions for the π modes, of course, is the relative lack of any tendency of π bond orbitals to concentrate about the metal–ligand vector. Overall, therefore, we discern the principles governing ${}^{F}t_{\pi}:{}^{P}t_{\pi}$ ratios relative to ${}^{P}t_{\sigma}:{}^{F}t_{\sigma}$, but allow empiricism to establish actual results.

5.12. *A computational study of the two-centre expansion*

Sharma [51] has described a two-centre expansion of the type, Eq. (134), in terms of a multipolar series of Slater-type orbitals (STO) within the expression:

$$R^{N-1}e^{-\zeta R}Y_{M}^{L}(\Theta,\Phi)=\sum_{\ell}\left(\frac{1}{r}\right)\alpha_{\ell}(N\zeta LM|ar)\,Y_{m}^{\ell}(\theta,\phi), \tag{139}$$

in which the STO are referred to one centre — which we take as the ligand — by the coordinates $\{R, \Theta, \Phi\}$ and the expansion functions to another centre — the metal — separated by distance a from the first, by the coordinates $\{r, \theta, \phi\}$. He also provides analytical expressions for the radial factors, a_{ℓ}.

In the computations [52] we review, the ligand functions were represented by the double-zeta atomic functions of Clementi [53], expanded as in Eq. (135). Double-zeta functions for metal d orbitals were taken from the same source. Using standard numerical integration methods, integrals of form $\langle d_{\lambda}|r_{\alpha}|^{\ell}L_{\lambda}\rangle$ — relating to Eq. (131) and the intensity parameters Eq. (134) — for $\ell=1$ and 3 were evaluated for a range of circumstances. Throughout the results summarized in the present section, these integrals will be labelled P or F according to $\ell=1$ or 3, respectively. We review them under four headings.

5.12.1 *General trends*

A representative sample of the computational results is shown in Fig. 14. Plots show variations in the P and F integrals with bond length for various orbitals of

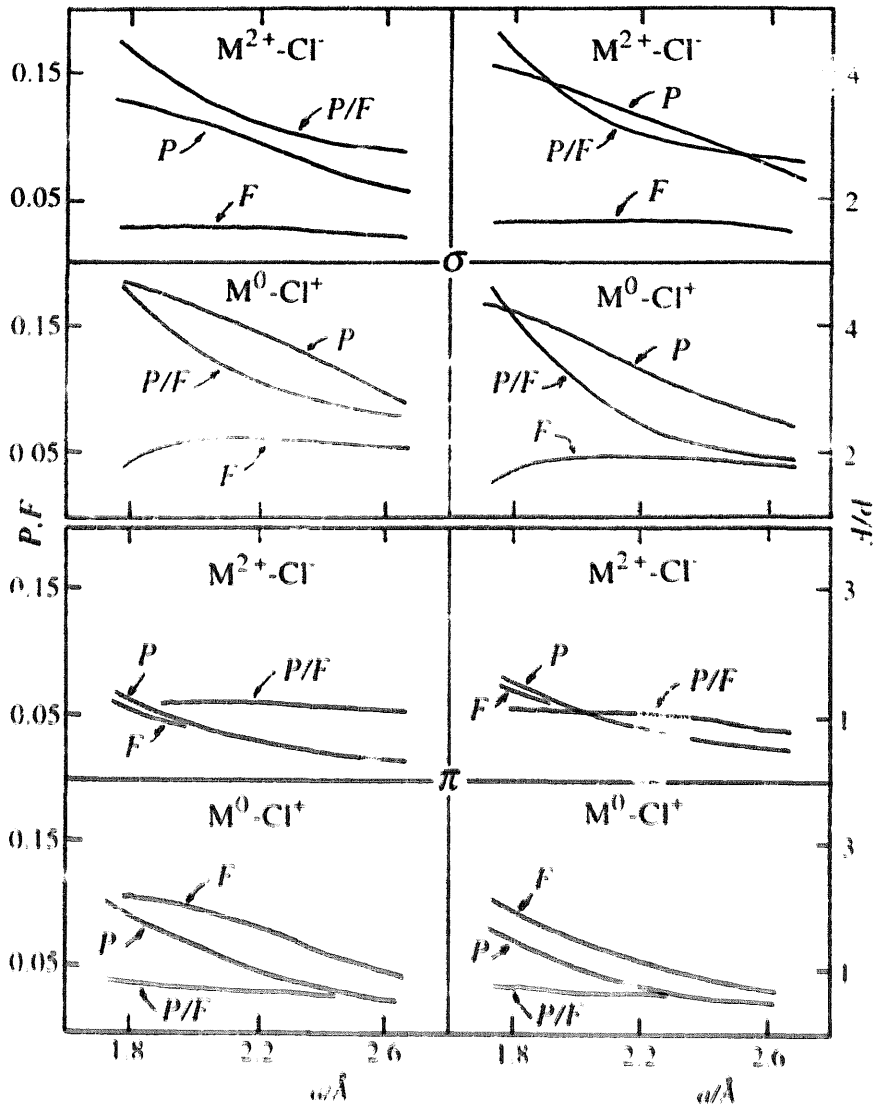

Fig. 14. Trends in P and F integrals, and in their ratios as functions of charge distribution and bond length for σ and expansions, after [52].

cobalt with a chlorine ligand. The results refer to valence orbitals associated with two widely extreme metal–ligand charge distributions: $M^{2+}\ L^{-}$ and $M^{0}L^{+}$. The latter distribution is deemed to have been achieved by donation of a pair of electrons into the metal 4*s* orbital, so retaining the same d^n configuration in the two limits.

Firstly, we note that contributions to P and F intensity parameters are of the same order of magnitude, confirming that neither set of t_λ parameter may be neglected. Secondly, we observe steady decreases in the magnitudes of both P and F integrals with increasing bond length, regardless of metal, ligand, atomic charge or orbital type. Equally general is the fact that the integrals for π interactions are smaller than those of σ type and decrease with bond length more sharply; both these features are shared with the corresponding overlap integrals, obtained by replacing the operator r_z by unity.

5.12.2. P:F *ratios*

The ratios of the integrals, *P*:*F*, which should serve as a good guide to the ratios ${}^{P}t_{\lambda}:{}^{F}t_{\lambda}$ as discussed above, decrease with increasing bond length in all cases. This result directly confirms the qualitative prediction (1) of the preceding section. In terms of the present atom-based computations, polarization of ligand orbitals towards the metal will be mimicked somewhat by shorter bond lengths and support for prediction (2) follows.

5.12.3. *The importance of the ligand functions*

Simultaneous variation of metal and ligand functions were included in the calculations summarized in Fig. 14. It is also revealing to consider the effects of such changes taken separately. A representative sample is presented in Fig. 15 for the combinations Co^{2+}, Co^{0} with Cl^{-} and Cl^{+}. Once again, we observe that values of both *P* and *F* integrals, and of the ratio *P*:*F*, all decrease with increasing bond length. Both *P* and *F* integrals increase with increasing negative charge on the metal as one would expect. Of particular interest is the way that the ratios *P*:*F* decrease markedly as the ligand $3p_z$ orbital contracts with the change $Cl^{-} \rightarrow Cl^{+}$ but hardly alter at all with contraction of the metal $3d_{z^2}$ orbitals. Thus, we conclude that *P*:*F* ratios are dominated by bond length and the *ligand* function; that is, by the multipolar expansion of the ligand orbitals. In essence, the metal *d* orbital and electronic dipole operator, er_z, act roughly as multipliers so far as *P*:*F* ratios are concerned. Analogous conclusions emerge from similar computations for π interactions.

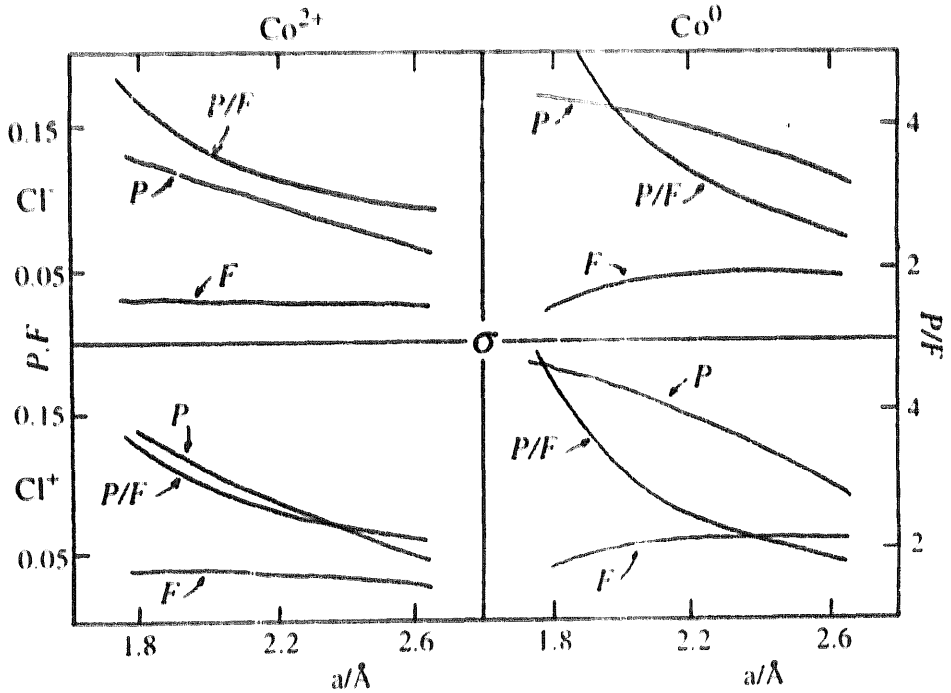

Fig. 15. Trends in *P* and *F* integrals for σ expansions as functions of metal and ligand charge separately [52].

5.12.4. A more realistic modelling

Thus far we have considered only expansions of outer ligand valence orbitals although possible charge variations have also been investigated. All this has been done within a simple atomic/ionic representation of the ligand functions. As discussed earlier, however, bond orbitals are expected to concentrate more about the bond vector than free atomic orbitals. This notion lies behind the greater lone pair–lone pair than lone pair–bond pair repulsions in valence shell electron-pair-repulsion (VSEPR) theory, for example. Simulation of tighter bond orbitals may be effected in part by inclusion of inner orbitals into the valence shell. A donor σ orbital for a chlorine ligand, for instance, will be better represented by some combination of $3p_z$ and $2p_z$ functions than by $3p_z$ alone. Fig. 16 illustrates the dependence of the P and F integrals, and their ratio, upon such a change. The most important conclusion to be drawn from these results is that, not only do the F and P integrals decrease in magnitude on replacing the chlorine ion $3p_z$ function by $2p_z$, but the ratio P:F also decreases markedly. Herein lies the numerical support for proposition (1.3) described in Section 5.11.

Altogether, while bearing in mind the role of metal-originating functions within ligand-field orbitals, the computational exercise summarized here fully confirms all qualitative predictions made earlier. Those predictions provide the guide to the bonding interpretation of the $^{L}t_{\lambda}$ parameter values obtained from a given analysis of intensity distribution in 'd–d' spectra. They have been remarkably well borne out empirically, as will be described in Section 7.

This concludes our review of the CLF intensity model as applied to acentric chromophores [11,52]. In due course, we will show that its extension to include intensity deriving by vibronic means does not require a corresponding increase in parametrization. It is therefore appropriate at this point to compare the CLF approach and its parametric structure with the modelling of (mostly) 'f–f' transitions that we have reviewed at such length in Section 4.

5.13. Symmetry and degrees of freedom

First, let us supplement Table 4 for the case of C_{2v} symmetry, as in Table 16. Table 13 listed Cartesian multipole coefficients — equivalent to $V_Q^k(\rho)$ for $\rho = x, y, z$

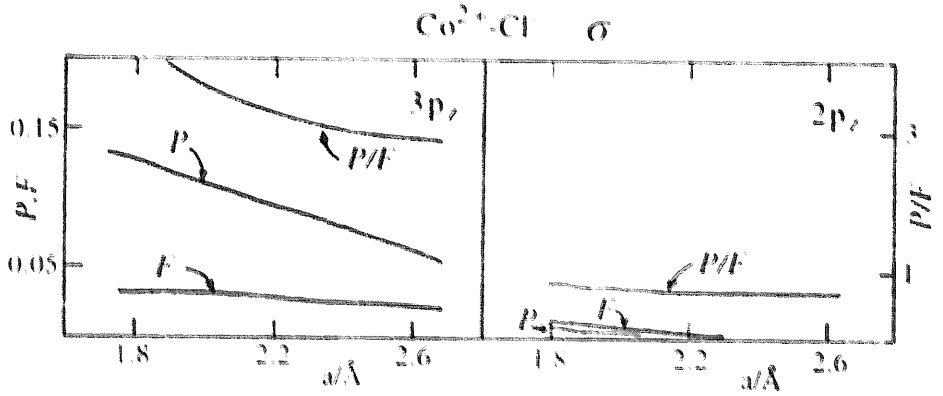

Fig. 16. The markedly smaller P:F ratios for inner orbitals [52].

Table 16
Vector field parameterizations for C_{2v} site symmetry

K	(a) Parameters $V_Q^K(\rho)$				Parameters A_{JKM}		
	Number for z	Number for x	Number for y	Totals	Number for $J=K$	Number for $J=K\pm1$	Totals
2	2	1	1	4	1	3	4
4	3	2	2	7	2	5	7
6	4	3	3	10	3	7	10
All	9	6	6	21	6	15	21

in C_{2v} symmetry. Compare the entries in Table 13 with those in Table 4(a) and Table 16(a) for $C_{\infty v}$ and C_{2v} local ligation symmetry, respectively. In $C_{\infty v}$ symmetry, ${}^{L}t_{\pi x} = {}^{L}t_{\pi y}$ and we find non-zero multipole components in Table 13 (ignoring c_{00}, which is without significance for observable transitions) with c_{20} and c_{40} for T_z, and with c_{21} and c_{41} for $T_{x,y}$, in agreement with the accounting in Table 4(a). Lowering the ligation symmetry to C_{2v}, ${}^{L}t_{\pi x} \neq {}^{L}t_{\pi y}$ and we find two non-zero multipole coefficients in Table 13 with $K=2$ (c_{20}, c_{22}) and two with $K=4$ (c_{40}, c_{42}) for T_z; for each of T_x and T_y, there is one with $K=2$ (c_{21}) and two with $K=4$ (c_{41} and c_{43}). These numbers of symmetry-required variables agree with those in Table 16(a) except that three are expected there for T_z instead of the two appearing in the CLF Table 13. The shortfall in the CLF scheme arises from our neglect of δ interactions in Eq. (91) *et seq.* The missing entry for T_z would involve the real part of $c_{44}(r)$ in Table 12(a) of the form $c_{44} \sim (t_{\delta x^2-y^2} - t_{\delta xy})$. Altogether, therefore, we observe the CLF parametrization to be properly behaved with respect to symmetry.

We discussed in Section 4.7 how the expression of the multipole expansions of the effective dipole operators in terms of vector spherical harmonics is especially revealing with respect to various intensity-generating mechanisms. The coefficients of these harmonics are labelled A_{JKM} by Newman and Balasubramanian [24], or $A^{t}_{\lambda p}$ by Richardson and Reed [43,46], and by Stewart [29,45]. Using Eq. (75), we may construct A_{JKM} coefficients in the C_{2v}, CLF scheme from either Tables 13 or 14; they are listed in Table 17. Once again, the entries in Table 17 correlate with the accounting in Tables 4(b) and 16(b). A_{444} and A_{544} are deemed negligible in the CLF approach following neglect of δ bonding interactions within the cellular ligand-field orbitals.

Let us consider the numbers of degrees of freedom within the CLF model. It is apparent that the nine significant A_{JKM} in Table 17 are functions of nine ${}^{L}t_{\lambda}$ ($L=P$, F, R; $\lambda=\sigma$, πx, πy) basic CLF parameters in local C_{2v} ligation symmetry. For the linear ligation of $C_{\infty v}$ symmetry, four A_{JKM} remain to be expressed in terms of six ${}^{L}t_{\lambda}$ ($L=P$, F, R; $\lambda=\sigma$, π) CLF parameters. With neglect of the CLF R contribution, there are six and four ${}^{L}t_{\lambda}$ parameters for C_{2v} and $C_{\infty v}$, respectively. So the numbers of A_{JKM} and ${}^{L}t_{\lambda}$ variables may or may not be equal, depending upon the nature of (reasonable) simplifying assumptions made. While a computation of the $\{A_{JKM}\}$

Table 17
Non-zero vector harmonic multipole coefficients in the CLF scheme

$$A_{120}=\left(\frac{1}{10}\right)^{1/2}[-{}^{P}\tilde{t}_{\sigma}+3{}^{P}\tilde{t}_{\pi x}+3{}^{P}\tilde{t}_{\pi y}-6{}^{F}\tilde{t}_{\sigma}-2{}^{F}\tilde{t}_{\pi x}-2{}^{F}\tilde{t}_{\pi y}]$$

$$A_{222}=\frac{5}{12}[2{}^{P}\tilde{t}_{\pi x}-2{}^{P}\tilde{t}_{\pi y}+3{}^{F}\tilde{t}_{\pi x}-3{}^{F}\tilde{t}_{\pi y}]$$

$$A_{320}=\left(\frac{1}{15}\right)^{1/2}[9{}^{P}\tilde{t}_{\sigma}+8{}^{P}\tilde{t}_{\pi x}+8{}^{P}\tilde{t}_{\pi y}+4{}^{F}\tilde{t}_{\sigma}+3{}^{F}\tilde{t}_{\pi x}+3{}^{F}\tilde{t}_{\pi y}]$$

$$A_{322}=\frac{1}{6}\left(\frac{1}{2}\right)^{1/2}[8{}^{P}\tilde{t}_{\pi x}-8{}^{P}\tilde{t}_{\pi y}+3{}^{F}\tilde{t}_{\pi x}-3{}^{F}\tilde{t}_{\pi y}]$$

$$A_{340}=\frac{1}{20}[12{}^{P}\tilde{t}_{\sigma}-8{}^{P}\tilde{t}_{\pi x}-8{}^{P}\tilde{t}_{\pi y}-88{}^{F}\tilde{t}_{\sigma}+67{}^{F}\tilde{t}_{\pi x}+67{}^{F}\tilde{t}_{\pi y}]$$

$$A_{342}=\frac{3}{8}\left(\frac{1}{30}\right)^{1/2}[16{}^{P}\tilde{t}_{\pi x}-16{}^{P}\tilde{t}_{\pi y}-29{}^{F}\tilde{t}_{\pi x}+29{}^{F}\tilde{t}_{\pi y}]$$

$$A_{442}=\frac{3}{40}\left(\frac{1}{2}\right)^{1/2}[32{}^{P}\tilde{t}_{\pi x}-32{}^{P}\tilde{t}_{\pi y}+27{}^{F}\tilde{t}_{\pi x}-27{}^{F}\tilde{t}_{\pi y}]$$

$$A_{444}\sim\Delta\delta$$

$$A_{540}=\frac{1}{2}\left(\frac{1}{5}\right)^{1/2}[24{}^{P}\tilde{t}_{\sigma}-16{}^{P}\tilde{t}_{\pi x}-16{}^{P}\tilde{t}_{\pi y}+4{}^{F}\tilde{t}_{\sigma}-{}^{F}\tilde{t}_{\pi x}-{}^{F}\tilde{t}_{\pi y}]$$

$$A_{542}=\frac{3}{20}\left(\frac{7}{6}\right)^{1/2}[16{}^{P}\tilde{t}_{\pi x}-16{}^{P}\tilde{t}_{\pi y}+{}^{F}\tilde{t}_{\pi x}-{}^{F}\tilde{t}_{\pi y}]$$

$$A_{544}\sim\Delta\delta$$

$$A^{*}_{JKM}=(-1)^{J+1+M}A_{JK,-M}.$$

from the $\{{}^{L}t_{\lambda}\}$ is always possible (and unique), the reverse process is generally unavailable. Shortly, we consider the parametrization in the SC and DC models described in Section 4. That has been implemented largely for '*f*–*f*' spectra while, to date, the CLF model has been developed only for '*d*–*d*'. We can, however, anticipate the outline of a CLF modelling of '*f*–*f*' electric dipole strengths.

Qualitatively, the bonding in lanthanoid complexes should resemble that in higher oxidation state compounds of the main transition metals. The bond orbitals are expected to be similar to those represented by the ϕ in Eq. (89); once more we would recognize σ and π contributions, but neglect δ and ϕ. The required parity mixing to be parametrized within the ligand-field orbitals now involves contributions from *d* and *g* functions, of course, so that we would take ${}^{L}t_{\lambda}$ parameters for '*f*–*f*' transitions for $L=D$, G, R. Although the detailed forms of the effective multipole expansions have not been derived at the time of writing, their general form will resemble those in Table 17 but will extend to the numbers given in Table 16. In C_{2v} local symmetry the 21 A_{JKM} (or a few less upon neglect of δ interactions) will be formed from just nine ${}^{L}t_{\lambda}$ parameters or, again, from six if the R contributions can be neglected. In $C_{\infty v}$ symmetry, six A_{JKM} variables will be constructed from six

or four ${}^{L}t_{\lambda}$ parameters depending upon the inclusion or neglect of R contributions, respectively.

5.14. The functional dependence of static- and dynamic-coupling parameters

5.14.1. Static coupling

Reid and Richardson [46] have expressed the A^{λ}_{tp}[SC] parameters in terms of the $\Xi(t, \lambda)$ of Eq. (53):

$$A^{\lambda}_{tp}[\mathrm{SC}] = -A_{tp}\Xi(t, \lambda)(2\lambda+1)/(2t+1)^{1/2}. \tag{140}$$

The $\Xi(t, \lambda)$ quantities are independent of ligand properties. They involve only angular factors and radial integrals relating to the electrostatic configurational mixing on the metal. The ligand dependence of the A^{λ}_{tp}[SC] is contained within the A_{tp} parameters which are the odd parity components of the crystal-field potential that are responsible for that configurational mixing. Within the crystal-field scheme, the $\{A_{tp}\}$ are modelled in terms of ligand point charges $\{eq\}$, sometimes with the addition of ligand polarizabilities, taken as mean, static polarizabilities, $\{\bar{\alpha}\}$. The polarizability refinement is problematic in practice, being fraught with the question of convergence, and is usually ignored. The functional dependence of the point-charge, crystal-field parameters, $\{A^{\lambda}_{tp}[\mathrm{SC}, \mathrm{chg}]\}$, for a single ligand, then involves the magnitude of the point charge, q; its distance from the metal, R; and the radial integrals $\langle nl|r|n'l'\rangle$ and $\langle nl|r^{t}|n'l'\rangle$. Within the philosophy of the crystal-field scheme, all of these quantities are taken from "known" data and, in this sense, the $\{A_{tp}[\mathrm{SC}, \mathrm{chg}]\}$ parameters are not really variables. On the other hand, practical applications of the model — one of which will be reviewed shortly — treat one or more of the basic properties parametrically.

In the $C_{\infty v}$ local symmetry of the point-charge model, A^{λ}_{tp} vanish unless $p = 0$, and $t = \lambda \pm 1$ only. For '*d–d*' transitions, therefore, we find four non-zero $A^{\lambda}_{\lambda\pm1,\,0}$ coefficients and for '*f–f*' transitions there are six, as in Table 4(b). These may be modelled in each case by a single charge magnitude, q; or by q, $\langle nl|r|n'l'\rangle$ and $\langle nl|r^{t}|n'l'\rangle$ depending upon the degree of confidence placed in the radial functions of the metal orbitals (*d*, *p* and *f*; or *f*, *d* and *g*).

5.14.2. Dynamic coupling

Reid and Richardson [46] derived a general expression for the effective transition dipole operator for the DC mechanism:

$$V_q[\mathrm{DC}] = -\sum_{\lambda}\sum_{q'}\sum_{jL}\left(\frac{(\lambda+1)(2\lambda+1)(2\lambda+3)}{3}\right)^{1/2}\langle r^{\lambda}\rangle R_L^{-(\lambda+2)}\{C^{\lambda}(j)C^{\lambda+1}(L)\}^{1}_{q}$$
$$\times\sum_{n,\,m}\langle 1q,\,1-q'|nm\rangle^{*}(-1)^{q'}\alpha^{n}_{m}(L). \tag{141}$$

Their V_q corresponds, in our notation, to T_n; that is, to one "spherical" polarization of the effective transition operator: $\langle r^{\lambda}\rangle$ is the radial integral $\langle {}^{t}R|r^{\lambda}|{}^{t}R\rangle$ where ${}^{t}R$ is the radial part of the orbitals between which the transition is taking place (${}^{d}R$ or

^fR, as appropriate). The $\{\alpha_m^n(L)\}$ are components of the dynamic, electric dipolar polarizability tensor for ligand L. Eq. (141) is for the most general circumstance in which there is no special orientation of a most generally formulated polarizability. Various special cases for Eq. (141) may be constructed. The first concerns the exclusion of $n=1$ within the range $n=0$, 1, 2. This omission relates to ligands with S ground states and corresponds to the irrelevance of the antisymmetric polarizability tensor discussed just before Eq. (67). The components with $n=0$ and 2 relate to the symmetric mean and anisotropic tensors, there labelled with $k=0$, 2. A_{tp}^{λ} parameters for the isotropic ($n=0$) case depend upon $\bar{\alpha}$, the mean polarizability, and are labelled A_{tp}^{λ}[DC, α]. A commonly favoured special case relates to the anisotropic ($n=2$) polarizability when this is taken to be cylindrically symmetric; that is, when the polarizability ellipsoid is a figure of revolution. Parameters for these circumstances are labelled A_{tp}^{λ}[DC, β] where β relates to the single anisotropy $(\alpha_{\parallel}-\alpha_{\perp})$; $\parallel$ and $\perp$ refer to the principal axis of the tensor.

From Eq. (141), we observe that A_{tp}^{λ}[DC] parameters are functions of the radial integrals for the metal atom, $\langle r^{\lambda}\rangle$; the bond length, R, and the ligand polarizability, α. That Eq. (141) relates to a sum of contributions from several perturbers (L) does not confuse this assessment of the functional dependency of the A_{tp}^{λ} parameters. We have already discussed the number of A_{tp}^{λ} parameters which may arise in $C_{\infty v}$ or C_{2v} local *pseudo*symmetry. Regardless of the symmetry, they are all functions of $\langle r^{\lambda}\rangle$, R and α. There arises, however, the question of how many system variables are involved. This can be a complicated matter depending upon how much is modelled and how it is done.

Consider first, $C_{\infty v}$ ligation symmetry. Here there are one, or two, polarizability parameters, $\bar{\alpha}$ and β. The radial integrals $\langle r^{\lambda}\rangle$, are either two or three in number according to the modelled transitions being of 'd–d' or 'f–f' type, respectively. Within an "*ab initio*" philosophy, these quantities are taken as known but they can, nevertheless, be considered as variables in a looser modelling scheme. In C_{2v} symmetry, we require three polarizability variables, corresponding to the three major axes of a general, symmetric polarizability tensor. Their orientations are surely not to be treated as variables for they are defined by the symmetry elements of that point group. In lower symmetry, however, six polarizability variables are required, although these may be taken in the form of the three principal polarizabilities plus three Euler angles describing their orientation with respect to the local ligation or global molecular- frame. One may anticipate that the complications for such low symmetry are not worth the candle. In due course, we briefly consider one low symmetry case within the CLF model. For the present it is enough to stay with C_{2v} which serves as a useful symmetry classification for very many chemical ligations.

In applications of the DC mechanism generally, problems arise in the modelling of ligand polarizabilities. One, of course, is that the $\{\alpha\}$ of Eq. (141) are *dynamic* properties rather than static and, within an *ab initio* approach, appropriate values may not be readily available. This problem is particularly severe for polarizability anisotropies. One measure of the difficulty is provided by the following brief review of a study by Dallara et al. [54].

5.14.3. *Modelling polarizability contributions — an example*

Following their presentation of the theory of '*f–f*' electric dipole intensities [from which Eq. (141) was quoted], the Richardson group described its first application for two acentric lanthanoid chromophores. The study [54] involved a more refined analysis of the $[Eu(ODA)_3]^{3-}$ and $Eu(DBM)_3H_2O$ chromophores that were the subject of earlier work [32] using the isotropic DC model: the chromophore geometries are of the ID and III types of Fig. 6. The oxydiacetate (ODA) and β-diketonate (DBM) ligands are shown in Fig. 17. Dallara et al. [54] list the ligand properties they require to model the appropriate A_{tp}^{λ} parameters. They are: (1) identification and selection of ligand perturber sites; (2) positional coordinates and, in some cases, spatial orientations of those perturbers; (3) ligand charges; and (4) ligand polarizabilities.

Their consideration of perturbers was remarkably comprehensive. Ligations were not represented as single entities. Instead, *all* atoms in the ODA ligands were included, and each assigned fractional charges, q_L, and isotropic polarizabilities, $\bar{\alpha}_L$. For the DBM system, all chelate ring atoms and the water oxygen atom were included, while the phenyl groups were each described by a single perturber site. All of these had already been considered in their earlier study [41]. In the Dallara et al. paper [54], this already-comprehensive list was supplemented with various sets of chemical bonds. Both isotropic ($\bar{\alpha}_L$) and anisotropic (β_L) polarizability values were assigned to each chemical bond and positioned at the bond midpoints. The phenyl groups of the DBM ligand were assigned $\bar{\alpha}$ and β values also. The spatial orientations required for all anisotropic DC perturbers were fixed from appropriate X-ray crystallographic data.

Initial modelling with all these perturbers quickly indicated that a large subset made little significant contribution to the calculated A_{tp}^{λ} parameters. The bulk of the study of Dallara et al. therefore relates to a so-called "reduced" basis of structural perturber sites. We reproduce these for the DBM chromophore in Table 18 to illustrate the detail of this work [54].

A major objective of the study of Dallara et al. [54] was to demonstrate the empirical need for non-zero parameters of the kind $A_{\lambda p}^{\lambda}$ (especially A_{20}^{2}) that reveal the relevance of the anisotropic DC mechanism. This they did. Their success in reproducing the experimental dipole strengths in these chromophores is illustrated in Table 19. A corresponding comparison of modelled and empirical A_{tp}^{λ} parameter values is presented in Table 20. Note that these values refer to the chromophores complete rather than to single ligation perturbers.

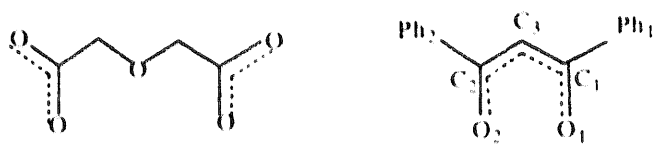

ODA DBM

Fig. 17.

Table 18
Ligand perturber site properties for $Eu(DBM)_3H_2O$ (after Dallara *et al.* [54])

Perturber site (L)	Positional coordinates					Orientation		
	R_L (Å)	θ_L (°)	ϕ_L (°)	q_L (e)	$\bar{\alpha}_L$ (Å^3)	β_L (Å^3)	θ'_L (°)	ϕ'_L (°)
H_2O	2.390	0	0	−0.30	1.490			
O_1	2.270	73.54	40.72	−0.625	0.026			
O_2	2.300	130.72	348.95	−0.625	0.026			
C_1	3.317	86.39	31.91	0.10	0.037			
C_2	3.322	119.78	2.86	0.10	0.037			
C_3	3.721	103.57	18.54	0.05	0.878			
Ph_1	5.994	74.22	42.54	0	10.60	−5.85	67.34	134.45
Ph_2	5.918	130.96	347.91	0	10.60	−5.85	55.98	112.95
C_1–O_1	2.850	81.40	34.22	0	0.987	0.26	109.79	15.88
C_2–O_2	2.868	123.31	357.73	0	0.987	0.26	96.77	22.22

Table 19
Comparison of relative dipole strengths within multiplet–multiplet transition (after Dallara *et al.* [54])

Transition	Relative dipole strength		
	Model calculation	Empirical fit	Experimental
(a) for $[Eu(ODA)_3]^{3-}$			
$A_1(^7F_0) \rightarrow E_a(^5D_2)$	1	1	1
$A_1(^7F_0) \rightarrow E_b(^5D_2)$	0.94	4.25	4.43
$E_b(^7F_2) \leftarrow A_1(^5D_0)$	1	1	1
$E_a(^7F_2) \leftarrow A_1(^5D_0)$	0.85	3.76	3.84
(b) for $Eu(DBM)_3H_2O$			
$A(^7F_0) \rightarrow E_a(^5D_2)$	1	1	1
$A(^7F_0) \rightarrow A(^5D_2)$	7.34	6.70	3.38
$A(^7F_0) \rightarrow E_B(^5D_2)$	1.89	11.01	22.22
$A(^7F_1) \leftarrow E(^5D_1)$	1	1	1
$A(^7F_1) \leftarrow A(^5D_1)$	109	2.38	2.21
$E(^7F_1) \leftarrow E_1A(^5D_1)$	59.7	4.28	6.52
$E_b(^7F_2) \leftarrow A(^5D_0)$	1	1	1
$A(^7F_2) \leftarrow A(^5D_0)$	3.49	7.52	3.80
$E_A(^7F_2) \leftarrow A(^5D_0)$	0.89	14.53	5.91

We make just two broad observations about the results summarized in Table 19 and Table 20. While the importance of the A^{λ}_{20} ($t = \lambda$ type) parameter has been well demonstrated in these systems: (1) the quantitative agreement between modelled and empirical parameters and dipole strengths is, at best, modest; and (2) even the quality of the empirical fits to experiment is not perfect. The empirical parameters are mechanism-independent, of course; not only do they not depend upon the SC and DC modelling, but their derivation is independent of any notion of superposition. It seems likely that the differences between the last two columns of Table 19

Table 20
Comparison of calculated intensity parameters with those determined by parameter fits (after Dallara *et al.* [54])

Parameter	$A^{\lambda}_{tp}/10^{-11}$cm			
	$[Eu(ODA)_3]^{3-}$		$[Eu(DBM)_3]H_2O$	
	Model calculation	Empirical fit	Model calculation	Empirical fit
A^2_{10}			−46	−40
A^2_{20}	15.3i	15.8i	8.49i	70i
A^2_{30}			69.5	50
A^2_{33}	−39.2i	−15.6i	−16.4+38.9i	−10+40i

derive from imperfect modelling of the ligand-field energies upon which the intensity analyses are predicated. As for the comparisons between the modelled and empirical fits, Dallara et al. comment, amongst other matters, upon the possibility that other mechanisms, not considered in their study, may play their part. We agree but reserve our commentary for the overview of a comparison we now make between the CLF approach and the SC+DC modelling of the Richardson and Mason groups.

5.15. *Covalency and the CLF approach*

The SC and DC mechanisms for forced electric dipole transitions are both examples of the "independent systems" approach. There is no recognition of the covalency and overlap between metal and ligands. The possible importance of these effects, however, was strongly argued for by Newman and Balasubramanian [24], and acknowledged repeatedly by Richardson and his group [43,55]. In 1983, the latter pointed out [43] that: "While it seems certain that overlap effects will contribute to the intensity...it is not at all clear how large these effects will be or how they should be modeled and calculated." The activity in this field was such that just one year later in 1984, Poon and Newman [40] made the first explicit attempt to consider covalency. Their results did not agree well with experiment, however, as we saw in Section 4.7 but one might not have expected too much of so simple a modelling within an *ab initio* approach; as was admitted by these workers at the time.

The CLF approach, though parametric, does attempt to incorporate all effects of covalency and overlap based upon an assumption that ligand-field theory is a generally successful *pseudo*potential model for *d*- or *f*- electron properties. The ligand-field orbitals $\{\psi_{LFO}\}$, from which the present intensity model is derived, correspond closely with the "best orbitals" notionally defined by density functional theory - allowance for the separation of *d–d* (or *f–f*) interactions having been made, as outlined above and elsewhere [7–9]. The ligand-field orbitals thus include the effects of all covalency, overlap and configurational mixing that go to make the molecule *as it is*. These italics emphasize the crucial distinction between the formed molecule and the promolecule comprising metal and ligands in their electronically free forms but located in the geometry of the real molecule. The optical (and other)

quantities that we seek to model are properties of the molecular ensemble after the electron redistribution we call bonding has taken place. Furthermore, since bonding varies between one molecule and another, the forms of both bond orbitals and d (or f) basis functions vary. An obvious corollary of this is that the magnitudes of all ligand-field parameters — both e_λ and ${}^{L}t_\lambda$ — will generally vary from system to system, and that exact, or even occasionally approximate, transferability of these parameter values between systems is not to be expected. For the energy parameters, e_λ, this question has been discussed at length recently [9]. No doubt there is rather little direct overlap between lanthanoid f orbitals and the ligands (or between higher oxidation state transition metal d orbitals and the ligands). However, that does not deny the relevance of covalency and overlap between metal and ligands in general — they are *bound* after all. Although the metal–ligand overlap presumably involves the metal s and p orbitals in particular, the consequences for covalency, in general, and for the d or f electron properties, in particular, must be expected to be important.

The centrally important contribution by Newman and Balasubramanian [24] was their demonstration that, within the single restriction to one-electron operators, all kinds of parity-mixing (which enables the electric dipole transitions that are our concern) will be subsumed within an effective vector operator like Eq. (72). The SC and DC mechanisms are constructs to model *some* contributions to that operator in terms selected by the theoretician. We argue that the CLF approach models *all* contributions in terms selected by nature. The SC terms refer to configuration mixing between functions of an imagined (promolecular) free ion. The DC terms relate to the construct of independent systems that are coulombically coupled transiently in the presence of the incident radiation field. These are ways of setting up a calculable scenario given the enormity of the task of some complete *ab initio*, all-electron computation, and, of course, covalency and overlap are explicitly excluded. However, the effects of covalency and overlap are also implicitly excluded. Our point, here, is that estimates of perturber charges and polarizabilities must relate to the bound structure rather than to various free units. To some extent, of course, Dallara et al. [54] attempted to take account of this by considering some bonds as pertubers; otherwise, however, their modelling referred to uncomplexed atoms. There arises the question of how much charges and polarizabilities change on complexation. No doubt those for the more distant entities — those outside the first coordination shell — will often be somewhat similar in bonded and promolecular structures. On the other hand, the DC contribution to intensity from the more distant perturbers will generally be less important than those from the immediate metal environment, and it is there where the largest changes to charge distribution on complexation are expected. Our discussions of the factors affecting trends in CLF ${}^{L}t_\lambda$ parameters centred around bond polarization effects and the "tightening" of bonding electron density about the metal–ligand line of centres. It is at least likely that the polarizabilities of ligand donor atoms will be much reduced relative to those in the corresponding free ligands. Without the benefit of all-electron *ab initio* calculations for object chromophores, however, it is obvious that we can do no more than make educated guesses. Our guess would be that previous "*ab initio*" estimates of the DC contributions to forced electric dipole intensities are too large. This opinion lies behind our

suggestion in Section 4.9 that the successful accounting for the '*d–d*' intensities in $[CoCl_4]^{2-}$ and the like is owed to cancellations between the neglect of covalency and overlap, and an overestimation of the polarizability of bound ligands; in effect, to cancellations between the explicit and implicit neglect of covalency.

The CLF approach merely recognizes that, *inter alia*, the functions involved in electric dipole transitions *are* of mixed parity and the model simply parametrizes the consequences of that. It might be objected that, in the absence of some prior calculation of that mixing from first principles, nothing has been put into the model. If so, we would observe that neither have there been included any unnecessary preconceptions that are artefacts of the independent systems proposition. Our assertion that the CLF approach is selected by nature derives from an observation that ligand-field theory works well, by and large, together with theoretical studies [5–9] of why it should. Those studies were made by tracing connections between the empirical procedures of ligand-field theory, on the one hand, and the well-established concepts of quantum chemistry at large, on the other. In so doing, it was possible to discern what ligand-field parameters must monitor and, hence, how they may be interpreted. This stance is to be contrasted with a "front-loaded" model that imbues parameters with meanings by assumption and definition. The former reveals the constructs of nature, the latter imposes the prejudices of the theoretician, however necessary they may be felt in the interests of tractability.

There can, of course, be no direct mapping of the SC and DC mechanisms onto the CLF modelling. It is possible, however, to see vaguely how the concepts of the former relate to the latter. Consider first, the SC contribution. The essence of Judd's [22] and Ofelt's [23] electrostatic modelling was to evaluate the consequences of parity mixing within the "optical" f^N states arising from configurational interaction with excited $f^{N-1}d^1$ or $f^{N-1}g^1$ states brought about by the crystal field. All such mixing is just one part of the (implicit) description of the ligand-field orbitals $\{\psi^{LFO}\}$ in the formed molecule. The dominant contribution to the $\{\psi^{LFO}\}$ is expected to comprise those metal and ligand orbitals most involved in overlap, of course. There will, however, be lesser contributions from higher-lying metal functions whose overlap with the ligands may be slight or vanishing. As in the Judd and Ofelt formalisms, such contributions will take a sign determined by energy separations like $E(4f)-E(5d)$. The sign opposition of SC and DC contributions to intensity has been noted many times. Our discussions of the CLF ${}^{L}t_{\lambda}$ parameters repeatedly referred to parity-mixing originating on the metal or originating on the ligand. The first of these *resembles* the SC contributions of the Judd and Ofelt models. We have emphasized the word *resemble* for it must not be forgotten that the differences between real molecules and promolecules render the exact forms of appropriate radial integrals and orbitals energies as unknown to us in practice.

Connections between the CLF scheme and the DC mechanism are hard to find. In principle, one could envisage a form of algebra that would achieve some artificial resemblance between them. One might propose a different independent-systems structure relating not to metal and ligands but to metal d (or f) functions and to the "rest" orbitals of Eq. (88). Expressions akin to Eq. (60) would result, but

subsequent relationships with polarizabilities appear to be without conventional meaning — and surely without utility.

There is a central point here to do with the question of drawing arbitrary boundaries: where does a chromophore begin and end? For the SC approach, the chromophore is the metal ion itself. For the DC model, we might say the same, but that intensity arises from coupling with atoms, groups and bonds surrounding the metal. As the ligand polarization mechanism is the same as the inhomogeneous dielectric approach, one may view it as a story about secondary radiation sources. The magnitudes of such contributions decrease rapidly with the distances of those sources from the central metal and with their number establishing an ever-closer approach to effective spherical symmetry in the lattice. How well does the CLF approach model the whole environment? There are two direct types of approximation involved. One is the restriction in the number of cells within the superposition to the number of ligand donor atoms in the first coordination shell (plus any void cells for the energy parametrization). The other is the neglect of δ (and perhaps ϕ etc.) bonding with the metal. Both are chemically reasonable assumptions that have proved totally satisfactory for the analysis of transition energies and various magnetic properties. Then there are indirect approximations. Given the "empirical" fitting of intensity distributions to the basic CLF model, including misdirected valency where appropriate, there follows the *interpretation* of the optimal ${}^{L}t_{\lambda}$ parameter values. Those values will, of course, subsume effects originating in (radially) distant parts of the molecule as well as in those close by that are the usual focus of our attention. In that sense the CLF model is complete (accepting always the basic ligand-field premis about mean d (f) orbitals and so on, as discussed in Section 5.1 and elsewhere [5–9]). Whether one is able or is bothered to resolve the undoubtedly small contributions from the periphery of the molecule or, indeed, from the lattice is another question. It seems neither sensible nor attractive to risk double counting by adopting a mix which one might label CLF + DC.

In Section 7 we will survey the successful application of the CLF approach to some 43 chromophores. The ${}^{L}t_{\lambda}$ parameter values deriving from both the static CLF model and the vibronic one we describe in Section 6 consistently correlate well, though qualitatively, with broader issues of chemistry and bonding. The quality of reproduction of experimental intensity distributions is uniformly good and rather better than that reported so far for the independent systems analyses. It must be acknowledged, however, that the reproduction of the generally broad — and usually spin-allowed — features of 'd–d' spectra, which have been the sole focus of CLF studies, may be less exacting than of those usually sharp and well-resolved transitions typical of 'f–f' spectra.

5.16. *Misdirected valency*

The local *pseudo*symmetry for many ligations is lower than C_{2v}. This circumstance tends to arise in two main ways: (1) when the constraints of chelation or intermolecular hydrogen bonding within the lattice result in bent bonds; and (2) when the ligand field of a non-dative lone pair on the donor atom lying to one side of the local

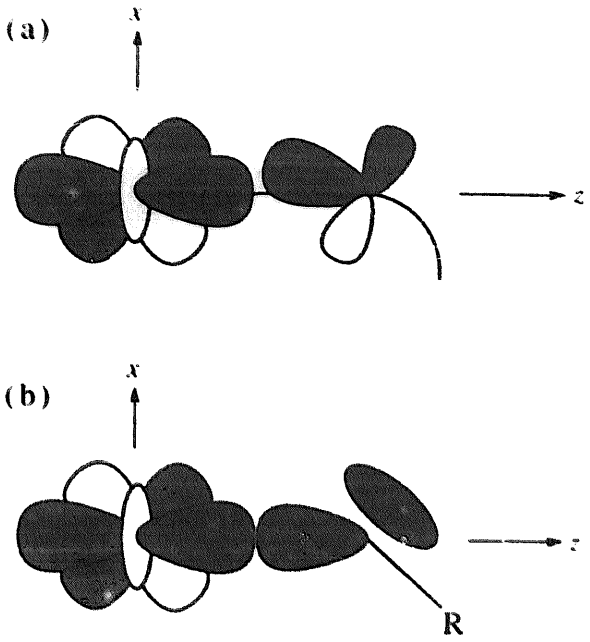

Fig. 18. Misdirected valency: (a) for bent bonding, perhaps due to chelation; and (b) from the effects of the non-dative ligand lone pair.

metal–ligand vector is significant. These situations are sketched in Fig. 18 and are collectively referred to by us as "misdirected valency". The local *pseudo*symmetry is C_s. The consequences for CLF analysis of transition energies have been studied extensively, both theoretically [9,10] and experimentally [10]. The local energy matrix ceases to be diagonal on lowering the symmetry from $C_{2v} \rightarrow C_s$ and an extra off-diagonal parameter $e_{\sigma\pi}$ is included in the parameter set:

$$\begin{array}{c} \\ d_{z^2} \\ d_{xz} \\ d_{yz} \end{array} \begin{array}{c} C_{2v} \\ \begin{pmatrix} e_\sigma & 0 & 0 \\ 0 & e_{\pi x} & 0 \\ 0 & 0 & e_{\pi y} \end{pmatrix} \end{array} \begin{array}{c} C_s \\ \begin{pmatrix} e_\sigma & e_{\sigma\pi x} & 0 \\ e_{\sigma\pi x} & e_{\pi x} & 0 \\ 0 & 0 & e_{\pi y} \end{pmatrix} \end{array} . \tag{142}$$

The consequences of these types of ligation for intensities are likely to be complicated. For the DC approach, the situation corresponds to the most general case studied, as in Eq. (141), and is an unappealing subject for analysis. It is equally, or perhaps even more, unappealing within the CLF model, though one study has been made [56]. We do not go over the tedious algebra here, however, confining ourselves to some general remarks. (1) ${}^{L}t_{\sigma\pi}$ parameters, akin to $e_{\sigma\pi}$ for energies, Eq. (142), are not required. (2) The main consequences of misdirected valency for the intensity parametrization are modified ${}^{L}t_{\pi x}$ (if the misdirected valency is defined within the local xz plane) values. These correspond to a positive contribution and will be most visible for the case of a formally non-π-bonding ligand when ${}^{L}t_{\pi x}$ values will be non-zero in the presence of a bent ML σ bond. Modifications to ${}^{L}t_{\sigma}$ values are expected

to be small. (3) The detailed forms of Tables 9–11, 13, 14 and 17 are all changed in the lower, C_s, symmetry but evidence to date suggests that neglect of these changes will not be too serious. (4) In summary, a practical *modus operandi* for systems with misdirected valency is to parametrize fully so far as energies and the ligand field are concerned (with e_σ, $e_{\pi x}$; and $e_{\sigma\pi x}$, and $e_{\pi y}$, of course) and to let ${}^{L}t_{\pi x}$ values subsume, as best they might, the consequences for the subsequent intensity analysis — in particular by allowing for non-zero ${}^{L}t_{\pi x}$ values in cases of pure σ-bonding chelates like ethylenediamine, for example.

5.17. Coordination voids

An important concept in the ligand-field analysis of planar and other sparsely coordinated complexes is that of the coordination void. The consequences for the CLF e_λ parametrization have been described many times and reviewed in great detail recently [9]. Our remarks here follow that discussion. The effective ligand-field potential associated with a coordinationally void region is not zero; as for a region or cell containing a ligand, the potential is established by any locally situated "rest" orbitals [see Eq. (88)]. In a void cell, the effective "rest" orbitals are dominated by an energetically high-lying s function. This cannot, of course, affect forced electric dipole moments because of the orbital selection rule $\Delta\ell = \pm 1$. Overall, therefore, the presence of coordination voids must be properly accounted for within prior ligand-field analysis but otherwise is without consequence for intensities.

The addenda of this and the preceding section complete our description of the CLF intensity model for acentric chromophores. We now consider the case of vibronic coupling in which parity mixing and the generation of effective electric dipole operators arise dynamically during the course of molecular vibrations.

6. The cellular ligand-field model for centric and near-centric chromophores

As discussed in Section 2, the Condon transition moment Eq. (34) will vanish in centric chromophores. Electric dipole intensity may arise in centrosymmetric species if induced by appropriate vibrational modes. In the harmonic approximation, the complex motions undergone by a vibrating molecule can always be resolved into a combination of independent normal modes. This independence means that normal vibrations are uncorrelated so that, in general, they coincide in neither frequency nor phase. Electric dipole intensities induced by several normal modes are then simply given by the sum of the intensities of each. There is no question here of forming the square modules of the sum of transition moments for each vibration. The uncorrelated nature of these independent intensity sources ensures that cross terms between different transition moments vanish over time. In the following development [12], therefore, we consider electric dipole intensity for a single normal vibration mode, η, modelling experiment by a simple sum of intensities at the end.

6.1. Effective operators

As in the "static" CLF model of Section 5 ("static" referring to the environment being acentric), we seek to construct effective operators, $e\mathbf{T}$, acting upon pure (electronic) d^N (or f^N) states that replace pure electric dipole operators $e\mathbf{r}$ acting upon "true" states. Within the electronic-nuclear space that we must now consider, however, those effective operators will also be functions of the nuclear displacements Q_η of the normal mode η. We begin by writing matrix elements of effective operators $e\mathbf{T}'$ acting in the electronic–vibrational basis of the Born–Oppenheimer approximation as equivalent elements of operators $e\mathbf{T}$ acting within the pure electonic basis:

$$\begin{aligned}&\langle\chi_d(r,\theta,\phi)V(Q_\eta)|e\mathbf{T}'(Q_\eta;r,\theta,\phi)|\chi'_d(r,\theta,\phi)V'(Q_\eta)\rangle\\&\quad\approx\langle\chi_d(r,\theta,\phi)|e\mathbf{T}(Q_\eta;r,\theta,\phi)|\chi'_d(r,\theta,\phi)\rangle,\end{aligned}\tag{143}$$

in which the approximation sign expresses an assumption that the vibrational wavefunction V' is effectively independent of which excited electronic state is involved in the chosen transition. In addition, the vibrational overlap integral is taken to be unity in recognition of the fact that the model will be applied to the reproduction of the broad features in 'd–d' corresponding to vibrational envelopes. We have thus assumed that the $e\mathbf{T}$ may be constructed by folding in the same vibrational product, $V(Q_\eta)V'(Q_\eta)$ throughout the ligand-field domain. This assumption is of the kind already used in the CLF model for acentric systems, in which one presumed that the description of any one d orbital is independent of the particular transition in which it is involved — the concept of the "mean" d orbital discussed earlier. One thus considers averaged parameters in parallel with the central strategy of ligand-field analysis of transition energies.

Expanding $\mathbf{T}$ in multipolar form:

$$\mathbf{T}(Q_\eta;r,\theta,\phi)=\sum_\alpha\sum_{kq}w_{kq\alpha}(Q_\eta;r)C_q^k(\theta,\phi)e_\alpha,\tag{144}$$

where $\mathbf{e}$ is a unit vector referred to Cartesian directions, $\alpha=x,y,z$, yields matrix elements in the basis of pure d (or f) electronic wavefunctions as

$$\begin{aligned}&\langle\chi_d(r,\theta,\phi)|\mathbf{T}(Q_\eta;r,\theta,\phi)|\chi'_d(r,\theta,\phi)\rangle\\&=\sum_\alpha\sum_k\sum_{q=-k}^{k}\langle\chi_d(r,\theta,\phi)|w_{kq\alpha}(Q_\eta;r)C_q^{(k)}(\theta,\phi)|\chi'_d(r,\theta,\phi)\rangle e_\alpha\\&=\sum_\alpha\sum_{kq}\langle R_d(r)|w_{kq\alpha}(Q_\eta;r)|R_d(r)\rangle\langle\hat\chi_d(\theta,\phi)|C_q^{(k)}(\theta,\phi)|\hat\chi'_d(\theta,\phi)\rangle e_\alpha\\&=\sum_\alpha\sum_{kq}c_{kq\alpha}(Q_\eta;r)\langle\hat\chi_d|C_q^{(k)}|\hat\chi'_d\rangle e_\alpha,\end{aligned}\tag{145}$$

in which $\hat\chi$ denotes the angular part of χ, and the $\{c\}$, given by

$$c_{kq\alpha}(Q_\eta;r)=\langle R_d(r)|w_{kq\alpha}(Q_\eta;r)|R_d(r)\rangle,\tag{146}$$

are functions of the nuclear displacements Q_η and of the radial functions R_d which are common to all the ligand-field states and d orbitals for the chromophore in question.

Once again we invoke a cellular superposition, $T=\Sigma_c T^c$, writing:

$$\mathbf{T}^c(Q_\eta^c; r^c, \theta^c, \phi^c)=\sum_{\alpha'}\sum_{k'q'} w^c_{k'q'\alpha'}(Q_\eta^c; r^c)C^{(k')}_{q'}(\theta^c, \phi^c)e^c_{\alpha'}, \tag{147}$$

for the cellular multipolar operators, T^c. The global matrix elements Eq. (145) then take the forms [12]:

$$\langle\chi_d(r, \theta, \phi)|\mathbf{T}(Q_\eta; r, \theta, \phi)|\chi'_d(r, \theta, \phi)\rangle=\sum_c\sum_{\alpha'\alpha}\sum_{k'}\sum_{q'q} \mathscr{L}^c_{\alpha'\alpha}c^c_{k'q'\alpha'}(Q_\eta^c; r^c)e_\alpha\mathscr{D}^{k'}_{q'q}(\hat{R}^c)$$
$$\times\langle\hat{\chi}_d|C^{(k')}_{q'}|\hat{\chi}'_d\rangle, \tag{148}$$

where

$$c^c_{k'q'\alpha'}(Q_\eta^c; r^c)=\langle R_d(r)|w^c_{k'q'\alpha'}(Q_\eta^c; r^c)|R_d(r)\rangle. \tag{149}$$

The multipolar coefficients $\{c^c_\alpha\}$ for each local Cartesian polarization, $\alpha'=x', y', z'$, are similar to those evaluated in Table 13 for the CLF "static" model except in two crucial respects. They depend upon the local orientation of cellular nuclear displacement, Q_η^c, and, as a second consequence of that, these $\{c^c\}$ differ even for cells involving otherwise identical ligations, as the nuclear displacements at a given instant in time generally vary from cell to cell within any given normal vibration. In this, we recognize a global phase structure in the $\{Q_\eta^c\}$ determined by the molecular normal vibration mode which persists even after resolution of that mode into the cellular components. Accordingly, the projection of Q_η to form the $\{Q_\eta^c\}$ is an important feature of the parameteric structure in this vibronic CLF model. Furthermore, each Q_η^c describes a vectorial displacement with, generally, different components relative to the locally defined axes, x', y', z'.

The core of the "static" CLF intensity model, of course, was the expression of the cellular multople effective operators in terms of the basic ${}^{l_\lambda}t_\lambda$ parameters. Analogous expressions within the present vibronic CLF model depend upon the nature of local nuclear displacements. We consider three types of motion — bends, stretches and torsions.

6.2. *Bending vibrational modes*

The cellular superposition of Eq. (148), like that of Eq. (127) for the "static" model, involves operator multipole expansions referred to mean or equilibrium ligation frames which are defined in practice by X-ray diffraction data. Let us consider a bending vibration mode in which an object ligation oscillates in the local xz plane and define a reference frame D associated with an instantaneous angular displacement of the ligation by θ^x from the equilibrium frame E, as shown in Fig. 19. It is recognized, of course, that the oscillation plane of a real bending motion need not coincide with a principal plane of the local ligation *pseudo*symmetry; the displacement θ^x, here, therefore represents merely the component of the real bend in the xz plane. The sense of the angular displacement, as indicated by the arrow in Fig. 19, is such that a positive θ^x is associated with frame D being displaced into the positive quadrant of the xz plane of frame E. In the harmonic approximation that we consider here, angular displacements are taken to be small, when $\cos^n\theta^x\rightarrow 1$,

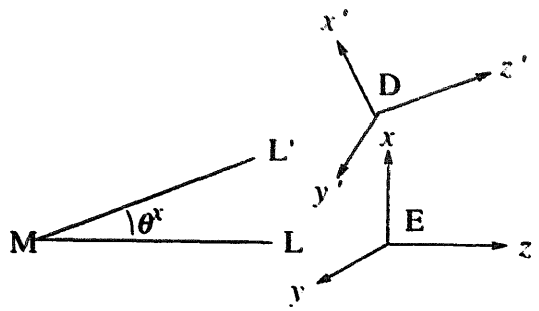

Fig. 19. Equilibrium, E, and displaced, D, frames for bending modes.

sin $\theta^x \to \theta^x$ and $\sin^n \theta^x \to 0$ $(n>1)$, and the two frames are related by:

$$\begin{array}{cc} & E \\ & \begin{array}{ccc} x & y & z \end{array} \\ D \begin{array}{c} x' \\ y' \\ z' \end{array} & \begin{pmatrix} \cos\theta^x & 0 & -\sin\theta^x \\ 0 & 1 & 0 \\ \sin\theta^x & 0 & \cos\theta^x \end{pmatrix} \end{array} \xrightarrow[\text{small}]{\theta^x} \begin{array}{c} E \\ D \begin{pmatrix} 1 & 0 & -\theta^x \\ 0 & 1 & 0 \\ \theta^x & 0 & 1 \end{pmatrix}. \end{array} \tag{150}$$

We further assume that small vibrational displacements do not significantly alter the character of the local electron density distribution. Therefore, effective electric dipole operators for the displaced ligation may be taken, with respect to frame D, as those given in Table 13: we write,

$$\begin{aligned} {}^{L}T_{z'} &= {}^{L}c^{z'}_{20}C^{(2)}_0 + {}^{L}c^{z'}_{22}(C^{(2)}_2 + C^{(2)}_{-2}) + {}^{L}c^{z'}_{40}C^{(4)}_0 + {}^{L}c^{z'}_{42}(C^{(4)}_2 + C^{(4)}_{-2}) \\ {}^{L}T_{x'} &= {}^{L}c^{x'}_{21}(C^{(2)}_1 - C^{(2)}_{-1}) + {}^{L}c^{x'}_{41}(C^{(4)}_1 - C^{(4)}_{-1}) + {}^{L}c^{x'}_{43}(C^{(4)}_3 - C^{(4)}_{-3}) \\ {}^{L}T_{y'} &= {}^{L}c^{y'}_{21}(C^{(2)}_1 + C^{(2)}_{-1}) + {}^{L}c^{y'}_{41}(C^{(4)}_1 + C^{(4)}_{-1}) + {}^{L}c^{y'}_{43}(C^{(4)}_3 + C^{(4)}_{-3}), \end{aligned} \tag{151}$$

where, for 'd–d' transitions, $L=P$ or F as before, and the $\{c\}$ coefficients are given in terms of the basic CLF "static" parameters ${}^{L}t_{\lambda}$ as in Table 13.

We now refer the operators of Eq. (151) in frame D to the equilibrium frame E [the reference frame for the later superposition, Eq. (148)]. The rotation by θ^x about the local y axis in Fig. 19 is implemented by the Euler rotation, $R(0, -\theta^x, 0)$, using the conventions of Brink and Satchler [57]. The Wigner rotation simplifies as:

$$\mathscr{D}^{(k)}_{q'q}(0, -\theta^x, 0) = d^{(k)}_{q'q}(-\theta^x), \tag{152}$$

so, using the tabulations of Buckmaster [58] for the $\{d\}$ and assuming small θ^x, we construct the transformations shown in Table 21.

Substitution of the relationships in Table 21 into Eq. (151) would yield effective transition moment operators for the light electric dipole oriented along the x', y', z' axes of frame D but referred to frame E. We require expressions for the base vector e referred to the equilibrium frame also. These are constructed with the aid of the

transformation Eq. (150) to yield:

$$
\begin{aligned}
{}^{L}T_z = {}^{L}c^{z}_{20}\left[C^{(2)}_{0} - \left(\frac{3}{2}\right)^{1/2} \theta^{x} C^{(2)}_{-1} + \left(\frac{3}{2}\right)^{1/2} \theta^{x} C^{(2)}_{1} \right] \\
+ {}^{L}c^{x}_{22}\left[C^{(2)}_{2} + C^{(2)}_{-2} + \theta^{x} C^{(2)}_{-1} - \theta^{x} C^{(2)}_{1} \right] \\
+ {}^{L}c^{z}_{40}\left[C^{(4)}_{0} - (5)^{1/2}\theta^{x} C^{(4)}_{-1} + (5)^{1/2}\theta^{x} C^{(4)}_{1} \right] \\
+ {}^{L}c^{z}_{42}\left[C^{(4)}_{2} + C^{(4)}_{-2} + \frac{3}{2}(2)^{1/2}\theta^{x} C^{(4)}_{-1} - \frac{3}{2}(2)^{1/2}\theta^{x} C^{(4)}_{1} \right. \\
\left. - \left(\frac{7}{2}\right)^{1/2} \theta^{x} C^{(4)}_{-3} - \left(\frac{7}{2}\right)^{1/2} \theta^{x} C^{(4)}_{3} \right] \\
+ \theta^{x}\left[{}^{L}c^{x}_{21}(C^{(2)}_{-1} - C^{(2)}_{1}) + {}^{L}c^{x}_{41}(C^{(4)}_{-1} - C^{(4)}_{1}) + {}^{L}c^{x}_{43}(C^{(4)}_{-3} - C^{(4)}_{3}) \right] \qquad (153)
\end{aligned}
$$

$$
\begin{aligned}
{}^{L}T_x = {}^{L}c^{x}_{21}\left[C^{(2)}_{1} - C^{(2)}_{-1} - 2\left(\frac{3}{2}\right)^{1/2} \theta^{x} C^{(2)}_{0} + \theta^{x} C^{(2)}_{-2} + \theta^{x} C^{(2)}_{2} \right] \\
+ {}^{L}c^{x}_{41}\left[C^{(4)}_{1} - C^{(4)}_{-1} - 2(5)^{1/2}\theta^{x} C^{(4)}_{0} + \frac{3}{2}(2)^{1/2}\theta^{x} C^{(4)}_{-2} + \frac{3}{2}(2)^{1/2}\theta^{x} C^{(4)}_{2} \right] \\
+ {}^{L}c^{x}_{43}\left[C^{(4)}_{3} - C^{(4)}_{-3} - \left(\frac{7}{2}\right)^{1/2} \theta^{x} C^{(4)}_{-2} - \left(\frac{7}{2}\right)^{1/2} \theta^{x} C^{(4)}_{2} + (2)^{1/2}\theta^{x} C^{(4)}_{-4} \right. \\
\left. + (2)^{1/2}\theta^{x} C^{(4)}_{4} \right] + \theta^{x}\left[{}^{L}c^{z}_{20} C^{(2)}_{0} + {}^{L}c^{z}_{22}(C^{(2)}_{-2} + C^{(2)}_{2}) + {}^{L}c^{z}_{40} C^{(4)}_{0} \right. \\
\left. + {}^{L}c^{z}_{42}(C^{(4)}_{-2} + C^{(4)}_{2}) \right]
\end{aligned}
$$

$$
\begin{aligned}
{}^{L}T_y = {}^{L}c^{y}_{21}\left[C^{(2)}_{1} - C^{(2)}_{-1} - \theta^{x} C^{(2)}_{-2} + \theta^{x} C^{(2)}_{2} \right] \\
+ {}^{L}c^{y}_{41}\left[C^{(4)}_{1} - C^{(4)}_{-1} - \frac{3}{2}(2)^{1/2}\theta^{x} C^{(4)}_{-2} + \frac{3}{2}(2)^{1/2}\theta^{x} C^{(4)}_{2} \right] \\
+ {}^{L}c^{y}_{43}\left[C^{(4)}_{3} - C^{(4)}_{-3} + \left(\frac{7}{2}\right)^{1/2} \theta^{x} C^{(4)}_{-2} - \left(\frac{7}{2}\right)^{1/2} \theta^{x} C^{(4)}_{2} - (2)^{1/2}\theta^{x} C^{(4)}_{-4} \right. \\
\left. + (2)^{1/2}\theta^{x} C^{(4)}_{4} \right].
\end{aligned}
$$

Table 21
Transformations of multipole operators upon small angular rotations θ^x about x (D→E)

Frame D	Frame E
$C_0^{(2)} \rightarrow$	$C_0^{(2)} + \left(\frac{3}{2}\right)^{1/2} \theta^x C_1^{(2)} - \left(\frac{3}{2}\right) \theta^x C_{-1}^{(2)}$
$C_{\pm 1}^{(2)} \rightarrow$	$C_{\pm 1}^{(2)} \mp \left(\frac{3}{2}\right)^{1/2} \theta^x C_0^{(2)} \pm \theta^x C_{\pm 1}^{(2)}$
$C_{\pm 2}^{(2)} \rightarrow$	$C_{\pm 2}^{(2)} \mp \theta^x C_{\pm 1}^{(2)}$
$C_0^{(4)} \rightarrow$	$C_0^{(4)} + \left(5\right)^{1/2} \theta^x C_1^{(4)} - \left(5\right)^{1/2} \theta^x C_{-1}^{(4)}$
$C_{\pm 1}^{(4)} \rightarrow$	$C_{\pm 1}^{(4)} \mp \left(5\right)^{1/2} \theta^x C_0^{(4)} \pm \frac{3}{2}\left(2\right)^{1/2} \theta^x C_{\pm 2}^{(4)}$
$C_{\pm 2}^{(4)} \rightarrow$	$C_{\pm 2}^{(4)} \mp \frac{3}{2}\left(2\right)^{1/2} \theta^x C_{\pm 1}^{(4)} \pm \left(\frac{7}{2}\right)^{1/2} \theta^x C_{\pm 3}^{(4)}$
$C_{\pm 3}^{(4)} \rightarrow$	$C_{\pm 3}^{(4)} \mp \left(\frac{7}{2}\right)^{1/2} \theta^x C_{\pm 2}^{(4)} \pm \left(2\right)^{1/2} \theta^x C_{\pm 4}^{(4)}$

With vanishing displacement, θ^x, in Eq. (153) we recover Eq. (151), but referred to frame E.

Note particularly that the expressions in Eq. (153) involve parts that are independent of the displacement, θ^x, and parts that are linear in θ^x. Vibrations in the global, centrosymmetric molecule are even (g) or odd (u). We therefore consider pairs of ligations which are centrosymmetrically disposed about the metal atom in their equilibrium condition. *Gerade* and *ungerade* bending displacements of such a ligation pair are shown in Fig. 20. Following procedures like those detailed above, we have established [12] three relevant conclusions: (1) the superposition of operators Eq. (153) for two diametrically opposite ligations suffering *gerade* angular displacements as in Fig. 20(a) vanishes identically, as required by the Laporte rule; (2) a similar superposition for ligations undergoing *ungerade* bending does not vanish; (3) only the θ^x-dependant parts of Eq. (153) contribute to that *ungerade*-type superposition. This latter is, of course, to be expected, for any vibronic intensity must derive from the *changes* associated with ligand displacement.

Within any harmonic vibration cycle, the displacement angle θ^x varies symmetrically about the equilibrium position. However, the *intensity* arising from a displacement of $-\theta^x$ will be identical with that from a displacement of $+\theta^x$. Accordingly,

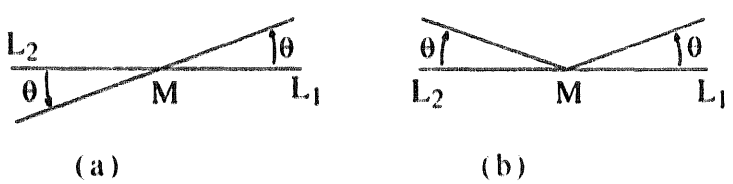

Fig. 20. (a) *Gerade* and (b) *ungerade* bending modes.

effective operator expressions like Eq. (153) are replaced by analogous expressions involving $\bar{\theta}^x$ rather than θ^x, where $\bar{\theta}^x$ defines a root-mean-square (rms) vibration amplitude. In this way, we recognize the time-averaged nature of experimental electronic transitions. As such rms amplitudes are unknown *a priori*, we parametrize them at this stage of development of the CLF vibronic model by their incorporation within the static ${}^{L}t_{\lambda}$ parameters as follows.

The surviving θ^x-dependent parts of Eq. (153) form multipole expansions of the ${}^{L}T_{\beta}$ ($\beta=x, y, z$) with coefficients of the form ${}^{L}c^{\beta}_{kq}\theta^{\alpha}$ ($\alpha=x$ so far but will be generalized to include $\alpha=x$ or y shortly). Let us define:

$$ {}^{\alpha L}c^{\beta}_{kq} \equiv {}^{L}c^{\beta}_{kq}\bar{\theta}^{\alpha}. \tag{154} $$

Table 13 defined the $\{{}^{L}c^{\beta}_{kq}\}$ as functions of the "static" parameters $\{{}^{L}t_{\lambda}\}$; $\lambda=\sigma, \pi x, \pi y$:

$$ {}^{L}c^{\beta}_{kq} = {}^{L}f^{\beta}_{kq}({}^{L}t_{\lambda}). \tag{155} $$

Because of *linear* dependence of the surviving terms in Eq. (153), and hence of Eq. (154), upon θ^x, we may concatonate the parametric natures of the $\{t\}$ and the $\{\theta\}$ and write:

$$ {}^{\alpha L}c^{\beta}_{kq} = {}^{L}f^{\beta}_{kq}({}^{L}t_{\lambda}; \bar{\theta}^{\alpha}) \equiv {}^{L}f^{\beta}_{kq}({}^{L}t^{\alpha}_{\lambda}). \tag{156} $$

Thus, intensity parameters $\{{}^{L}t_{\lambda}\}$ appearing without a right-hand superscript refer to the usual "static" parameters of Eq. (134), while those $\{{}^{L}t^{\alpha}_{\lambda}\}$ appearing with a right-hand superscript refer to "vibronic" parameters relating to the ligand bending displacements in the αz plane of the local equilibrium ligation frame. Within that equilibrium frame, the effective transition moment operators for bending in the local xz plane take the forms:

$$ \begin{aligned} {}^{L}T^{x}_{z} = {}& {}^{xL}c^{z}_{20}\left[\left(\frac{3}{2}\right)^{1/2}(C^{(2)}_{1} - C^{(2)}_{-1})\right] + {}^{xL}c^{z}_{22}(C^{(2)}_{-1} - C^{(2)}_{1}) \\ & + {}^{xL}c^{z}_{40}[(5)^{1/2}(C^{(4)}_{1} - C^{(4)}_{-1})] \\ & + {}^{xL}c^{x}_{42}\left[\frac{3}{2}(2)^{1/2}(C^{(4)}_{-1} - C^{(4)}_{1}) - \left(\frac{7}{2}\right)^{1/2}(C^{(4)}_{-3} - C^{(4)}_{3})\right] \\ & + {}^{xL}c^{z}_{21}(C^{(2)}_{-1} - C^{(2)}_{1}) + {}^{xL}c^{x}_{41}(C^{(4)}_{-1} - C^{(4)}_{1}) + {}^{xL}c^{x}_{43}(C^{(4)}_{-3} - C^{(4)}_{3}) \end{aligned} \tag{157} $$

$$ \begin{aligned} {}^{L}T^{x}_{x} = {}& {}^{xL}c^{z}_{21}\left[-2\left(\frac{3}{2}\right)^{1/2}C^{(2)}_{0} + C^{(2)}_{-2} + C^{(2)}_{2}\right] \\ & + {}^{xL}c^{x}_{41}\left[-2(5)^{1/2}C^{(4)}_{0} + \frac{3}{2}(2)^{1/2}(C^{(4)}_{-2} + C^{(4)}_{2})\right] \\ & + {}^{xL}c^{x}_{43}\left[-\left(\frac{7}{2}\right)^{1/2}(C^{(4)}_{-2} + C^{(4)}_{2}) + (2)^{1/2}(C^{(4)}_{-4} + C^{(4)}_{4})\right] \\ & + {}^{xL}c^{z}_{20}C^{(2)}_{0} + {}^{xL}c^{z}_{22}(C^{(2)}_{-2} + C^{(2)}_{2}) + {}^{xL}c^{z}_{40}C^{(4)}_{0} + {}^{xL}c^{z}_{42}(C^{(4)}_{-2} + C^{(4)}_{2}) \end{aligned} $$

$$^{L}T_{y}^{x} = {}^{xL}c_{21}^{y}(C_{2}^{(2)} - C_{-2}^{(2)}) + {}^{xL}c_{41}^{y}\left[\frac{3}{2}(2)^{1/2}(C_{2}^{(4)} - C_{-2}^{(4)})\right]$$

$$+ {}^{xL}c_{43}^{y}\left[\left(\frac{7}{2}\right)^{1/2}(C_{-2}^{(4)} - C_{2}^{(4)}) + (2)^{1/2}(C_{4}^{(4)} - C_{-4}^{(4)})\right].$$

By way of emphasis, the $\{^{xL}c_{kq}^{\beta}\}$ bear the same functional relationships to the $\{^{L}t_{\lambda}^{x}\}$ as the $\{^{L}c_{kq}^{\beta}\}$ of Table 13 do to the $\{^{L}t_{\lambda}\}$. The right-hand superscript x on the $\{^{L}t_{\beta}^{x}\}$ in Eq. (157) refers, once more, to the ligand movement in the local xz plane. These expressions are thus the (xz) vibronic analogues of the "static" expressions in Eq. (151). Equivalent expressions for $\{^{L}t_{\beta}^{y}\}$ relating to ligand angular displacements in the local yz plane have been derived in a similar manner and are given elsewhere [12].

6.3. *Stretching vibrational modes*

Throughout pure stretching vibrations, or equally for components of more complex motions parallel to the metal ligand vector, the relationships between effective electric dipole multipole operators and CLF $^{L}t_{\lambda}$ parameters remain exactly as given in Table 13. However, the magnitudes of the $^{L}t_{\lambda}$ parameters vary throughout the vibration cycle. The variations will not be linear with respect to vibration amplitude but rather something like that sketched in Fig. 21. Superposition of effective operators for a pair of diametrically opposite ligations will comprise only those parts arising from the *differences* in $^{L}t_{\lambda}$ parameters for the displaced ligations. *Gerade* modes accordingly yield a null result in agreement with Laporte's rule. At some

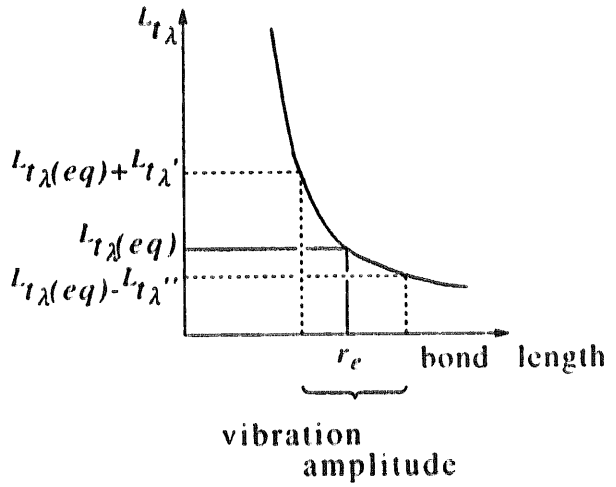

Fig. 21. The variation of $^{L}t_{\lambda}$ values in stretching modes.

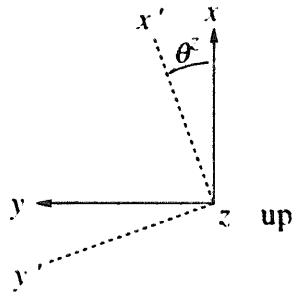

Fig. 22. Equilibrium and displaced (unprimed and primed, respectively) frames for a librating ligation.

non-equilibrium instant within an *ungerade* stretch, the differences between oppositely referred CLF parameters will be $({}^{L}t_{\lambda}(\mathrm{eq})+{}^{L}t_{\lambda}')-({}^{L}t_{\lambda}(\mathrm{eq})-{}^{L}t_{\lambda}'')={}^{L}t_{\lambda}'+{}^{L}t_{\lambda}''$ in the notation of Fig. 21. In the harmonic approximation, therefore, we assign CLF parameters to one ligand as:

$$ {}^{L}t_{\lambda}^{z}=({}^{l}t_{\lambda}'+{}^{L}t_{\lambda}'')_{\mathrm{rms}} \tag{158} $$

and ${}^{L}t_{\lambda}^{z}=0$ for the other. This ensures that the global $\{{}^{L}T^{z}\}$ operators do not vanish within the cellular superposition.

6.4. *Torsional modes*

These vibrations describe oscillatory rocking motions of a ligand about the metal–donor atom vector. They are not, of course, defined for an atomic ligand. As our original presentation of the CLF vibronic model was developed for various MX_n species; X = halogen, torsions were irrelevant. The discussions below are presented for the first time.

We consider a rotation of a single ligation by θ^z about the M–L(z) axis. The displaced, D, and equilibrium, E, frames in Fig. 22 are related as in Eq. (159):

$$ D\begin{array}{c} \\ x' \\ y' \\ z' \end{array}\overset{E}{\begin{array}{c} \begin{array}{ccc} x & y & z \end{array} \\ \begin{pmatrix} \cos\theta^z & \sin\theta^z & 0 \\ -\sin\theta^z & \cos\theta^z & 0 \\ 0 & 0 & 1 \end{pmatrix} \end{array}} \underset{\text{small}}{\overset{\theta^z}{\rightarrow}} D\overset{E}{\begin{pmatrix} 1 & \theta^z & 0 \\ -\theta^z & 1 & 0 \\ 0 & 0 & 1 \end{pmatrix}}. \tag{159} $$

Equivalent to Table 21 for a bending displacement, we have for this rotation the simple relationships:

$$ \text{For D}\rightarrow\text{E:}\quad C_q^{(k)}\rightarrow e^{-iq\theta^z}C_q^{(k)}\sim(1-iq\theta^z)C_q^{(k)};\quad \theta^z \text{ small.} \tag{160} $$

Transformation of the operators Eq. (151) from frame D to frame E, equivalent to

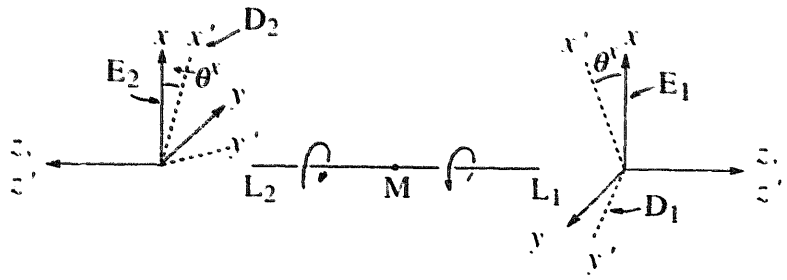

Fig. 23. Equilibrium (E) and displaced (D) frames for opposite ligands engaged in a torsion.

the "bend" expressions Eq. (153), yields:

$$
\begin{aligned}
{}^{L}T_z &= {}^{L}c^{z}_{20}C^{(2)}_0 + {}^{L}c^{z}_{22}(C^{(2)}_2 + C^{(2)}_{-2}) + {}^{L}c^{z}_{40}C^{(4)}_0 + {}^{L}c^{z}_{42}(C^{(4)}_2 + C^{(4)}_{-2}) \\
&\quad - 2i\theta^{z}\,{}^{L}c^{z}_{22}(C^{(2)}_2 - C^{(2)}_{-2}) - 2i\theta^{z}\,{}^{L}c^{z}_{42}(C^{(4)}_2 - C^{(4)}_{-2}) \qquad (161)\\
{}^{L}T_x &= {}^{L}c^{x}_{21}(C^{(2)}_1 - C^{(2)}_{-1}) + {}^{L}c^{x}_{41}(C^{(4)}_1 + C^{(4)}_{-1}) + {}^{L}c^{x}_{43}(C^{(4)}_3 - C^{(4)}_{-3}) \\
&\quad - i\theta^{z}\,{}^{L}c^{x}_{21}(C^{(2)}_1 + C^{(2)}_{-1}) - i\theta^{z}\,{}^{L}c^{x}_{41}(C^{(4)}_1 + C^{(4)}_{-1}) - 3i\theta^{z}\,{}^{L}c^{x}_{43}(C^{(4)}_3 + C^{(4)}_{-3}) \\
&\quad - \theta^{z}\,{}^{L}c^{y}_{21}(C^{(2)}_1 + C^{(2)}_{-1}) - \theta^{z}\,{}^{L}c^{y}_{41}(C^{(4)}_1 + C^{(4)}_{-1}) - \theta^{z}\,{}^{L}c^{y}_{43}(C^{(4)}_3 + C^{(4)}_{-3}) \\
{}^{L}T_y &= {}^{L}c^{y}_{21}(C^{(2)}_1 + C^{(2)}_{-1}) + {}^{L}c^{y}_{41}(C^{(4)}_1 + C^{(4)}_{-1}) + {}^{L}c^{y}_{43}(C^{(4)}_3 + C^{(4)}_{-3}) \\
&\quad - i\theta^{z}\,{}^{L}c^{y}_{21}(C^{(2)}_1 - C^{(2)}_{-1}) - i\theta^{z}\,{}^{L}c^{y}_{41}(C^{(4)}_1 - C^{(4)}_{-1}) - 3i\theta^{z}\,{}^{L}c^{y}_{43}(C^{(4)}_3 - C^{(4)}_{-3}) \\
&\quad + \theta^{z}\,{}^{L}c^{x}_{21}(C^{(2)}_1 - C^{(2)}_{-1}) + \theta^{z}\,{}^{L}c^{x}_{41}(C^{(4)}_1 - C^{(4)}_{-1}) + \theta^{z}\,{}^{L}c^{x}_{43}(C^{(4)}_3 - C^{(4)}_{-3}).
\end{aligned}
$$

Now consider the counter-rotations of two identical ligations sited diametrically opposite to one another relative to the central metal. The displaced and equilibrium frames for ligands undergoing this torsion are shown in Fig. 23. The relationship of the displaced frame D_2 for ligation 2 relative to E_2 is identical to that of D_1 relative to E_1. Hence, the expressions in Eq. (161) for the operators for ligation 1 in frame E_1 also serve for the operators for ligation 2 in frame E_2. Transformation from E_2 to E_1 involves rotation by π about their common axis x; that is, $R(0, \pi, \pi)$. Now:

$$
\mathscr{D}^{(k)}_{q'q}(0, \pi, \pi) = \exp(iq\pi)d^{(k)}_{q'q}(\pi) = \exp(iq\pi)(-1)^{k+q'}\delta_{q,-q'} \qquad (162)
$$

so that the $C^{(k)}_q$ in E_2 transform to $+C^{(k)}_{-q}$ in E_1 for all q. The Cartesian transformation from E_2 to E_1 is given by:

$$
\begin{array}{cc} & E_1 \\ & \begin{array}{ccc} x & y & z \end{array} \\ \begin{array}{c} x \\ E_2 \quad y \\ z \end{array} & \begin{pmatrix} 1 & 0 & 0 \\ 0 & -1 & 0 \\ 0 & 0 & -1 \end{pmatrix} \end{array} . \qquad (163)
$$

In transforming the operators Eq. (161) from E_2 to E_1, we use Eqs. (162) and (163)

together and find that:

$$\text{for } {}^{L}T_x\text{:}\quad C_q^{(k)} \rightarrow +C_{-q}^{(k)} \tag{164}$$

$$\text{for } {}^{L}T_z, {}^{L}T_y\text{:}\quad C_q^{(k)} \rightarrow -C_{-q}^{(k)},$$

and hence that the θ^z-independent parts of Eq. (161) transform to their negatives while the θ^z-dependent parts transform to themselves. In forming the superposition over the two centrically related ligations, therefore, only the θ^z-dependent terms survive so that, for the reference ligation undergoing a torsion, we have:

$$\begin{aligned}
{}^{L}T_z^{\tau} &= -2i\theta^z {}^{L}c_{22}^z(C_2^{(2)} - C_{-2}^{(2)}) - 2i\theta^z {}^{L}c_{42}^z(C_2^{(4)} - C_{-2}^{(4)}) \qquad (165)\\
{}^{L}T_x^{\tau} &= -\theta^z(i^{L}c_{21}^x + {}^{L}c_{21}^y)(C_1^{(2)} + C_{-1}^{(2)}) - \theta^z(i^{L}c_{41}^x + {}^{L}c_{41}^y)(C_1^{(4)}) + C_{-1}^{(4)})\\
&\quad -\theta^z(3i^{L}c_{43}^x + {}^{L}c_{43}^y)(C_3^{(4)}) + C_{-3}^{(4)})\\
{}^{L}T_y^{\tau} &= \theta^z(-i^{L}c_{21}^y + {}^{L}c_{21}^x)(C_1^{(2)} - C_{-1}^{(2)}) + \theta^z(-i^{L}c_{41}^y + {}^{L}c_{41}^x)(C_1^{(4)} - C_{-1}^{(4)})\\
&\quad +\theta^z(-3i^{L}c_{43}^y + {}^{L}c_{43}^x)(C_3^{(4)} - C_{-3}^{(4)}).
\end{aligned}$$

Note, however, that from Table 13, ${}^{L}c_{22}^z$ and ${}^{L}c_{42}^z$ coefficients are each of the form $({}^{L}t_{\pi x} - {}^{L}t_{\pi y})$, and, similarly, that $(i^{L}c_{21}^x + {}^{L}c_{21}^y)$, $(i^{L}c_{41}^x + {}^{L}c_{41}^y)$, $(3i^{L}c_{43}^x + {}^{L}c_{43}^y)$, $(i^{L}c_{21}^y + {}^{L}c_{21}^x)$, $(-i^{L}c_{41}^y + {}^{L}c_{41}^x)$ and $(-3i^{L}c_{43}^y + {}^{L}c_{43}^x)$ all take the form $({}^{L}t_{\pi x} - {}^{L}t_{\pi y})$. Thus, we see that the effective multipole operators for torsion depend solely upon the ligation π anisotropy. They will survive for torsions of opposite pyridine ligations, for example, but vanish for linear ligators like the halogens.

Equivalent to Eq. (154) we may define:

$${}^{tL}c_{kq}^{\beta} \equiv {}^{L}c_{kq}^{\beta}\bar{\theta}^z, \tag{166}$$

where $\bar{\theta}^z$ is the rms value of θ^z (the semi-torsion angle for the ligation pair) and employ four torsional intensity parameters, ${}^{L}t_{\lambda}^{\tau}$; $L = P, F$; $\lambda = \pi x, \pi y$.

6.5. *Relationships between the static and vibronic CLF parameters*

In Table 22, we summarize the variables that are engendered by the CLF vibronic model as described so far. $L = R$ parameters are not included in the CLF vibronic model on the assumption that their effects will tend to cancel in centric and near-centric geometries. The parameter lists in Table 22 relate to the three different kinds of ligand displacement rather than to discrete types of normal vibration mode. In general, normal modes may involve contributions from one or more of these kinds

Table 22
Vibronic CLF parameters

(a) For bends (tangential displacements)	${}^{L}t_{\sigma}^{x}$ ${}^{L}t_{\pi x}^{x}$ ${}^{L}t_{\pi y}^{x}$ ${}^{L}t_{\sigma}^{y}$ ${}^{L}t_{\pi x}^{y}$ ${}^{L}t_{\pi y}^{y}$
(b) For stretches (longitudinal displacements)	${}^{L}t_{\sigma}^{z}$ ${}^{L}t_{\pi x}^{z}$ ${}^{L}t_{\pi y}^{z}$
(c) For torsions (rotational displacements)	${}^{L}t_{\pi x}^{\tau}$ ${}^{L}t_{\pi y}^{\tau}$
All for $L = P, F$ ('d–d') or $L = D, G$ ('f–f')	

of displacement, and, even for pure bends, the normal mode may comprise displacements in both tangential directions (x and y) normal to the metal–ligand vector. Potentially, therefore, any one real normal mode may require up to 11 CLF variables per ligation, and since a complete vibronic analysis would include consideration of several normal modes — by summing the intensities associated with each — the number of degrees of freedom are increased considerably. Practicality demands that this freedom be curtailed dramatically.

One criterion by which to judge any discounting of these variables is that of the magnitude of ligand displacements. Definitions like Eq. (154) establish the CLF vibronic parameters to be linearly dependent upon rms displacements. As discussed in Section 2, these tend to be smaller for higher frequency vibrations. Stretches are generally of higher frequency than bends or torsions so an immediate simplifying strategy for vibronic intensities is to discard all but the softer torsions and bends. Our first applications of the vibronic CLF model was to square planar, tetrahalocopper(II) [54] and -platinum(II) [60] chromophores. For these, consideration of normal mode contributions to intensity was limited to the three, *ungerade* bending modes — of b_{2u}, a_{2u} and e_u symmetry (torsions are irrelevant in these systems, of course). Within each mode, many fixed relationships exist between the different displacements of each ligation: for example, all ligands move away and essentially normal to the coordination plane by equal amounts in the a_{2u} mode, or, in pairs, by equal but opposite amounts in the b_{2u} mode, as illustrated in Fig. 24. There are, however, no fixed relationships between the magnitudes of the displacements for the different modes. A large parameter list remained even for this simple model. The analyses were tedious and lengthy, and characterized by many correlations between optimal parameter values — often, though not always, the indicator of an overparametrized model. Nevertheless, good reproductions of observed intensity distributions were obtained for several different chromophores in this series and the relative magnitudes of the various t parameters for different modes qualitatively correlated inversely and well with known vibrational frequencies. We do not review these studies in any further detail; their importance lay in providing confidence in the CLF approach enough to implement the next phase in its development that we now describe.

The parameters of Table 22 subsume both electronic and vibrational characteristics in the various ligations, the latter being particularly responsible for the proliferation of variables. However, the theoretical development that we have reviewed defines. for each angular displacement, a simple proportionality between the vibronic and

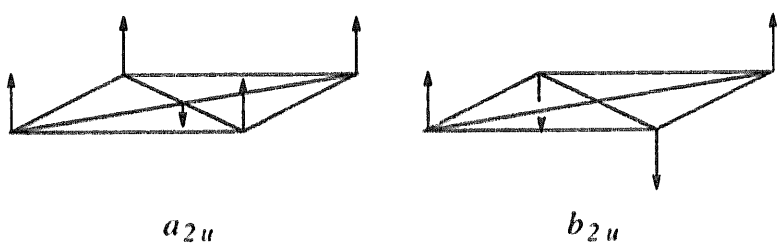

Fig. 24. The a_{2u} and b_{2u} bending modes in square planar coordination.

static $\{t\}$ parameters: *viz* that a vibronic ${}^{L}t_{\lambda}$ parameter equals the equivalent static ${}^{L}t_{\lambda}$ parameter times the appropriate rms ligand displacement. Rather than parametrize these rms displacements, as done implicitly within Table 22, we predicate our vibronic analysis upon a prior vibrational analysis that provides them as fixed, known quantities. Normal coordinate analysis (NCA) of the vibration frequencies (from IR and/or Raman spectroscopy) provides the means by which the necessary ligand displacements are determined. Though modelled through an assumed force field, the process of NCA is utterly independent of the ligand-field analysis it precedes.

The combination of NCA+CLF vibronic analysis constitutes the present stage of development of the ligand-field model. We can discern a number of significant gains over the bare CLF vibronic model. (1) For bends and torsions, the parameters of Table 22 are proportional to the corresponding "static" parameters, the constants of proportionality being furnished by prior NCA. Accordingly, the only CLF variables used for bending and torsional components of any normal vibrational mode (however complex otherwise) are the "static" parameters ${}^{L}t_{\lambda}$; $L=P$, F, $\lambda=\sigma$, πx, πy. (2) This parameter set is not increased as more (bending and/or torsional) modes are included, for the dynamics of each are determined by the same NCA and the parameters of Table 22 (bends and torsions) all relate to the *same* "static" t parameter set. In this way, a rather comprehensive description of the vibrational character of a chromophore can be included in the overall model without penalty so far as the vibronic degrees of freedom are concerned. (3) Not only can the description of the vibrational motion be so easily extended but a similar lack of penalty attaches to an analysis of near-centric chromophores in which intensity accrues from both static and dynamic sources. In practice, these are common circumstances; we review one such study [61] in Section 7 — of $[Ni(en)_3]^{2+}$, which is only approximately octahedral. The *same* set of ${}^{L}t_{\lambda}$ parameters suffice for the "static" contribution as for all vibronic bends and torsions. (4) The temperature dependences of all ligand displacements are calculable from the NCA and so predictions about the temperature dependence of the CLF vibronic intensities may be made and compared with experiment. (5) Only for stretches (or the stretching components of normal modes) are extra t parameters required. An important — and surely reasonable — assumption made within the CLF modelling of bends and torsions is that the electronic character of the bonds remains essentially constant; ultimately this assumption is responsible for the proportionality between static and bending or torsional t parameters. For stretches, on the other hand, that bonding character is all that can change so that the simple proportionality does not result in this case. The relationship between ${}^{L}t_{\lambda}$ (static) and ${}^{L}t_{\lambda}^{z}$ [Eq. (158)] is unknown and must be parametrized; nor need we expect exactly the same relationship for $L=P$ as for $L=F$. Altogether, therefore, a consideration of stretching modes or components requires ${}^{L}t_{\lambda}^{z}$ parameters in addition to the set of "static" ${}^{L}t_{\lambda}$ parameters required for either "static" contributions or bending/torsional modes, or both. As stretching normal modes are usually of rather higher frequency than bends or torsions, stretching displacements are relatively small. Similarly, the stretching displacements within impure bends or torsions are frequently small. We suggest that

the neglect of all stretching modes or components — in the interests of minimizing parameterization — might not be too serious. The analyses summarized in Section 7 have incorporated such an assumption. (6) Finally, for all NCA+CLF vibronic analyses parametrized solely in terms of "static" ${}^{L}t_{\lambda}$ parameters (i.e. stretches being neglected), all remarks concerning the significance of static-type parameters discussed in Section 6 carry over *in toto* to the vibronic systems.

7. A survey of CLF analytical results

Our focus in this article has been on the CLF modelling of transition metal '*d–d*' spectral intensities and we end with a brief but comprehensive summary of its application to some 43 chromophores. All CLF intensity analyses to date are from this laboratory and all have been conducted in a similar fashion. Each intensity study is built upon detailed CLF analysis of transition energies. We do not describe these ligand-field analyses here, however, although appropriate discussion of optimized e_{λ} parameter values will be given. Similarly, we do not provide sources for the spectroscopic and crystallographic data upon which each study depends; these are to be found within the cited CLF intensity papers. Our presentation is as follows.

First we list all chromophores investigated within the CLF intensity approach. Then we exemplify the quality of reproduction of experimental data with a few typical examples. There follow several subsections in which optimized CLF $\{t\}$ parameter values are collected and discussed with reference to the theoretical predictions of Section 5. We end with an illustration of the relevance of these studies to selection rules and spectral assignment.

7.1. *The chromophores*

The 43 chromophores studied within the CLF approach are listed in Table 23. They are assembled according to coordination number and geometry type. There are 12 complexes with approximately tetrahedral geometry; one with a highly compressed tetrahedral geometry that departs only a little from planar; 13 with exactly planar coordination geometry; 14 five-coordinate species with essentially trigonal–bipyramidal geometry; 2 five-coordinate systems with near square–pyramidal geometry; and one nominal octahedron with D_3 trischelate symmetry. Also listed are the types of data that have been reproduced: solution spectra, linearly polarized spectra from single-crystal studies, or circularly polarized spectra from solution or crystal work. Some CLF studies were performed within the "static" model alone, some within the "vibronic" model, and some included both parity-mixing sources. For convenience, we also provide labels of subsections in the present review in which more detailed discussion is made.

Table 23
Chromophores analysed within the CLF intensity model

Index[a]	Geometry[b]	Chromophore[c]	Complex[d]	Data type[e]	CLF type[e]	Analysis reference	Section reference[g]
1	Tet.	$CoCl_4$	Cs_3CoCl_5	S, C	S	[62,63]	7.3.1
2	Tet.	$NiCl_4$	Cs_3NiCl_5	C	S	[62,63]	7.3.1
3	Tet.	$CuCl_4$	Cs_2CuCl_4	C	S	[62,63]	7.3.1, 7.3.5
4	Tet.	CoP_2Cl_2	$Co(PPh_3)_2Cl_2$	C	S	[62,63]	7.3.1, 7.2.1
5	Tet.	CoP_2Br_2	$Co(PPh_3)_2Br_2$	C	S	[62,63]	7.3.1
6	Tet.	NiP_2Cl_2	$Ni(PPh_3)_2Cl_2$	C	S	[62,63]	7.3.1
7	Tet.	NiP_2Br_2	$Ni(PPh_3)_2Br_2$	C	S	[62,63]	7.3.1
8	Tet.	CoN_2S_2	$Co(amt)_2$	C	S	[64]	7.3.1
9	Tet.	CoO_2S_2	$Co(etu)_2(OAc)_2$	C	S	[62,64]	7.3.1
10	Tet.	CoN_2Cl_2	(−)Co(α-isospar)Cl_2	S, CD	S	[65]	7.2.4, 7.3.6
11	Tet.	CoN_2Cl_2	(−)Co(spar)Cl_2	S, CD	S	[65]	7.3.6
12	Tet.	CoN_2Cl_2	(+)Co(tmpd)Cl_2	S, CD	S	[65]	7.3.6
13	Tet./pla.	$CuCl_4$	NBZP	C	S+V	[59,66]	7.3.4
14	Pla.	$CuCl_4$	METH	C	V	[59,66]	7.3.4
15	Pla.	$CuCl_4$	CREAT	C	V	[59,66]	7.3.4
16	Pla.	$CuCl_4$	NMPH	C	V	[59,66]	7.3.4
17	Pla.	$CuCl_4$	NAEM	C	V	[66]	7.3.4
18	Pla.	$PdCl_4$	K_2PdCl_4	C	V	[66]	7.3.4, 7.2.5
19	Pla.	$PtCl_4$	K_2PtCl_4	C	V	[60,66]	7.3.4, 7.2.5
20	Pla.	$PtBr_4$	K_2PtBr_4	C	V	[60,66]	7.3.4
21	Pla.	$PtCl_3N$	$KPtCl_3NH_3$	C	S+V	[67]	7.3.4
22	Pla.	$CuCl_2N_2$	PDMP	C	V	[68]	7.3.5
23	Pla.	$CuCl_2N_2$	2,3-LUT	C	V	[68]	7.3.5
24	Pla.	$CuCl_2N_2$	2,6-LUT	C	V	[68]	7.3.5
25	Pla.	$CuCl_2O_2$	4-PICNO	C	V	[68]	7.3.5
26	Pla.	$CuCl_2O_2$	DIAQ	C	V	[68]	7.3.5
27	TBP	$CoNN_3Br$	Co(Me_6tren)Br_2	S	S	[62,63]	7.3.2
28	TBP	$NiNN_3Br$	Ni(Me_6tren)Br_2	S	S	[62,63]	7.3.2
29	TBP	$CoNN_3N$	Co(Me_6tren)NCS_2	C	S	[62,63]	7.3.2
30	TBP	$NiNN_3N$	Ni(Me_6tren)NCS_2	C	S	[62,63]	7.3.2, 7.2.2
31	TBP	$CoNS_3Br$	Co(S-tren)Br.PF_6	C	S	[62,63]	7.3.2
32	TBP	NiN_3O_2	Ni(salmedpt)	C	S	[56]	7.3.2
33	TBP	$CoNN_3N$	Co(S-tan)NCS.ClO_4	S, CD	S	[69]	7.3.2, 7.3.6
34	TBP	$CoNN_3Cl$	Co(S-tan)Cl.ClO_4	S, CD	S	[69]	7.3.2, 7.3.6
35	TBP	$CoNN_3Br$	Co(S-tan)Br.ClO_4	S, CD	S	[69]	7.3.2, 7.3.6
36	TBP	$CoNN_3I$	Co(S-tan)I.ClO_4	S, CD	S	[69]	7.3.2, 7.3.6
37	TBP	$NiNN_3N$	Ni(S-tan)NCS.ClO_4	S, CD	S	[69]	7.3.2, 7.3.6
38	TBP	$NiNN_3Cl$	Ni(S-tan)Cl.ClO_4	S, CD	S	[69]	7.3.2, 7.3.6
39	TBP	$NiNN_3Br$	Ni(S-tan)Br.ClO_4	S, CD	S	[69]	7.3.2, 7.3.6
40	TBP	$NiNN_3I$	Ni(S-tan)I.ClO_4	S, CD	S	[69]	7.3.2, 7.3.6
41	SP	CoO_4O	Co(ars.O)$_4$(NO_3)$_2$	C	S	[70]	7.3.3, 7.2.3
42	SP	NiO_4O	Ni(ars.O)$_4$(NO_3)$_2$	C	S	[70]	7.3.3, 7.2.3
43	Oct.	NiN_6	Ni(en)$_3$(NO_3)$_2$	C, CCD	S+V	[61]	7.2.6, 7.3.6

[a]Used throughout Section 7 to identify systems.
[b]Describing approximate geometry of first coordination shell (exact for planar).
[c]First coordination shell; all M(II).

7.2. Reproduction of experimental data

The following exemplify the quality of reproduction of experimental intensity distributions. While spectral transition intensities, or oscillator strengths, may be measured absolutely, they are frequently not; sometimes absorbance is reported on an arbitrary scale, sometimes polarization studies are dependent on poorly determined crystal thickness. Accordingly, we are more concerned with intensity distributions than with absolute values.

7.2.1. Bis(triphenylphosphine)dichlorocobalt(II)

Molecules of chromophore **4** (Table 23) are ideally aligned in the monoclinic ($P2/c$) lattice such that equivalent axes of the (nearly exactly) C_{2v} chromophores are coparallel and oriented along the crystal a', b, c directions ($a' = b \wedge c$). The observed polarization ratios for absorbances determined parallel to these three directions are maximal in consequence. There are six discrete (spin-allowed) transitions. Optimizing the fit between these — throughout the three polarizations together — and relative intensities calculated within the "static" CLF intensity model has yielded the agreements shown in Fig. 25. The bar graphs represent intensities integrated over the band intervals: 5.0–7.0, 7.0–9.0, 9.0–12.0, 12.0–15.0, 15.0–19.0 $cm^{-1} \times 10^3$. Parametrization of the prior energy analysis included both interelectron repulsion and spin-orbit coupling as well as the ligand field proper [B, ζ, e_σ(Cl), e_σ(P), e_π(Cl), e_π(P)].

7.2.2. Hexamethyltrendithiocyanate nickel(II)

Polarized spectra parallel to two principal axes of the orthorhombic crystals of chromophore **30** have been reported. Optimizing fits between the "static" CLF model and the three observed, spin-allowed bands yielded the results given in

---

(*Table* 23 *continued*)

[d]Further identification with abbreviations given below; for counter ions in ionic species see CLF analysis references.

[e]S = solution, C = linearly polarized single-crystal, CD = solution circular dichroism, CCD = crystal CD.

[f]S = "static" contributions to parity-mixing, V = vibronic contributions.

[g]Section labels locate discussions in this article.

Abbreviations: amt — 3-amino-2-methylpropane-2-thiolato; etu — ethylenethiourea; OAc — acetato; α-isospar — α-*iso*spartein; spar — spartein; tmpd — (+)*N*,*N*,*N*′,*N* tetramethyl-1,2-propylenediamine; NRZP — bis(*N*-benzylpiperazinium)tetrachlorocopper(II); METH — bis(1-methyl-4-oxo-3,3-diphenylhexyldimethylammonium)tetrachlorocopper(II); CREAT — bis(2-imino-1-methyl-4-imidazolidinium)tetrachlorocopper(II); NMPH — bis(*N*-methylphenylethylammonium)tetrachlorocopper(II); NAEM — bis(*N*-2-aminoethylmorpholinium)tetrachlorocopper(II); PDMP — bis(1-phenyl-3,5-dimethylpyrazole)dichlorocopper(II); 2,3-LUT — bis(2,3-dimethylpyridine)dichlorocopper(II); 2,6-LUT — bis(2,6-dimethylpyridine)dichlorocopper(II); 4-PICNO — bis(4-methylpyridine-N-oxide)dichlorocopper(II); DIAQ — $Cu(H_2O)_2Cl_2.4(C_6H_5)_3PO$; Me_6tren — tris(2-dimethylaminoethyl)amine; S-tren — tris(2-*tert*-butylthioethyl)amine; salmedpt — bis(salicylidene-γ-aminopropyl)methylaminato; S-tan — $Me_2NCH_2CH(Me)N(CH_2CH_2NMe_2)_2$; ars.O — diphenylmethylarsineoxide; en — ethylenediamine.

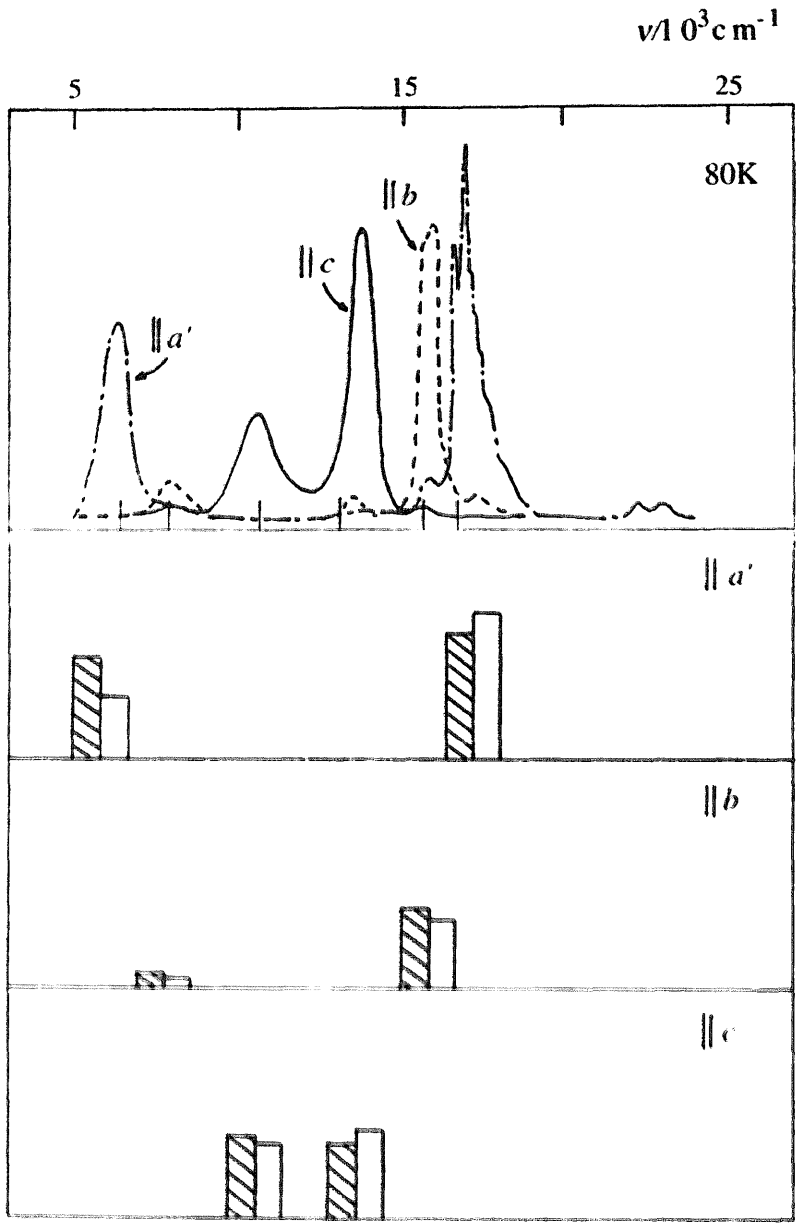

Fig. 25. Observed and calculated (hatched) intensities for CoP_2Cl_2.

Table 24. An entirely similar quality of fit was obtained for other chromophores in this series (**27**, **28**, **29**, **31**).

7.2.3. Tetrakis(diphenylmethylarsineoxide)nitrato-cobalt(II) *and -nickel*(II) *nitrates*

The near-square pyramidal coordination in chromophores **41** and **42** is established by four basal arsine oxide ligands plus an apical nitrate. Polarized absorption spectra parallel and perpendicular to the tetrad of these tetragonal crystals — perpendicular to which lies the M(arsine oxide)$_4$ plane — have been recorded at 80 K for the nickel(II) complex and at 20 K for the cobalt(II). Four spin-allowed regions were fitted within the "static" CLF scheme for each system. Polarization ratios for the

Table 24
Observed and calculated intensity distributions in the $[Ni(Me_6tren)NCS]^+$, chromophore **30**

Spectral range (cm^{-1})	Polarization $\|b$		Polarization $\|c$	
	Observed	Calculated	Observed	Calculated
4000–11 000	8	8	4	3
11 000–20 000	9	6	16	15
20 000–30 000	30	27	33	41

nickel compound are particularly strong. The excellent reproductions of intensity distributions are shown in Table 25. The ligand-field analysis of transition energies, paramagnetic anisotropies and esr g values upon which these intensity analyses were based were very detailed and incorporated a study of misdirected valency with respect to all ligations — non-dative lone pairs on the arsine oxides and bent bonding with the apical nitrates.

7.2.4. (-) (α-isospartein)dichlorocobalt(II)

Chromophores **10**, **11**, **12** comprised a series for the study of (solution) circular dichroism: we review just one here, namely **10**. The unpolarized and circularly polarized solution spectra of this compound are shown in Fig. 26. Drake et al. [71] selected these systems for study because the rigid, bicyclic spartein ligands impose a chirality upon the coordination, as shown in Fig. 27, which is not lost by racemization in solution. Our reproduction of the relative band areas under the unpolarized trace are shown at the top of Fig. 26 together with calculated transition energies from the prior ligand-field analysis. A simultaneous reproduction of the CD signs and areas is shown at the bottom of the figure; note the much smaller magnitudes

Table 25
Observed and calculated intensity distributions in the spin-allowed bands of $[M(OAsPh_2Me)_4NO_3]^+$; M = Co(II), Ni(II); **41**, **42**

Spectral range (cm^{-1})	Polarization $\|c$		Polarization $\perp c$	
	Observed	Calculated	Observed	Calculated
M = Co(II)				
5000–9500	6	6	7	6
9500–15 500	8	8	14	13
15 500–18 500	11	11	14	14
19 200–23 000	24	25	18	18
M = Ni(II)				
5000–10 000	3	3	5	5
10 000–16 000	12	11	18	18
18 500–19 800	2	3	10	10
19 800–26 900	9	9	41	41

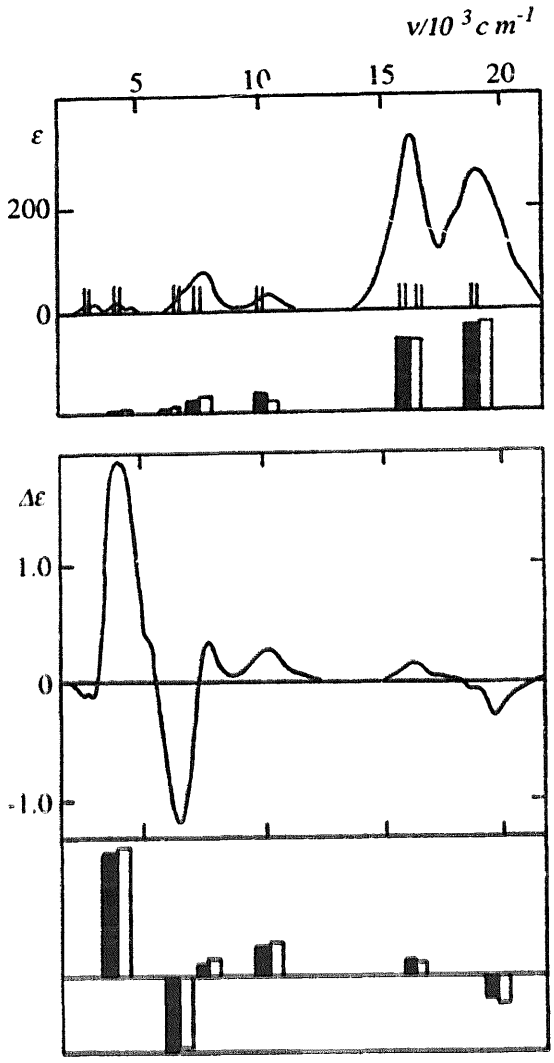

Fig. 26. Co(α-isospartein)Cl_2; unpolarized (top) and circularly polarized spectra with reproductions of band areas.

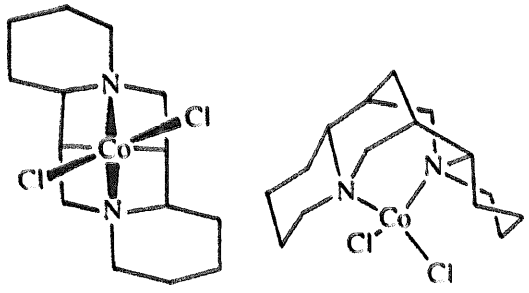

Fig. 27. The bulk of the rigid, bicyclic spartein ligand imposes a twisting of the Cl–Co–Cl plane away from the normal to the N–Co–N plane.

of the differential absorbances ($\epsilon_R - \epsilon_L$) in the CD experiment than of $\bar{\epsilon}$ in the unpolarized spectrum.

The literature on the theory of circular dichroism is extensive: Richardson has published a review [72] on the subject and focusses upon the SC + DC modelling of

the electric dipole transition moments appearing in the Rosenfeld [73] expression for the rotatory strength R_{ij} that is measured by the CD experiment:

$$R_{ij} = \mathrm{Im}[-\langle\psi_i|\mu|\psi_j\rangle\langle\psi_j|m|\psi_i\rangle], \tag{168}$$

where Im signifies the imaginary part of the product between electric dipole and magnetic dipole matrix elements (μ_{ij} and m_{ji}), respectively. Within the CLF model, the electric dipole matrix elements are calculated as described in Section 5 and the magnetic dipole matrix elements as for any other study of paramagnetic properties (see, for example, [8]). Apart from an orbital reduction factor k appearing in the magnetic moment operators, $\mu_\alpha = k\ell_\alpha + 2s_\alpha$; $\alpha = x, y, z$, no further parameterization is required for the evaluation of rotatory strengths. However, as described fully elsewhere [65], a satisfactory and simultaneous reproduction of the unpolarized and circularly polarized spectra, as demonstrated by Fig. 26, requires a detailed recognition of the misdirected valency present in those chromophores. This misdirected valency arises, in the present systems, from ring strain in the chelation to the spartein (or propylenediamine) ligands and from the relative twisting of the CoN_2 and $CoCl_2$ planes caused by the steric constraints imposed by the bulky sparteins, as exemplified in Fig. 27.

7.2.5. *Tetrahaloplatinum*(II) *and -palladium*(II)

Rather few ligand-field studies of second- and third-row transition metal complexes have been reported. Within those that have, K_2PtCl_4 and K_2PtBr_4 have been the subjects of much detailed work, mostly concerned with the question of spectral assignment. That question is now resolved [60]. We have reproduced the relative intensities of chromophores **18**, **19**, **20** within the vibronic CLF approach. As shown in Table 26, excellent fits have been achieved for five absorption regions in each platinum complex and for two in the less rich spectrum of K_2PdCl_4; in each case, for incident light polarized parallel and perpendicular to the crystal tetrad. All calculations, including those for the energy analyses upon which the intensity work was based, were performed within the full d^8 basis. The large magnitude of spin-orbit coupling in these second- and, particularly, third-row species causes considerable mixing of spin character amongst the states involved in the spectroscopic transitions. These more exacting circumstances provided no special difficulties for the intensity analyses, although computation times were naturally much longer. The fits summarized in Table 26 were obtained within the "complete" vibronic CLF model, meaning NCA+CLF. It is interesting to note that closely similar fits with similar t parameter values (described later) were obtained earlier in the more freely parameterized vibronic CLF scheme, thus lending considerable support to the NCA+CLF approach. The histograms in Fig. 28 summarize the relative contributions to overall intensities in these three chromophores from the three inducing bending modes.

7.2.6. *Tris(ethylenediamine)nickel(II) dinitrate*

The molecular symmetry of $[Nien_3]^{2+}$ is D_3 and chiral; the complex spontaneously resolves on crystallization. The dinitrate chromophore **43** crystallizes in the hex-

Table 26
Observed and calculated intensity distributions in the 15K polarized crystal spectra of $[PtCl_4]^{2-}$, $[PtBr_4]^{2-}$ and $[PdCl_4]^{2-}$

Spectral range (cm^{-1})	Polarization a (x, y)		Polarization c (z)	
	Observed	Calculated	Observed	Calculated
$[PtCl_4]^{2-}$				
16 000–19 000	4	9	4	1
19 000–23 000	22	33	21	13
23 000–25 000	21	24	11	25
25 000–28 000	41	24	0	0
28 000–31 000	115	99	129	140
$[PtBr_4]^{2-}$				
15 000–17 500	9	11	0.1	0.1
17 500–21 000	30	20	35	10
21 000–23 500	22	43	32	35
23 500–25 500	63	67	0	0
25 500–29 000	138	132	126	137
$[PdCl_4]^{2-}$				
15 000–20 000	8	6	3	3
20 000–25 000	318	317	103	106

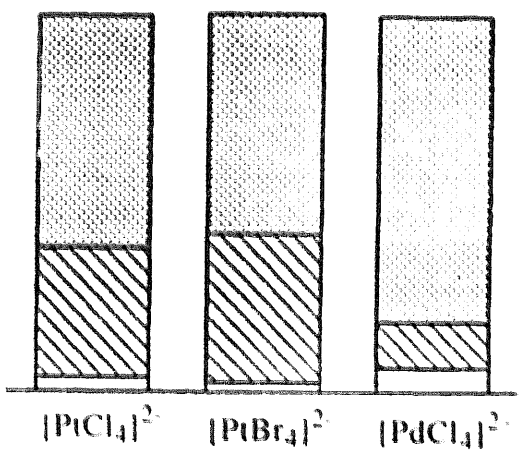

Fig. 28. Relative contributions of the three *ungerade* bonding modes (open for a_{2u}, hatched for b_{2u} and shaded for e_u) to the intensity in the ligand-field spectra (integrated over all 'd–d' bands) for $[PtCl_4]^{2-}$, $[PtBr_4]^{2-}$ and $[PdCl_4]^{2-}$.

agonal class. The linearly polarized, single-crystal 'd–d' spectrum comprises three spin-allowed transitions in each of the two unique polarizations but the highest energy transition is marked by the charge-transfer spectrum in the $\|c$ polarization. A single-crystal, axial CD spectrum of the chromophore has been reported independently by two groups and is characterized by three rotatory strengths of the same sign, one very much greater than the other two. Both linearly and circularly polarized spectral intensities have been reproduced within the CLF scheme.

The departure of the chromophore symmetry from centric octahedral is significant so that parity-mixing to force the electric dipole transitions arises by both static and dynamic means. The CLF analysis was therefore of the "static+vibronic" type described at the end of Section 6. All vibronic t parameters were related to the "static" t parameters by prior NCA. The latter was performed as a full 37-body problem, fitting to IR frequencies observed over the range 120–3267 cm^{-1} with a force field defined for the geometry of the $[Nien_3]^{2+}$ ion. Significant nickel–nitrogen bend contributions are made to the 10 lowest energy vibrations. The vibronic CLF modelling included bending displacements of the ligands for each of these 10 vibration modes. However, the vibronic and static parameterization in this system was as simple as the NCA was complex. Thus, all ligations are identical and involve metal–ligand σ bonding only. For the energy analysis, only one CLF parameter is required (e_σ) in addition to the usual Racah B and spin-orbit coupling ζ. For the *complete* vibronic+static intensity analysis, only two CLF parameters are needed ($^Pt_\sigma$, $^Ft_\sigma$). However, as absolute intensities are not calculated within the parametric CLF scheme, only the ratio $^Pt_\sigma$:$^Ft_\sigma$ survives as a system variable. The fits to the linearly polarized intensities in Table 27 were obtained in short order. The signs and relative intensities of the axial CD spectrum were calculated concurrently without further parameterization; the excellent agreement with experiment is shown in Table 27 also.

7.2.7. *Reproduction of spectral traces*

The present article is about spectral intensities. These correspond to the areas under absorption bands and, for much '*d–d*' spectroscopy, those bands are envelopes of many components like spin-orbit splittings and, in particular, vibrational progressions. The analysis of band shapes forms no part of our discussions. However, for demonstration and teaching purposes [74] it might be desirable to append an analysis of band areas with a simulation of an experimental spectral trace. We have considered this within an extremely simple model.

We suppose all bands to be gaussian in shape and synthesize a spectral trace by superposition of one such gaussian for each electronic transition. Each gaussian is defined by its total area and its half-width. Relative areas are proportional to computed intensities and are thus directly available at the end of a CLF (or other)

Table 27
Observed and calculated intensities for $[Nien_3]^{2+}$

Spectral range (cm^{-1})	Linear polarizations				Axial CD	
	σ		π			
	Observed	Calculated	Observed	Calculated	Observed	Calculated
9000–15 000	24.2	23.0	30.1	30.6	−957	−952
15 000–24 000	18.6	20.7	9.9	10.2	−36	−42
28 000–32 000	17.3	15.5	a	7.9	−7	−6

[a]Transition obscured by charge-transfer feature.

intensity analysis. Band widths are estimated as follows. We assume that relative band widths are proportional to the relative energy dependences of the transitions upon the ligand-field strength. This supposition is based upon the idea that transition frequencies vary most strongly with respect to the bond length changes that accompany a symmetric breathing mode. Our calculations are implemented by comparing transition energies computed with optimized ligand-field parameters (for example, the CLF $\{e\}$ variables) with those deriving from the same parameter values but increased by 5%. In effect, we are computing slopes in a Tanabe–Sugano-like diagram. Finally, we estimate the absolute bandwidths required for spectral simulation by multiplication of the relative band widths by a "mean bandwidth" scale factor. Altogether, therefore, progress from the intensity analysis proper to a simulation of a spectral trace requires just the one extra variable. We illustrate a particularly favourable example in Fig. 29. These traces relate to the experimental polarizations $\|b$ and at 45° to a in the (010) plane of chromophore **16**. The intensities in this planar, centric $[CuCl_4]^{2-}$ system were reproduced within the vibronic CLF model. It is to be emphasized that the computation of spectral traces does not affect the prior calculation of intensity distribution. Though rather successful in this example, it is not universally so pleasing; one could have expected little more from so crude a simulation.

7.2.8. Temperature dependence of vibronic intensities

Hitchman and his colleagues [75–77] have measured the '*d–d*' spectra of several centric, planar $[CuCl_4]^{2-}$ chromophores in different lattices over extended temperature ranges (**14-17**). Their intensities have been analysed within the vibronic CLF model. Our practice has been to fit the experimental data recorded at the lowest temperature for two reasons: (1) the band resolution is greater at the lowest temperatures; and (2) essentially only the lowest ($v=0$) member of the vibrational series

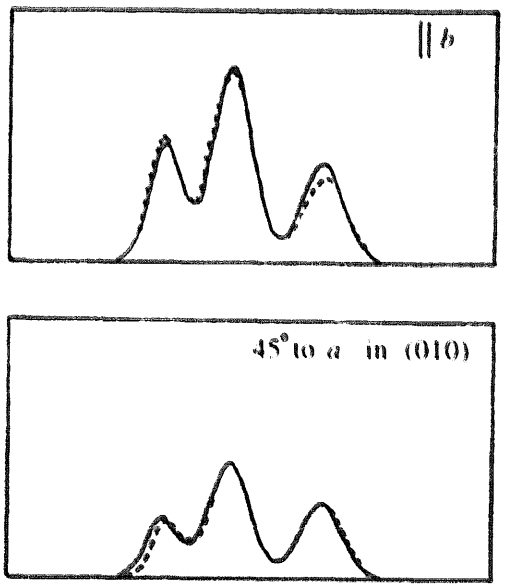

Fig. 29. Reproduction of spectral traces in NMPH (**16**).

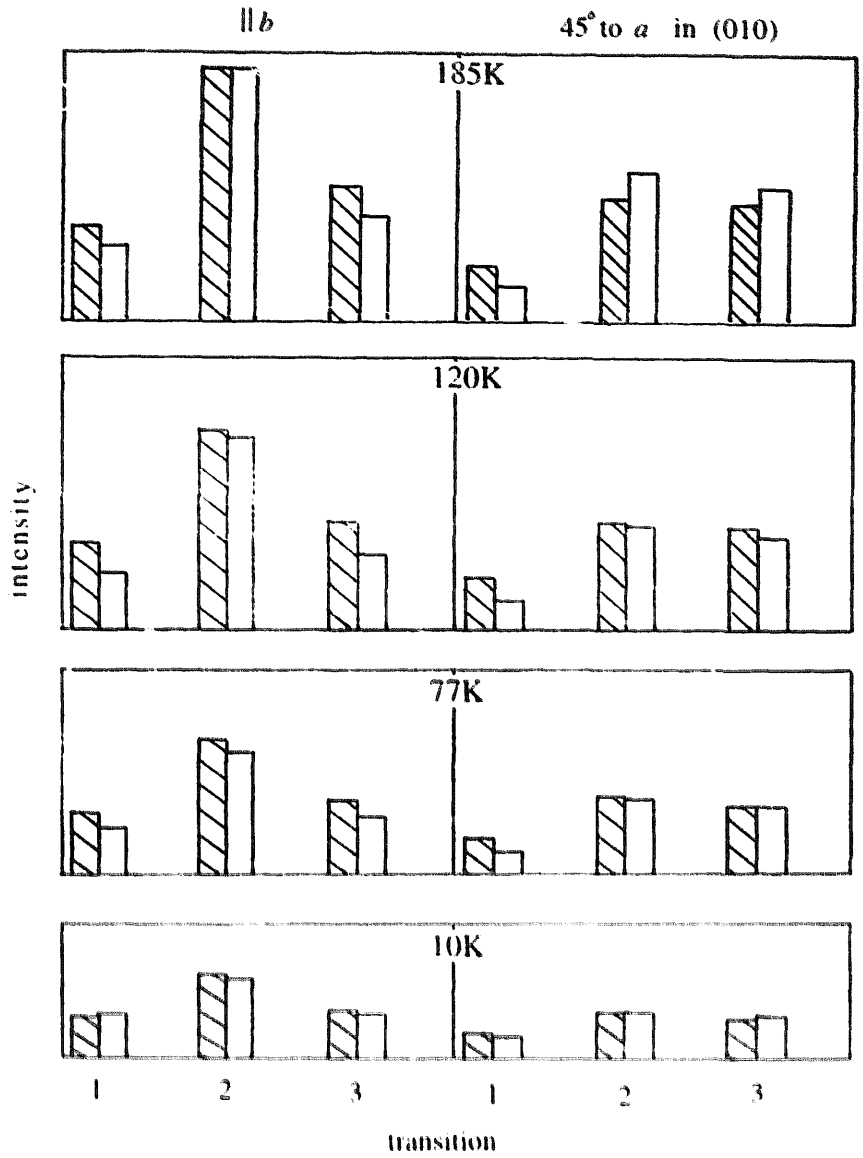

Fig. 30. Observed (hatched) and calculated intensities in NMPH (16) at several temperatures. All plots are on a common, but arbitrary, scale.

of each inducing mode is then populated and one expects the closest approach to harmonicity. Following such a CLF optimization, '*d–d*' intensity calculations at higher temperatures used the same "static" *t* parameter set together with variation of ligand displacements as functions of temperature and determined from NCA. In short, we sought to reproduce the temperature dependences of the various spectra by reference to the ligand dynamics alone. The results of one such analysis — on chromophore **16** — are illustrated in Fig. 30.

7.3. Parameter values

We refer to the *CLF* energy and *CLF* intensity models because they both parameterize aspects of the same ligand-field domain. It is therefore appropriate to discuss

the energy and intensity parameter values that reproduce experiment at the same time. This was performed fully in the primary literature cited in Table 23. As our accent in this review is on intensities, we reduce discussion of the energy parameterization to a minimum although we must emphasize the connections between the two sets of variables.

Throughout the summaries presented below we keep to the fore the various theoretical ideas and predictions described in Section 5. For ease of reference, these are:

(1) The signs of the ${}^{L}t_{\lambda}$ values are expected to be the same as those of the corresponding e_{λ} values. Such has been found to be the case in all CLF analyses to date.

(2) Ratios of ${}^{L}t_{\pi}:{}^{L}t_{\sigma}$ will often be larger than corresponding $e_{\pi}:e_{\sigma}$ ratios because the electric dipole operator is a more "outer" function than is the effective ligand field operator. This expectation has also been borne out in practice.

(3) The effects of misdirected valency must be properly accounted for within energy analyses. The main consequence for intensities will be a positive contribution to ${}^{L}t_{\pi}$ values (for ligand donors) even if the ligands have no formal π bonding function. There are several examples of this throughout the analyses cited in Table 23.

(4) *P*:*F* ratios, meaning ${}^{P}t_{\lambda}:{}^{F}t_{\lambda}$, are expected to be affected mostly by the two-centre expansion of ligand functions onto the metal. Our earlier discussions predicted that *P*:*F* ratios will be larger for:

(*1*) shorter bond lengths;

(*2*) ligand functions which are more polarized toward the metal; and

(*3*) ligand functions which are laterally more diffuse. The role of direct metal *p*–metal *d* mixing may also be important and is a question we consider later.

(5) Early attempts [11] to reproduce intensity distributions of octahedral and near-octahedral chromophores within the "static" CLF model failed utterly. This was, of course, a constructive failure showing that the effects of vibronic coupling could not be subsumed within the inappropriate static scheme. Similarly, preliminary attempts to model the vibronic field in $[Nien_3]^{2+}$ with octahedral or D_3 symmetry modes instead of the normal modes determined by NCA were unsuccessful. In the last section, we illustrate the crucial importance of accurate representations of both ligand field and spin-orbit coupling within the prior energy analyses.

(6) At the end of this section, we collect together the various examples in which CD has been modelled and emphasize the simplicity of the CLF approach to rotatory strengths.

7.3.1. Tetrahedral chromophores

Chromophores **10**–**12** in Table 23 are discussed under the CD heading later. The remaining nine tetrahedral molecules comprise the simple chlorides of cobalt, nickel and copper (**1**–**3**), the bishalobisphosphine complexes of cobalt and nickel (**4**–**7**) and the pair, CoN_2S_2 and CoO_2S_2 (**8**, **9**). CLF e_{λ} values for **1**–**7** are presented in Table 28 and ${}^{L}t_{\lambda}$ values in Table 29. Chromophores **8** and **9** are discussed shortly. While e_{λ} parameter values have been determined on an absolute scale, ${}^{L}t_{\lambda}$ values

Table 28
Optimal ligand-field parameter values (cm^{-1}) for chromophores 1–7

(a) Complex	B	ζ	$e_\sigma(X)$	$e_\pi(X)$	$e_\sigma(P)$	$e_\pi(P)$
$[CoCl_4]^{2-}$	750	500	3600	1000		
$[NiCl_4]^{2-}$	780	550	3800	900		
$Co(PPh_3)_2Cl_2$	575	500	3400	2000	3800	−1500
$Co(PPh_3)_2Br_2$	575	500	3500	1500	3500	−1000
$Ni(PPh_3)_2Cl_2$	550	350	4600	2000	4600	−2500
$Ni(PPh_3)_2Br_2$	550	300	4000	1500	4000	−1500

(b) Complex	ζ	e_σ	$e_{\pi\parallel}$	$e_{\pi\perp}$	$e_{\pi\sigma}$	e_ϵ (void)
$[CuCl_4]^{2-}$	700	4475	950	750	200	−850

are only relative, having been established by reproduction of intensity *distributions*. Reference ${}^{L}t_\lambda$ parameters are marked with an asterisk.

CLF e_λ values do not vary markedly throughout the short series of tetrachlorides (**1–3**) although there is some tendency towards larger $e_\sigma(Cl)$ values as cobalt(II) is replaced by nickel(II) and the copper(II). The more extensive parameterization [78] for $[CuCl_4]^{2-}$ is associated with its more distorted geometry. For the CLF ${}^{L}t_\lambda$ values, we note generally that each takes the same (positive) sign as its e_λ counterpart and that ${}^{L}t_\pi:{}^{L}t_\sigma$ ratios are considerably greater than $e_\pi:e_\sigma$. The most obvious trend, however, is the steady increase in ${}^{P}t_\sigma:{}^{F}t_\sigma$ along the series Co, Ni, Cu. To some extent, the underlying increase in the effective nuclear charge on the metal atoms along this series, which we presume to be the cause of that trend, also appears to increase the metal character in the π bonds as evidenced somewhat by the increasing ${}^{P}t_\pi:{}^{F}t_\pi$ ratios.

The CLF ${}^{L}t_\lambda$ values for the phosphine chromophores reflect their ligand fields and bonding especially well. The small and negative ${}^{L}t_\pi(P)$ values accord with π acceptor phosphines having π electron density well polarized away from the metal. The much greater $F{:}P$ ratio for the phosphine σ bonding in comparison with the halogen σ bonding presumably reflects a greater polarizability of the formally negatively charged halogens compared with the neutral phosphorus donors. Early ligand-field analyses of transition energies and of single-crystal paramagnetism in the bisphosphine complexes established two main conclusions, as indicated by the e_λ values in Table 28. The phosphines act as significant π acceptors, and, in consequence, the halogens in these complexes have much enhanced π donor function, relative to the tetrahalides, reflecting the operation of the electroneutrality principle as they act to compensate the central metal for its consequent loss of negative charge. This has been reviewed recently [9]. This view of the electron density distribution in the bisphosphine complexes is nicely confirmed by the intensity ${}^{L}t_\lambda$ parameter values in Table 29. Thus, we observe much larger ${}^{P}t_\pi:{}^{F}t_\pi$ ratios for the halogens indicating their greater polarization towards the metal as compared with the halogens in the $[MCl_4]^{2-}$ species. A similar result is to be seen for the $P{:}F$ values

Table 29
Optimal intensity parameters for chromophores 1–7

(a) For $[MCl_4]^{2-}$ species

Complex	$^{F}t_{\sigma}$(Cl)	$^{P}t_{\sigma}$(Cl)	$^{F}t_{\pi}$(Cl)	$^{P}t_{\pi}$(Cl)
$[CoCl_4]^{2-}$	100[a]	54	65	110
$[NiCl_4]^{2-}$	100[a]	155	120	125
$[CuCl_4]^{2-}$	100[a]	300	40	400

(b) For MP_2X_2 species; P = PPh_3

Complex	$^{F}t_{\sigma}$(P)	$^{P}t_{\sigma}$(P)	$^{F}t_{\sigma}$(X)	$^{P}t_{\sigma}$(X)	$^{F}t_{\pi}$(P)	$^{P}t_{\pi}$(P)	$^{F}t_{\pi}$(X)	$^{P}t_{\pi}$(X)
NiP_2Cl_2	100[a]	0	45	125	−10	−10	5	70
CoP_2Cl_2	100[a]	10	80	200	−40	−50	10	120
CoP_2Br_2	100[a]	10	120	200	−20	−40	0	120

[a]Fixed (reference) values.

for the $^{L}t_{\sigma}$ (halogen) ratios. Much smaller *P*:*F* ratios are evident for the π bonding of the phosphines, again to be associated with their more distant acceptor orbitals (which are probably the P–R σ antibonding functions).

The pair of chromophores **8** and **9** nicely illustrate the conflict between trends 4.2 and 4.3, discussed more fully in Section 5. Their CLF e_{λ} and $^{L}t_{\lambda}$ values are collected together in Table 30. Molecular geometries and some coordination dimensions are shown in Fig. 31. The e_{π} values attest a greater basicity of the thiolate than of the amine in CoN_2S_2 and much greater than for the thiourea in CoO_2S_2. Neither sulfur ligand shows much π bonding character so that, overall, the thioketone furnishes a very weak ligand field. This net weak donor function appears to be compensated for by strong donicity in both σ and π modes from the acetates in CoO_2S_2. The large π donicity no doubt draws upon the delocalized π electron density in the

Table 30
Optimal energy (cm^{-1}) and intensity (arbitrary units) parameter values for CoN_2S_2 and CoO_2S_2 chromophores (**8**, **9**)

CoN_2S_2				CoO_2S_2			
e_{σ}(N)		3900		e_{σ}(O)		5800	
				$e_{\pi\perp}$(O)		2000	
e_{σ}(S)		5800		e_{σ}(S)		2600	
$e_{\pi\perp}$(S)		0		$e_{\pi\perp}$(S)		−200	
B		620		*B*		690	
ζ		500		ζ		500	
$^{P}t_{\sigma}$(N)	30	$^{F}t_{\sigma}$(N)	0	$^{P}t_{\sigma}$(O)	83	$^{F}t_{\sigma}$(O)	100[a]
				$^{P}t_{\pi\perp}$(O)	50	$^{F}t_{\sigma\perp}$(O)	0
$^{P}t_{\sigma}$(S)	100[a]	$^{F}t_{\sigma}$(S)	25	$^{P}t_{\sigma}$(S)	4	$^{F}t_{\sigma}$(S)	17
$^{P}t_{\pi\perp}$(S)	0	$^{F}t_{\pi\perp}$(S)	0	$^{P}t_{\pi\perp}$(S)	0	$^{F}t_{\pi\perp}$(S)	0

[a]Fixed (reference) values.

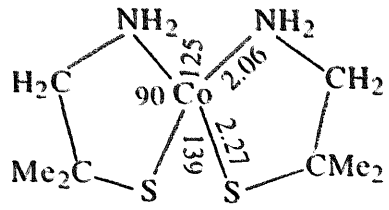

CoN_2S_2

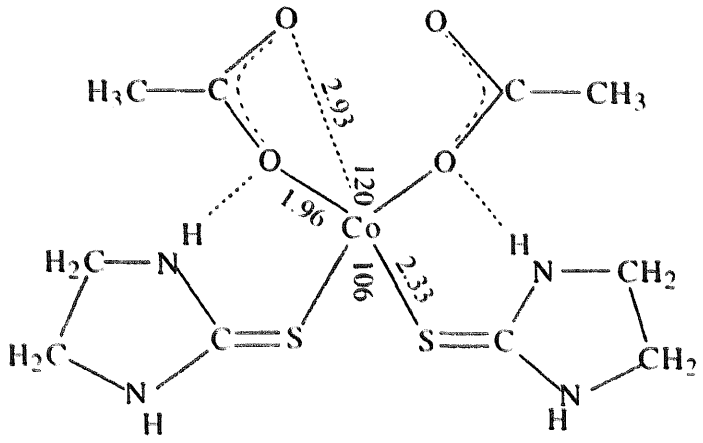

CoO_2S_2

Fig. 31. Chromophores **8** and **9**.

carboxylate anions. The metal–ligand bond lengths in the two chromophores broadly correlate with these ligand-field strengths. Now consider the ${}^{L}t_{\lambda}$ values established independently from the spectral intensities. As the spectra for the CoO_2S_2 chromophore were reported on arbitary scales, it is not possible to compare the magnitudes of the parameter values between the two systems. Once again, the ${}^{L}t_{\lambda}$ values are reported, in Table 30, relative to fixed values for one parameter in each system, as indicated. We observe, however, that large e_{λ} values are consistently associated with large ${}^{L}t_{\lambda}$ values, small with small, and even middle with middle. The lack of any significant π bonding role of either sulfur ligand is confirmed as is the greater basicity of thiolate than of amine in CoN_2S_2 and of acetate over thiourea in CoO_2S_2. Of particular interest are the *P*:*F* ratios determined by these analyses.

The greater *P* contributions for t_{σ}(N), t_{σ}(thiolate), and $t_{\pi\perp}$(O) all attest the relatively short bonds and good electron donation towards the metal atoms. Similarly, the relatively greater *F* contribution for t_{σ}(thiourea) accords with a longer bond and poor ligand donicity. All of these features illuminate propositions 4.*1* and 4.*2* above. By contrast, the very strong σ donor function of the acetates in CoO_2S_2 are associated with ${}^{P}t_{\sigma}(O) < {}^{F}t_{\sigma}(O)$. We consider this result to illustrate 4.*3*, relating to the circumstance in which bond "tightening" about the M–L vector arises when σ electron donation away from the atom-like field of the donor atom is more pronounced, as discussed in Section 5. Confidence in the reality of this result derives

from the consistently good correlations observed for all the other e_λ and ${}^{L}t_\lambda$ values in these analyses.

7.3.2. Trigonal bipyramidal chromophores

Of the 14 TBP complexes in Table 23, all but one (**32**) involve tetradentate, tripodal ligands. Twelve of these ligands furnish pure amine ligation, NN_3, and one (**31**) provides an NS_3 donor set. Optimal energy parameter values for all tripod-containing complexes are listed in Table 31. We will discuss Ni(salmedpt)–chromophore **32** — in due course.

The 13 complexes listed in Table 31 involve the d^7 cobalt(II) and d^8 nickel(II) metal centres. We have discussed elsewhere [79] the changing pattern of axial versus equatorial metal–amine bond lengths along the transition metal series. In the strong-field limit, the d orbital configurations for ions in TBP coordination are $(d_{xz,\ yz})^4(d_{xy,\ x^2-y^2})^2(d_{z^2})^1$ for d^7 and $(d_{xz,\ yz})^4(d_{xy,\ x^2-y^2})^3(d_{z^2})^1$ for d^8. The increased occupancy of the equatorial orbitals frustrates ligation with the equatorial amines more in the nickel complexes than in the cobalt ones. However, the general increase in effective nuclear charge as one traverses the periodic table from left to right combines with this factor to yield the overall trend that axial bonding increases in strength as cobalt(II) is replaced by nickel(II). Bond lengths reflect this trend [79] as do the ligand-field parameters in Table 31.

The corresponding ${}^{L}t_\lambda$ values for the 13 chromophores in Table 31 are presented in Table 32. Those for the S-tan complexes are given as absolute values being derived from analysis of solution spectra on absolute scales. The remainder are given relative to reference values marked with an asterisk. All the CLF analyses are of the "static" type. Parity mixing for the diametrically opposed axial ligations would cancel for identical ligations. The ${}^{L}t_\lambda$(ax) values accordingly refer to differences of ${}^{L}t_\lambda$ parame-

Table 31
Optimal CLF energy values (cm^{-1}) for chromophores **27**–**31** and **33**–**40**

Complex		$\bar{e}_\sigma$(ax)[a]	e_π(ax)[b]	e_σ(eq)	e_π(eq)
27	$[CoNN_3Br]^+$	4250	2000	4250	
28	$[NiNN_3Br]^+$	5100	2000	4500	
29	$[CoNN_3NCS]^+$	5600	2000	4400	
30	$[NiNN_3NCS]^+$	6000	2000	4000	
31	$[CoNS_3Br]^+$	4200	1500	3000	−500
33	[Co(S-tan)NCS]$^+$	4650	1000	3700	
34	[Co(S-tan)Cl]$^+$	4300	1200	3800	
35	[Co(S-tan)Br]$^+$	4100	1250	3900	
36	[Co(S-tan)I]$^+$	3800	1250	4100	
37	[Ni(S-tan)NCS]$^+$	5300	700	3500	
38	[Ni(S-tan)Cl]$^+$	5050	900	3500	
39	[Ni(S-tan)Br]$^+$	4900	900	3600	
40	[Ni(S-tan)I]$^+$	4700	950	3200	

[a]Mean value for axial ligands; $\bar{e}_\sigma(ax) = [e_\sigma(N_{ax}) + e_\sigma(X)]/2$.
[b]$e_\pi(N_{ax})$ assumed zero.

Table 32
Optimal CLF intensity parameter values for the chromophores **27–31** and **33–40**

Complex		$^{F}t_{\sigma}$(ax)	$^{P}t_{\sigma}$(ax)	$^{F}t_{\sigma}$(eq)	$^{P}t_{\sigma}$(eq)	$^{F}t_{\pi}$(ax)	$^{P}t_{\pi}$(ax)	$^{F}t_{\pi}$(eq)	$^{P}t_{\pi}$(eq)
(a) For $[MNR_3Br]^+$; ax = (Br-amine)									
27	$[CoNN_3Br]^+$	−100[a]	−90	50	0	0	0		
28	$[NiNN_3Br]^+$	−100[a]	−100	60	0	10	10		
31	$[CoNS_3Br]^+$	−100[a]	−80	25	3	0	0	0	−3
(b) For $[MNN_3NCS]^+$; ax = (NCS-amine)									
Complex		$^{F}t_{\sigma}$(ax)	$^{P}t_{\sigma}$(ax)	$^{F}t_{\sigma}$(eq)	$^{P}t_{\sigma}$(eq)	$^{F}t_{\pi}$(ax)	$^{P}t_{\pi}$(ax)		
29	$[CoNN_3NCS]^+$	100[a]	50	100	50	0	0		
30	$[NiNN_3NCS]^+$	100[a]	20	45	0	50	20		
(c) For $[M(S\text{-tan})X]^+$; ax = (X-amine)									
Complex		$^{F}t_{\sigma}$(ax)	$^{P}t_{\sigma}$(ax)	$^{F}t_{\sigma}$(eq)	$^{P}t_{\sigma}$(eq)	$^{F}t_{\pi}$(ax)	$^{P}t_{\pi}$(ax)		
33	[Co(S-tan)NCS]$^+$	43[b]	0	11	0	8	16		
34	[Co(S-tan)Cl]$^+$	−92	−92	12	0	12	0		
35	[Co(S-tan)Br]$^+$	−70	−70	14	0	7	7		
36	[Co(S-tan)I]$^+$	−83	−83	16	0	16	0		
37	[Ni(S-tan)NCS]$^+$	86	34	34	5	17	17		
38	[Ni(S-tan)Cl]$^+$	−26	−26	34	0	0	0		
39	[Ni(S-tan)Br]$^+$	−36	−36	36	0	0	7		
40	[Ni(S-tan)I]$^+$	−37	−37	37	0	0	0		

[a]Fixed (reference) values.
[b]All values as $^{L}t_{\lambda}/10^{-20}$D.

ters associated with the apical amine and the non-tripodal ligand. This has obvious consequences for the quoted signs of all $^{L}t_{\lambda}$(ax) values. Thus, throughout Table 32, we note that positive $^{L}t_{\pi}$ values are to be associated with the π donor, non-tripodal ligations if it is assumed that there is no π bonding role for the apical amines. Similarly, the signs of all $^{L}t_{\sigma}$(ax) parameters are comprehensible if axial contributions follow the sequence NCS > amine > halogen. Furthermore, assuming that the signs of $^{L}t_{\lambda}$ parameters are the same as those of their e_{λ} counterparts, as theoretically predicted in Section 5, this ordering establishes a similar ordering of ligand-field strengths which is identical to that indicated by the relative e_{σ}(ax) values in Table 31. This ordering of ligand σ bascisity accords with general chemical experience. It is worth noting, however, that the *energy* analyses for *these* systems cannot, of themselves, firmly establish that ordering because the e_{σ}(ax) values of Table 31 merely record the averages of e_{σ}(amine) and e_{σ}(X).

With this ordering in mind, we note from the e_{λ} values of Table 31 that the equatorial ligations are generally weaker than the axial. In line with this conclusion, are the somewhat smaller $^{L}t_{\sigma}$(eq) values in Table 32 as compared with $^{L}t_{\sigma}$(ax). More significant is the characterization of these weaker equatorial ligations by dominant F contributions over P; F and P contributions to the $^{L}t_{\sigma}$ are more equal for the more strongly donating axial ligands.

Finally, we note that the relative magnitudes of t_σ and t_π parameters for the equatorial sulfur donors of $[CoNS_3Br]^+$ and their small magnitudes with respect to those for the axial ligations are once more qualitatively consistent with the weak donor function of these ligands evidenced by the e_σ and e_π values in Table 31.

In several respects, then, the ${}^Lt_\lambda$ and e_λ parameterizations for these 13 TBP complexes correlate well with each other and with geometric features quoted in the primary literature. Some lack of clarity is evident, however, which stems in part from many of the analyses being based upon unpolarized, solution spectra [80] or, in the case of $[CoNN_3NCS]^+$, upon the unavailability of precise structural parameters [62]. Overall, however, there can be no doubt that the theoretical predictions of Section 5 have been reasonably well confirmed in these species.

The ligand-field and intensity analyses for chromophore **32** — Ni(salmedpt) — illustrate some of the complexities associated with misdirected valency. The coordination geometry of this complex is summarized in Fig. 32. Ligand-field analyses of the '*d*–*d*' transition energies optimized values for the parameter set: Racah *B* and *C* for interelectron repulsion; and for the ligand field proper, the CLF parameters, e_σ(im), $e_{\pi\perp}$(im) for the Schiff-base imines lying at the axial sites of the trigonal bipyramidal coordination, e_σ(am) for the equatorial amine, and e_σ, $e_{\pi\perp}$, $e_{\pi\parallel}$ and $e_{\sigma\pi\parallel}$ for the equatorial phenolic oxygen donors; $\parallel$ and $\perp$ refer to directions parallel and perpendicular to the salicylidene rings, respectively; the spin-orbit coupling coefficient, ζ, was held fixed at 450 cm^{-1} throughout. The parameters $e_{\pi\parallel}$ and $e_{\sigma\pi\parallel}$ were required to account for the misdirected valency arising from the non-dative oxygen lone pairs lying in the planes of the sal rings. Good representation of the experimental transition energies yielded the optimal parameter values listed in Table 33.

The axial imines are approximately centrosymmetrically related through the metal. Were this precise, contributions to intensities in this "static" CLF analysis from these ligations would cancel exactly. The main departure from this centric relationship lies in the inexact parallelism of the N=C bonds. We therefore omitted ${}^Lt_\sigma$(im) parameters from the intensity analysis and only included ${}^Lt_{\pi\parallel}$(im) towards the end

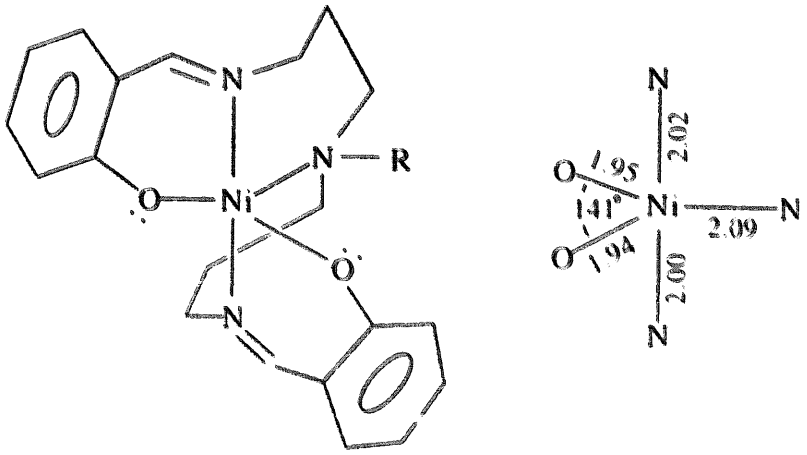

Fig. 32. Chromophore **32**.

Table 33
Optimal energy parameter values (cm^{-1}) for chromophore **32**

Parameter	e_σ(im)	$e_{\pi\perp}$(im)	e_σ(am)	e_σ(O)	$e_{\pi\perp}$(O)	$e_{\pi\parallel}$(O)	$e_{\sigma\pi\parallel}$(O)	B	C	ζ
Value	5100	0	3300	4000	1100	25	1200	820	3000	450

of the process. However, contributions from this source were found to be trivial. The optimal values for ${}^{L}t_\lambda$ parameters, given in Table 34 thus refer only to the equatorial ligands. *R*-type contributions were considered explicitly in this analysis but found to be very slight due, no doubt, to the triangular coordination, as discussed in Section 5.

The e_σ values in Table 33 describe M–L σ bonding which decreases along the series imine > oxygen > amine. We suppose the much larger e_σ(im) value to reflect the greater *d* electron density and its repulsive role in the equatorial plane of the TBP coordination, as for the tripodal complexes above. The larger fields of the phenolic oxygens relative to those of the amines, on the other hand, appears to describe a greater electron donation from the formally negatively charged oxygen donors. The dominance of ${}^{F}t_\sigma$(O) over ${}^{P}t_\sigma$(O) in Table 34 supports this conclusion and indicates, as for the acetate ligations in chromophore **9**, a tightening of the M–O σ bond as electron density tends to leave the atomic field of the donor atom. The lesser donation from the amines, on the other hand, is characterized by a laterally more diffuse σ bonding density when ${}^{P}t_\sigma$(am) > ${}^{F}t_\sigma$(am).

The positive sign found for $e_{\sigma\pi\parallel}$(O) places off-axis perturbation in the Ni–O ligation on the same side as the non-dative lone pair. This situation is quite typical of misdirected valency from such sources [10]. The misdirected valency is also strongly evidenced by the relative magnitude of the ${}^{P}t_{\pi\parallel}$(O) parameter. That the *P* contribution here so overwhelms the *F* cannot be understood in terms of a strong polarization towards the metal, but rather in terms of a relatively wide lateral spread of the non-dative lone pair that would concur with its expected diffuseness.

The CLF intensity analysis of this chromophore included a detailed theoretical consideration of the consequences of misdirected valency upon the *t* parametrization. Wide ranging empirical variation of the many extra parameters spawned in these circumstances suggest that the effects of misdirected valency are adequately monitored by the energy parameters, $e_{\sigma\pi\parallel}$ and $e_{\pi\parallel}$, and just the pair of intensity variables, ${}^{P}t_{\pi\parallel}$ and ${}^{F}t_{\pi\parallel}$.

Table 34
Optimal intensity parameter values for chromophore **32**

Parameter	${}^{P}t_\sigma$(am)	${}^{F}t_\sigma$(am)	${}^{P}t_\sigma$(O)	${}^{F}t_\sigma$(O)	${}^{P}t_{\pi\perp}$(O)	${}^{F}t_{\pi\perp}$(O)	${}^{P}t_{\pi\parallel}$(O)	${}^{F}t_{\pi\parallel}$(O)
Value	100[a]	64	0	53	45	8	61	2

[a]Fixed (reference) value.

7.3.3. Square pyramidal chromophores

Our examples of SP coordination are the pair of arsine oxide complexes $[M(diphenylmethylarsineoxide)_4NO_3]^+NO_3^-$; M = Co(II), Ni(II) — chromophores **41** and **42**. These systems have been extensively studied. CLF energy analyses have successfully reproduced '*d–d*' transition energies and single-crystal paramagnetic susceptibilities over the temperature range 90–300 K for both complexes, and single-crystal esr *g* tensors for the cobalt system. The molecules are isostructural and crystallize isomorphously in tetragonal lattices. The metal atoms are sited on crystallographic four-fold axes but the apical nitrates are disordered. Some details of the coordination geometry of the nickel complex are given in Fig. 33. Misdirected valency effects are associated with all ligations; with the non-dative lone pairs of the arsine oxide donor oxygen atoms and with bent bonding between metal and nitrate. Optimal CLF e_λ values affording reproduction of all the ligand-field properties listed above are presented in Table 35 . Throughout, significant magnitudes for the various $e_{\sigma\pi\|}$ and $e_{\pi\|}$ parameters evince the expected misdirected valency. It is particularly obvious, however, that the characters of the metal–nitrate ligations differ markedly between these two molecules. This is to be understood in terms of the steric role of the d_{xy} orbital again, being doubly filled in the nickel complex, but only singly filled

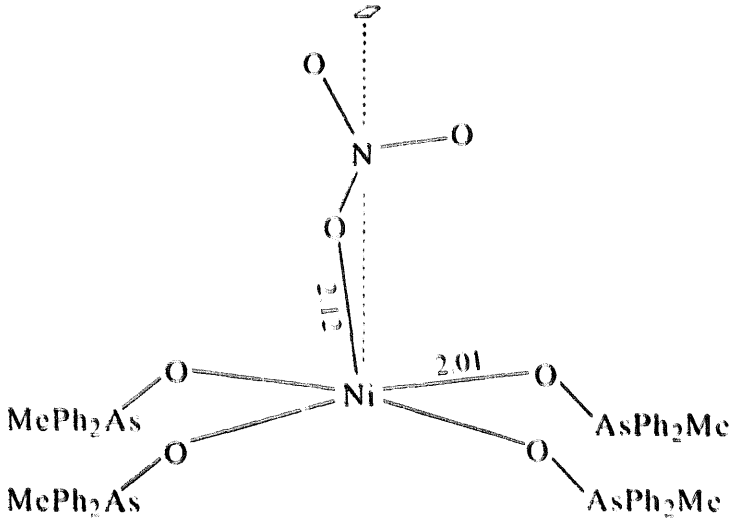

Fig. 33. Chromophore **42**.

Table 35
Optimal CLF e_λ values (cm^{-1}) for chromophores **41** and **42**

Parameter	M = Co(II)		M = Ni(II)	
	Arsine oxide	Nitrate	Arsine oxide	Nitrate
e_σ	3500	100	3550	1700
$e_{\pi\perp}$	980	−200	950	100
$e_{\pi\|}$	875	650	675	350
$e_{\sigma\pi\|}$	945	950	880	1650

in the cobalt. Bond strengthening that is to be expected with increasing effective nuclear charge on replacing cobalt by nickel is frustrated for the basal coordination by the extra d_{xy} electron and must be compensated for by a shorter bond and increased ligand field of the nickel–nitrate ligation. In both chromophores, of course, the low value for $e_\sigma(NO_3^-)$ also reflects the negative ligand-field contribution from the coordination void opposite.

CLF intensity parameter values yielding optimal reproduction of the polarized crystal spectra are collected together in Table 36. We have generally opted in the present review not to recount details of the analytical processes that have yielded the various e_λ and ${}^Lt_\lambda$ parameter values. Table 36 includes mention of ${}^Rt_\lambda$ parameters, however, for which a brief commentary is appropriate. As discussed in Section 5, R contributions for the incident electric dipolar field oriented normal to any local bond are discarded. The remaining $R(z)$ contributions yield local transition moments oriented parallel to each M–L vector and their sum will vanish for the global chromophore symmetries of bipyramids and antibipyramids. There will be some tendency for similar cancellation in the present square pyramids also. The basal ligands are oriented at about 101° to the formal molecular tetrad, so that the axial contribution from the nitrate R terms will cancel those from the four basal ligands when ${}^Rt_\lambda(NO_3) \sim 0.73\,{}^Rt_\lambda(AsO)$. The ligand-field energy analyses established weaker interactions between metal and nitrate than for metal and arsine oxide and the Ni–ONO_2 and Ni–OAs bond lengths are 2.01 and 2.12 Å, respectively. It was anticipated from the beginning of the intensity analyses that overall R contributions would be small and not well-defined. The analyses were therefore carried out in two steps. In the first, all R contributions were ignored. Surprisingly and fortunately, an essentially unique region of $P+F$ parameter space for each chromophore provided good reproduction of the experimental intensity distributions. In the second step,

Table 36
Optimal CLF intensity parameter values for chromophores **41** and **42**

Parameter	M = Co(II)		M-Ni(II)	
	Arsine oxide	Nitrate	Arsine oxide	Nitrate
${}^Pt_\sigma$	100[a]	0	100[a]	15
${}^Ft_\sigma$	20	0	25	50
${}^Pt_{\pi\perp}$	20	0	25	0
${}^Ft_{\pi\perp}$	70	−20	85	0
${}^Pt_{\pi\parallel}$	35	0	35	0
${}^Ft_{\pi\parallel}$	0	10	0	10
$\Delta^Rt_\lambda = {}^Rt_\lambda(AsO) - {}^Rt_\lambda(NO_3)$				
Δ^Rt_σ	10	0		
$\Delta^Rt_{\pi\perp}$	10	−10		
$\Delta^Rt_{\pi\parallel}$	0	0		

[a]Fixed (reference) value.

the response of these regions to variations in the differences between R contributions for arsine oxide and nitrate ligations, $\Delta^R t_\lambda$, were investigated. Little correlation between the model's response to these ΔR values was noted and values quoted in Table 36 are subject to estimated uncertainties of about ± 10.

The ${}^L t_\lambda$ values in Table 36 accord with the e_λ values in Table 35 and associated discussion reasonably well. The good, but not exceptional, donor function of the arsine oxides are characterized by a ${}^P t_\sigma$ parameter which dominates over ${}^F t_\sigma$. The contrary domination of the F contribution over the P for the ${}^L t_\pi$(AsO) parameters merely reflects the greater distance from the metal of π functions relative to σ together with the only modest π donor role of the arsine oxide ligand. The dominance of the ${}^P t_{\pi\|}$(AsO) over ${}^F t_{\pi\|}$(AsO), on the other hand, like that in Ni(salmedpt) above, reflects the lateral diffuseness of the non-dative lone pair on the oxygen atom.

The energy analyses provided a view of weak metal–nitrate bonding in the nickel complex, but weaker still in the cobalt one. The intensity analyses confirm this result. While a significant contribution to the spectral intensity arises from the nickel–nitrate coordination, rather little derives from the cobalt–nitrate interaction. Furthermore, ${}^F t_\sigma > {}^P t_\sigma$ for the Ni–NO_3 ligation, in contrast to the situation for the metal–arsine oxide bonding, once more attesting the relative weakness of the nitrate coordination. That same weakness is presumably responsible for the dominance of ${}^F t_{\pi\|}(NO_3)$ over ${}^P t_{\pi\|}(NO_3)$.

7.3.4. Planar chromophores I

Here, we particularly address the square planar, tetrahalo complexes of copper(II), palladium(II) and platinum(II) — chromophores **14–20** — but include a near-planar $[CuCl_4]^{2-}$ system (**13**) and the acentric, planar species $[PtCl_3NH_3]^-$, **21**. Chromophores **14–17** comprise $[CuCl_4]^{2-}$ ions in different lattices. Their polarized crystal spectra differ because of the varied environment of the tetrachlorocopper ions. Spectral resolution throughout the group varies and the detail of their experimental spectroscopic study varies also. Each system has been subjected to independent CLF analysis. Unsurprisingly, their parametrizations are closely similar; this does, of course, go some way to support the general integrity of the analytical process. In the present review, we represent the group by a single chromophore. The $[CuCl_4]^{2-}$ group, and K_2PtCl_4 and K_2PtBr_4, were the first systems to be analysed within the CLF vibronic model. In those early studies [59] the vibronic t parameters were not related to an underlying set of static t parameters by NCA. The optimization procedures were very lengthy and complex and are not reviewed here. Nevertheless, they furnished conclusions that were well supported by the more refined, "complete", CLF+NCA vibronic analysis [66] we describe now. The opportunity was taken in this study to make comparisons with some related but non-planar chromophores and also to include an analysis of K_2PdCl_4. The experimental data base for the latter complex is far less rich than those for the platinum chromophores, K_2PtCl_4 and K_2PtBr_4, and would not support analysis within the highly parameterized CLF vibronic model that did not link all vibronic variables to a common static set.

In addition, then, to the square planar platinum and palladium tetrahalides, the present group of chromophores includes the planar CREAT complex (**15**); NBZP

(13), which possesses a strongly compressed tetrahedral coordination with two Cl–Cu–Cl angles averaging 166° and four averaging 90°, and, as reported in Section 7.3.1, Cs_2CuCl_4 (3) being much more nearly tetrahedral with the two larger Cl–Cu–Cl angles averaging 129°. The CLF intensity analyses for these complexes were of the vibronic+NCA type for $[PtCl_4]^{2-}$, $[PtBr_4]^{2-}$, $[PdCl_4]^{2-}$ and the planar $[CuCl_4]^{2-}$ of CREAT; static+vibronic+NCA for the compressed tetrahedral $[CuCl_4]^{2-}$ ions in NBZP; and static only for the "tetrahedral" $[CuCl_4]^{2-}$ ions in Cs_2CuCl_4. All *ungerade bending* modes were included in the vibronic contribution to these analyses. Values of the ${}^{L}t_{\lambda}$ parameters for the chromophores are compared in Table 37 . Let us first consider the ${}^{L}t_{\sigma}$ values.

The ratio ${}^{P}t_{\sigma}:{}^{F}t_{\sigma}$ for the planar chromophore CREAT is about 0.3; for $[PtCl_4]^{2-}$ and $[PtBr_4]^{2-}$, it is 1.6 and 0.9, respectively. The values for ${}^{P}t_{\sigma}$ and ${}^{F}t_{\sigma}$ for the d^8 planar species are absolutely larger than those for the d^9 planar $[CuCl_4]^{2-}$ complex. Both of these observations correlate well with the magnitudes of nephelauxetic effects that have been observed in these, and related, species. Thus, $F_2:F_2$(free ion) ratios for $[PtCl_4]^{2-}$ and $[PtBr_4]^{2-}$ chromophores have been estimated [60] to lie within the bounds 0.49–0.78 and 0.35–0.54, respectively. For the planar, low-spin d^7 complexes, Co(salen) and Co(clamben), [salen = *N*,*N*′-ethylenebis-(salicylideneaminato)] and clamben = *N*,*N*′-ethylenebis(2-amino-5-chlorobenzyl-ideneaminato)], $F_2:F_2$(free ion) values are 0.41 and 0.28, respectively [81]. In all these low-spin d^7 and d^8 species, the empty $d_{x^2-y^2}$ orbital is similarly reflected in larger ${}^{P}t_{\sigma}:{}^{F}t_{\sigma}$ ratios. The smaller *P*:*F* ratios for $[PtBr_4]^{2-}$ with respect to $[PtCl_4]^{2-}$ does not conflict with the opposite trend for nephelauxetic effects as longer M–L bonds are otherwise associated with lower *P*:*F* ratios.

Similar reasoning applies when we compare ${}^{P}t_{\sigma}:{}^{F}t_{\sigma}$ ratios for the planar d^8 and d^9 species. The $d_{x^2-y^2}$ orbital houses no electrons in the d^8 molecules but one electron in the d^9. The steric activity of this nearly non-bonding electron tends to loosen the d^9 M–Cl bonds relative to those in the d^8 metals and this is reflected in the marked decrease in intensity *P*:*F* ratio from 1.6 for $[PtCl_4]^{2-}$ to 0.3 for $[CuCl_4]^{2-}$.

Having argued that trends in Z_{eff} account for the variation in *P*:*F* ratios for tetrahedral chloro Co(II), Ni(II) and Cu(II) complexes in Section 7.3.1 and that variations in the steric role of the open *d* shell rationalize those for the planar chloro Pt(II) and Cu(II) chromophores, we focus now on the marked differences between intensity parameter values for tetrahedral and planar chlorocuprates. Insofar that

Table 37
Optimal CLF ${}^{L}t_{\lambda}$ values[a] for chromophores **3**, **13**, **15**, **18**–**20**

Parameter	$[PtCl_4]^{2-}$	$[PtBr_4]^{2-}$	$[PdCl_4]^{2-}$	CREAT	NBZP	Cs_2CuCl_4
${}^{P}t_{\sigma}$	225	249	229	19	246	452
${}^{F}t_{\sigma}$	142	281	46	69	73	70
${}^{P}t_{\pi}$	0	0	0	21	176	374
${}^{F}t_{\pi}$	247	411	286	62	115	70

[a]All values in units of $D \times 10^{-2}$ except for Cs_2CuCl_4 whose arbitrary values have been scaled, as described in the text.

the Cu–Cl σ bonds are built from Cu 4*s* plus ligand σ functions, no first-order variation with Cl–Cu–Cl angle is to be expected. We similarly expect no first-order variations in either the magnitudes of the ${}^{L}t_{\lambda}$ parameters nor in the ${}^{P}t_{\sigma}$:${}^{F}t_{\sigma}$ ratio with respect to the Cl–Cu–Cl bond angle. On the other hand, however, contributions to the bond orbitals from Cu 4*p* functions *are* expected to vary with the geometry change from planar to tetrahedral. No such contribution can occur at all in the centric planar environment, of course. As discussed in Sections 3 and 5, contributions to a ${}^{P}t_{\sigma}$ parameter arise from the multipole expansion of the ligand function onto the metal centre *and* from the admixture 4*s*–4*p* brokered by covalency with the ligands. While similar contributions to ${}^{F}t_{\sigma}$ are expected from the multipole expansion, analogous 4*s*–4*f* mixing will be trivial. Altogether, therefore, we expect to see similar ${}^{F}t_{\sigma}$ parameter values in planar and tetrahedral $[CuCl_4]^{2-}$ species, but larger ${}^{P}t_{\sigma}$ values in the acentric tetrahedral environment than in the centrosymmetric planar one. The ${}^{F}t_{\sigma}$ value for the near-planar NBZP is similar to that for CREAT. All ${}^{L}t_{\lambda}$ values for Cs_2CuCl_4 in Table 37 have been scaled to the value 70 for ${}^{F}t_{\sigma}$, accordingly, and we observe a dramatic increase in ${}^{P}t_{\sigma}$ as the chromophore geometry of the chlorocuprates changes from planar to "tetrahedral". The magnitude of this trend is by no means to be laid at the door of the SC mechanism discussed in Section 4, however, for, as described in Section 3, the magnitude of 4*s*–4*p* mixing is greatly enhanced by covalency.

We now consider the intensity parameters relating to π bonding. Firstly within the chlorocuprate species, we discern a somewhat similar pattern for the ${}^{L}t_{\pi}$ values in Table 37 as for the ${}^{L}t_{\sigma}$. The ${}^{F}t_{\pi}$ values do not vary markedly while those of the ${}^{P}t_{\pi}$ increase dramatically with the trend from planar to tetrahedral. Again, we ascribe this to an increasing participation of the Cu 4*p* orbitals within the bond orbitals. Turning to the d^8 chromophores, the dominance of ${}^{F}t_{\pi}$ over ${}^{P}t_{\pi}$ appears to reflect their low-spin configuration. Thus, we emphasized above how the unoccupancy of the $d_{x^2-y^2}$ orbital facilitates increasing M←L σ donation. In the same way, the double occupancy of all other *d* orbitals tends to frustrate M←L π donation. Precise e_{λ} values for these complexes are unavailable because of inevitable parameter correlations that characterize analyses of the transition energies. Nevertheless, "midrange" CLF e_{λ} values [60] do support a relatively minor π functionality in these d^8 bonds: for $[PtCl_4]^{2-}$, $e_{\sigma} = 11980\ cm^{-1}$ and $e_{\pi} = 2300\ cm^{-1}$; for $[PtBr_4]^{2-}$, $e_{\sigma} = 10000\ cm^{-1}$ and $e_{\pi} = 940\ cm^{-1}$; for $[PdCl_4]^{2-}$, $e_{\sigma} = 9200\ cm^{-1}$, and $e_{\pi} = 1300\ cm^{-1}$. A lesser polarization of the halogen π functions towards the platinum and palladium metal atoms is then reflected in the dominance of ${}^{F}t_{\pi}$ over ${}^{P}t_{\pi}$ intensity parameters.

We conclude this section with a brief mention of a static + vibronic CLF intensity analysis of complex **21** — $[PtCl_3NH_3]^-$ — being the only other such study of a platinum chromophore. The acentric, planar coordination requires consideration of *cis* and *trans* Pt–Cl bonding as well as Pt–N; *cis* and *trans* relate, as usual, to Pt–Cl bonds lying adjacent or opposite the Pt–N bond, respectively. The consequently high degree of parameterization resulted in CLF e_{λ} and ${}^{L}t_{\lambda}$ parameter values that were less well established than for the tetrahalo complexes above. Best estimates of the ${}^{L}t_{\lambda}$ are given in Table 38. As detailed elsewhere [67], most of the observed intensity arises from the static environment. The more strongly bound ammine is

Table 38
CLF intensity parameters[a] for chromophore **21**

Parameter[b]	Range
${}^{P}t_{\sigma}(N)$	165–225
${}^{F}t_{\sigma}(N)$	0 ± 15
${}^{P}t_{\sigma}(Cl^{t})$	103–185[c]
${}^{F}t_{\sigma}(Cl^{t})$	108–99[d]
${}^{P}t_{\pi}(Cl^{t})$	0 ± 8
${}^{F}t_{\pi}(Cl^{t})$	140 ± 23
${}^{P}t_{\sigma}(Cl^{c})$	150
${}^{F}t_{\sigma}(Cl^{c})$	118 ± 23
${}^{P}t_{\pi}(Cl^{c})$	26 ± 18
${}^{F}t_{\pi}(Cl^{c})$	90 ± 8

[a] In units of $D\times10^{-2}$.
[b] Cl^{t} = *trans* Cl, Cl^{c} = *cis* Cl.
[c] Correlation: $1.33\,{}^{P}t_{\sigma}(N)-115$.
[d] Correlation: $-0.1\,{}^{P}t_{\sigma}(n)+122$.

associated with a ${}^{P}t_{\sigma}$:${}^{F}t_{\sigma}$ ratio that strongly favours the *P* contribution. The smaller *P*:*F* ratios for the chlorine σ bonding resemble those in Table 37 for the tetrachloroplatinate. Once again the Pt–Cl ligations are characterized by ${}^{F}t_{\pi}$ parameters dominating over ${}^{P}t_{\pi}$.

7.3.5. Planar chromophores II

In this section, we look at a series of five $CuCl_2X_2$ complexes — chromophores **23–26** — all of which possess exact or near-exact *trans*, centric planar coordination of the metal. The '*d*–*d*' intensities of each have been analysed within the CLF + NCA vibronic scheme. In three complexes, the X ligands are cyclic amines — lutidines or a pyrazole — and in two, they are oxygen donors — water or a pyridine-*N*-oxide.

The study of these five chromophores is very detailed. We confine ourselves here to three main issues. One concerns the question of band assignment and selection rules for the DIAQ complex **26** and is a matter we return to in Section 7.4. The others relate to the CLF e_{λ} and ${}^{L}t_{\lambda}$ values. The emphasis here is on the unusually large e_{σ} values for ligations with the nitrogen heterocycles and we shall see how the conclusions from the energy analyses are supported by the reproduction of spectral intensities.

Optimal CLF e_{λ} values for the five $CuCl_2X_2$ systems are listed in Table 39 and Table 40. The $d_{x^2-y^2}$ orbital in these systems is uniquely shifted by interaction with both Cu–Cl and Cu–X bond orbitals; accordingly, separate $e_{\sigma}(Cl)$ and $e_{\sigma}(X)$ values cannot be determined. It is obvious, nevertheless, that e_{σ} values for the $CuCl_2N_2$ species are unusually large; those for the $CuCl_2O_2$ complexes are more typical. At the same time the values for e_{σ}(void) for the first group are significantly less than for the second, the latter of which are again more normal for planar copper(II) species. Values for the ligand-field trace, Σ, being the sum of all diagonal e_{λ} parameter values in a complex have been found [9,82] to be about 23 000 cm^{-1} in very many

Table 39
Optimal CLF e_λ values (cm^{-1}) for chromophores **22–24**

Parameter	PDMP	2,3-LUT	2,6-LUT
$\bar{e}_\sigma^a$	6550	6550	6350
e_π(Cl)	1800	1280	1280
$e_{\pi\perp}$(N)	950	940	940
e_σ(void)	−2500	−2690	−2690
Σ^b	30 300	27 820	27 020

[a] $\bar{e}_\sigma = [e_\sigma(\mathrm{N}) + e_\sigma(\mathrm{Cl})]/2$
[b] The ligand-field trace,

$$\Sigma = \sum_{i}^{\text{cells}} (e_\sigma + e_{\pi\perp} + e_{\pi\parallel})_i$$

Table 40
Optimal CLF e_λ values (cm^{-1}) for chromophores **25** and **26**

Parameter	DIAQ	Parameter	4-PICNO
$\bar{e}^a$	5700	$\bar{e}_\sigma^a$	5450
e_π(Cl)	1000	e_π	830
$e_{\pi\perp}$(O)	1800		
$e_{\pi\parallel}$(O)	0[b]		
$e_{\sigma\pi\parallel}$(O)	0[b]	$e_{\sigma\pi\parallel}$(O)	700
e_σ(void)	−3110[c]	e_σ(void)	−3110
Σ	24 180	Σ	22 220

[a] $e_\sigma = [e_\sigma(\mathrm{O}) + e_\sigma(\mathrm{Cl})]/2$.
[b] Fixed values.
[c] Set equal to e_σ(void) for 4-PICNO.

six-, five- and four-coordinate molecules of Fe(II), Co(II), Ni(II) and Cu(II). Trace values for the $CuCl_2O_2$ species in Table 40 fit this pattern while those for the $CuCl_2N_2$ species do not. Arguments presented in the original paper [68] suggest that these unusual features derive from particularly large ligand-field strengths for the M–N σ interactions in these molecules. The strong ligand fields derive not so much from an unexpectedly large σ donicity, but from an intact ligand polarization that puts significant negative charge on the donor nitrogen atom.

The optimal CLF intensity parameter values ($D \times 10^{-2}$) for all five $CuCl_2X_2$ chromophores are listed in Table 41. Although all $^Lt_\lambda$ values are presented on an absolute scale, comparisons between chromophores must be made with care as the values have involved the difficult measurement of crystal thickness. All values for the 2,3-LUT are similar to the corresponding ones for 2,6-LUT. In view of the rather different appearance of the experimental spectra of these systems (for reasons of polarization directions and experimental crystal planes), it is gratifying to see the chemical similarity of these two compounds reflected in this way. The most obvious difference between the lutidine and pyrazole complexes is in the ratio $^Pt_\sigma(\mathrm{N}):{}^Ft_\sigma(\mathrm{N})$, being about 3 in the LUT species, but only about 1/30 for PDMP. On the other

Table 41
Optimal CLF intensity parameters ($D \times 10^{-2}$) for $CuCl_2X_2$ chromophores, **22–26**

Parameter	PDMP	2,3-LUT	2,6-LUT	DIAQ	4-PICNO
${}^{P}t_{\sigma}(Cl)$	87	45	33	126	166
${}^{F}t_{\sigma}(Cl)$	24	38	30	1	0
${}^{P}t_{\pi}(Cl)$	5	3	2	57	118
${}^{F}t_{\pi}(Cl)$	5	3	2	19	35
${}^{P}t_{\sigma}(X)$	3	100	72	68	158
${}^{F}t_{\sigma}(X)$	87	32	31	116	10
${}^{P}t_{\pi\parallel}(X)$	0[a]	0[a]	0[a]	0[a]	48
${}^{F}t_{\pi\parallel}(X)$	0[a]	0[a]	0[a]	0[a]	0
${}^{P}t_{\pi\perp}(X)$	25	11	0	24	48[b]
${}^{F}t_{\pi\perp}(X)$	21	9	2	125	0[b]

[a]Fixed.
[b]$\parallel$ set equal to $\perp$.

hand, the e_{σ} values for these three complexes are virtually identical. The pK_a values for pyridine and pyrazole are 5.2 and 2.5, respectively. A less good donor σ function for the pyrazole ligation would be expected to be reflected in a lower *P*:*F* ratio, as observed. At the same time, however, we anticipate a somewhat greater polarity on the pyrazole ligand than a pyridine (or lutidines, here) so that their similar e_{σ} values probably result from a compensation of poorer donor functions in the pyrazole by a larger ionic contribution to the M–L bonding. Turning to the copper–chlorine ligations in the $CuCl_2X_2$ complexes, we observe the ${}^{P}t_{\sigma}(Cl)/{}^{F}t_{\sigma}(Cl)$ ratio for the pyrazole complex to be significantly larger than those for the LUT systems. This presumably reflects a larger Cl→Cu donation in the PDMP molecule than in the LUT species to compensate for the poorer σ donor function of the pyrazole relative to the lutidines in concert with the operation of the electroneutrality principal at the metal. The unusually strong donicity of the nitrogen ligands as a group compared with the water and pyridine-*N*-oxide ligands also appears to be evinced by all ${}^{L}t_{\lambda}(Cl)$ values throughout the five $CuCl_2X_2$ chromophores. In recognition once more of the operation of the electroneutrality principle at the metal centre, the chlorine ligands appear to be better donors in the $CuCl_2O_2$ species than in the $CuCl_2N_2$ as indicated by larger ${}^{L}t_{\sigma}(Cl)$ and ${}^{L}t_{\pi}(Cl)$ in the former and by large ${}^{P}t_{\lambda}:{}^{F}t_{\lambda}$ ratios also. The global view of the electron distributions throughout the series of five $CuCl_2X_2$ chromophores is consistent only upon recognition of the "ionic" contribution to the large e_{σ} values [$e_{\sigma}(N)$ underlying] in the $CuCl_2N_2$ systems. Here is a good example of how the combined analysis of transition energies and intensities can illuminate our understanding of the bonding in transition metal complexes.

7.3.6. The reproduction of rotatory strengths

Circular dichroism was the focus of studies on three formal tetrahedral chromophores, **10–12**, eight trigonal bipyramidal chromophores, **33–40**, and of incidental interest for the "octahedral" system **43**. As the present article addresses the reproduction and understanding of forced electric dipole strengths in '*d–d*' and '*f–f*'

spectra, we will not dwell upon the calculation of rotatory strengths, except to make one general observation about their origins in these chromophores.

The sources of the chirality in these complexes are seemingly obvious. In the spartein complexes, discussed in Section 7.2.4, the twisting of the Cl–Co–Cl and N–Co–N planes, arising from the steric roles of the bulky spartein ligands, defines an obvious structural chirality. An equally clear, though obviously smaller, structural chirality is evident in the propylenediamine complex, illustrated in Fig. 34. Similar and familiar twisting of the diamine chelate rings in the tripodal ligand, S-tan, define the structural handedness in chromophores **33–40**. In the six-coordinate complex, $[Nien_3]^{2+}$, the structural chirality is evident both in the rotation of opposite "octahedral" faces normal to the molecular three-fold axis and in the ethylenediamine twisting itself.

In all cases, however, good reproduction of the magnitudes of rotatory strengths was possible only upon recognition of the bent bonding that these geometrical features imply. The "purest" illustration of this was provided by chromophore **12** — the propylenediamine system shown in Fig. 34. In that molecule, the Cl–Co–Cl and N–Co–N planes are nearly exactly orthogonal so that any ligand-field modelling expressed, as usual, in terms of the first coordination sphere with local M–L ligations of C_{2v} pseudosymmetry will necessarily yield null rotatory strengths. Within an independent-systems approach, the source of the *optical* chirality in such a chromophore is viewed as a physically separated perturber located within the propylenediamine backbone. The literature on this subject is very large and has an extensive provenance; Mason, for example, has provided a delightfully readable account [83] and Richardson a thoroughgoing review [72] at a more technical level. The independent-systems approach is, of course, only a model and, as we have discussed at length, explicitly neglects covalency and overlap. We have argued that the CLF approach, though necessarily parametric, should take account of all contributions to one-electron processes contributing to the effective operators of forced electric dipole transitions. In chromophore **12**, for example, the structural chirality imposed by the chelate obliges the nitrogen σ donor orbitals to be inexactly directed towards the central metal atom (a) because of the tendency of the nitrogens to be tetrahedrally bound and (b) in view of some degree of chelate ring strain. Misdirected valency in

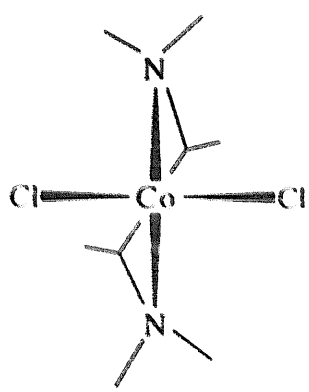

Fig. 34. Chromophore **12**.

the Co–N bonding results, monitored in the CLF model by appropriate $e_{\sigma\pi}$, e_{π} and ${}^{L}t_{\pi}$ parameters, and non-zero rotatory strengths ensue. In the spartein chromophores, it has been argued that the electronic chirality is much less than the structural chirality defined by the donor atom coordinates because of the effects of misdirected valency arising from both ring strain and the misalignment of cobalt and nitrogen σ functions due to the primary twisting of the coordination geometry. Much smaller effects, but ones originating in the same way, are responsible for the electronic chirality observed in the S-tan chromophores **33–40**; the same consequences of ethylenediamine chelation probably contribute to the circular dichroism in $[Nien_3]^{2+}$.

These effects are small, but rotatory strengths respond sensitively to them. Unfortunately, none of the analyses surveyed in this section were able to define the parameters of misdirected valency very accurately. In each case, however, the signs of the $e_{\sigma\pi}$ parameters were such as to concur with the physical siting of the bent bonding proposed. The reader is referred to the original papers, cited in Table 23, for full details.

For completeness' sake, we list best estimates of the ${}^{L}t_{\lambda}$ parameters for the "tetrahedral" chromophores, **10–12**, in Table 42. All *P*:*F* ratios are greater than unity and appear to describe "normal" ligand→metal electron donation throughout. Typical CLF e_{λ} values for the group are $e_{\sigma}(Cl) \sim 4000\ cm^{-1}$, $e_{\pi}(Cl) \sim 1300\ cm^{-1}$ and $e_{\sigma}(N) \sim 4800\ cm^{-1}$; details of other e_{λ} values will be found in the original paper. CLF ${}^{L}t_{\lambda}$ values for the S-tan complexes were discussed in Section 7.3.2. As described in Section 7.2.6, after lengthy NCA, only one variable was required (in first-order, at least) for $[Nien_3]^{2+}$. It was found that the ratio ${}^{P}t_{\sigma}(N):{}^{F}t_{\sigma}(N)$ was about 4, again in line with a typically good N→Ni σ donation.

7.4. A correlation between bond character and an optical selection rule

Chromophore **26** provides an interesting example of how the *character* of chromophore bonds can falsify bond assignments made by conventional application of

Table 42
Optimal CLF ${}^{L}t_{\lambda}$ values for chromophores **10–12**

Parameter	Spartein	α-isospartein	Propylenediamine
${}^{P}t_{\sigma}(Cl)$	85	129	102
${}^{F}t_{\sigma}(Cl)$	22	9	0
${}^{P}t_{\pi}(Cl)$	78	82	86
${}^{F}t_{\pi}(Cl)$	9	12	18
${}^{P}t_{\sigma}(N)$	100[a]	100[a]	100[a]
${}^{F}t_{\sigma}(N)$	38	35	33
${}^{P}t_{\pi x}(N)$	57	74	64
${}^{F}t_{\pi x}(N)$	18	19	19
${}^{P}t_{\pi y}(N)$	58	83	52
${}^{P}t_{\pi y}(N)$	3	12	17

[a]Fixed (reference) values.

symmetry alone; we do not, of course, imply any violation of group theory. The central issue here is the observed weakness in crystal b polarization (which corresponds very closely with the molecular z polarization, where z lies parallel to the Cu–O bonds in the coordination of the DIAQ chromophore) of what our analysis assigns as the $xz \rightarrow x^2-y^2$ transition. This transition is formally enabled by a b_{3u} vibration and, because of this, Hitchman and McDonald [84,85] had favoured an alternative assignment. This alternative assignment did not yield a satisfactory intensity analysis, as detailed in the original paper. The issue we review here is the reason for the weakness of this transition even though the chromophore does undergo the deformations of a b_{3u} bend.

The transition moment $\langle xz|ez|x^2-y^2\rangle$ involves electronic displacement in the xz global frame alone. As shown in Fig. 35, the b_{3u} bend involves tangential displacements of the chlorine atoms lying along the global y axis, parallel to z. This ligand motion is the source of vibronic parity mixing into the d orbital basis that ultimately generates spectral intensity. The odd-parity functions admixed into the d that circumvent the orbital selection rule $\Delta\ell = \pm 1$ are of p or f type. If p, the chlorine atom displacement admixes p_y into $d_{x^2-y^2}$. However, the resulting $p_y - d_{x^2-y^2}$ hybrid differs from the pure $d_{x^2-y^2}$ function only in spatial regions on either side of the xz plane. The $\langle xz|ez|x^2\rangle$ transition moment is not, therefore, expected to be affected or enabled by this particular parity-mixing process. The same is not true for d–f mixing. Consider, for example, the admixture of $fx(z^2-y^2)$ character into the $d_{x^2-y^2}$ orbital as will be facilitated by the b_{3u} bend. As shown in Fig. 36, the f function is concentrated in *both* xy and xz planes. Changes in the d–f mixing in the xy plane brought about by the displacement of the chlorine atoms are necessarily accompanied by changes in d–f mixing in the xz plane. Accordingly, the $\langle xz|ez|x^2-y^2\rangle$ transition moment is expected to be sensitive to the b_{3u} bend *via* the d–f mixing but not, as we have seen, by any d–p mixing. However, the CLF $^{L}t_{\lambda}$ values of Table 41 are characterized by a total dominance of $^{P}t_{\sigma}(\mathrm{Cl})$ over $^{F}t_{\sigma}(\mathrm{Cl})$, associated with good Cl→Cu σ donation, as described in Section 7.3.5. The inevitable result is that the $\langle xz|ez|x^2-y^2\rangle$ transition is very weak. The relevance of bond character in deciding selection rules is not normally considered when evaluating appropriate direct

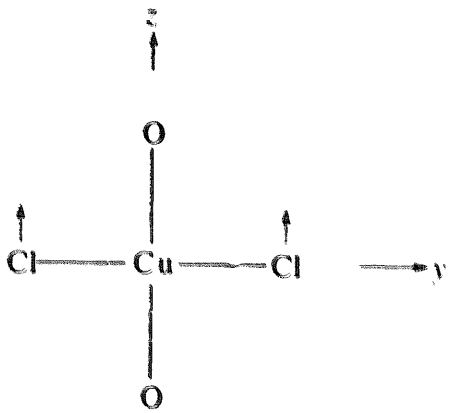

Fig. 35. The b_{3u} bend in the planar $CuCl_2O_2$ moieties.

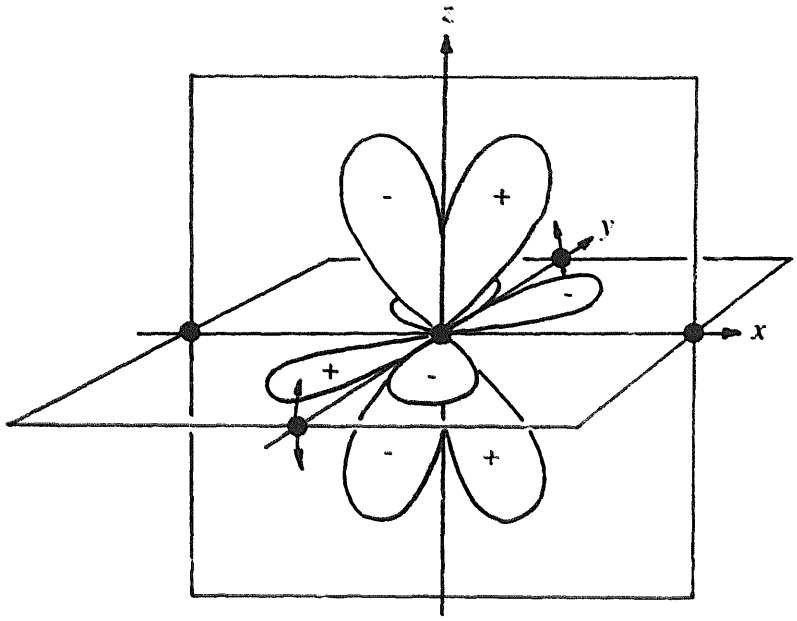

Fig. 36. The $fx(z^2-y^2)$ function in relation to the global molecular frame for DIAQ (26).

products at the outset of (or in the absence of) an intensity analysis. This intriguing example illustrates how one may be misled.

7.5. *Concluding remarks*

The past 40 years have seen an impressive attack on the intensities of open *d*- and *f*-shell spectra with imaginative and technical contributions from many laboratories. It is now apparent that intensity distributions can be well reproduced for a wide range of chromophores in which the parity mixing required to force formally disallowed, electric dipole transitions may arise statically within acentric environments or vibronically in centric ones. It is probably true that relative intensities of '*d–d*' transitions have been reproduced more accurately by the CLF model than '*f–f*' by the independent-systems approach. It is, however, only fair to acknowledge that the main-block studies have addressed the broader envelopes of less-well resolved transitions while those of the lanthanoids have mostly been concerned with typically sharper and more fully resolved transitions. In our CLF analyses, for example, we have often noted the insensitivity of calculated intensities to the magnitude of the spin-orbit coupling coefficient. This must be due, in large measure, to our seeking to reproduce intensities of spin-orbit coupling coefficient. This must be due, in large measure, to our seeking to reproduce intensities of spin-orbit-split components within a single band. No doubt variations in the magnitude of spin-orbit coupling would redistribute intensity amongst appropriate unresolved components of the band and so be invisible to the analytical process.

In common with other contributions to this field, we have been much concerned with the question of mechanism. Of central importance to that issue is the paper by Newman and Balasubramanian [24] in identifying the essence of Judd's early work

[22] as the construction of a quite general effective electric dipole operator for one-electron processes. Within that effective operator will be contained, albeit implicitly, contributions to dipole intensity from *all* one-electron sources, including covalency. Problems of dealing with covalency and overlap *ab initio* are horrendous and it was only natural to see their explicit and hopeful neglect by those espousing the independent-systems models. An accounting for them *parametrically*, however, within the CLF approach is not fundamentally difficult and appears to be generally remarkably successful. It is, of course, sad that the well-founded, theoretical generalities of the CLF model cannot be illustrated numerically and explicitly. This limitation is broadly the same as that governing the computation of molecular wavefunctions in these complex open-shell systems. Nevertheless, it is the case, that optimal values for the system variables generally make good qualitative sense in relation to chemistry and bonding theory in general. This success is undoubtedly to be ascribed to nature having (seemingly adventitiously) established the ligand-field regime itself in which *d* and *f* orbitals remain sufficiently uncoupled from all others.

As for future work, it is obviously desirable to apply the CLF model within the lanthanoid *f* block and to address the details of magnetic circular dichroism. Clearly there is much work ahead. Richardson ended at least one of his papers [46] with a plea for more, and detailed, experimental studies of '*f*–*f*'- and, by implication, of '*d*–*d*'-spectra. We concur.

References

[1] C.K. Jørgensen, R. Pappalardo, H.-H. Schmidtke, J. Chem. Phys. 39 (1963) 1422.
[2] C.E. Schäffer, C.K. Jørgensen, Molecular Phys. 9 (1965) 401.
[3] C.E. Schäffer, Struct. Bonding 5 (1968) 68.
[4] C.E. Schäffer, Struct. Bonding 14 (1973) 69.
[5] M. Gerloch, J.H. Harding, R.G. Woolley, Struct. Bonding 46 (1981) 1.
[6] R.G. Woolley, Molecular Phys. 42 (1981) 703.
[7] M. Gerloch, R.G. Woolley, Progress in Inorganic Chemistry, vol. 31, Wiley, New York, 1984, p. 371.
[8] M. Gerloch, Magnetism and Ligand-Field Analysis, Cambridge University Press, Cambridge, 1983.
[9] A.J. Bridgeman, M. Gerloch, Progress in Inorganic Chemistry, vol. 45, Wiley, New York, 1996, p. 179.
[10] M.J. Duer, N.D. Fenton, M. Gerloch, Int. Rev. Phys. Chem. 9 (1990) 227.
[11] C.A. Brown, M. Gerloch, R.F. McMeeking, Molecular Phys. 64 (1988) 771.
[12] M.J. Duer, S.J. Essex, M. Gerloch, K.M. Jupp, Molecular Phys. 79 (1993) 1147.
[13] G. Fischer, in: C.D. Flint (Ed.), Vibronic Processes in Inorganic Chemistry, NATO ASI Series, Kluwer, Dordrecht, 1989, p. 7.
[14] S.B. Piepho, P.N. Schatz, Group Theory in Spectroscopy, Wiley, New York, 1983.
[15] C.J. Ballhausen, A.E. Hansen, Ann. Rev. Phys. Chem. 23 (1972) 15.
[16] R.G. Denning, in: C.D. Flint, Vibronic Processes in Inorganic Chemistry, NATO ASI Series, Kluwer, Dordrecht, 1989, p. 111.
[17] G. Fischer, in: C.D. Flint (Ed.), Vibronic Processes in Inorganic Chemistry, NATO ASI Series, Kluwer, Dordrecht, 1989, p. 103.
[18] C.J. Ballhausen, Molecular Electronic Structures of Transition Metal Complexes, McGraw-Hill, London, 1979.
[19] L.L. Lohr, Jr, J. Chem. Phys. 50 (1969) 4596.
[20] A.D. Liehr, C.J. Ballhausen, Phys. Rev. 106 (1957) 1161.

[21] C.J. Ballhausen, A.D. Liehr, J. Molecular Spectra 2 (1958) 342.
[22] B.R. Judd, Phys. Rev. 127 (1962) 750.
[23] G.S. Ofelt, J. Chem. Phys. 37 (1962) 511.
[24] D.J. Newman, G. Balasubramanian, J. Phys. Chem.: Solid State Phys. 8 (1975) 37.
[25] C.K. Jorgensen, B.R. Judd, Molecular Phys. 8 (1964) 281.
[26] S.F. Mason, R.D. Peacock, B. Stewart, Molecular Phys. 30 (1975) 1829.
[27] C.G. Gray, Can. J. Phys. 46 (1968) 135.
[28] B.R. Judd, Angular Momentum Theory for Diatomic Molecules, Academic Press, New York, 1975, p. 98.
[29] B. Stewart, in: C.D. Flint (Ed.), Vibronic Processes in Inorganic Chemistry, NATO ASI Series, Kluwer, Dordrecht, 1989, p. 327.
[30] B.R. Judd, J. Chem. Phys. 70 (1979) 4830.
[31] F.S. Richardson, Chem. Phys. Let. 86 (1982) 47.
[32] F.S. Richardson, J.D. Saxe, S.A. Davis, T.R. Faulkner, Molecular Phys. 42 (1981) 1401.
[33] J.R. Quagliano, G.W. Burdick, D.P. Clover-Fischer, F.S. Richardson, Chem. Phys. 201 (1995) 321.
[34] J.D. Axe, J. Chem. Phys. 39 (1963) 1154.
[35] W.F. Krupke, J.B. Gruber, Phys. Rev. 139A (1965) 2008.
[36] P.J. Becker, Phys. Stat. Solidi 43 (b) (1971) 583.
[37] R. Reisfeld, J. Hormodaly, B. Barnett, Chem. Phys. Lett. 17 (1972) 248.
[38] Z. Jaeger, R. Engleman, Chem. Phys. Lett. 19 (1973) 242.
[39] A.R. Edmonds, Angular Momentum and Quantum Mechanics, Princeton University Press, New Jersey, 1960.
[40] Y.M. Poon, D.J. Newman, J. Phys. Chem.: Solid State Phys. 17 (1984) 4319.
[41] M.F. Reid, J.J. Dallara, F.S. Richardson, J. Chem. Phys. 79 (1983) 5743.
[42] M.F. Reid, F.S. Richardson, Chem. Phys. Lett. 95 (1983) 501.
[43] M.F. Reid, F.S. Richardson, J. Chem. Phys. 79 (1983) 5735.
[44] R. Kuroda, S.F. Mason, C. Rosini, Chem. Phys. Lett. 70 (1980) 11.
[45] B. Stewart, Molecular Phys. 50 (1983) 161.
[46] M.F. Reid, F.S. Richardson, J. Phys. Chem. 88 (1984) 3579.
[47] R. Gale, R.E. Godfrey, S.F. Mason, R.D. Peacock, B. Stewart, J. Chem. Soc., Chem. Comm. (1975) 329.
[48] P. Hohenberg, W. Kohn, Phys. Rev. 136B (1964) 864.
[49] V. Heine, Solid State Phys. 35 (1980) 1.
[50] M. Gerloch, R.F. McMeeking, J. Chem. Soc. (Dalton) (1975) 2443.
[51] R.R. Sharma, Phys. Rev. 13A (1976) 517.
[52] C.A. Brown, M.J. Duer, M. Gerloch, R.F. McMeeking, Molecular Phys. 64 (1988) 825.
[53] E. Clementi, IBM J. 9 (1965) 2.
[54] J.J. Dallara, M.F. Reid, F.S. Richardson, J. Phys. Chem. 88 (1984) 3587.
[55] E.M. Stephens, M.F. Reid, F.S. Richardson, Inorg. Chem. 23 (1984) 4611.
[56] M.J. Duer, M. Gerloch, Inorg. Chem. 28 (1989) 4260.
[57] D.M. Brink, G.R. Satchler, Angular Momentum, Oxford University Press, Oxford, 1968.
[58] H.A. Buckmaster, Can. J. Phys. 42 (1961) 386.
[59] M.J. Duer, S.J. Essex, M. Gerloch, Molecular Phys. 79 (1993) 1167.
[60] A.J. Bridgeman, M. Gerloch, Molecular Phys. 79 (1993) 1195.
[61] A.J. Bridgeman, K.M. Jupp, M. Gerloch, Inorg. Chem. 33 (1994) 5424.
[62] C.A. Brown, M.J. Duer, R.F. McMeeking, Molecular Phys. 64 (1988) 793.
[63] C.A. Brown, M.J. Duer, R.F. McMeeking, Molecular Phys. 64 (1988) 825.
[64] M.J. Duer, M. Gerloch, J. Chem. Soc. Dalton Trans. (1989) 2109.
[65] N.D. Fenton, M. Gerloch, Inorg. Chem. 29 (1990) 3718.
[66] A.J. Bridgeman, M. Gerloch, Inorg. Chem. 34 (1995) 4730.
[67] A.J. Bridgeman, M. Gerloch, J. Chem. Soc., Dalton Trans. (1995) 197.
[68] A.J. Bridgeman, S.J. Essex, M. Gerloch, Inorg. Chem. 33 (1994) 5411.
[69] N.D. Fenton, M. Gerloch, Inorg. Chem. 29 (1990) 3726.
[70] N.D. Fenton, M. Gerloch, Inorg. Chem. 28 (1989) 2975.

[71] A.F. Drake, S.J. Hirst, R. Kuroda, S.F. Mason, Inorg. Chem. 21 (1982) 533.
[72] F.S. Richardson, Chem. Rev. 79 (1979) 17.
[73] L. Rosenfeld, Z. Physik 52 (1928) 161.
[74] M. Gerloch, Comments Inorg. Chem. 18 (1996) 101.
[75] R.G. McDonald, M.A. Hitchman, Inorg. Chem. 25 (1986) 3273.
[76] M.A. Hitchman, P.J. Cassidy, Inorg. Chem. 18 (1979) 1745.
[77] R.G. McDonald, M.J. Riley, M.A. Hitchman, Inorg. Chem. 27 (1988) 894.
[78] R.J. Deeth, M. Gerloch, J. Chem. Soc., Dalton Trans. (1986) 1531.
[79] R.J. Deeth, M. Gerloch, Inorg. Chem. 24 (1986) 4490.
[80] M. Ciampolini, Struct. Bonding 6 (1969) 52.
[81] R.J. Deeth, M.J. Duer, M. Gerloch, Inorg. Chem. 26 (1987) 2573.
[82] R.J. Deeth, M. Gerloch, Inorg. Chem. 24 (1985) 1754.
[83] S.F. Mason, Molecular Optical Activity and the Chiral Discriminations, Cambridge University Press, Cambridge, 1982.
[84] M.A. Hitchman, R.G. McDonald, Inorg. Chem. 29 (1990) 3074.
[85] M.A. Hitchman, R.G. McDonald, Inorg. Chem. 29 (1990) 3081.